The Dissertation Committee for Shichao Liu Certifies that this is the approved version of the following dissertation:

The Effects of Indoor Air Jets on Air Distribution and Human Exposure to Particles

Committee:

Atila Novoselac, Supervisor

Richard L. Corsi

Ying Xu

Ofodike A. Ezekoye

James Bennett

Qingyan (Yan) Chen

The Effects of Indoor Jets on Air Distribution and Human Exposure to Particles

by

Shichao Liu, B.E., M.E.

Dissertation

Presented to the Faculty of the Graduate School of

The University of Texas at Austin

in Partial Fulfillment

of the Requirements

for the Degree of

Doctor of Philosophy

The University of Texas at Austin

December, 2014

Dedication

To Yi, for her unwavering love, support and encouragement.

Acknowledgements

First and foremost, I would like to thank my advisor, Dr. Atila Novoselac, for taking me as his student among numerous applicants. He always encourages me when I get stuck in the mud and supports me whenever I confront challenges regarding to research and life.

I would also like to acknowledge Dr. Richard L. Corsi, Dr. Ying Xu, Dr. Ofodike A. Ezekoye, Dr. James Bennett and Dr. Qingyan (Yan) Chen, for sparing time to serve on my committee and reviewing my work.

I would like to express my profound gratitude to the American Society of Heating, Refrigerating and Air-Conditioning Engineers, for granting me support to pursue my graduate studies.

My thanks to Dr. Neil Crain for his discussion with me, and to Ms. Dori Eubank for her dedication and management of crises.

My experiment helpers, Shane Riley, Adrian Saldanha, Steve Bourne, Yirui Liang, Qiang Liu, Guangyu Cao, Chenyang Bi and Xinke Wang, gave me hands when I swapped diffusers/ grilles beyond my ability.

Special thanks are due to my English mentors, Steve Bourne, Brandon Boor, Jordan Clark and Kristen Cetin, for their kindness and patience when hanging out with me and proof-reading my documents.

Finally, I would like to acknowledge my family: my parents Xiping and Xinai, my brother Shizhen, and my new family, Yi. This dissertation work is possible because of you!

The Effects of Indoor Air Jets on Air Distribution and Human Exposure to Particles

Shichao Liu, Ph.D.

The University of Texas at Austin, 2014

Supervisor: Atila Novoselac

Indoor jets considerably dominate air movement and distribution of temperature and velocity, as well as transport of particles and other pollutants. Indoor air temperature and velocity distribution substantially impact occupants' thermal comfort and productivity, heat and mass transfer on indoor surfaces. In addition, jets produced by human respiratory activities, such as coughing and sneezing, enhance the spread of particles that might carry bacteria or viruses. Understanding and characterizing indoor jets and their impacts on air distribution, temperature and velocity fields, and particle transport are crucial for advancing heating, ventilation, and air conditioning (HVAC) systems when considering thermal comfort and developing strategies for exposure mitigation.

This dissertation contributes to the scientific understanding regarding to indoor air distribution and particle transport associated with indoor air jets. Current HVAC system design defines indoor air distribution related to the selection of diffusers/ grilles that distribute supply air jets, according to the specifics of the space and internal heating and cooling loads. However, current design guidance was developed over 40 years ago. It requires expansion of diffuser/ grille types and the update for air distribution by diffuser/ grille air jets supplying warm air at heating mode. Unlike jets from diffusers/ grilles, jets

created by human activities are inherently transient in nature and might perform quite differently from steady-state ones. Understanding the dynamics of unsteady-state jets, such as coughs, enhances the current state of understanding of the mechanisms of respiratory disease transmission, which enables development of exposure reduction measures.

The investigations presented in this dissertation extend the state-of-the-art knowledge on indoor jets and analyze the effect of steady-state and unsteady-state jets on particle transport in indoor environments. This dissertation addresses two objectives by conducting six investigations. The first objective includes four investigations that deal with air distribution and particle transport associated with steady-state jets created by diffusers/ grilles, and the remaining two investigations relate to the second objective on unsteady-state cough jets.

The first objective of this dissertation characterizes air distribution and particle transport in a space with steady-state jets created by diffusers/ grilles. One of the major contributions of this objective to the-state-of-the-art knowledge on indoor air distribution is the newly developed method for diffuser performance assessment and design when considering heating mode. It advances the current diffuser/ grille selection guide that was outdated decades ago. Furthermore, based on 650 experimental set-ups this objective provides a systematic analysis of indoor air velocity that can be further used in indoor heat transfer and pollutant emission and transport.

The second objective investigates velocity fields in unsteady-state cough jets and transport of coughed particles. This objective provides a theoretical analysis of the dynamics of cough jets and examines how human thermal plume affects the exposure to coughed particles when considering different particle sizes.

Ultimately, these investigations fill the knowledge gaps in indoor air distribution and particle transport associated with steady-state and unsteady-state jets in spaces using all-air HVAC systems. The newly developed diffuser guideline will improve HVAC design for both heating and cooling conditions when considering thermal discomfort or air stagnant zones caused by a wrong diffuser selection. In addition, the systematic analysis of indoor air velocity will improve the prediction of indoor heat transfer, mass transfer, particle resuspension rate, pollutant emission rate from the floor and other indoor surfaces. Finally, the theoretical analysis of unsteady-state jets contributes the knowledge for fluid dynamics of unobstructed human coughs and also transport of coughed particles, including the distribution in the vicinity of an exposed person.

Table of Contents

List of Tables

List of Figures

Chapter 1: Introduction

1.1 PROBLEM STATEMENT

1.1.1 Steady-state and unsteady-state jets

Air jets are used to move indoor air and particulate matter in various built environments ranging from buildings - such as homes and offices - to specific indoor spaces - such as automobile and airplane cabins. Jets created by air diffusion terminal units (diffusers/ grilles) distribute supply air throughout the indoor space, while maintaining occupant thermal comfort and diluting indoor airborne pollutants. The jets generated by diffusers/ grilles are usually associated with HVAC (heating, ventilating and air conditioning) systems running: (1) intermittently (on-off HVAC control) with a constant flow rate when the HVAC is on; (2) continuously at a constant flow rate but with variable jet temperatures (Constant Air Volume (CAV) control); or (3) at a variable flow rate but with a constant supply temperature (Variable Air Volume (VAV) control). Even when using a VAV system, however, supply air flow rates change quite slowly. As a result, these types of jets can be considered to be in a quasi-steady-state.

Other types of jets in the indoor environment are unsteady ones often caused by human activities, such as closing a door or walking, and these jets can also affect pollutant distribution (Gomes et al. 2007). Other specific important unsteady-state jets impacting pollutant transport are those associated with human respiratory activities; for instance, breathing, coughing and sneezing. A cough can have a long penetration length, carrying and dispersing potentially infectious particles such as influenza virus (Lindsley et al. 2010). This dissertation considers the jets induced by human respiratory activities as unsteady-state jets.

1.1.2 Indoor air distribution related to steady-state and unsteady-state jets

Steady-state jets generated by diffusers/ grilles dominate overall indoor air distribution and particle dispersion, while unsteady-state jets influence only local dynamics of air and particles due to their short periods. A good air distribution contributes towards

meeting human comfort requirements, and incurs a lower energy penalty for air distribution, while satisfying fresh air ventilation needs.

Indoor air distribution affects air velocity and temperature distributions that are important factors concerning thermal comfort (Fanger 1970). A recent survey suggests that thermal comfort is of greater importance than visual or acoustic comfort (Frontczak and Wargocki 2011). There is also a potential for productivity improvement among workers who are provided with greater thermal comfort. It is suggested that task-related performance is significantly correlated with the human perception of thermal environment, and that the value of the productivity loss is quite closely related to thermal dissatisfaction (Kosonen and Tan 2004).

By adjusting diffuser/ grille air jet characteristics, such as temperature and velocity, indoor thermal comfort can be achieved. The adjustment to some extent determines total building energy performance, which can also impact national energy consumption. Buildings are responsible for 41% of source energy consumption in the United States (U.S. Department of Energy 2012), and the energy use for HVAC systems accounts for 50% of building consumption and 20% of total consumption in the USA (Pérez-Lombard et al. 2008). Since indoor air distribution is dominated by steady-state jets from diffusers/ grilles, the reduction of the number of diffusers/ grilles required to be supplied into a space without compromising thermal comfort will in turn reduce required capacity of energy consumption by HVAC systems.

Air distribution is also an indicator of ventilation effectiveness. Previous studies have shown that the ventilation effectiveness is significantly influenced by the arrangement and type of supply diffusers/ grilles in the room (Chung and Hsu 2001; He et al. 2005; Lee et al. 2007). Improvement of air distribution/ ventilation effectiveness reduces the creation of poorly ventilated areas with stagnant air and removes contaminants before they can spread throughout a conditioned space. Increases in the fresh air delivered to an occupied zone decreases subject dissatisfaction of air quality and reduces sick building syndrome - (SBS) (Wargocki et al. 2000). Fisk (2000) estimated that the potential annual savings and

productivity gains possible from reduced incidences of SBS are between $10 billion and $30 billion.

Furthermore, indoor air distribution is related to particle resuspension and organic compound emission from indoor surfaces (Xu and Little 2006; Hafner et al. 2012; Goldasteh et al. 2013). Particle detachment from the floor is usually characterized in terms of free-stream velocity close to the floor (Ibrahim et al. 2003). Generally, the amount of particles that resuspend from a surface rises with increasing air velocity (Boor et al. 2013). Clausen et al. (2010) measured the specific emission rates of DEHP and found that the emission rates doubles as free-stream velocity doubles. In addition, air distribution is responsible for the human exposure to airborne particles. Previous studies have measured the fraction of particles inhaled as a function of air velocity (Ogden and Birkett 1977; Vincent and Mark 1982; Armbruster and Breuer 1982).

Compared with steady-state jets provided by diffusers/ grilles, human coughs are representatives of unsteady jets influencing local air motion. A typical cough has a peak velocity in a range of 6-22 m/s with a duration ranging from 0.25s to 0.8s (Zhu et al. 2006; Gupta et al. 2009). An individual human cough jet in a calm indoor environment can expel saliva droplets further than two meters (Zhu et al. 2006). As a violent event, human coughs play a key role in transferring respiratory diseases between infectious and susceptible individuals. Previous studies found an association between cough frequency and tuberculous aerosol production and infection (Loudon and Spohn 1969; Fennelly et al. 2004), and for human exposure studies it is important to understand the dynamics of these unsteady-state jets.

1.1.3 Particle transport related to steady-state and unsteady-state jets

Epidemiological studies have demonstrated adverse effects of particulate matter exposure on human health, as evidenced by the London smog of 1952 that caused approximately 4000 excess deaths (Wilkins 1954). Particles smaller than 2.5μm in diameter pose the greatest health issues because they can be carried into human lungs. Short-term exposures to such particles can aggravate lung disease, causing asthma attacks and acute

bronchitis, and may also increase susceptibility to respiratory infections. Long-term exposures are associated with chronic problems such as reduced lung function, development of chronic bronchitis and even premature death (U.S. EPA 2003).

As humans spend nearly 90% of their time indoors (Klepeis et al. 2001), particle transport and distribution in indoor environments contribute greatly to the impacts of particle exposure on human health. Indoor particle transport is driven by indoor airflow distribution, gravity, and other forces such as Brownian force. The location of particle sources, room configuration and particle size also contribute to the transport of particles (Bouilly et al. 2005; Holmberg and Chen 2003; Lu et al. 1996; Mundt 2001; Whicher et al. 2002; Zhao et al. 2004). Unlike the steady-state jets only transporting particles, a cough generates and spreads particles; Lindsley et al. (2012) found that the average number of particles expelled by each cough ranges from 900 to 302,200. Due to its high discharge velocity, a cough jet might dominate the transport and dispersion of released coughed particles. Typically, most indoor sources of particles are intermittent or unsteady because of human activities, for instance cooking, printing, walking on the floor and coughing. Hence, understanding the transport of particles generated from unsteady sources in a space associated with steady-state and unsteady-state jets would guide strategies for diminishing exposure level to particles.

1.1.4. Indoor air distribution index in a space

The current technique used to predict and represent indoor air distribution created by steady-state jets from diffusers/ grilles is the Air Diffusion Performance Index (ADPI) method. ADPI is defined as the percentage of occupied zone falling into the comfortable zone determined by measuring local effective draft temperature (EDT). The effective draft temperature is a calculated temperature combining indoor air temperature and velocity distributions (ASHRAE Standard-113 2013). ADPI also defines the maximum acceptable velocity in the occupied zone.

Values of ADPI for typical diffuser/ grille air jets and indoor thermal loads have been aggregated into a selection guide to direct diffuser selection and layout (Miller and Nevins 1970; Miller 1971; Miller and Nash 1971; Miller and Nevins 1972; Miller 1979).

Current diffuser guidelines (e.g. ASHRAE-*Fundamentals* 2009) list the ADPI values for five common types of diffusers. Based on required airflow rates, HVAC system designers are able to select and layout diffusers/ grilles to achieve the maximum ADPI and indoor air distribution. However, the available types of diffusers/ grilles have increased over time and are not all reflected in the design guidelines. Moreover, the manufacturing methods for many of the diffusers/ grilles in the current guidelines have changed since the original testing occurring in the 1960s (Miller and Nevins 1970; Miller 1971), which may have changed the performance characteristics of these devices.

When the first ADPI-based diffuser/ grille selection guide was developed, HVAC systems for delivering warm air in heating mode were uncommon. Nowadays, however, the operation of HVAC systems for heating has become much more popular, and HVAC systems need be designed to meet both heating and cooling requirements in most climates (Buratti et al. 2013; Krarti 2008; Platt et al. 2010; Vakiloroaya et al. 2014). Even though ASHRAE Standard-113 (2013) states that "the ADPI method for mixing systems should be applied to traditional overhead air distribution systems under cooling operation only", the same diffusers are used for heating in the winter. The lack of ADPI method for heating mode often causes underperformance of all-air delivery systems when used for heating. When diffusers/ grilles supply air at a low airflow rate but at a high temperature, the thermal stratification causes not only thermal comfort issues, but also stagnant air in the occupied zone resulting in low ventilation effectiveness (Novoselac and Srebric 2003; Krajčík et al. 2012; Tomasi et al. 2013). Therefore, further development of the ADPI method is required for applications at heating mode.

1.1.5. Unsteady cough jets: velocity and particle transport

The velocity field of human coughs has been extensively examined using various experimental methods, including Particle Image Velocimetry (PIV) (Zhu et al. 2006; Chao et al. 2009; VanSciver et al. 2011; Nishimura et al. 2013) and Schlieren imaging (Tang et al. 2009). However, the velocity variation in a cough jet has been rarely analyzed as steady-steady jets. A theoretical analysis of coughed droplets characterized the trajectories of

different size droplets driven by a cough jet assuming the cough jet was steady (Xie et al. 2007). Although this analysis is very helpful to understand the dynamics of different size droplets in a cough, the simplification related to the steady state jet limits the findings from being generalized to real cough conditions. Kouros et al. (1993) found that an unsteady-state jet, such as puff, has significantly different properties from a steady-state jet with the same inlet velocity. Another study has shown that the momentum of a puff is constant in time and flow, and self-persevering (self-similarity) can be achieved downstream from the puff source (Kovasznay et al. 1975). The short duration of a cough jet classifies it as a puff and using a puff theory helps the theoretical analysis of the velocity field in the cough, and consequently the trajectories of various size particles within the cough jet.

While the previously mentioned studies (Yin et al. 2011; Gupta et al. 2011; Zhang and Li 2012; Zhao et al. 2005) were concerned with the dispersion of coughed particles in indoor environments, Lai et al. focused on the interpersonal transport of expiratory particles in scaled and full-scale chambers (Berrouk et al. 2010; Lai and Wong 2010, 2011; Seepana and Lai 2012). In these studies, coughs were simulated by using a spray gun with the results providing fundamental data regarding to interpersonal transmission of coughed particles. However, further improvement of experimental studies of interpersonal transport is possible, especially when considering the size of the discharge opening ("human mouth") and more details on discharge concentration. The discharge concentration of a cough allows an analysis of to what extent expiratory particle concentration decays during transport. Furthermore, much less is known about the effect of particle size on coughed particles transporting in the jet and vicinity of an exposed occupant. Most particle sampling instruments, e.g. Optical Particle Counters (OPC) and Aerodynamic Particle Sizes (APS), have a response time of 1s or larger. This prevents the measurement of particle concentration in the cough jet region where coughed particles pass through a position quickly, especially when the cough velocity is high. This may explain why previous studies measured only long-duration and low-discharge-velocity coughs (Lai and Wong 2010; Seepana and Lai 2012; Chen et al. 2013). Detailed studies about the transport of particles expelled from a typical cough are scarce.

The investigations presented in this dissertation are concerned with how two types of jets - unsteady and steady - influence indoor air distribution and particle transport. This dissertation advances the understanding of the effects of steady jets produced by HVAC diffusers/ grilles on air distribution and particle transport at both cooling and heating modes. In addition, the dissertation seeks to fill the knowledge gaps regarding to velocity distribution in cough jets and the transport of coughed particles, which pose a health hazard to humans through the spread of infectious particles.

The knowledge gaps regarding to characterization of indoor air distribution and particle transport in an indoor space with steady-state and unsteady-state jets require further investigations. Specifically, the current ADPI method characterizing indoor air distribution needs to be updated and expanded. In addition, in order to guide diffuser/ grille selection for heating condition, a heating mode ADPI method must be developed. Furthermore, the transport of particles from an unsteady cough needs an investigation that considers short period but strong momentum unsteady jets. To address the challenges identified by previous research, this dissertation conducts six investigations in regard to steady-state and unsteady-state jets occurring in the indoor environment, as described in the following section.

1.2 OBJECTIVES AND SCOPE OF THIS DISSERTATION

This dissertation is poised to examine the impact of indoor steady-state and unsteady-state jets on air distribution and particle transport. Indoor steady-state jets are provided by air diffusers/ grilles for HVAC systems that are commonly used in commercial office buildings. Since commercial office-type buildings mostly apply diffusers/ grilles to generate mixing ventilation. This dissertation focuses air distribution and particle transport related to steady-state jets only for mixing ventilation. In addition, indoor air motion and particles are driven only by the momentum of jets from diffusers/ grilles or coughing and indoor thermal plumes from heat sources in this work. Additional momentum sources, such as the case of using a fan, are not considered herein.

The overall objectives of this dissertation illustrated in Figure1 are summarized as follows:

(1) Characterize air distribution in indoor spaces equipped with different diffusers/ grilles, and investigate the transport of particles released from different locations in these spaces.

(2) Analyze the velocity field in a cough jet region, and examine the transport of coughed particles as affected by the cough jet and an exposed occupant's thermal plume.

Four investigations related to steady-state jets support the first objective:

(A) The investigation and measurement of indoor velocity and temperature distributions in the occupied zone of a full-scale test room when the diffusers are providing cold air (cooling mode operation). ADPI values over a large range of air exchange rates (ACHs) are calculated using temperature and velocity data for a specific set of thirteen diffuser types. This investigation expands and updates the ADPI method in cooling mode.

(B) An investigation uses Fanger's thermal comfort model (Fanger 1970), to develop an ADPI diffuser selection methodology for all-air heating systems (heating mode operation). Beside the impact of local temperature and velocity, the heating ADPI model takes into account the negative impact of thermal stratification (when warm steady-state jets are provided into a space) and its influence on the generation of stagnant zones.

(C) An investigation to systematically analyze indoor air velocity in the occupied zone of a full-scale test room, as well as in the region including the floor affected by the diffuser/ grille air jet(s). This investigation explores factors influencing indoor air velocities, such as air exchange rate, diffuser/ grille type and indoor thermal loading.

(D) Finally, an investigation into steady-state jets to measure and numerically simulate the transport of particles released from two locations: (1) inside the steady-state jet region; and (2) outside the jet region. The impact of particle size - 0.77, 2.5 and 7μm - and mode (cooling or heating mode) -is also considered in this investigation.

Two additional investigations support the second objective related to unsteady-state cough jets:

(E) The first unsteady-state-jet investigation applies fundamental fluid dynamics to analyze velocity field of a cough jet; in this analytical study a dimension analysis is used to define key jet parameters assuming jet momentum self-preservation theory (Kovasznay et al. 1975).

(F) The final investigation examines the distribution of coughed particles in the vicinity of an exposed occupant in a close proximity to the coughing source.

The organization of this dissertation is as follows: “Literature review” provides the current research background and knowledge gap; “Methodology” summarizes experimental measurements and CFD numerical simulations for all related investigations; “Results” presents the major findings from this dissertation work; “Conclusion” provides a brief summary. “Appendices” include four full-length articles related to the investigations in this dissertation.

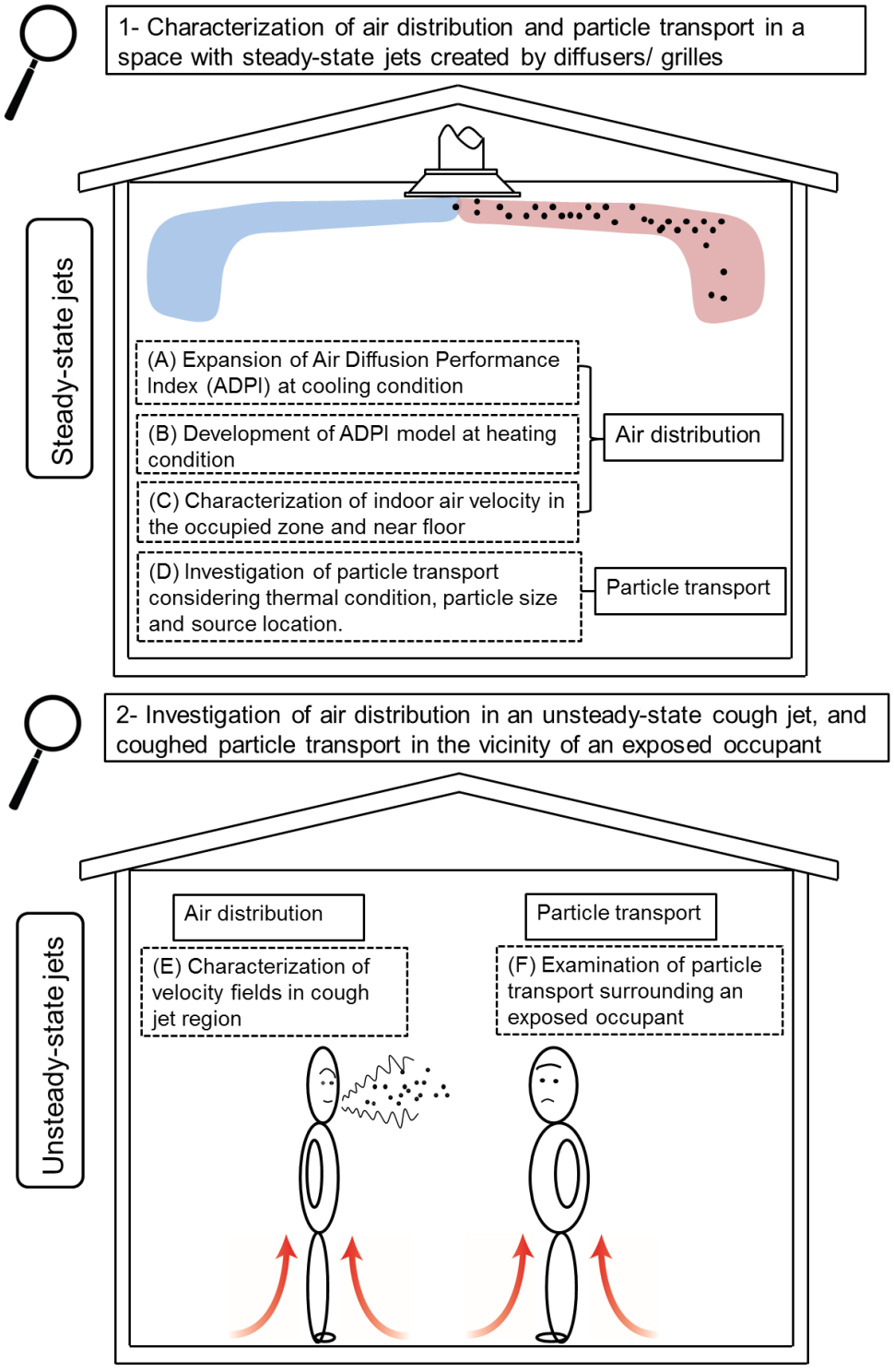

Figure 1: Illustration of the two research objectives and six (A-F) specific investigations conducted to address these objectives.

Chapter 2: Critical literature review and relevant background

This section summarizes previous research relevant to this dissertation and distinguishes the dissertation work from them. The literature review is divided into four sections. Section 2.1 and 2.2 discuss previous studies in the field of steady-state diffuser air jets considering air distribution and particle transport, respectively. Section 2.3 reviews the literature on human coughing and interpersonal exposure to coughed particles. Specifically, it discusses the discharge velocity and particle size distribution of an individual cough that is followed by a summary of previous work related to particle dispersion caused by a cough. Lastly, in Section 2.4, the numerical calculation of particle dispersion in a space with steady-state or unsteady-state jets is discussed focusing on the comparison of Large Eddy Simulation (LES) and Reynolds-average Navier-Stokes (RANS) models.

2.1 AIR DISTRIBUTION IN A SPACE WITH STEADY-STATE JETS FROM DIFFUSERS / GRILLES (INVESTIGATIONS 1A AND 1B)

This section focuses on the air distribution in a space with different diffusers/ grilles and summarizes the previous studies on ADPI. In a ventilated space, the air supplied into the space through various types of diffusers/ grilles, such as round ceiling diffuser, square ceiling diffuser, adjustable blade grill and fixed blade grille, is distributed by turbulent air jets. Air jets from diffusers/ grilles have different characteristics. For instance, an attached jet is produced when the supply air jet is attached to a ceiling or a wall. ASHRAE Handbook-*Fundamentals* (2009) classifies jets into six groups when air is supplied through different diffusers/ grilles as summarized in Table 1.

Jet type	Diffusers/ grills	Characteristics
Compact jets	Grille, nozzle, opening with a small aspect ratio	Three-dimensional, axis-symmetric, maximum velocity on the jet axis
Linear jets	Slot, opening with a high aspect ratio	Two-dimensional, axis-symmetric, transforming into compact jets away from the diffuser
Radial jets	Ceiling cylindrical air diffusers, such as round ceiling, square ceiling, plaque diffuser	Directing air horizontally in all directions.
Conical jets	Cone or regulated multi-diffuser ceiling-mounted device	Axis – symmetric
Incomplete radical jets	Grilles with diverging vanes and a forced angle of expansion	Transforming into a compact jet away from the diffuser
Swirling jets	Vortex-forming diffuser	Creating rotation

Table 1: The types of jets created by various diffusers/ grills.

Employing Computational Fluid Dynamics (CFD) method, numerous studies have simulated air jets provided by diffusers/ grilles, and indoor air distribution in a space with such jets (Luo and Roux 2004; Bin and Sekhar 2007; Lee et al. 2007; Zhou and Haghighat 2007; Cao et al. 2011). Aziz et al. (2012) numerically investigated the characteristics of airflow provided by round, square and swirl ceiling diffusers. The results showed that round and square ceiling diffusers have a similar performance to distribute supply air, while swirl jet decays faster than the ones created by round and square ceiling diffusers, suggesting a greater entrainment ratio when using swirl diffusers than round and square ceiling diffusers (Hu 2003).

Numerical studies related to diffuser/ grille types include indoor air distribution in an enclosed space installed with diffusers/grilles at different layouts. Sun and Smith (2005) compared indoor airflow characteristics in a room using one square cone diffuser with using two such diffusers. The results suggested that a single diffuser is capable to improve the mixing effect than two diffusers when maintaining total supply airflow rate. However, numerical studies mostly focused on the verification of diffuser modeling rather than how different diffuser/ grill air jets impact indoor air distribution (Srebric and Chen 2002; Abanto et al. 2004; Xu and Niu 2004; Zhang et al. 2009; Cehlin and Moshfegh 2010).

Because of cost-prohibitiveness, experimental studies on air distribution in a ventilated room using different diffuser/ grille types and layouts are scarce. Chow and Wong (1994) measured indoor air distribution induced by a linear diffuser in an environmental chamber. Cao et al. (2010) identified the airflow patterns of different attached plane jets and developed an empirical mode to predict the decay of jet velocity. The velocity field, throw and drop of a jet created by a high side-wall grille were measured recently (Martinez-Almansa et al. 2014). However, these studies mainly are concerned with air velocity only in the jet region.

ADPI is an indicator of air diffusion performance of a diffuser/ grille at a specific air delivery rate and space load (ASHRAE Standard-113 2013). ADPI reflects indoor air uniformity in terms of velocity and temperature distribution using a single index. The currently used ADPI method for cooling mode developed by Miller and Nash (1971) was derived from the subjective response to draft (air temperature difference and velocity) proposed by Houghten et al. (1938).

ADPI is determined by the maximum air speed and Effective Draft Temperature (EDT). It is the percentage of testing points falling into the range of EDT at an acceptable air speed. The EDT was first introduced by Rydberg et al. (1949) and then modified by Straub in a discussion of the paper by Koestel and Tuve (1955) as

$$EDT = T_i - T_a - 8.0(V_i - 0.15)\ ^oC \quad (1)$$

where T_i is temperature at the test point, i ; T_a is spacious average temperature and V_i is local air speed.

The criterion's range of cooling mode EDT is between -1.7 ^{o}C and 1.1 ^{o}C with an air speed less than or equal to 0.35 m/s. The lower boundary of EDT (-1.7^{o}C) shows a good agreement with Houghten's data for 80% of the occupants reporting comfort (Nevins and Miller 1972). Koestel and Tuve (1955) indicated that the upper limit of EDT=1.1^{o}C is satisfactory. Furthermore, the velocity 0.15m/s in the EDT Equation 1 represents the effect of human thermal plume. Additionally, the maximum acceptable velocity of 0.35m/s that

occupants can tolerate was recommended by Nevins and Miller (1972). The range derived from subjective thermal sensation defines the variation in EDT with air temperature difference and speed.

The ADPI method has been broadly applied to guide diffuser/ grille selection and layout after extensively work on the relationship of ADPI with the characteristics of diffusers/ grilles, room geometry and thermal load (Miller and Nevins 1969; Miller and Nevins 1970; Miller 1971; Miller and Nash 1971; Miller and Nevins 1972; Miller 1979). The ADPI of each diffuser/ grille type is described as a function of the ratio of diffuser/ grille air jet's throw length (T_v) to room characteristic length (L): T_v/L, and room load (ASHRAE - HVAC Application 2007; ASHRAE-*Fundamentals* 2009). Most studies under cooling condition have shown: (1) that ADPI curves have a concave-like shape as illustrated in Figure 2, (2) that the ADPI is low for small and large $T_{0.25}/L$ ratios, and (3) that there is a point with the maximum ADPI (Miller and Nevins 1970; Miller 1971; Miller and Nevins 1972; Nevins and Miller 1972; Miller 1979).

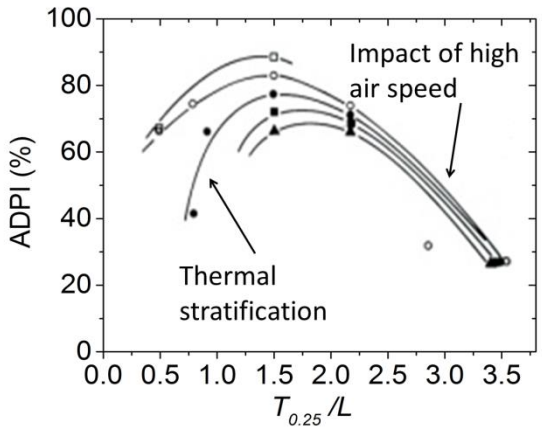

Figure 2: General ADPI profiles as a function of $T_{0.25}/L$ under cooling mode; Symbols are real data of high sidewall grilles from Miller and Nash (1971) at different cooling loads.

Furthermore, as an indicator of occupants' comfort (John 2012), the ADPI method has been used to evaluate thermal comfort along with PMV (Predicted Mean Vote) and PPD (Predicted Percentage of Dissatisfied) that involves four additional factors including (1) mean

radiant temperature, (2) relative humidity, (3) metabolic rate, and (4) clothing insulation. Chung and LEE (1996) reported the evaluation of thermal comfort under three ventilation patterns in terms of PPD and ADPI. The results concluded that ADPI may not be adequate to represent draft risk. Another studies investigated experimentally the jet-flow characteristics from a high sidewall grill and a linear diffuser (Chow and Wong 1994; Chow and Wong 1996). The ADPI was found to be linearly related to PPD for the high sidewall grill. Besides PPD, previous studies attempted to correlate ADPI with other parameters, such as Archimede's number, jet momentum and supply air temperature (Chow et al. 1996; Rutman et al. 2005; Ng et al. 2008; Corgnati et al. 2009; Gao and Lee 2009). Meanwhile, the ADPI method was also employed to optimize the design of a floor-based air-conditioner (Corgnati et al. 2009). The literature review illustrates that previous studies have made efforts to correlate ADPI with the characteristics of diffusers or the thermal comfort model described in ASHRAE-Standard 55 (2010). However, such efforts are still insufficient to take account of more diffuser types, heating mode and the association of thermal comfort and ADPI. In addition, ASHRAE-Standard 113 (2013) states that "the ADPI method for mixing systems should be applied to traditional overhead air distribution systems under cooling operation only" with the explanation that humans are overly sensitive to temperature variation in heating mode (Int-Hout 2002). But many studies have applied the current ADPI method for heating mode to evaluate the performance of diffusers/ grilles and to guide HVAC system design (Cho and Liu 2009; Corgnati et al. 2009; Fontanini et al. 2011). Currently there is neither recommendation nor study that proposes ADPI model when supply diffuser/ grill provides warm air into a room.

2.2 INDOOR AIR VELOCITY IN A SPACE WITH STEADY-STATE JETS (INVESTIGATIONS 1C)

The review in this section provides a summary of air velocity in a space with HVAC systems. Air velocity is a prevalent parameter related to over a large range of building science studies including thermal comfort, particle dynamics, gaseous pollutant transport, heat

transfer and energy saving (Mallick 1996; Posner et al. 2003; Schiavon and Melikov 2008; Xu et al. 2012; Walker and Sherman 2013).

Previous studies on air velocity in occupied zone mainly focused on the effects of heat source location and air exchange rate when indoor spaces were installed with a certain type of diffuser (Chow and Wong 1999; Bennett et al. 2000; Cho and Awbi 2007), or on filed measurements in different places (Hahnzawa et al. 1987; Matthews et al. 1989; Baldwin et al. 1998). For example, a study conducted by Chow and Wong (1999) indicated that indoor air velocity linearly increases with air exchange rate. In addition, Wasiolek et al (1999) measured indoor air velocity in a mockup and a plutonium work-room using sonic anemometries. The average velocity varies from 0.015m/s to 0.097m/s in the mockup room and 0.1m/s to 0.36m/s in the workroom. A further study in the plutonium work-room revealed that the average velocity at a height of 1.5m (approximately the height of human breathing zone) ranges from 0.08m/s to 0.41m/s with a median velocity of 0.18m/s (Whicker et al. 2000). In addition, a survey of air movement preference in office buildings suggested that the average indoor velocity is only 0.04m/s in summer and 0.09m/s in winter (Zhang et al. 2007). Besides the climate's effect, indoor air velocity might be affected by many other factors such as diffuser/ grille type and indoor thermal loading (heating or cooling). In general, very few studies have systematically investigated indoor air velocity when the space is mechanically ventilated using various types of diffusers/ grilles or under different thermal conditions: cooling and heating.

2.3 PARTICLE TRANSPORT IN AN ENVIRONMENT WITH STEADY-STATE DIFFUSER/ GRILLE AIR JETS (INVESTIGATIONS 1D)

Terminal diffusers/ grilles are characterized with creating various air flow patterns and consequently by air diffusion performance index (ADPI). For instance, a ceiling diffuser should always deliver supply air attached to the room ceiling. Compared to a standard diffuser/ grill, a vortex diffuser causes a greater entrainment of surrounding air, which leads to jet velocity decay quickly and draft reduction (Hu 2003). Furthermore, a high side-wall

grill generates a plane jet that develops into an axisymmetric jet. Due to Coanda effect, the flow moves along the ceiling and comes down along the opposite wall for a small value of Grashof (Gr) number. At a large Gr number, however, supply air moves along the ceiling and then turns downwards at a certain distance (Tripathi and Moulic 2007). For a displacement diffuser at floor level, in contrast, supply air flows along the floor toward various heat sources in the space, then it rises along these sources, forms thermal plume and finally exits the room at the ceiling height.

As particle dispersion is affected by airflow pattern created by diffuser/ grille air jets, various diffusers/ grilles dilute and remove particles from the room at different levels of efficiency. Although a few dozens of diffuser/ grille types are prevalent on the market, the resulting airflow patterns could be categorized into three main regimes: Mixing Ventilation (MV), Displacement Ventilation (DV) and Under-Floor Air-supply Distribution (UFAD). For instance, round ceiling diffusers, slot ceiling diffusers and high side-wall grills produce well-mixed air distribution, while displacement distribution can be obtained by using a grill or multi-hole diffuser at the floor level. Even though this dissertation focuses on only MV, the following literature review discusses particle distribution in the environments with the two popular ventilation patterns: MV and DV. Nevertheless, the dispersion of particles released from unsteady jets, such as coughing, sneezing and breathing, is not included in this review. The literature review in this section focuses on particle concentration in a room considering jet types, particle source locations, and source dynamics (continuous or intermittent). Table 2 summarizes research studies investigating the transmission of particles in various built environments. Of the ten studies summarized in Table 2, six were conducted in a room with heat sources. Two major conclusions can be drawn from the literature listed in Table 2.

1) Particle dispersion is determined by many factors, including air distribution created by diffuser/ grille air jets, the location of particle sources, room configuration and particle size (Bouilly et al. 2005; Holmberg and Chen 2003; Lu et al. 1996; Mundt 2001; Whicker et al. 2002; Zhao et al. 2004). Among these factors, ventilation tends to affect

significantly the particle distribution. However, Bouilly et al. (2005) found that this effect is less notable for coarse particles (> 2.5μm).

2) DV presents a higher performance on the removal of particulate matter than MV (Bolster and Linden 2008). This is because indoor thermal plume has a similar positive mechanism as DV for particle removal, causing upwards airflow (Bolster and Linden 2009; Rim and Novoselac 2009). However, DV might lead to a high concentration in breathing zones when particles are suspended by human plumes (Salmanzadeh et al. 2012).

The literature review shows that numerous studies have been conducted on the dispersal of particles continually released. However, studies on the transmission of intermittently generated particles are still in demand. For instance, there are few studies on the transport of resuspended (induced) particles from floor across a space with steady-state jets produced by diffusers/ grilles. In addition, there remains little knowledge of how steady-state jets provided by diffusers/ grilles affect the transmission of particles released inside and outside the jet regions. Another knowledge gap is that most reviewed studies focused on particle transmission at cooling condition, while the heating condition has been seldom included in these studies. In summary, the transport of particles in a space with steady-state jets requires further investigation, especially when the particle source is intermittent and exhibits different effects by the jets and indoor thermal conditions: cooling and heating.

Reference	Method	Flow mode	Building	Thermal	ACH (hr^{-1})	Location of Particle Source	Particle Size (μm)	Findings
Bolster and Linden (2008)	Simulation & Experiment	DV &MV	Box chamber with a predefined plume	Thermal		Point source in the plume		1) DV shows better performance than MV for particle removal for small particles. 2) Thermal plume enhances removal for DV. 3) The exposure to coarse particles may be increased in DV.
Bouilly et al. (2005)	Simulation & Experiment	MV &DV	Experimental chamber without furniture	Isothermal	0.5, 1	Full of particles initially in the room	0.3-15	1) The dispersal of particles depends on particle sizes. 2) The effect of inlet and outlet locations is less notable for coarse particles.
Holmberg and Chen (2003)	Simulation	DV &MV	Classroom with 25 student simulators	Thermal	6.4	Diffuser air jet	10	Ventilation pattern plays an important role in particle dispersion.
Lu et al. (1996)	Simulation & Experiment	MV	Two interconnected zones without furniture	Isothermal	9.2& 10.3	Diffuser air jet	0.5-5	Particle concentration depends on particle properties, ventilation conditions and airflow patterns (ACH).
Mundt (2001)	Experiment	DV	Office with human simulators and furniture	Thermal	2, 3 &4	1).Talcum powder on the floor; 2).Suspension by the supply airflow	Multi-dispersed	Particle removal efficiency is dependent on the position of sources.
Rim and Novoselac (2009)	Experiment	DV &MV	Room with a human simulator	Thermal	3	1). Close to manikin. 2).1.6m in front of head	0.03, 0.77 &3.2	1) The uniform concentration is only in MV. 2) Due to thermal plume, the concentration for DV is not uniform. 3) Thermal plume is important in transporting resuspended particles. 4) Exposure to particles is depended on source locations.

Table 2: Summary of studies on particle removal due to steady-state jets.

Reference	Method	Flow mode	Building	Thermal	ACH (hr-1)	Location of Particle Source	Particle Size (μm)	Findings
Rim and Novoselac (2010)	Simulation	DV &MV	Full scale chamber with heated wall	Thermal	1.93, 3.86 &7.72	1) At floor, 2) In thermal plume, and 3) Close to a diffuser air jet	1 &7	The size and position of sources have a very small impact on human exposure variation.
Salmanzadeh et al. (2012)	Simulation	DV	Room with a human simulator	Thermal	6.45	Diffuser air jet	1	Thermal plume flow leads to a high concentration of suspended particles.
Whicker et al. (2002)	Experiment	MV & Ceiling In-Out	working room with furniture	Isothermal	6 &12	Short duration release (60s)	Lognormal (median: 0.52μm)	1) Ventilation rate has a strong influence on particle dispersion rate. 2) Changes in room geometry, room furnishing has significant effects on the dispersion.
Zhao et al. (2004)	Simulation	MV and DV	Two interconnected zones without furniture	Isothermal	9.216	Diffuser air jet	1, 2.5, 5 &10	1) Particle concentration is mainly influenced by ventilation. 2) Average particle concentration for DV is higher than MV. 3) Particle sizes have different movements.

Table 2: Summary of studies on particle removal due to steady-state jets (continued).

2.4 VELOCITY AND PARTICLE TRANSPORT ASSOCIATED WITH AN UNSTEADY-STATE COUGH JET (INVESTIGATIONS 2E AND 2F)

A human cough is a representative of an unsteady-state jet that frequently occurs in indoor environments. The literature review in this section focuses on the dispersion of particles due to a cough jet. The spread of airborne particles can be enhanced by a cough jet characterized by a high discharge velocity and particle injection rate.

Experimental research on the velocity field of coughs is challenging and often applies the state-of- the-art measuring technology. The velocity profile and turbulence statistics of a cough can be precisely measured by an optical apparatus, such as Schlieren optical system, Particle Image Velocimeter (PIV), Laser Doppler Velocimeter (LDV) or electric resistance based apparatus such as a hot-wire anemometer. The maps of coughing velocity obtained using sequential Schileren images showed that the maximum air speed of a cough is roughly 8m/s (Tang and Settles, 2008; Tang et al., 2009). PIV technology has been employed to measure the airflow pattern, velocity profile and other variables of voluntary subject coughs (Zhu et al. 2006; Chao et al. 2009; VanSciver et al. 2011; Nishimura et al. 2013). A cough jet carrying particles travels swiftly, up to 11.7m/s, and lasts a short period, at a level of 0.5s (Chao et al. 2009; Gupta et al. 2009). Visualization of coughed airflow showed that an individual cough has an average cough velocity, 11.2 m/s, and travels as far as 1.7m (Zhu et al. 2006). Kwon et al. (2012) measured the initial velocity and exhaled airflow angles from coughing and speaking in an indoor chamber. They found that the average initial coughing velocity was 15.3 m/s and 10.6 m/s for the males and females respectively, which yielded an average initial velocity of 12.9 m/s. Also, the males present a higher exhaled air angle, 38^{o} than the females with 32^{o}.

The size distribution of a cough jet was also determined by Chao et.al (2009) using Mie imaging technique (IMI) and PIV. The measurements showed that the geometric mean diameter of coughed droplets is 13.5μm. The average number and size of particles coughed by an influenza-infected subject ranges from 900 to 302,200 and 0.35 to 10μm, respectively (Lindsley et al. 2012). An extensive review conducted recently by Gralton et al. (2011) summaries the size

range of coughed particles from a large quantity of studies and concludes that the size scale of particles ranges from 0.1 to 100μm for individuals prior to and after 1979. The characteristics of coughing velocity and particle size range are summarized in Table 3. The table shows that cough jets are characterized with large ranges of discharge velocity and particle sizes.

Authors	Maximum velocity (m/s)	Particle size(μm)
Duguid 1946	N/A	4-8μm
Zhu et al. 2006	6-22m/s with an average of 11.2m/s	N/A
Yang et al. 2007	N/A	0.62-15.9μm with an average 8.35μm
Chao et al. 2009	11.7m/s (average)	13.5μm
Gupta et al. 2009	5.5-21m/s (1.7m,70Kg male occupant)	N/A
VanSciver et al. 2011	1.5-15.8	-
Tang et al. 2012	Male 3.2-14 Female 2.2-5	-
Wells 1955	16-48	-
Fennelly, 2004	-	0.65-3.3
Li et al. 2008	-	50-100
Heymann 1899	-	30-500
Morawska et al. 2008	-	0.4-10
Xie et al 2009	-	50-75
Lindsley et al. 2012	N/A	0.35-10μm
Kwon et al. 2012	15.3 male 10.6 female	N/A

Table 3: Cough velocity and size range of injected aerosols.

Increasing interests in the prevention of interpersonal exposure has caused many researchers to investigate the dispersal of airborne particles expelled from a respiratory jet in different indoor environments, numerically and/or experimentally. Yin et al. (2011) presented the

spatial distribution of particles coughed and breathed by a resting patient in a medical ward with two ventilation modes. They concluded that the difference in particle distribution between two cases were insignificant only when the supply jet provided mixing ventilation. The numerical simulation in an airline cabin showed that the dispersion of particles released by a passenger was predominately affected by the bulk airflow (Gupta et al. 2011). The modeling of a cough in railway cabins pointed out that the transmission of coughed particles contained two regimes: particles generated in the first 0.2s escaping from the body plume, and particles generated in the next 0.2s following the upward body plume (Zhang and Li 2012).

The transport of coughed and/or sneezed aerosols has also been measured in both small-scale and full-scale chambers (Lai and Wong 2010; Lai and Wong 2011; Seepana and Lai 2012). The interpersonal exposure to the aerosols was estimated in these studies as well. The results concluded that a cough jet can easily penetrate the boundary layer of a manikin. Ventilation modes, cough directions and particle sizes affect the level of exposure to coughed particles. However, studies are still needed to provide extensive understanding of the coughed-particle dispersion and the consequent exposure. Spread of infectious diseases by airborne particles released by human cough has gained a lot of attention in the indoor air research community. However, further improvement of experimental studies regarding interpersonal transport is needed, especially when considering the size of the discharge opening ("human mouth") and more details on discharge concentration as mentioned in Chapter 1.

This dissertation will address these limitations to provide analysis of air velocity field of cough jets with different discharge velocities and durations, and data of dispersion of coughed particles with various sizes.

2.5 NUMERICAL SIMULATION OF PARTICLE DISPERSION CAUSED BY STEADY AND UNSTEADY JETS (A TOOL TO SUPPORT INVESTIGATIONS 1D AND 2F)

As Computational Fluid Dynamics (CFD) provides a valuable tool to achieve the objectives in this dissertation, this section provides a review of previous studies employing CFD to track indoor particles. CFD simulations utilizing RANS and LES turbulent models have been widely performed and accepted coupled with a Lagrangian particle-tracking scheme (Wang and Squires 1996; Béghein et al. 2005; Gao and Niu 2007; Tian et al. 2007; Zhang and Chen 2009; Rim and Novoselac 2010; Wang et al. 2012). When compared to LES, RANS shows more benefits at the conditions that computational resource is limited. As a result, previous numerical studies on particle tracking associated with steady-state and unsteady-state jets mainly employed RANS-Lagrangian method (Worth Longest and Vinchurkar 2007; Zhao et al. 2008; Gupta et al. 2011; Chang et al. 2012; Chen et al. 2012; Chang et al. 2013; King et al. 2013; Sadrizadeh et al. 2014).

Despite the increase of computation resources, few studies have applied LES-Lagragian scheme to simulate particle dispersion and deposition in indoor application regarding jets (Beghein et al. 2005; Bouilly et al. 2005; Chang et al. 2006; Tian et al. 2007; Chang and Hu 2008; Choi and Edwards 2008; Wang et al. 2012). A good example for unsteady-state jet is the study of a LES simulation of expiratory droplet dispersion from a sneezing jet conducted by Berrouk et al. (2010). Most of the studies have revealed that LES generates reasonably better prediction. For instance, Wang et al. (2012) found that the Lagrangian method predicted more accurate particle concentration coupled with LES than RANS and URANS.

Since the grid number is the major impact related to computation resources for numerical simulation, Figure 3 summarizes the grid numbers employed in the studies of indoor air modeling since 2001 published in the most impacting journals: “Atmospheric Engineering”, “Building and Environment”, “Energy and Buildings” and “Indoor Air”. Results in Figure 3

summarize the grid numbers in 292 papers using RANS and 19 papers using LES or DES (Detached Eddy Simulation).

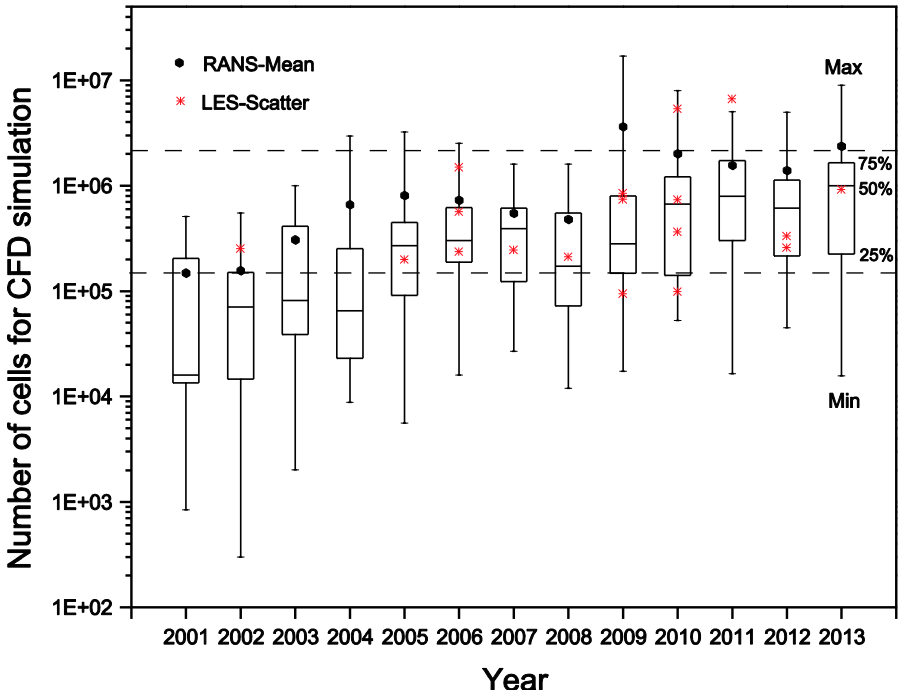

Figure 3: Number of discretization grids for indoor air simulation.

Figure 3 demonstrates that the mean grid number for RANS has increased one order of magnitude from 2001 to 2010. Up to 2013, half of studies are performing simulation using approximate one million cells. Moreover, the grid numbers in LES simulation present insignificant increase when compared to RANS. This implies that in today's CFD applications for indoor modeling, both RANS and LES simulations are using relatively similar cell numbers.

In general, the literature review presented in this chapter highlights substantial efforts related to characterizing indoor air distribution and particle transport in a space associated with steady-state or unsteady-state jets. ADPI method is widely used by HVAC designers, but the knowledge gaps in the performance of new diffuser/ grille types operating at both cooling and heating mode limit further advancement of this method. Systematic characterization of indoor air

velocity in the presence of various diffusers/ grilles is needed, and examination of transport of particles in both cooling and heating mode will improve our ability to design HVAC systems. Secondly, there is growing recognition that unsteady-cough jets spread disease-carrying particle in a violent level, but their complex dynamics of fluid and particles fluid dynamics require deeper understands of transport mechanisms. Last, this literature review only includes a small fraction and more review is shown in the appendices.

Chapter 3: Methodologies used in Investigation 1A – 2F

This chapter describes the methods applied in the investigations reported in this dissertation. Experimental measurements for indoor air distribution and particle transport for steady-state jet scenarios were conducted in a full-scale environmental room, while the experimental investigation explored unsteady-state cough jets in a small-scale test room. In addition to experimental measurements, this dissertation employed CFD numerical simulations to model indoor velocity and temperature distribution, and particle transmission that were validated using experimental results. Analytic analysis provided a valuable tool to investigate the velocity field in unsteady-state cough jets varying with time, as well as particle trajectory of a single particle injected by a cough jet.

Table 4 summarizes the methodologies in all the six investigations. This dissertation reports around 750 experiments consisting of (1) nearly 650 experiments for determining ADPI values in the full-scale test room ventilated using thirteen types of diffusers/ grilles, (2) five experiments for determining particle concentration in the full-scale room with a ceiling attached jet at cooling condition, (3) six smoke visualizations and velocity measurements in the center-section plane (76 locations) downstream of a cough jet, and (4) twenty-four measurements of particle concentration in the vicinity of a recipient near a cough jet source. To assess the uncertainty of the experimental studies, each measurement was repeated at least three times with the exception of the ADPI values. The reason is that ADPI values are of more dependent of other factors, such as diffuser/ grill size and manufacturer.

A CFD numerical method was first validated using previously established experimental results in the literature (Lu et al. 1996). As particle concentration is partially determined by air distribution, numerical studies, in this dissertation focus only on particle tracking. This dissertation employed a CFD numerical method to explore particle spreading in the scenarios that were not examined experimentally, such as particle concentration associated with steady-state jets at heating mode.

Unlike steady-state jets, the fluid dynamics of unsteady-state jets has not been theoretically characterized. Using the results of smoke visualization, this dissertation developed a similarity analysis of six artificial jets and one real cough jet measured by PIV in the literature (Nishimura et al. 2013). Obtaining the fluid dynamics of cough jets, in addition, this dissertation was capable to calculate the trajectory of a sing particle utilizing Newton's second law, which would provide an improved understanding of coughed particle transport.

Methodology	Jet type	Objective	Description
Experimental measurement (each measurement was repeated at least 3 times except for ADPI values)	Steady-state jets (full-scale room)	Air distribution (Investigation 1A-1C)	Approximately 650 experiments of ADPI values in the room installed with various diffusers/ grilles.
		Particle transport (Investigation 1D)	Five concentration measurements of particles (0.77,2.5 and 7μm) released from inside and outside a ceiling-attached jet under cooling condition
	Unsteady-state jets (small-scale room)	Air distribution (Investigation 2E)	1. Six smoke visualizations of 6 cough jets with different durations and discharge velocities. 2. Velocity measurements at 76 locations in a weak cough jet (6m/s, 1s).
		Particle transport (Investigation 2F)	Twenty-four Concentration measurement of coughed particles (0.77, 2.5 and 7μm) in the vicinity (8 locations) of a recipient near a cough source
CFD numerical simulation (focus on only particle transport)	Steady-state jets	Particle transport (Investigation 1D)	1. Validation using established experimental data reported in previous literature (Lu et al. 1996). 2. Concentration simulation of particles (0.77, 2.5 and 7μm) released from inside and outside a ceiling-attached jet under both cooling and heating conditions.
Analytical analysis (focus on only unsteady-state jets)	Unsteady-state jets	Air distribution (Investigation 2E)	Dimension analysis of penetration distance of six artificial cough jets and a real human cough jet as reported by Nishimura et al. (2013).
		Particle transport (Investigation 2F)	Trajectory calculation of a single coughed particle with three sizes (0.77, 2.5 and 7μm).

Table 4: Summary of methodologies applied for Investigation 1A-2F.

3.1 EXPERIMENTAL FACILITY

3.1.1 Environmental test rooms (Investigations 1A-2F)

The study carried out all measurements of indoor air distribution and particle transport in two test rooms. The measurements on steady-state jets were performed in a full-scale chamber (5.5m×4.5m×2.7m) that precisely controls supply air temperature and airflow rate (Figure 4). The chamber has a dedicated and modifiable control system that is capable of a supply air between 6 and 50 ^{o}C at an air exchange rate (ACH) of 3.5 to 14 hr^{-1}. The test room has all interior walls made of stainless steel capable of minimizing particle deposition. One wall of the test rooms contains embedded hydronic cooling/ heating coils capable of simulating a cool/warm window or external wall, such as occurs during the winter/summer in perimeter zones. In addition, the test room can be used to generate various ventilation patterns by changing the ventilation configuration. To increase the accuracy of particle experiments, furthermore, background particle concentration was minimized by the use of a high-efficiency particulate air (HEPA) filter in the air supply duct.

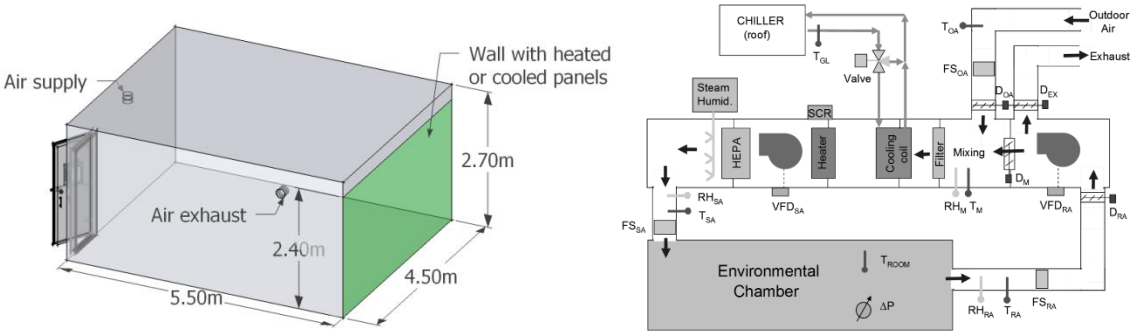

Figure 4: Schematic of the full-scale test room and the HVAC system for environmental control.

The experiments about unsteady cough jets were carried out in a smaller test room (2.4m×2.4m×2.4m) as shown in Figure 5. This small-scale test room had a ventilation rate of approximately 3.5hr^{-1} and supply air that was filtered by a HEPA filter was provided from the bottom level of the room. The supply air created displacement ventilation and indoor air motion was determined by thermal plume and unsteady cough jets. Similar to the full-scale room, the interior walls were stainless steel to reduce particle deposition. For all test conditions associated with steady-state and unsteady-state jets, indoor air distribution and particle transport were affected by the jets and thermal plumes due to heat sources only. There were no other additional momentum sources, such as a fan or moving occupant.

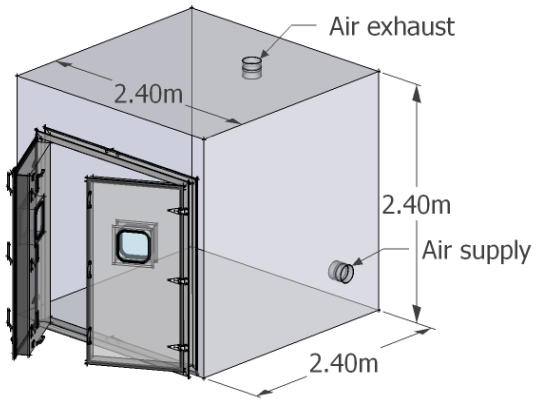

Figure 5: Schematic of the small-scale test room.

3.1.2 Instrumentation (Investigations 1A-2F)

State-of-the-art instruments recorded the temporal and spatial distribution of velocity, temperature and particle concentration in the test rooms. The selection of the measurement instrumentation focused on increasing measurement accuracy. Table 5 shows the specifications of all the instruments used in the experiments.

Instruments	Model	Accuracy	Measuring variable and comments
Air flowmeter	EBTRON GT Type A 116	5% of reading	Supply airflow rate, verified with duct bluster and Pitot probe
Electricity usage monitor	Kill-A-Watt, P4400	0.5% of reading	Indoor heat simulator power, maximum accuracy 2% of reading
Hotwire anemometer	CTA, DANTEC, Denmark	Calibrated using Pitot probe with DG-700	Velocity distribution and boundary condition of an unsteady jet
Digital pressure gauge	DG-700, ENERGY CONSERVATORY, US	1% of reading or 0.15Pa	Calibrate Hotwire Anemometer
Hot-sphere anemometer	HT-400, SENSOR, Poland	±0.03m/s+-3% Temperature:±0.3°C	Airflow and thermal field in all set-ups except in the unsteady cough jet region
Thermistor	Model 44033, OMEGA	±0.1°C	Supply, return air and interior surface temperature
Fog machine	EF-1000, Eliminator Lighting, Los Angeles, USA	-	Visualization of various jets
Camera	1080p @ 60 frames per second	-	Record smoke visualization of jets
Aerotrak	Model 9306 and 8220, TSI, US	<12% in terms of performance comparison of 5 Aerotraks	Concentration in the cough generator/ box and full-scale test room
APS	Model3321, TSI, US	10% of reading plus variation from counting statistics	Particle concentration in the unsteady cough jet region and vicinity of a receiver occupant in the small-scale test room

Table 5: A summary of the instruments and associated uncertainties.

3.1.3 Test particles and particle generators (Investigations 1D & 2F)

This study investigated the transport of three characteristic sizes (0.77μm, 2.5μm and 7μm) of particles for the cases of steady-state and unsteady-state jets. For 0.77 and 2.5μm particles, a Collison nebulizer sprayed particle solution and atomized it into nuclei. The solution contained latex spherical mono-dispersed particles (coefficient of size variation 1%-3%) with a

density of 1.05 g/cm^3. Careful attention was paid to ensure that all solution except particle nuclei was evaporated shortly after injection. Such mono-dispersed particles can be monitored without size categorization issues if the background concentration is negligibly low. However, the Collison nebulizer had difficulties generating enough mono-dispersed 7μm particles. Therefore, in this study we developed a large-particle disperser that can generate a large quantity of Arizona Test Dust (ATD) (nominal 5-10μm, density of 2.65g/cm^3) particles. Figure 6 shows the particles and generators for the three particle sizes.

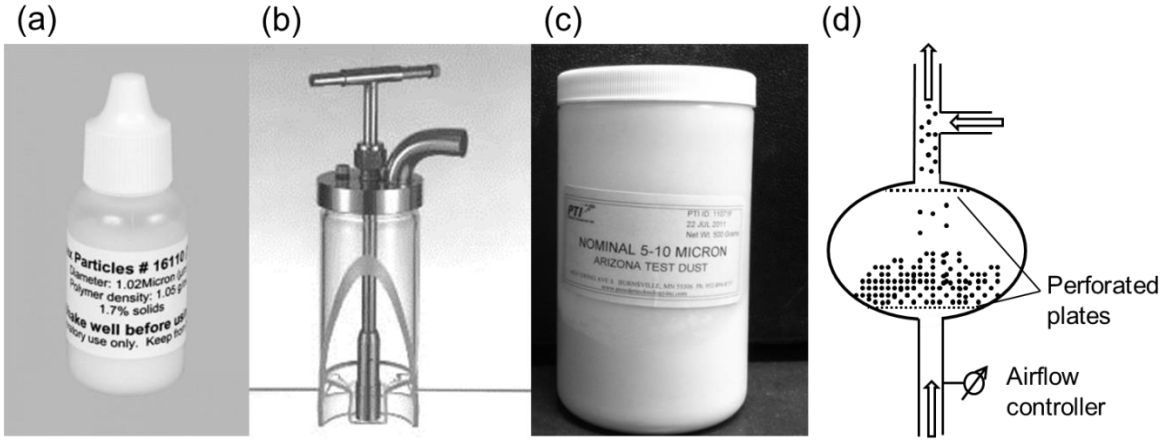

Figure 6: Test particles and generators for three particle sizes; (a) Latex particle solution; (b) Collison nebulizer particle generator; (c) Arizona test dust; (d) Arizona test dust generator.

3.1.4 Diffusers/ grilles to generate steady-state jets (Investigations 1A-1D)

This section provides a description of diffusers/ grilles used in the full-scale room to create indoor steady jets. The investigations (1A-1D) employed various types of air terminal diffusers/ grilles as applied in all-air HVAC systems for mechanical mixing-ventilation. The selected diffuser types are commonly used in commercial buildings and available on the major market. To include the uncertainty due to diffuser size and manufacturer, this study selected three to four manufacturers randomly for most diffuser types. The impact of sizes was also

considered by testing two sizes for each type. The specific sizes were selected based on real applications of such diffusers, such as diffuser's airflow rate delivery capacity and room size. Unsuitably large diffusers/ grilles would provide too weak jets to mix the occupied zone well, leading to a stagnant zone that is prohibited in real application. In contrast, too small sizes would cause great pressure resistance of diffusers, which would cause unaccepted energy penalty and disruptive noise. Table 6 shows the description of thirteen diffuser/ grille types. All the thirteen types create well-mixed ventilation patterns.

#	Diffuser type	Size (cm)	Manufacturer	Deflector adjustment	Installation location
1	Adjustable blade grille	41×15 & 61×15	A, B & D	45° upward 0° horizontal 45° downward	High sidewall
2	Fixed blade grille	41×15 & 61×15	A, B, C & D	15° upward 15° downward	High sidewall
3	Linear bar grille	41×15 & 61×15	A, B, C & D	-	High sidewall
4	Nozzle	13* & 15*	A, B & C	-	High sidewall
5	Round ceiling	15* & 25*	A, B, D & E	-	Ceiling
6	Square ceiling	15* & 20*	A, B & C	-	Ceiling
7	Perforated-Round pattern	15* & 20*	A, B & C	-	Ceiling
8	Perforated-Directional pattern	15* & 20*	A, B, C & D	-	Ceiling
9	Louvered face-lip	15* & 23*	A, B, C & D	-	Ceiling
10	Louvered face-no lip	15* & 23*	D & E	-	Ceiling
11	Plaque face	15* & 20*	A, B, C & D	-	Ceiling
12	Linear slot	2 & 4 slots, 120cm long	A, B, D & E	-	Ceiling
13	Swirl	15* & 20*	A, B & C	-	Ceiling

§ A: Krueger; B: Price; C: Titus; D: Nailor; E: Metalaire

* Size in duct diameter

Table 6**:** Description of the 13 types of diffusers on the market.

3.1.5 Unsteady-state jet generator (Investigations 2E & 2F)

A cough box / generator depicted in Figure 7, was constructed to model an unsteady cough jet. The cough box has dimensions of 0.25m×0.25m×0.25m (15.6L), and a cough jet was released by injecting pressurized air into the box. The cough box used a 6cm long stainless steel tube with an inner diameter of 2.4cm as the discharge opening to simulate a human mouth, 4cm^2 (Gupta et al. 2009). Before the cough event, a high concentration of particles in the box was secured by injection of particles over a certain period of time. To prevent particles from leaving the box during the particle injection period and before start of the cough event, a suction pump connected to the box generated slightly negative pressure inside the box. The spatial uniformity of particle concentration in the box was achieved by using a small fan. The coughed flow was controlled by a fast-response solenoid valve operating in an "on-off" (square wave) manner that controls the inflow of high pressure air in the box. An airflow straightener was built inside of the box to create a unidirectional vertical flow (Figure 7). In ideal conditions, the unidirectional flow in the box carries particles at a low deposition rate towards the jet exit. In this study, the supply pressure and the corresponding cough jet was adjusted to have a discharge velocity of 6.08m/s (Reynolds number of 9700), and turbulence intensity 4.25% at the center of the tube opening. The duration of the cough jet was 1 second.

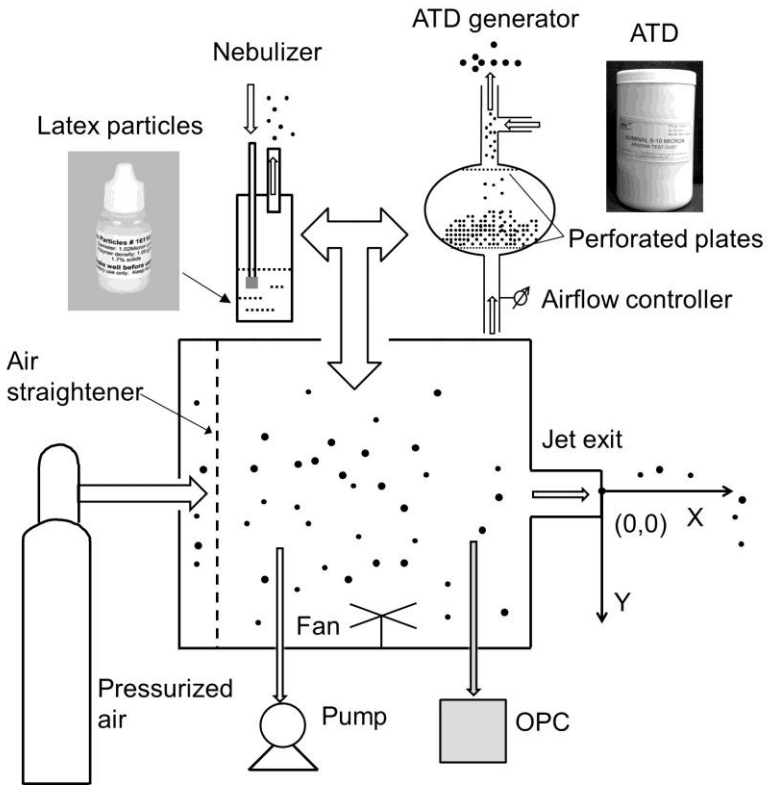

Figure 7: Schematic of the cough box / generator and the particle generators (Liu and Novoselac 2014).

3.2 EXPERIMENTAL SETUPS AND PROCEDURES - INDOOR AIR DISTRIBUTION (INVESTIGATIONS 1A-1C & 2E))

To address the research objectives, experiments of indoor air distribution in an environmental room with steady-state jets and unsteady-state jets were needed. This section describes experimental set-ups and measurement procedures for various scenarios concerning steady-state and unsteady-state jets.

As indoor jets create air distribution represented by velocity and temperature distribution, the investigations measured all indoor velocity and temperature fields. The spatial velocity and temperature at a given location were measured at a frequency of 5Hz for 3 minutes when considering the spatial distribution created by steady-state jets (ASHRAE Standard-113 2013).

For analyses related to unsteady cough jet, however, a fast-response hot-wire anemometer (frequency of 5,000 Hz) and several hot-anemometers (frequency of 5Hz) captured the velocity variations of an unsteady cough jet (high frequency) and jet's impact on the surrounding regions (low frequency).

3.2.1 The effects of steady jets on air distribution in occupied zone (Investigations 1A-1C)

To include various types of steady jets generated by air diffusers/ grilles, this investigation employed three diffuser mounting configurations in order to install all diffusers listed in Table 6. In accordance with practical application, the experimental setups allowed three mounting positions: (1) ceiling position for ceiling diffusers; (2) ceiling position for linear slot diffusers and (3) high side-wall position for grilles. The full-scale test room was modified to fulfill the three configurations, for example building ductwork ceiling plenum. Moreover, the buoyancy effect was considered by creating cool jets and warm jets corresponding to summer condition and winter condition, respectively. Cool jets denote that jet temperature is higher than indoor average temperature, while warm jets refer to the reverse conditions. Figure 8 shows the experimental setups and the three configurations for diffuser/ grille installation. Position 1 and 2 used two identical diffusers while Position 3 employed only one grille to generate a steady-state jet. The two diffusers for Position 1 (or 2) were balanced to have the maximum airflow rate difference within 10%. The experiments employed a plenum box at each duct terminal to ensure that the airflow was uniformly distributed by a diffuser in relevant directions (ASHREAE Standard 70 2006).

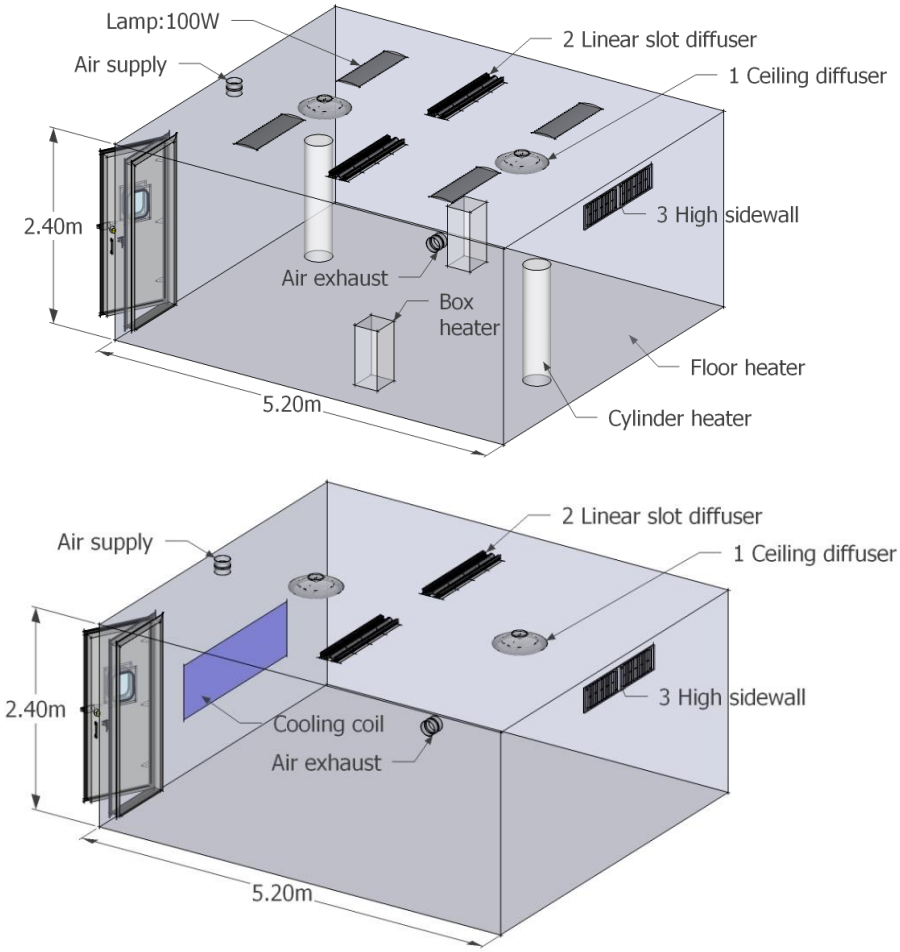

Figure 8: Experimental setup and three configurations for diffuser installation 1: Ceiling diffusers, 2: Ceiling linear slot diffusers and 3: High sidewall grilles or nozzles (0.1m from the upper frame to the ceiling); (top) Setup for cool steady-state jets with heat simulators in the test room; (bottom) Setup for warm steady-state jets with cooling coil in the test room.

When generating cool air jets, as the room control temperature in the experiments was maintained at 23±0.5^{o}C (typical temperature in an office), this study used several adjustable electric heaters simulating indoor occupants, computers, lamps and floor heat gains in the room. Table 7 describes the apportionment of the total heat generated by indoor heaters for two loads: 25 and 50W/m2 representing typical loads of an office space (ASHRAE Handbook-*Fundamentals* 2009; Huang and Zhang 1999). The heating operation (for experiments with heating condition investigated) was modeled by employing a cooling water coil attached to the

middle part of a wall and very low-speed fans drew air towards the cooled wall (Figure 8b). The low-speed fans provided no disturbance in the occupied zone while generating downward cool draft along the cooled-wall that is a representative of a window or an eternal wall in winter time. This cooling coil provided the room a specific heating load in a range of 35-40W/m2. This load value was selected to represent a typical heating load of an office space (ASHRAE Handbook-*Fundamentals* 2009; Huang and Zhang 1999).

Heaters	**Room Loads**	
	25 W/m^2	50 W/m^2
Lamps	100W ×4	100W ×4
Box heaters	47W×2	100W ×2
Cylinder heaters	47W×2	100W ×2
Floor heater	0W×1	370W ×1

Table 7: Heat simulators for two cooling loads.

3.2.1.1 Sample positions: velocity and temperature

To obtain indoor air distribution, twelve hot-sphere anemometers with an accuracy of 0.03m/s and 0.1^{o}C monitored velocity and temperature at 60 locations in the occupied zone at four heights above the floor (0.1, 0.6, 1.1, and 1.7m) according to ANSI/ASHRAE Standard-113. Figure 9 describes the positions of the 60 sampling sensors at 15 horizontal locations evenly distributed across the floor and two reference points (1.1 and 2.3m above the floor). To obtain data at sixty locations with 12 available sensors, the study repeated each experiment five times by moving three tripod-stands with each containing 4 sensors in five specific locations. Among all the repeated measurements in the five locations, the temperature varied within 1oC and the measured local temperatures for different repeats were corrected using the temperature data at the reference point (1.1m) according to ANSI/ASHRAE Standard-113. This measure ensured compensation for temperature variation among different repeats. Furthermore, to identify

temperature stratification, the temperature gradient was calculated based on five vertical locations by using the average temperature at the same height of 0.1, 0.6, 1.1 and 1.7m, and the temperature of the reference point at 2.3m. Once velocity and temperature distributions are measured, this study is capable to obtain the indoor air distribution for various steady-state jets.

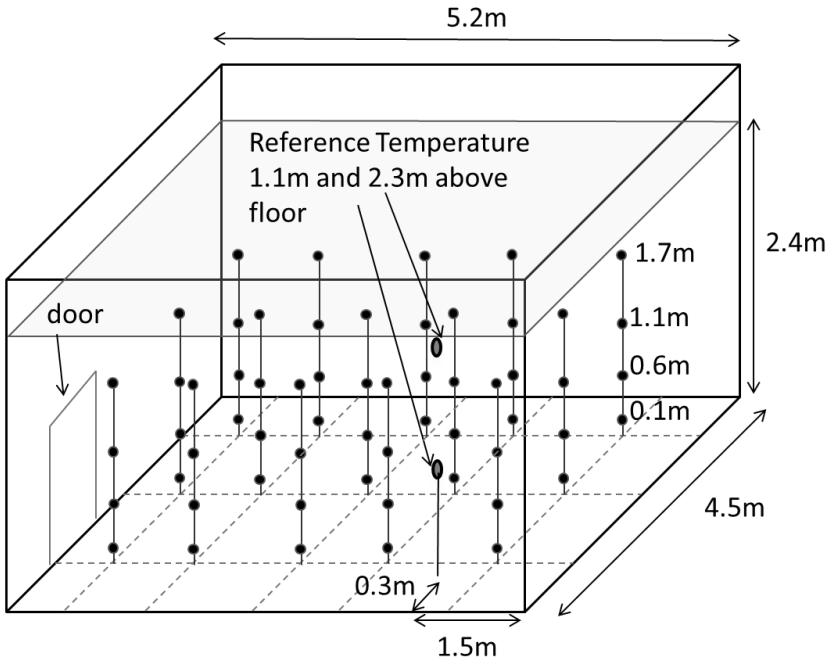

Figure 9: Locations for velocity and temperature measurement related to steady-state jets.

3.2.1.2 Methodology used for defining air distribution performance index (ADPI)

ADPI is defined as the percentage of occupied zone falling into the acceptable velocity and temperature region determined by measuring local Effective Draft Temperature (EDT) for cooling steady-state jets; the EDT is a calculated temperature difference that combines air temperature and velocity (ASHRAE Standard-113 2009). The cooling EDT, first introduced by Rydberg et al. (1949), is based on the subjective response to draft (air temperature and velocity) obtained by Houghen et al. (1938), and then modified by Straub in a discussion in the

paper by Koestel and Tube (1955), as shown in Equation 1 in the chapter of the Literature review. It is worthy to note that Equation 1 is only valid for cooling operation.

3.2.1.3 Connection between ADPI and thermal comfort model

Since EDT is a function of air temperature and velocity, it relates to thermal comfort. However, thermal comfort also depends on other important factors such as relative humidity (RH), mean radiant temperature, metabolic rate and clothing insulation (Fanger 1970; ASHRAE-Standard 55 2010). Fanger (1970) has developed a well-accepted Predicted Mean Vote (PMV) index to describe human thermal comfort. The PMV model uses heat balance principles to relate air temperature, air speed, humidity, radiant temperature, metabolic rate and clothing insulation (ASHRAE Standard 55, 2010). PMV=0 refers to a neutral sensation scale under which 90% of occupants would feel thermally comfortable.

When considering mean radiant temperature, in many office buildings radiant temperature is relatively close to room air temperature (Int-Hout 1983), suggesting a small impact of radiation. When considering the metabolic rate (Unit: Met.) and clothing insulation (Unit: Clo.), an office worker normally has a rate ranging from 1.0 to 1.3 Met and a typical insulation of 0.5 Clo. in summer and 1.0 Clo. in winter (ANSI/ASHRAE Standard-55 2010). The only variable that may vary significantly in commercial office buildings is relative humidity (RH); because the EDT doses not take into account RH, this study adopts a most desirable RH of 50% for cool steady-state jets and warm steady-state jets. Consequently, for a fixed RH and the clothing insulation defined by heating or cooling season, the thermal comfort in an office environment mainly depends on air temperature and air speed that define EDT. Therefore EDT can be derived from Fanger's thermal comfort models under summer (cooling mode) and winter (heating mode) condition.

3.2.1.4 EDT vs. PMV for cooling mode

The temperature range of the acceptable EDT (-1.7 ^{o}C to 1.1 ^{o}C) in Equation 1 at cooling mode illustrates the relationship between velocity and air temperature difference as shown in Figure 10a. Figure 10b shows the PMV range from -0.5 to 0.5 in a plot of air velocity versus temperature for a typical office space in summer (cooling mode). The plot was generated using PMV index according to ANSI/ASHRAE Standard-55 (2010), and the region of PMV in this investigation is limited to air speeds below 0.2m/s as described in the standard. Neutral thermal sensation is achieved when PMV is equal to zero, and since both EDT =0 and PMV=0 represent the condition of neutral thermal sensation, Figure 10c shifts the PMV region (-0.5 to 0.5) in Figure 10b to overlap PMV=0 with EDT=0 in Figure 10a. It shows that the boundaries of PMV region -0.5 and 0.5 overlap with the EDT's boundaries of -1.7 ^{o}C and 1.1 ^{o}C, respectively. This suggests that the PMV index for 80% thermal acceptance agrees with Houghen's 80% thermal acceptance proposed in 1938 (Houghten et al. 1938), directly connecting PMV and EDT.

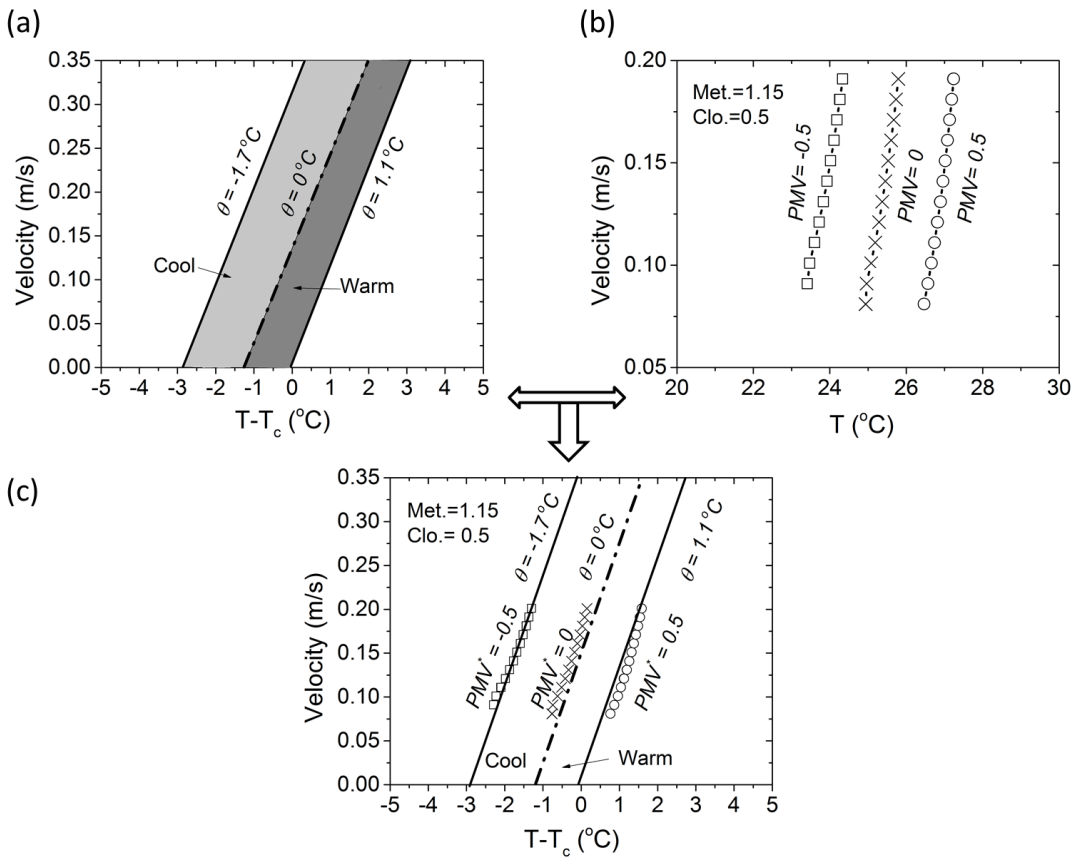

Figure 10: EDT and PMV as a function of air temperature and velocity for cooling mode (Metabolic activity: 1.15Met., Clothing condition: 0.5 Clo., and Relative humidity: 50%); (a) The range of 80% comfort acceptance using the cooling EDT; (b) The range of 80% comfort acceptance using PMV; (c) Comparison of the comfort ranges of the cooling EDT and PMV.

3.2.1.5 New air distribution performance index for heating mode

The EDT for heating mode is not available. However, based on the connection between PMV and EDT (described in the previous section), it can be developed by adjusting parameters that characterize heating mode in the model described in Section 3.2.1.4. Figure 11 (a) provides plots with the 80% comfort acceptance region calculated using PMV index for heating condition (Clothing condition: 1.0 Clo.). Because EDT is a function of local air temperature difference and air velocity, heating EDT should have a format of Equation 2:

$$\theta_1 < EDT\ (\theta) = T_i - T_a - k(V_i - 0.15)\ ^oC < \theta_2 \quad (2)$$

where θ_1 and θ_2 are the boundaries of EDT's range for heating mode, and k is a coefficient connecting temperature difference to air speed while considering thermal sensation.

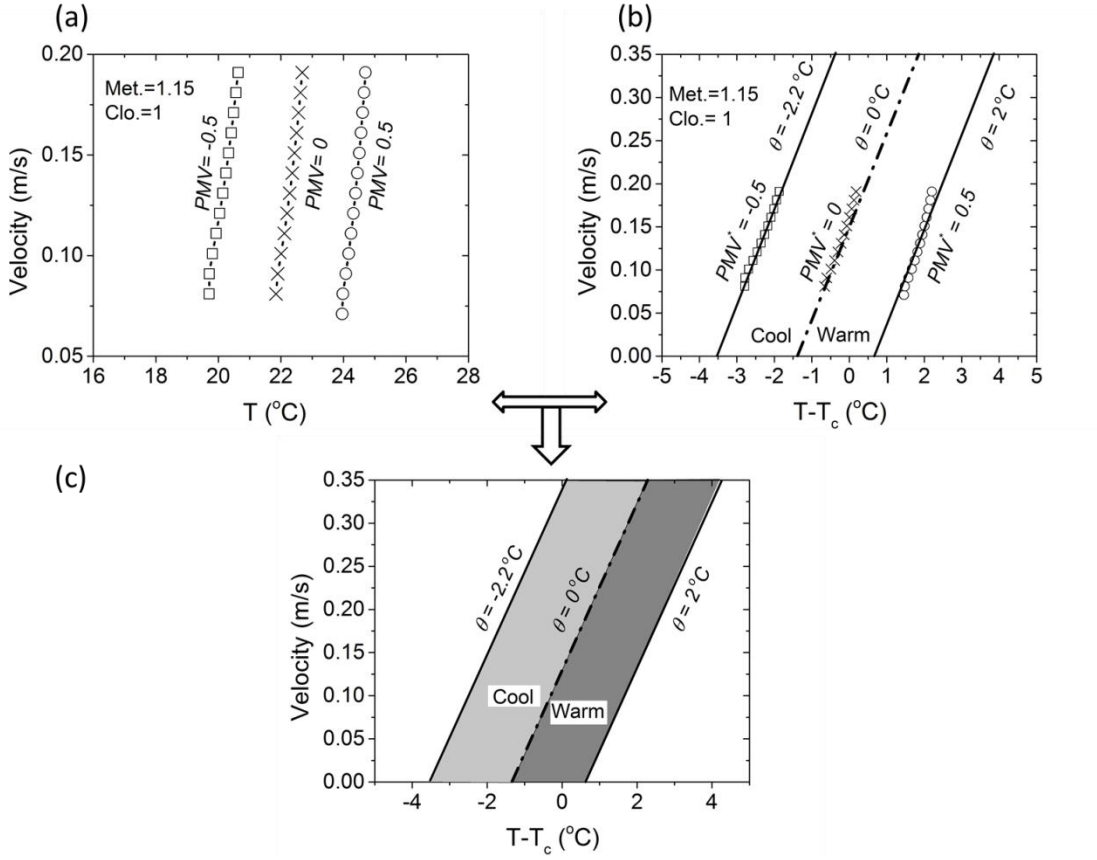

Figure 11: ADPI and PMV as a function of air temperature difference and velocity for heating mode (Metabolic activity: 1.15Met., Clothing condition: 1 Clo., and Relative humidity: 50%); (a) The range of 80% comfort acceptance using PMV; (b) EDT boundaries collapsing to those of PMV for 80% comfort acceptance. (c) The range of 80% comfort acceptance using EDT.

The heating EDT can be resolved if the coefficient k and two boundaries (θ_1 and θ_2) are determined. Due to the consistence of EDT and PMV regions for 80% thermal acceptance, one can derive the heating EDT by curve fitting EDT boundaries with those of PMV. Figure 11(b)

shows the best curve fitting of EDT's range according to PMV regions, which gives *k=9.1,* θ_1*=-2.2* and θ_2*=2*. Therefore, the heating mode EDT can be written as Equation 3**:**

$$EDT\ (\theta) = T_i - T_a - 9.1(V_i - 0.15)\ ^oC \quad (3)$$

The criterion's range of EDT (Equation 3) is between -2.2 ^oC and 2 ^oC. Similar to cooling mode EDT, the velocity of 0.15m/s in Equation 3 stands for the velocity of human thermal plume. This study keeps the criterion of air speed less than or equal to 0.35 m/s because occupants generally accept air speed greater than 0.2m/s for warm air circumstances as stated in ANSI/ASHRAE Standard 55 (2010).

Another important criterion for heating mode is the vertical air temperature difference and thermal stratification. ANSI/ASHRAE Standard 55 (2010) allows the maximum vertical air temperature of 3^oC between head (1.1m) and ankles (0.1m). In addition, higher vertical temperature gradient prohibits an efficient air mixing in the room. Therefore, this study adds an additional thermal stratification criterion to the ADPI method for warm steady-state jet conditions. In general, the ADPI for warm steady-state jets consists of three criteria: (1) EDT (Equation 3) ranging from -2.2 ^oC to 2 ^oC; (2) local air speed less than or equal to 0.35 m/s; and (3) Overall vertical temperature gradient lower than 3 ^oC/m, and local maximum temperature difference between 0.1m to 1.1m of less than 3 ^oC.

3.2.1.6 Steady-state jet length and the interpretation of indoor air distribution

The jet length, often referring to jet throw length (*T*), is defined as the distance from a diffuser to a point where the maximum velocity in the stream cross section has been reduced to a selected terminal velocity (*v*), such as 0.25m/s (ANSI/ASHRAE Standard-70 2006). Figure 12 illustrates throw lengths of various jets by diffusers over a range of airflow rates, when the jet terminal velocity decays to 0.25m/s. It is observed that the linear slot diffuser can create the largest jet throw length at a given airflow rate.

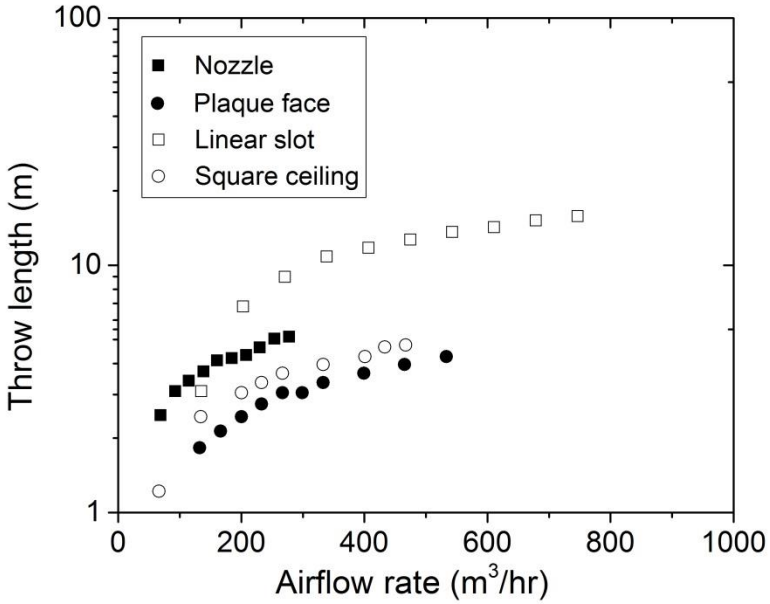

Figure 12: Throw lengths (terminal velocity=0.25m/s) of jets created by various diffusers.

The air distribution index method (ADPI) for steady-state jets from diffusers/ grilles typically relates diffuser air jet throw length ($T_{0.25}$ - distance at which jet velocity decreases to 0.25m/s) and the room characteristic length (L), which is defined as a distance from the diffuser to a wall perpendicular to jet or to the closest wall. Previous studies have shown that ADPI for a certain steady-state jet from an air diffuser/given is significantly dependent of the ratio of jet throw length ($T_{0.25}$) to room characteristic length (L) at a fixed indoor cooling load (Miller and Nevins 1970; Miller 1971; Miller and Nevins 1972; Nevins and Miller 1972; Miller 1979). Figure 2 in the Literature review chapter illustrates that the relationship curves of ADPI values versus $T_{0.25}/L$ have a concave-like shape for cool steady-state jets. Therefore, the indoor air distribution in the Chapter of Results is represented as the relationship of ADPI with $T_{0.25}/L$ as shown in Figure 2.

3.2.2 The effects of unsteady cough jets on air distribution in the cough jet region (Investigation 2E)

An unsteady-state cough jet is a violent respiratory activity associated with a large quantity of disease-carrying particles emission and interpersonal transmission. The short duration and high discharge velocity of a cough jet classifies it as a puff that appears more complex than a steady-state jet. This investigation describes the experimental setups in the small-scale test room for velocity field measurements in the cough jet region. The measurements consist of smoke visualization and velocity sampling using anemometers. To reduce the disturbance of background airflow on the cough jets, this investigation applied a low air exchange rate (~ACH=3.5hr^{-1}) to ventilate the small-scale test room.

3.2.2.1 Smoke visualization

Flow visualization offered an illustration of a cough jet penetrating into an environment. The penetration distance of a cough jet as a function of time and the spreading rate can be easily obtained from visualization. The visualization was created by using a water based fog machine (Model EF-1000, Eliminator Lighting, Los Angeles, CA, USA) that atomizing unscented water based fog juice (density of 1.043×10^3 kg/m^3 at temperature 23.0 °C) into particles with 60% in number smaller than 1.0μm and 99% smaller than 2.5μm. As the cough discharge velocity is as large as 6-22 m/s (Zhu el al. 2006), the cough jet profile was captured by such smoke. The smoke temperature was only slightly higher than background yielding a nearly isothermal turbulent cough jet. The visualization video was recorded by a camera at 60 frames per second. Five different cough jets were investigated using the smoke visualization as described in Table 8. The results of smoke visualization were used to derive the decay cough jet velocity using analytical analysis shown in the following sections. The investigation visualized the penetration distances with time for five intensities of isothermal cough jets and compared the results with a real human cough reported in the literature (Nishimura et al. 2013).

	Artificial coughs						Real cough
Discharge velocity (m/s)	15	12	9	6	6	6	~5.5
Cough duration (s)	0.4	0.4	0.4	0.4	0.8	1	0.3

Table 8: Discharge velocity and duration of five cough jets in smoke visualization.

3.2.2.2 Velocity sampling in the cough jet region

A one-dimensional hot-wire anemometer and a hot-sphere anemometer measured axial velocity in the center-section plane (76 positions) downstream a cough jet with the discharge velocity of 6m/s and duration of 1 second. The sampling points were located downstream at 4.2, 6.3, 8.3, 16.7, 25, 33.3 and 41.7 times of the diameter of the jet exit tube. In addition, the dynamics of discharge velocity was measured along the cough box exit tube. The hot-wire anemometer measured high velocities (>0.1m/s) with a large frequency of 5000Hz to capture a high velocity fluctuation, while the hot-sphere anemometer measured velocities between 0.05m/s to 0.1m/s with a frequency of 5Hz because low velocity eddies have a relatively longer lifetime. The hot-wire anemometer was calibrated using a Pitot-static system with a pressure transducer (0.1Pa resolution). The measurement at each position was repeated three times.

3.3 PARTICLE TRANSPORT (INVESTIGATIONS 1D & 2F)

Particle transmission reflects a combined effect of particle properties and air motion on particle dynamics. Because of short relaxation time, for instance, small particles follow airstream strictly even for low air motion. Indoor particle transport scenarios consist of particles spreading across the whole room that is ventilated by steady-state jets from air diffusers/ grilles and regionally transmitting associated with unsteady-state human respiratory jets, such as coughs. This dissertation places focus on the investigation of particle transport in a whole room for

steady-state jets created by air diffusers /grilles, and in the vicinity of a human recipient exposed to an unsteady-state cough jet affected by thermal plume.

3.3.1 The transmission of particles in a room ventilated by a steady-state mixing-type jet (Investigation 1D)

Table 6 in Section 3.1.4 lists 13 types of diffusers /grilles that are widely used to create a well-mixed ventilation pattern in a room. It is likely to infer that indoor particles generated from a source less affected by ventilation jets, such as re-suspension and infiltration from outdoors, have a similar fate for steady-state jets created by various diffusers/ grilles. However, particle transmission might be much different when the source is outside of a supply air jet from the cases that the source is inside. The examples are the transport of unfiltered particles emitted with a supply air jet, and of particles released by resuspension from the floor due to human movement. Furthermore, particle transmission might vary in the space installed with diffusers/ grilles when operating at cooling and heating condition.

The experiments compared the transport of three particle sizes of 0.77, 2.5 and 7μm at five locations as shown in Figure 13. The steady-state jet from the ceiling diffuser ventilated the full-scale test room at an air exchange rate (ACH) of $3.2hr^{-1}$. The temperature of the steady-state jet was maintained at approximately $17.6^{o}C$ under cooling conditions and $25.5^{o}C$ under heating conditions. The heated or cooled wall as shown in Figure 13a provided total convective heat of 320W heating or cooling. Two occupants were simulated with two simple-geometry cylinders, which had a diameter of 0.3m and a height of 1.5m. Both cylindrical manikins were fully coated with heaters, which generated a constant heat flux of 90W. The heaters were coated with aluminum foil, minimizing radiation to a negligible level. Beside the two thermal manikins, two unheated boxes and tables were placed against two walls to represent furniture.

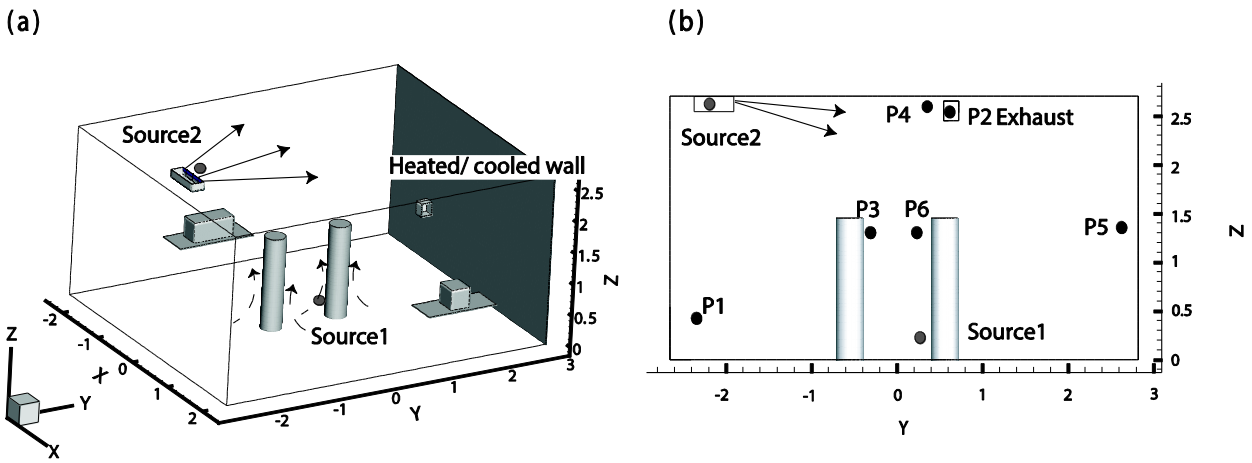

Figure 13: Particle measurements in the full-scale test room ventilated by a ceiling attached jet; (a). The locations of two particle sources; (2) Sampling positions for particle concentration.

This investigation compared the particle transmissions in two scenarios when the full-scale test room is ventilation by a ceiling attached steady-state jet. The first scenario shown in Figure 13 shows the experimental setup when the particle sources are outside (source 1) the supply jet, while the second one examines the transport of particles released outside (source 2) the steady-state supply jet. In addition, experimental measurements for the two scenarios were conducted only for cooling operation, while CFD numerical simulation considered both cooling and heating operations. The CFD numerical simulation will be described in Section 3.4.

Source 1 was positioned 0.3m above the floor and 0.02m from the cylinder occupant close to the heated wall. This source location was less impacted by the steady-state jet from the supply diffuser. In addition, particles emitted from source 1 can simulate the transmission of resuspended particles from the floor due to occupant activities, such as stepping on the floor, or by the occupant's thermal plume. Source 1 injected 0.77 and 2.5 μm particles using a Collison nebulizer at a low injection velocity of smaller than 0.1m/s to minimize the disturbance of the injection on local thermal plume. However, the 7μm particle generator (Figure 6 in section 3.1.3) required a substantial airflow that could influence the thermal plume. Therefore, only two particle sizes were considered when using Source 1. Located in supply diffuser, source 2 allowed

emitted particles (0.77, 2.5 and 7μm) well mixed with the steady-state jet. Particles generated source 2 modeled outdoor particles (and indoor particles recirculated by return diffusers) that spread through the ventilation system. To generate sufficient particles, the injection period for 0.7μm and 2.5μm particles was 100 seconds, while the large particles (or ATD) were injected for only 30 seconds due to a high injection rate.

For particle concentration measurements, five Aerotraks were used in five locations as shown in Figure 13b (P4 was not measured by numerical simulated). The five Aerotraks were calibrated side-by-side before the measurements. It was observed that the maximum discrepancy in transient particle concentration was about 12%. They monitored the variation of particle concentration in the breathing zones (P3 and P6) of the two thermal manikins, at the room exhaust (P1), and one other characteristic position (P1) in the space. Table 9 provides details about the five locations. The particle concentrations were recorded for a period of 1200 seconds. The experiments of the particle transmission were repeated three times for both scenarios. The background concentration was subtracted from all the values of the concentration. Moreover, the measurement concentrations for 0.77 and 2.5μm particles were normalized by a reference value C_{ref}. The ideal reference value is the particle emission concentration. However, the injection concentration of the particles was difficult to measure because of the unsteady emission rate, especially in the case of 7μm particles. For this reason, this dissertation used the average concentration over 1200 seconds at the exhaust of the chamber, C_{ref}, as the reference value for 0.77μm and 2.5μm particles. This is acceptable because: (1) the deposition loss on the wall was relatively low compared to ventilation effect, and (2) the exhaust concentration was close to the average concentration of the chamber. Nevertheless, particle deposition loss tends to be of importance for 7μm particles. To diminish this effect, the concentration of 7μm particles was normalized by the instantaneous average concentration, C^*_{ref}, at all the five sampling locations.

Samples	X, [m]	Y, [m]	Z, [m]
1	0	-2.35	0.59
2	2.05	0.63	2.55
3	0	-0.35	1.3
4	0	0.55	2.65
5	0	2.72	1.3
6	0	0.35	1.3

Table 9: Sample positions of the particle concentration associated with steady-state jets.

3.3.2 The transmission of coughed particles in the vicinity of a human recipient (Investigation 2F)

To examine how different size particles from coughing dispersed around a receiver occupant, this study carried out experiments of interpersonal transport of coughed particles in the small-scale chamber with two thermal manikins insides as shown in Figure 14. The chamber had a ventilation rate of approximately $3.5hr^{-1}$ and the supply air was filtered with a HEPA filter. The temperatures of supply air and exhausted air were 21.6 to 21.9^{o}C and 24.2 to 24.6^{o}C during the experiments, respectively. Thermal plumes were created by two thermal manikins, referred to as the source and the receiver, which were coated with electric heater sheets generating 45W of convective heat each. We compared the velocity 0.25m above the cylindrical manikin with that in our previous study using a full-scale manikin. It was observed that 45W heat can generated a thermal plume with a velocity of 0.19m/s at the region of 0.25m above the head which was consistent to that for the full scale thermal manikin (Rim and Novoselac 2009). To decrease the radiant heat transfer between the manikins and interior surfaces of the chamber, aluminum foil with very low emissivity was used to cover the exterior surfaces of the manikins.

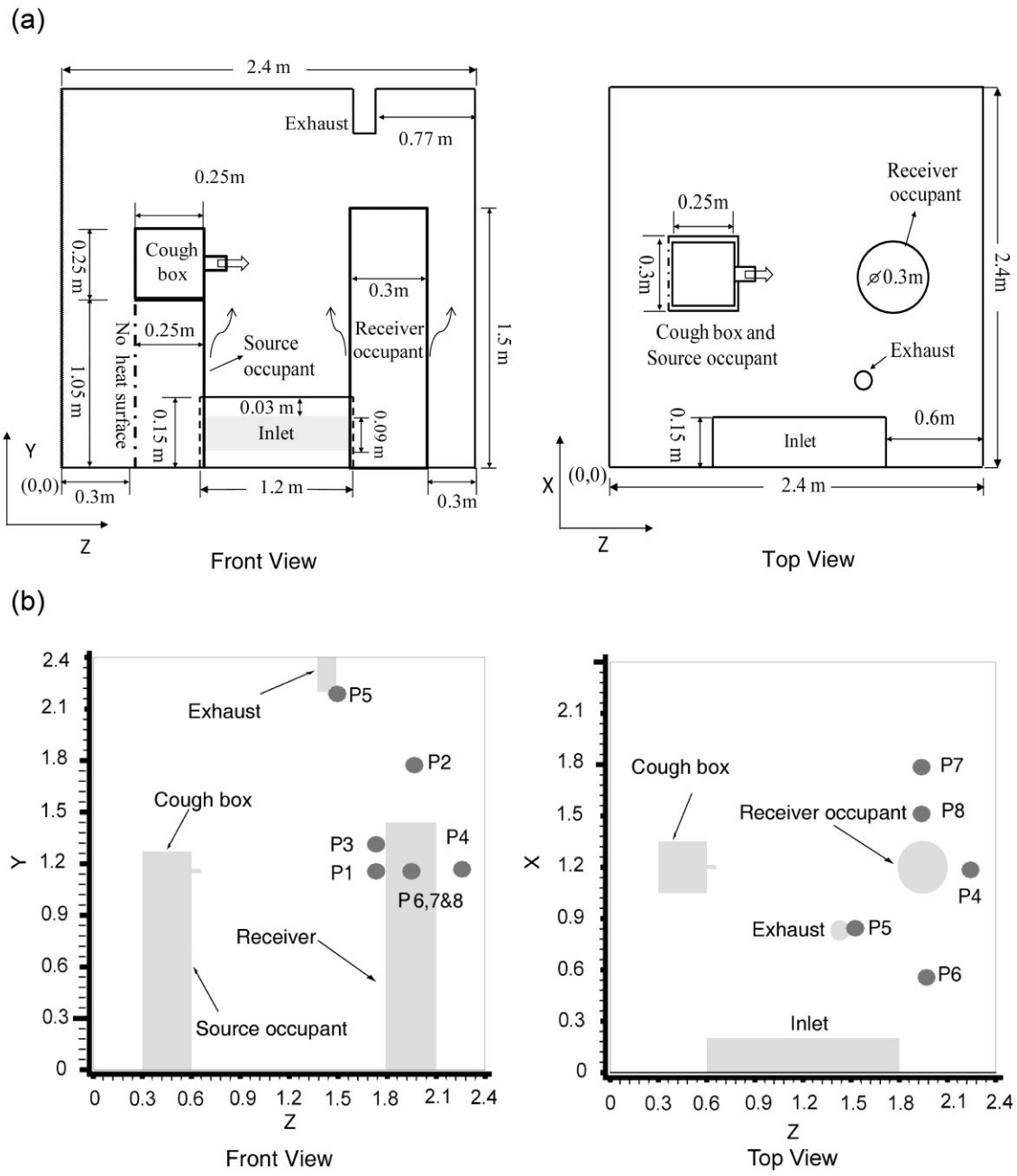

Figure 14**:** (a) Schematics of the experimental setup; and (b) measurement locations of particle concentration.

Two particle sensors sampled particles in the chamber and cough box, respectively. An APS is capable of measuring the concentration of particles from 0.5 to 20μm using a sophisticated time-of-flight technique which enables high resolution sizing over the entire

particle size range. Due to its "high" sampling frequency (up to 1Hz), the APS was used to monitor the dispersed particles in the surrounding of the receiver occupant as depicted in Figure 14, whereas an OPC sampled particles in the cough box to measure the injection concentration of a cough. The performance of two particle sensors was calibrated side-by-side before experiments. Before tracking the particle dispersion of an individual cough, the chamber was stabilized and cleaned by ventilation to minimize background concentration. In the data interpretation, the background concentration in the chamber was subtracted in the Results chapter. Table 10 shows the coordinates of sample locations of coughed particles.

(Origin is shown in Figure 14)

Locations	Measurement			Coordinates (m)		
	0.77μm	2.5μm	7μm	X	Y	Z
P1	×	×	×	1.2	1.157	1.765
P2	×	T.L.	×	1.2	1.94	1.945
P3	N.M.	×	N.M.	1.2	1.307	1.765
P4	×	×	×	1.2	1.157	2.25
P5	×	×	×	0.83	2.2	1.54
P6	×	×	T.L.	0.745	1.157	1.945
P7	×	T.L.	T.L.	1.655	1.157	1.945
P8	N.M.	×	N.M.	1.505	1.157	1.945

N.M.: not measured; T.L.: too low concentration

Table 10: Measurement locations and corresponding coordinates.

Although the concentration at other locations in the vicinity of the receiver occupant was also measured, the readings were too low to achieve statistically reliable results. The measurements at each location were repeated at least three times; for example, measurements at P1 were repeated thirteen times for 0.77μm particles. To faciliate the comparison of number concentrations of different size particles, all experimental results were normalized by the injection concentration in the cough box.

3.4 CFD NUMERICAL SIMULATION AND ANALYTICAL ANALYSIS

CFD simulation numerically calcuates fluid and particle dynamics in each geometry cell and iterates the calculation till a very small residual. The method is capable of providing more detailed information that is otherwise difficult to measure. In addition, an analytical approach, such as dimention analysis, is valuable to reveal the mechanism and property of jet dynamics. Because of multiple assumptions, both applied methods require experimental validation. This section first describes the methodology of CFD numerical simulation and analytical analysis used in this dissertaion. Then it provide a description of setups of steady-state jets and unsteady-state jets that were applied for CFD numerical simulation and analytical analysis, respectively. Additionally, CFD simulation of particle tracking was valided by using the experimental data reported in the literature (Lu et al. 1996).

3.4.1 CFD numerial simulation (Investigation 1D)

Since indoor air flow is turbulent, two widely accepted turbulent models – RANS and LES – were used in the numerical simulation. As recommended by previous studies (Chen 1995; Rim and Novoselac 2008; Liu et al 2011), the RNG k-ε model generally performs better for indoor airflows and buoyancy-driven flow than other eddy-viscosity models. By directly resolving the large scale eddies, LES turbulent model in this dissertation applied the dynamic Smagorinsky subgrid scale model (SGS) to model the small-scale eddies (Germano 1986). The numerical applied an Eulerian approach to simulate the airflow field and a Lagrangian method to track particles.

This investigation considers three catogories of numercial simulation setups: (1) validation of particle tracking using two-zone data (Lu et al. 1996); and (2) air distribution and particle transport in the full-scale test room with a steady-state jet. CFD models of the steady-state jet were developed with the commercially available ANSYS-FLUENT (version 12.1 2010) package for simulating indoor air distribution and particle transport. Addionally, the data processing for particle concentation was described in this section.

3.4.1.1 Validation of particle tracking using experimental results in literature

This subsection applied the establied experimental data obtained by Lu et al. (1996) to validate the CFD numerical simulation for particle tracking. By comparing numerical predictions in this investigation with the previous experimental results, the CFD modeling of airflow and particle concentration that was applied in the investigation of this dissertation can be verified. The following part of this subsection provides a description of experiements (Lu et al. 1996) and numerical setting (this investigation).

The experimental study conducted by Lu et al. (1996) released particles with supply air into a room divided into two zones by a partition with a lage opening. The geometrical configuration of the room is shown in Figure 15a. The opening was on the centerline of the room and had the size height × width of 0.95m × 0.7m. The room was ventilated through the supply section (0.15m × 0.5m× 1m) in Zone 1 at an air exchage rate (ACH) of 9.216 hr^{-1}. The exhaust section with the same geometry as the supply section was located a a low level in Zone2. Before the experiment, the particles are assumed to uniformly distribute in zone1 with partition opening was in the close condition. The smoke particles used in the experiment had sizes in a range of 0.5-5μm with a density of 0.85g/cm^3. More information about the two-zone room can be found in the literature (Lu et al. 1996).

(a) (b)

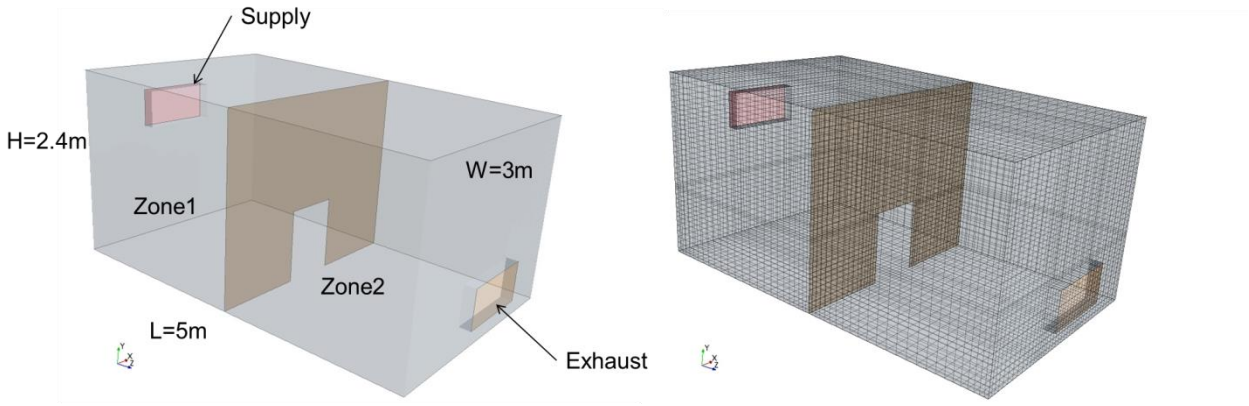

Figure 15: Geometry and sample mesh of the room with two zones; (a) Room geoemtry in the literature (Lu et al. 1996); (b) Mesh geometry generated by the validation effort in this dissertation.

The validation in this investigation applied the experimental setup to numerically simulate the particle concentration varying in the two zones using both RANS and LES models. The number of the hexahedral grids for the cases using RANS and LES is 62,000 and 500,000, respectively. The injected particles in the simulation was grouped into five sizes -1μm ,2 μm , 3 μm, 4 μm and 5 μm - to represent the smoke particles (0.5-5 μm) in the experiment. According to the study conducted by Chang et al. (2006), 6000 particles (1200 particles for each size) is sufficient to capture the variation of particle concentration in each zone. Therefore, this investigation injected 1200 particles for each size. Tracking the position of each particle, the simulation is capable to calculate particle mass concentration using the following equation:

$$Mass\ concentration\ (C) = \frac{Total\ mass\ of\ suspending\ particles\ (M_s)}{zone\ volume\ (V)} \qquad (4)$$

Miguel et al. (2005) investigated that indoor particle deposition is particularly significant for the floor surface, while deposition on vertical and ceiling surfaces becomes important only when these surfaces are electrically charges. Herein, particles are assumed to deposit on the

room's floor and bounce off other walls and ceilings. Table 11 summaries the parameter settings for the validation cases.

Set-up	RANS-RNG	LES
# of cells	62,000	500,000
Cell geometry	Hexahedral	Hexahedral
Supply velocity (m/s)	0.09216	0.09216
Air exchange rate(hr^{-1})	9.216	9.216
Turbulence intensity	5.2%	5.2%
Turbulent length scale of supply air (m)	0.091	0.091
Number of particles injected (#)	6,000	6,000
Time step size (s)	0.2	0.05
Physical time(s)	1600	1600
Particle deposition on surfaces	floor	floor

Table 11: Numerical setting for the validation of particle tracking.

3.4.1.2 Air distribution and particle transport in a room with a ceiling-attached steady-state jet

This subsection presents the numerical investigation conducted in this dissertation. The numerical simulations in this section first employed the measurements of parcticle concentration at cooling condition in the full-scale test room described in Figure 13 for verification. Then the transport of particles under both cooling operation and heating operation were investigated in the test room ventilated by a ceiling-attached jet.

The entire geometry of the test room was comprised of 496,650 hexahedral cells for both RANS and LES simulations. The grid number was justified using a grid independence check for RANS simulation. The cells were refined gradually with a ratio of roughly 1.4 (247,000, 500,000 and 1,000,000) to generate grid-independence results for RANS simulation. The study found that the predicted velocity and temperature changed at a negligible level for the three meshes. Considering LES simulation, the decreasing cell size reduces the effects of sub-grid model and enables the calculation to approach DNS. Therefore, the grid independence was not performed

for LES. In this study, the same mesh (500,000 cells) was utilized for the RNG and LES models in order to compare their performance. The minimum and maximum cell volumes in the domain are approximately 3.4×10^{-7} m^3 and 1.1×10^{-3} m^3, respectively. Figure 16 describes the mesh geometry developed in this investigation. In addition, the sensitivity of the number of released particles was checked using three settings, 100,000, 300,000 and 600,000. It turned out that 600,000 can generate a statistically stable concentration at a given location.

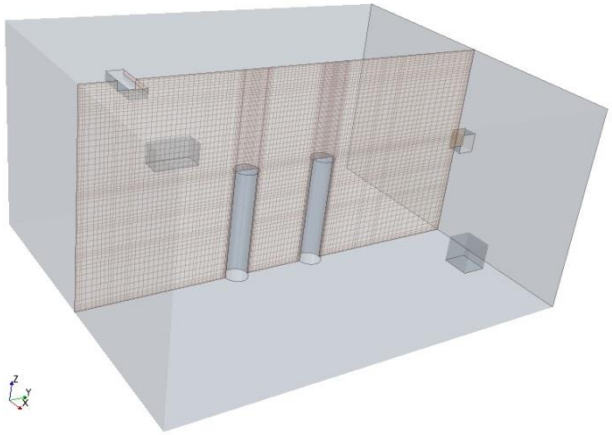

Figure 16: Mesh geometry of the room with a ceiling-attached steady-state jet.

Table 12 summaries the information of simulations in this investigation. All of the discretizations followed a second-order upwind scheme except for the momentum equation of the LES, which used a bounded central differencing scheme. The PISO algorithm was used as the pressure-velocity coupling method. The staggered scheme, PRESTO!, was employed for the pressure interpolation concerning the buoyancy flow. Due to the low particle load in the bulk environment, the particle simulation used one way coupling of airflow and particles. The convergence criteria were assumed to have been met when the iteration residuals became less than 10^{-6} for the energy equation, and 10^{-4} for the other parameters in all simulations.

Two time steps needed to be determined in order to solve the unsteady flow and particle dispersion. The time step for calculation of particle movement should make sure that each particle stays in the same eddy during each time step. Although the simulation was able to adopt time steps for airflow and particle movement, only one time step was used for both calculations in order to avoid the time interpolation error. The selection of the time step (t) in the simulation was made based on calculation stability and physical flow conditions:

(1) Iteration stability requires the time step to be smaller than the time a fluid parcel resides in one cell, which is usually indicated by the Courant-Frerichs-Lewy (CFL) number defined as Equation 5.

$$CFL = \Delta t \left(\frac{|u|}{\Delta x}, \frac{|v|}{\Delta y}, \frac{|w|}{\Delta z} \right)_{max} \quad (5)$$

Where *u, v, w* are the velocities at three directions, and Δx, Δy, Δz are grid size

in the corresponding directions.

(2) The selection of time step is also dependent on local flow characteristics, such as velocity gradient, and time scale of the flow eddies. The Kolmogorov time scale, shown in Equation 6, was adopted in the RANS and LES simulations.

$$\tau = (\nu/\varepsilon)^{1/2} \quad (6)$$

where τ is the Kolmogorov time scale(s), ν is kinematic viscosity (m^2/s), and ε is turbulent dissipation rate (m^2/s^3), calculated with RANS. The resulting Kolmogorov time scale of most eddies was roughly 0.05s.

Set-up	Cooling mode	Heating mode
Chamber volume (m^3)	67	67
Ventilation Patten	Mixing using a ceiling-attached jet	Mixing using a ceiling-attached jet
Number of cells	500,086	500,086
Cell geometry	Hexahedral	Hexahedral
Minimum cell volume(m^3)	3.43×10^{-7}	3.43×10^{-7}
Maximum cell volume(m^3)	1.07×10^{-3}	1.07×10^{-3}
Maximum aspect ratio	23	23
Supply velocity distribution	Measured	Measured
Air exchange rate(hr^{-1})	3.2	3.2
Turbulence intensity	5%	5%
Hydraulic diameter of openings (m)	0.15	0.15
Supply air temperature(^oC)	17.6	25.5
Thermal load (W)	Thermal wall (320 heating) + occupants (180 heating)	Thermal wall (320 cooling) + occupants (180 heating)
Number of particles injected(#)	600,000	600,000
Time step size (s)	0.05	0.05
Minimum CFL number	1.8	1.8
Particle deposition on surfaces	No	No

Table 12: Summary of numerical simulations adopted in the Investigation 1D associated with steady-state jets.

3.4.1.3 Data processing for particle concentration

To numerically calculate particle concentration at a certain location, the CFD simulation counted the number of particles residing in a volume surrounding the location and the number concentration can be obtained at each time step. The approach defined volumes that can be spherical, cubic, or cylindrical, depending on the local airflow pattern and particle transmission characteristics. Equation 7 describes the particle concentration calculation in the CFD simulations,

$$C_p = \lim_{V \to 0} \frac{N_p}{V} \tag{7}$$

where C_p is the particle number concentration in a predefined volume V, and Np is the particle number in the volume.

The volume needed to calculate the particle number concentration was determined by considering resolution requirements and the sampling airflow rate of particle counters. The volume size should be small enough to obtain the concentration at a specific location. This study used a volume of 0.05m in diameter at all sampling locations illustrated in Figure 13.

3.4.2 Analytical analysis for unsteady cough jets (Investigation 2E and 2F)

This investigation provides a mathematical description of the penetration distance and velocity field of a cough jet, and the trajectories of particles driven by the jet. As the short duration of a cough prevents detailed measurements of particle dynamics due to the limited capabilities of particle counters, theoretical or numerical analysis are the alternatives. In this study, analytical methods were applied to analyze the flow and particle dynamics in the cough jet region where the airflow was dominated by the jet. In this jet-dominant region, particles especially fine ones (PM 2.5), strictly follow jet streamlines because of the high discharge velocity. The dispersion of particles is mainly driven by drag force for fine particles and by gravity for coarse ones. When the cough jet decays and travels to another occupant, the body's thermal plume may affect dispersion. Other factors, such as receiver occupant's movement and respiratory activities, might also impact the transport and dispersion of coughed particles. The influence level of these factors depends on the characteristics of a cough jet.

Most coughs last 1 second or less with a velocity of 6m/s or higher (Gupta et al. 2009; Nishimura et al. 2013). For a commonly used particle sampler, e.g. OPC or APS, it is improbable that the sampler will have enough time to measure particle dispersion accurately in the cough jet region. Fortunately, momentum conservation allows a parameter analysis in the jet region before the jet decays to room background (Kovasznay et al. 1975). In the vicinity of a receiver occupant, including the breathing zone, the momentum conservation of the cough jet is broken

by additional buoyancy force due to the body thermal plume. In such region, flow and particle dynamics become increasingly complex and limit the theoretical analysis.

The characteristics of an unsteady cough jet are strongly related to: injected volume flow rate and duration of the jet besides the parameters defining a steady jet such as discharge velocity and inlet geometry. Due to the self-preserving (or momentum conservation) of a cough jet flow in the downstream region, the penetration distance S_p referring to the distance from injection source to jet frontal tip, can be written as Equation 8:

$$S_p = f(U_0, D, \tau) \tag{8}$$

where U_0 is discharge velocity, τ is time, and D is the diameter of jet source. The volume flow rate of the jet is $\pi U_0 D^2/4$. A dimensionless analysis results in a relationship for the jet at a constant discharge velocity U_0,

$$\frac{S_p - X_0}{D} \sim \left(\frac{U_0 \tau}{D}\right)^n \tag{9}$$

where X_0 is the virtual origin. The power n (n=1/2) reflects the relationship between penetration distance with time, which varies in different studies (Lee and Chen 1998; Sangras et al. 2002; Song and Abraham 2003).

After taking the derivative of the penetration distance, S_p, with respect to time, τ, we arrive at Equation (10),

$$\frac{U_{0m}}{U_0} = K_1 \left(\frac{S_p - X_0}{D}\right)^{-1} \tag{10}$$

where U_{om} is the maximum centerline velocity at the jet tip with a penetration of Sp. U_{om} can also refer to the peak average velocity at the cough jet center following the tip. The cough jet center is defined as a location of maximum velocity. Equation 10 shows that the tip velocity of a cough jet has a similar relationship with the dimensionless distance, S_p/D, as a steady jet (Chen and Rodi

1980). The coefficient K_1 is a constant value that can be determined via experiments described in Section 3.2.2.1.

Ghaem-Maghami and Johari (2010) reported that the axial velocity profile through a puff center follows a Gaussian function similar to a steady jet as described in Equation (11),

$$\frac{U}{U_{0m}} = \exp(-K_2(r^* - r_0^*)^2) \tag{11}$$

where $r^*=r/S_p$, $r_0^*= r_0/S_p$, and r is the vertical distance from the cough jet center. r_0^* is used because the cough jet center may be slightly off-center.

Furthermore, the velocity profiles of a steady jet with an identical Reynolds number as the cough jet in the literature were used for comparison with the cough jet (Wygnanski and Fiedler 1969; Bocksell 1998),

$$\frac{U_{0m}}{U_0} = B\left(\frac{S_p}{D}\right)^{-1} \tag{12}$$

$$\frac{U}{U_{0m}} = \text{sech}^2(\sigma r^*) \tag{13}$$

where B is velocity-decay constant, 5.5 , and σ is 10.4 through curve-fitting.

Once the velocity field is determined, the trajectory of a particle injected with a cough jet can be obtained according to Newton's second law of momentum conservation. Because the particle sizes concerned in this study were in the range of 0.35-10μm and the density of coughed particles is approximately equal to water liquid (Havel et al. 1955), only drag, buoyant and gravity forces dominate particle momentum. For the unobstructed cough and particle sizes considered in this study, these forces are several orders of magnitude greater than Brownian force, thermophoresis force and lift force (Talbot et al. 1980; Li and Ahmadi 1992). It is worth noting that this study focuses on an isothermal cough jet. This phenomenon can be reflected by

r_0* in Equation (11). Furthermore, the particle momentum and displacement equations can be written as follows:

$$\frac{\mathrm{d}\,\overrightarrow{U_p}}{\mathrm{d}\tau} = \frac{3C_d\rho_a}{8\rho_p r_p}\left|\overrightarrow{U_a} - \overrightarrow{U_p}\right|\left(\overrightarrow{U_a} - \overrightarrow{U_p}\right) + \vec{g}\left(1 - \frac{\rho_a}{\rho_p}\right) \tag{14}$$

$$\frac{\mathrm{d}\,\overrightarrow{X_p}}{\mathrm{d}\tau} = \overrightarrow{U_p} \tag{15}$$

where $\vec{U}$ is velocity, ρ is density, r_p is particle size and $\vec{g}$ refers to gravitational acceleration. The subscripts, *p* and *a*, represents particle phase and air phase, respectively.

C_d is the drag coefficient represented by a general function of particle Reynolds number, Re, as shown in Equation (16),

$$C_d = \mathrm{a}_1 + \mathrm{a}_2 Re^{-1}\mathrm{a}_2 + \mathrm{a}_3 Re^{-2} \tag{16}$$

where *a1*, *a2* and *a3* are constants that apply to spherical particles over a large range of *Re* (Morsi and Alexander 1972).

In terms of Equations (9)-(16), the trajectory of a single particle in a cough jet or steady jet can be determined. In this study, the fourth-order Runge-Kutta method was employed to numerically solve the differential equations. The calculation applied the same initial condition as experiments described before.

3.5 QUALITY CONTROL AND UNCERTAINTY ANALYSIS

For all six investigations (1A-2F) using experimental methodology, measures were taken to generate reliable results when considering: experimental design, measurement procedure and data processing. The uncertainty in the measured and processed data for all results was investigated in detail. Whenever possible, experiments were repeated three times to evaluate the

uncertainties in the measurements. In all figures in the results chapter, the error bars represent the propagated uncertainty determined by standard deviation. In addition, measures were taken to enhance the quality of experiments in all investigations. The following sections briefly describe the control measures for various parameters.

3.5.1 Velocity, temperature, and air flow rate measurements

High – precision instruments were utilized to measure indoor distribution of velocity and temperature, and supply airflow rate of the test rooms. To minimize possible disturbance, all investigations related to steady conditions conducted measurements after the three parameters became statistically stable. Also, the energy balance in test rooms was checked for each experiment by comparing the energy supplied to a test room with energy removed. For each experiment, the investigations minimized the net energy, energy supplied minus energy removed, in a range of not exceeding 10% of the supplied energy.

3.5.2 Uncertainty of ADPI due to diffuser/ grille selection

The uncertainty of the measured ADPI values depends on several factors. Specifically, the measurement uncertainty depends on the accuracy of the instruments used and factors relates to experimental set-up, such as diffuser installation, and flow adjustment and balancing. Other factors, such as variation in the geometry of diffusers produced by different manufacturers, as well as variations in diffuser size for the same diffuser type, introduce different levels of uncertainty. Because of the high accuracy of velocity and temperature sensors used (±0.03m/s and ±0.1^{o}C respectively) in this study, the error propagation analysis showed that the uncertainty caused by instrumentation had a small impact on calculated effective draft temperature, and consequently even smaller influence on ADPI compared with the impacts caused by the variation in the experimental set-ups. The uncertainty caused by the experimental set-up was evaluated by repetitions of experiments for the same diffuser at various stages of the project. The result showed that uncertainty caused by experimental set-ups generated a variation in ADPI of roughly ±2.7% (absolute value, 95% confidence interval). When considering the variation in

ADPI versus $T_{0.25}/L$ curves, however, the largest impact is caused by the variation in diffuser sizes, and in the geometries of diffusers produced by different manufacturers for most of the 13 diffuser types. The uncertainty caused by different manufactures and diffuser sizes is expressed by 95% confidence interval for the maximum ADPI and this uncertainty is presented in the major results tables.

3.5.3 Uncertainty in particle concentration measurement

Investigations 1D and 2F measured the concentration of particles (0.77, 2.5 and 7μm) using five optical particle counters (OPCs) and one aerodynamic particle sizer (APS). Since the particle concentrations presented in next chapter are normalized, a high quality measurement entails comparing the performance of the particle sensors. This section presents the two experimental results to assess the variations of particle sensors. First, Investigation 1D employed the five OPCs side-by-side to measure the particle concentration in a given environment. Second, Investigation 2F compared the performance of the APS and one OPC over a large range of particle concentrations.

Figure 17 shows the measured concentrations by the five OPCs side-by -side. It is observed that the five OPCS can generate almost equivalent results when measuring given particle concentrations. The results ensure the quality of particle measurements in the full-scale room associated with steady-state jets.

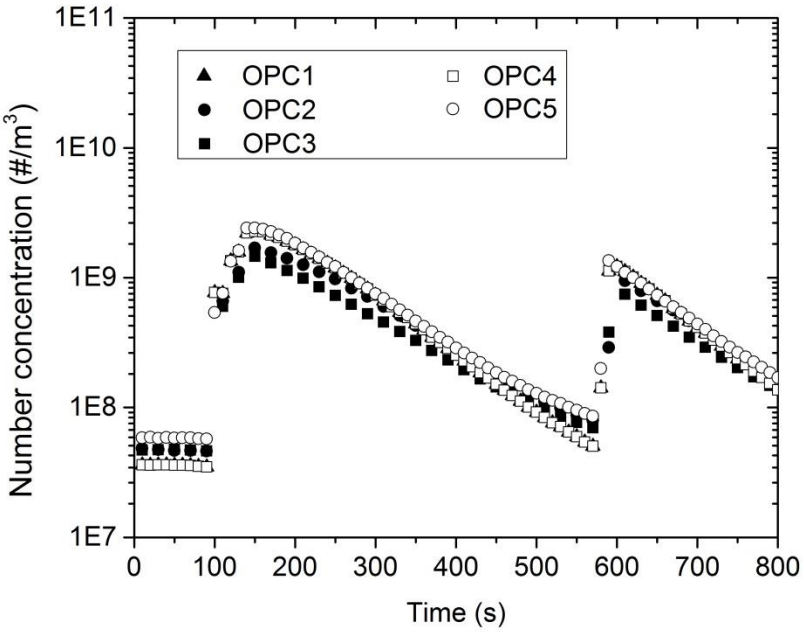

Figure 17: Comparison of measured sample particle (Arizona test dust, nominal 5-10µm) concentration using the five optical particle counters (OPCs) used in Investigation 1D.

Since OPC and APS applied different mechanisms to sample particles, it is crucial to ensure the two devices to generate equivalent results. Before measuring the transport of coughed particles, Investigation 2F compared the response of OPC and APS over a range of concentrations for 0.77 or 2.5µm particles, as shown in Figure 18. The measured concentrations by APS and OPC generate a linear curve for 0.77 and 2.5µm particles, indicating good performance of the two instruments for particle sampling. In addition, Appendix D discusses their performance measuring 7µm particles.

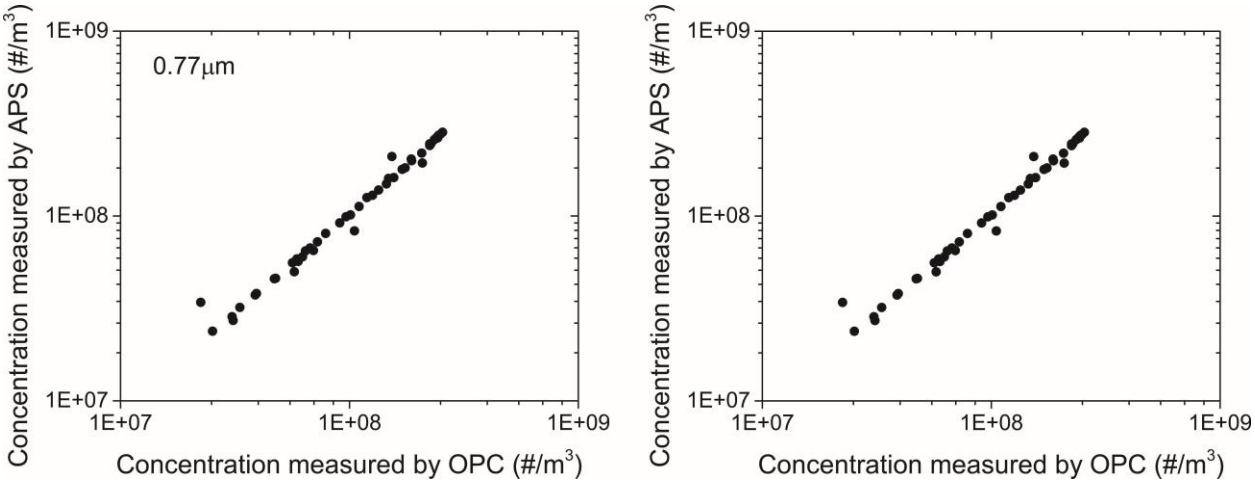

Figure 18: Comparison of measured sample particle (0.77 and 2.5μm latex particles) concentration by the aerodynamic particle sizer (APS) and optical particle counter (OPC) used in Investigation 2F.

The systematic uncertainty minimized as described above enabled precise evaluation of the uncertainty associated with reported data. Overall, the quality of measurement can be improved by careful experimental design. The experimental uncertainties of the particles measurement were mainly caused by experimental design, and this was assessed by statistical analysis, such as standard deviation and 95% confidence interval.

Chapter 4: Results

This dissertation addresses the effects of steady-state jets created by air diffusers/ grilles and unsteady-state cough jets on indoor air distribution and particle transport. Chapter 1 outlines the specific research objectives listed as Investigations 1A - 2E, and this chapter presents the major findings for each investigation and provides relevant implications. It constitutes two major sections: (1) Indoor air distribution while considering steady-state diffuser/ grille-created jets and unsteady-state cough jet; (2) The transport of three size particles carried by air flow. As the air distribution and particle transport were investigated using various research methodologies, such as experimental measurement, numerical and analytical modeling, and this dissertation compress the experimental and modeling results, whenever applicable.

4.1 INDOOR AIR DISTRIBUTION RELATED TO STEADY-STATE JETS CREATED BY AIR DIFFUSERS/ GRILLES

The indoor air distribution in the full-scale test room with steady-state jets is represented by a combined velocity and temperature factor of ADPI. This dissertation measured the distribution of velocity and temperature in the full-scale room mounted with various diffusers/ grilles under both heating and cooling conditions. For a given supply airflow rate and steady-state jet condition, the results of velocity and temperature in sixty locations (Figure 9) were represented by a single ADPI. This section (1) reports ADPI values under cooling and heating conditions and (2) analyzes possible factors influencing indoor air velocity.

4.1.1 ADPI values at Cooling Condition (Investigation 1A)

The ADPI values for each diffuser type are shown in Figure 19 when the supply air is cooler than indoor environment. As described in the methodology section, this investigation focuses on two cooling loads, 25W/m^2 and 50W/m^2. Figure 19 shows that ADPI decreases

with an increase of cooling load, especially for lower values of $T_{0.25}/L$. The reason for this is the fact that larger cooling load requires a larger temperature difference between supply air and room air for a given supply airflow rate (given $T_{0.25}/L$). The large temperature difference reduces the thermal uniformity in the occupied zone and therefore a larger percentage of space is exposed to cool draft.

At a given airflow rate for adjustable blade diffusers, upward or downward blade position causes a shorter throw length than deflector blades positioned horizontaly. Also, buoyancy may afect the direction of jets from the diffusers; cooled jet tends to travel downward which may result in draft in the occupied zone. This is particularly true for downward deflectors and Figure 19 shows that 45^o downward blade diffusers fail to generate aceptable air distribution (ADPI >80%) for all measures $T_{0.25}/L$ ratios regardless of the cooling loads (25W/m^2 and 50W/m^2). For upward angled blades (45^o upward in Figure 19), however, suppy air jets travel along the ceiling before moving downward along a side-wall, producing high ADPI values (almost as high as 90%) over a wide range of $T_{0.25}/L$. This indicates that air distribution design should not just include diffuser selection procedure but also diffuser adjustment.

The impact of diffuser adjustment is even more important for linear slot diffusers where even a very small imperfection of diffuser deflector adjustment could cause significant failing in the air distribution. The Appendix D discusses the poor air distribution resulted from poor adjustment of linear slot diffusers. Figure 19 shows the ADPI values of linear slot diffusers when deflectors are well adjusted, but the experiments related to the adjustment of this diffuser type show that ADPI may reduce more than 20% just due to poor adjustment. The detailed results about the impact of the blade adjustment for ceiling slot and grill diffusers are provided in Appendix D.

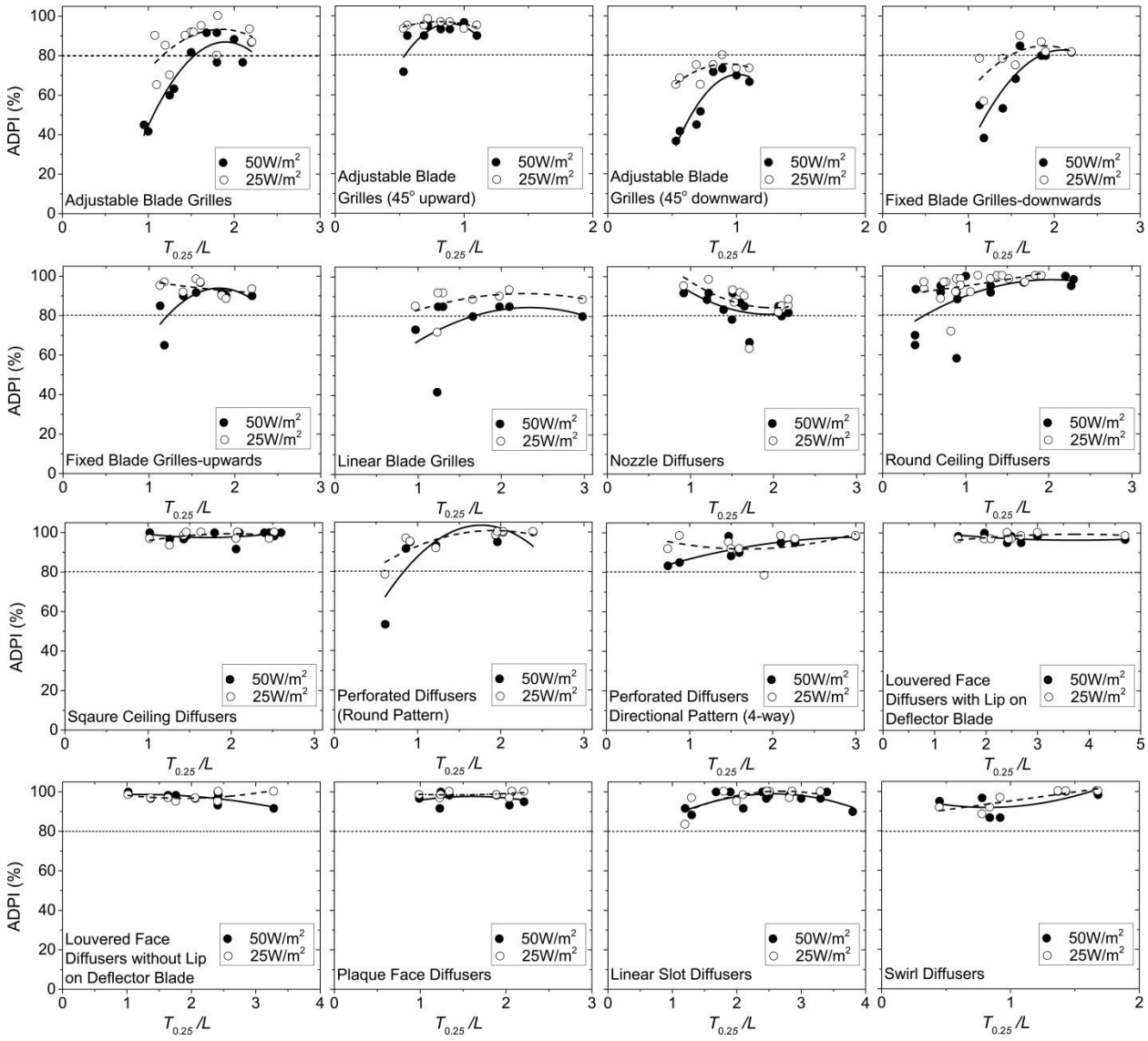

Figure 19: ADPI values *vs.* $T_{0.25}/L$ for the diffusers at 25W/m^2 and 50W/m^2 under cooling condition.

Table 13 shows the maximum ADPI values and $T_{0.25}/L$ ranges in which ADPI values are greater than 80% for different diffuser/ grille types at two cooling loads. The uncertainty of the maximum ADPI for each diffuser type is represented by 95% confidence interval for the mean response at various $T_{0.25}/L$. Overall, all 13 diffuser types are capable to create an indoor air distribution with ADPI greater than 80%, when excluding incorrect positioning of grill diffusers. In addition, upward deflectors can generate greater ADPI values than horizontal deflectors as

shown in ASHRAE Handbook-*Fundamentals* (2009). The downward deflector configuration for blade grilles should be avoided because the occupied zone will likely be exposed to a cold draft. Linear slot and louvered face diffusers are the least sensitive to $T_{0.25}/L$ for creating an indoor air environment with ADPI values greater than 80%.

Results in Figure 19 and Table 13 show the optimum $T_{0.25}/L$ ranges used for specific diffuser type selection. The major difference among the 13 diffuser types is the acceptable range of $T_{0.25}/L$ ratios. For example, louvered face diffusers with lip on deflector blade have maximum ADPI (100%) for a wide range of $T_{0.25}/L$ ratios (from 1.5 to 5) while grill diffusers with upward blades just in the narrow range around $T_{0.25}/L = 0.7$ (Figure 19). Since for a given type of diffusers/ grilles positioned in a certain room with varying supply flow rates, the range of the accptable $T_{0.25}/L$ ratios (ADPI>80%) indicate how the type of diffusers/ grilles perform when using with variable air volume (VAV) HVAC systems. Consequently, results in Figure 19 show the optimum of diffuser/ grille selection (selection of diffuser type suitable for the largest acceptable $T_{0.25}/L$ range) but also idicate suitability of diffuser typses for VAV-HVAC systems.

Terminal Device	Loads (W/m^2)	$T_{0.25}/L$ for Max. ADPI	Maximum ADPI (≤100%, 95% confidence interval)	$T_{0.25}/L$ range (ADPI>80 %)
Adjustable Blade Grilles (High Sidewall installation)- 45° upward blades	25	0.8	97±1%	0.5-1.1
	50	0.9	96±4%	0.6-1.1
Adjustable Blade Grilles (High Sidewall installation)- 0° horizontal blades	25	1.8	93±6%	1.2-2.2
	50	2	87±6%	1.7-2.2
Adjustable Blade Grilles (High Sidewall installation)- 45° downward blades	25	0.9	75±4%	-
	50	1	70±8%	-
Fixed Blade Grills(High Sidewall installation)-15° upward blades	25	1.1	95±5%	1.1-2.2
	50	1.9	92±8%	1.2-2.2
Fixed Blade Grills(High Sidewall installation)-15° downward blades	25	1.9	85±9%	1.6-2.2
	50	1.9	81±10%	1.9-2.2
Linear Bar Grilles (High Sidewall installation)	25	2.1	91±7%	1.0-3.0
	50	2	83±14%	1.6-3.0
Nozzles(High Sidewall installation)	25	0.9	99±13%	0.9-2.2
	50	0.9	94±8%	0.9-2.2
Round Ceiling Diffuser	25	1.8	100±4%	0.5-2.3
	50	2.2	100±11%	0.7-2.3
Square Ceiling Diffuser	25	2.1	99±2%	1-2.6
	50	2.6	100±3%	1-2.6
Perforated Diffusers-Round Pattern	25	1.9	100±5%	0.6-2.4
	50	1.9	100±10%	0.8-2.4
Perforated Diffusers- Directional Pattern (4-way)	25	3	99±11%	0.7-3
	50	3	98±6%	0.7-3
Louvered Face Diffusers-with Lip on Deflector Blade	25	3	99±1%	1.4-4.7
	50	1.5	99±3%	1.4-4.7
Louvered Face Diffusers-without Lip on Deflector Blade	25	3.3	100±3%	1-3.3
	50	1	99±3%	1-3.3
Plaque Face Diffusers	25	2.2	99±2%	1-2.2
	50	1.3	98±3%	1-2.2
Linear Slot Diffusers	25	2.8	100±3%	1.7-3.8
	50	2.5	99±3%	1.7-3.8
Swirl Diffusers	25	1.7	100±4%	0.4-1.7
	50	1.7	100±6%	0.4-1.7

Table 13: ADPI Selection Guide for Cooling Mode ($25W/m^2$ and $50W/m^2$).

Figure 20 summarizes the ranges of $T_{0.25}/L$ for each diffuser type to generate an indoor air distribution with an ADPI value higher than 80% at two indoor cooling loads – $25W/m^2$ and $50W/m^2$. These $T_{0.25}/L$ ranges for acceptable ADPI are a major improvement over existing

ADPI method for HVAC all-air system design. First, the ranges obtained by this work provide an expansion and updating of current ADPI method that was established in 1970s and only includes a very limited number of diffuser/ grille types. In fact, numerous new types, such as plaque face diffusers, are widely used but not specified by current ADPI guideline, which likely results in poor indoor air distribution. For this reason, they offer much better guideline for indoor air distribution design. Second, the manufacturing method for many diffusers/ grilles have changed since the original testing that occurring in the 1970s or before and may change the performance characteristics of these terminal devices. The results shown in this dissertation revised the current guideline by testing currently used diffusers/ grilles, which will greatly enhance the efficacy of the design of air distribution.

(a)

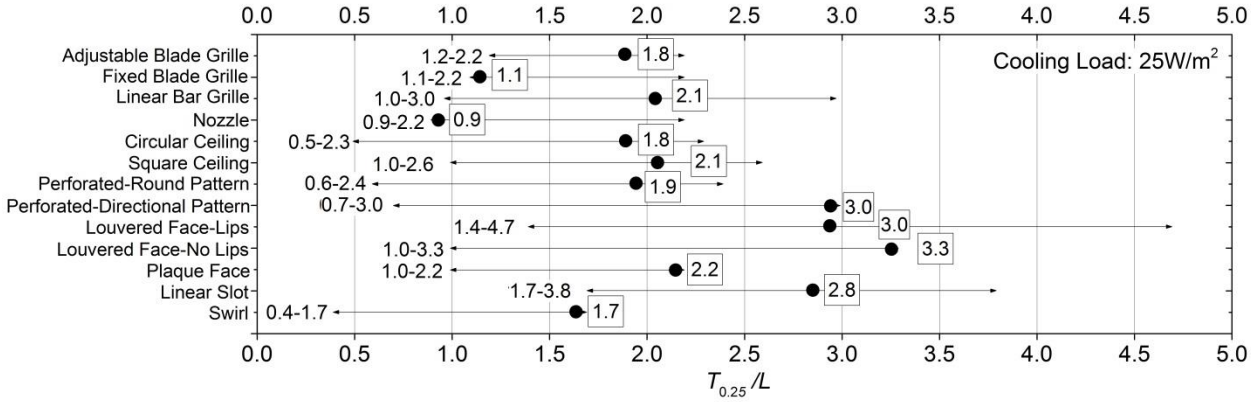

(b)

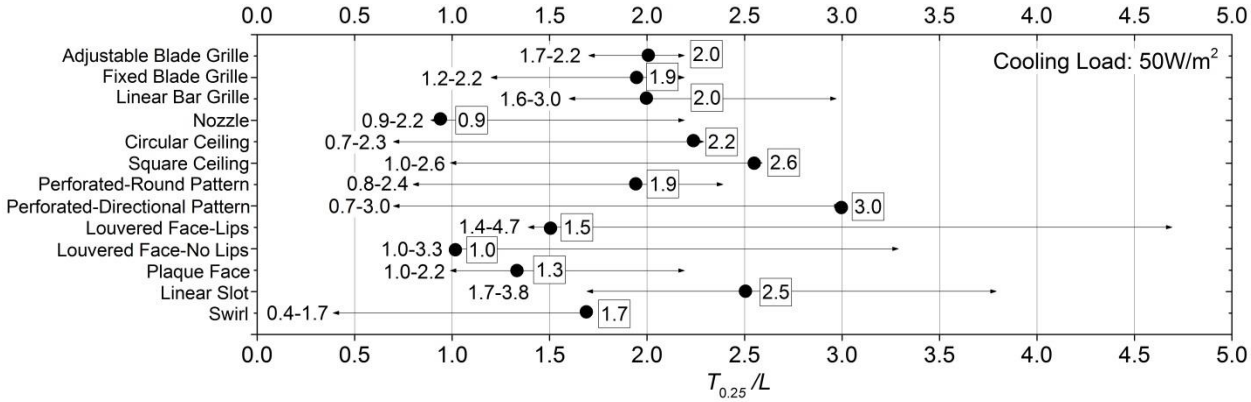

Figure 20: The ranges of $T_{0.25}/L$ for various diffuser types when ADPI higher than 80% at cooling condition; (a) 25W/m^2; (b) 50W/m^2; Dot denotes the maximum ADPI.

Lastly, this work generates results of ADPI at more realistic room loads. The current guideline (ASHRAE-*Fundamentals* 2009) includes a minimum of cooling load of 60W/m^2. With today's significantly reduced room loads, however, the load is too high to be applicable. For instance, current guideline requires the highest $T_{0.25}/L$ ratio not exceeding 1.9 for high side-wall grilles. Nevertheless, this dissertation indicates that the ratio can be as large as 3.0 for linear bar grilles as shown in Figure 20b. Therefore, the work will justify reduction of the number of diffusers required to be supplied into a space.

4.1.2 ADPI values at Heating Condition (Investigation 1B)

When warm air is provided in a room, possible thermal-stratification prohibits indoor pollution removal in the occupied zone because warm air stagnates in the upper region of the room. This dissertation section first exemplifies possible thermal stratification issues when $T_{0.25}/L$ ratio is small, then shows ADPI data for the studied diffuser types. It is followed by an ADPI selection guide for heating mode. Results for this heating mode are presented using the measured ADPI data in the same manner as the cooling mode in the section 4.1.1.

Figure 21 illustrates two examples of average vertical temperature distributions in the test chamber using round ceiling diffusers at two different supply airflow rates. The two cases both have an ADPI nearly 95% in terms of the heating ADPI model. The diffuser for the high thermal stratification case shown in Figure 21a has a low $T_{0.25}/L$ ratio of 0.75. Hence, the warm air provides a decreased momentum to mix with the air in the occupied zone and stagnates above due to buoyancy. A greater temperature gradient can be observed in the upper region. As a result, the ventilation strategy might be flawed due to the stagnant air in the lower and occupied space, even though the calculated ADPI may be as high as 95%. In contrast, the second example presented in Figure 21b shows a low thermal stratification in the whole space because of a greater $T_{0.25}/L$ ratio of 2.1 and as a result of a stronger mixing effect. Figure 21 implies that a low $T_{0.25}/L$ in the diffuser selection and layout may result in poor indoor air quality even though ADPI is high in the occupied zone. Therefore, this investigation adds an additional criterion of the acceptable maximum vertical temperature gradient of 3^{o}C to the heating mode ADPI method as described in last chapter.

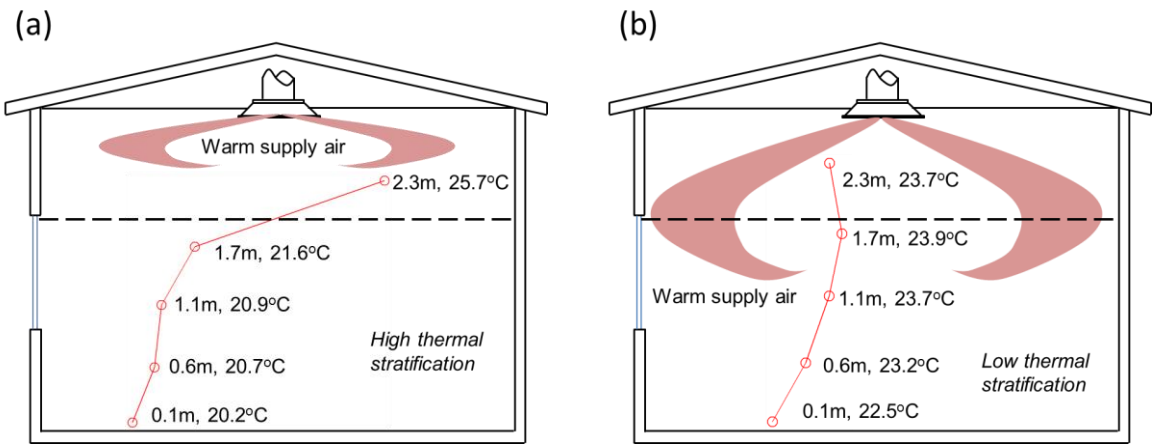

Figure 21: Examples of thermal stratifications in the chamber using round ceiling diffusers; (a) High thermal stratification; (b) Low thermal stratification.

The ADPI as a function of $T_{0.25}/L$ for the 13 diffuser types is shown in Figure 22. The results for each diffuer type aggregate measured ADPI for different diffuser sizes and manufactures. The second-order polynomial curve fitting is applied to generate ADPI profiles described in the illustration of Figure 2 (Chapter 2.1). In Figure 22**,** the ADPI of the adjustable blade grilles statistically increases gradually with $T_{0.25}/L$ because a greater $T_{0.25}/L$ can create better mixing while maintaining an acceptable air speed. In the range of $T_{0.25}/L$ from 0.5 to 2.2, ADPI is higher than 80% except for the point with the largest $T_{0.25}/L$. The reason is that the grille used in the measurement of this point has a smaller net area. This results in the jet from the grille having an air speed exceeding 0.35m/s at more regions in the occupied zone. It should also be noted that high thermal stratification occurs when $T_{0.25}/L$ is less than 1.1 resulting in the warm supply air stagnating in the upper region of the room and leaving the occupied zone poorly ventilated. Consequently, ventilation designs for heating mode should avoid this lower $T_{0.25}/L$ range.

The highest ADPI for round ceiling diffusers occurs in the lower and higher $T_{0.25}/L$ ratios. However, when $T_{0.25}/L<1.4$, warm air stays above the occupied zone and most locations in the occupied zone fall into the EDT comfort region only because of low air movement. However, the

temperature gradient in this range of $T_{0.25}/L$ exceeds the ADPI criterion (3^{o}C per meter vertically), so this range should be avoided.

The airflow delivered by plaque face diffusers has an increased Coanda effect because of a small opening height (~1 to 2cm). Hence, the airflow from these diffusers tends to be attached to the ceiling especially for heating mode conditions. To overcome possible thermal stratification, $T_{0.25}/L$ needs to be at least as large as 2.1 as demonstrated in Figure 22**.** The linear slot diffuser shows ADPI values greater than 80% at a large $T_{0.25}/L$ range of 1.3-3 without thermal stratification issues.

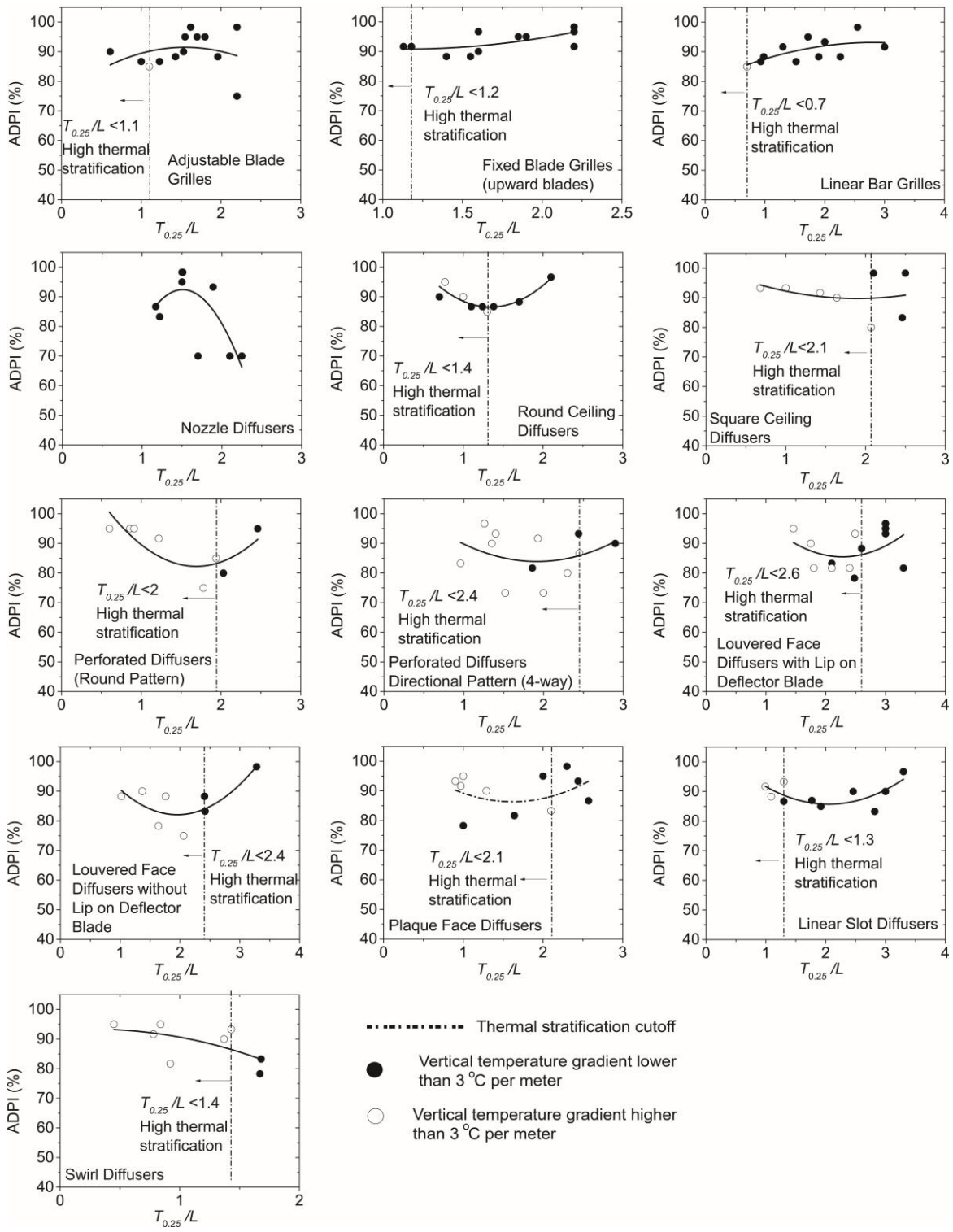

Figure 22: ADPI values *vs.* $T_{0.25}/L$ for diffusers/grilles under heating condition (35-40 W/m^2).

Figure 22 shows that a larger $T_{0.25}/L$ could reduce thermal stratification for all types of diffusers/ grilles. The reason is that jet momentum will be increased and therefore exert greater impact on the jet than buoyant effect. The comparison of buoyant effect and jet momentum (inertial) effect can be represented by Archimedes number. A smaller Archimedes number denotes a lower effect of buoyancy force due to temperature difference, leading to a higher ADPI value. Even though Archimedes number might be an indicator of ADPI for heating mode, it is not directly linked as $T_{0.25}/L$ to diffuser/ grille properties. The Archimedes number is also very useful to characterize the impact of the height of the room on the buoyancy effect under heating condition. Nevertheless, this investigation considers a fixed room height and therefore the Archimedes number is a function of only temperature difference between supply and room air, and also jet momentum rather than room size. To use Archimedes number as a design parameter in diffuser/ grille selection procedure, an HVAC designer needs more input variables; among them is the jet discharge velocity that is not often provided in the diffuser/ grille manufacturer catalogs. Consequently, this dissertation reports ADPI as a function of $T_{0.25}/L$ rather than Archimedes numbers.

By summarizing the ADPI data for diffusers in Figure 22**,** the paper provides an ADPI selection guide for heating mode when using one of the 13 diffuser types presented in Table 14. The selection guide provides the maximum ADPI for each diffuser type and the range of $T_{0.25}/L$ that can create an ADPI greater than 80%. The uncertainty of the maximum ADPI for each diffuser type is represented by 95% confidence interval for the mean response at various $T_{0.25}/L$. The linear bar grilles and round ceiling diffusers have larger ranges of $T_{0.25}/L$ ratios (0.7-3 and 1.4-2.1) that generate a large ADPI (>80%) for high sidewall and ceiling diffusers, respectively. The ceiling slot diffusers have a range from 1.3 to 3 for ADPI higher than 80%. The large ranges indicate the robustness of diffusers for variable air volume (VAV) systems.

Additionally, it should be pointed out that the ADPI methods in this dissertation are only applicable for well-mixed office-type buildings. ADPI methods could be misleading for other

ventilation systems, for instance underfloor and displacement ventilation, One should be very cautious to apply ADPI results from this dissertation in the spaces far different from office-type ones, such as airport terminal.

Terminal Device	$T_{0.25}/L$ for Max. ADPI	Maximum ADPI (95% confidence interval)	$T_{0.25}/L$ range (ADPI>80%)
Adjustable Blade Grilles (High Sidewall installation)- 45° upward blades	1.1	100±7%	0.6-1
Adjustable Blade Grilles (High Sidewall installation)- 0° horizontal blades	1.6	91±4%	1.1-2.2
Adjustable Blade Grilles (High Sidewall installation)- 45° downward blades	0.7	85±7%	0.6-0.8
Fixed Blade Grills(High Sidewall installation)-15° upward blades	2.2	97±3%	1.2-2.2
Fixed Blade Grills(High Sidewall installation)-15° downward blades	1.3	87±4%	1.1-2.2
Linear Bar Grilles (High Sidewall installation)	2.5	93±3%	0.7-3
Nozzles(High Sidewall installation)	1.5	92±7%	1.2-1.9
Round Ceiling Diffuser	2.1	96±3%	1.4-2.1
Square Ceiling Diffuser	2.5	91±9%	2.1-2.5
Perforated Diffusers-Round Pattern	2.5	91±9%	2-2.5
Perforated Diffusers- Directional Pattern (4-way)	2.4	90±10%	2.4-2.9
Louvered Face Diffusers-with Lip on Deflector Blade	3	93±6%	2.6-3.3
Louvered Face Diffusers-without Lip on Deflector Blade	3.3	90±10%	2.4-3.3
Plaque Face Diffusers	2.3	90±6%	2.1-2.6
Linear Slot Diffusers	3	91±4%	1.3-3
Swirl	1.7	91±9%	1.4-1.7

Table 14: ADPI Selection Guide for Heating Mode (35-40W/m^2).

Figure 23 compares the ranges of $T_{0.25}/L$ values that are capable to create an indoor air distribution with ADPI greater than 80%. It turns out that linear bar grilles and linear slot ceiling diffusers have the largest range for the heating condition.

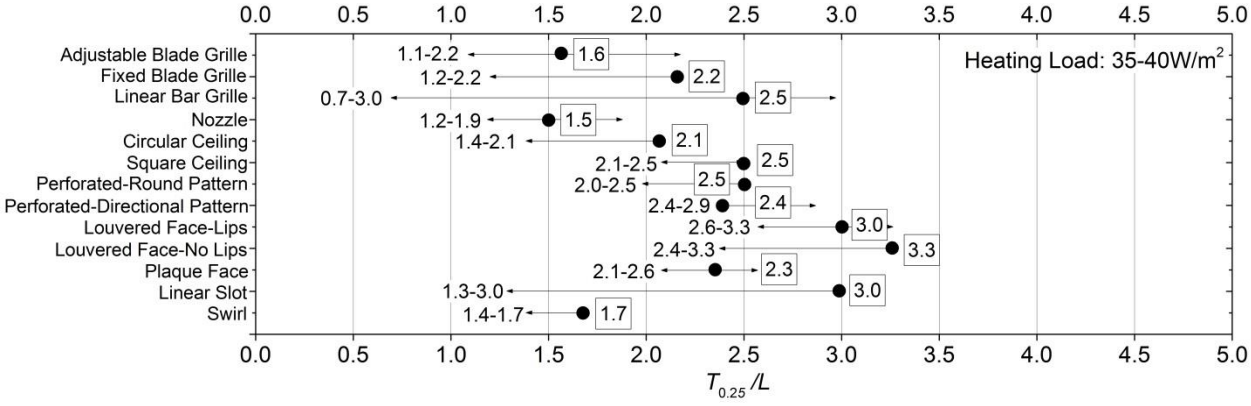

Figure 23: The ranges of $T_{0.25}/L$ for various diffuser types when ADPI higher than 80% at heating condition (35-44W/m^2).

The greatly different ADPI values of diffusers/ grilles under heating condition from cooling condition illustrate that current design guideline based on cooling operation only may result in unacceptable thermal stratification or stagnant air in the occupied zone, when the selected diffusers/ grilles operating at low $T_{0.25}/L$ ratios, such as for VAV systems. As a result, HVAC design should consider the operation under both cooling and heating conditions. Furthermore, this investigation compares the effects of blade angle and deflector adjustment on ADPI values (Appendix A). The findings would guide manufacturers to improve the design of their products to generate a more satisfied air distribution.

4.1.3 Average velocity above the floor and in the occupied zone (Investigation 1C)

At a given supply airflow rate, a certain type of diffuser/grille generates a unique steady-state jet. For example, round ceiling diffusers create radial jets, while high sidewall grilles generate compound jets. Entrainments of different jet type might drive indoor air motion differently, causing variations in velocity values. Indoor air velocity is a critical parameter

affecting many factors related to building science and engineering. The velocity in the occupied zone impacts human thermal sensation and exposure to pollutants, while velocity near a surface influences heat and mass transfer coefficient, and particle re-suspension rate.

This investigation systematically analyzes the measured velocity for ADPI values described in Investigation 1A and 1B. Since all the diffusers explored in this dissertation generally create a mixing ventilation pattern, the results presented herein are valid for a typical office environment. Figure 24 and 25 aggregate the indoor air average velocity in the occupied zone (region in-between 0.1 and 1.7 m above floor) and at the floor level (0.1m above) for different diffuser/ grille types under cooling conditions and heating conditions, respectively. The prediction bands for each correlation represent the expectation to enclose 95% of future data points. The correlations only include the cases for ADPI values greater than 80%, because air distribution design is supposed to maintain an ADPI value above 80%.

Figure 24 and 25 demonstrate that indoor average velocity generally increases linearly with air exchange rate in both the occupied zone (60 sampling locations) and near the floor (15 sampling locations 0.1m above the floor). Other factors, such as diffuser/ grill mounting position and room load, contribute the variation in velocity. The type of ceiling diffusers appears to be less sensitive to air exchange rate than the type of high sidewall grilles. Also, the uncertainty of velocity for the high sidewall type is greater, as suggested by wider prediction bands of the correlations. When compared to cooling operation, the overall velocity for all scenarios under heating conditions is smaller and varies slightly with air exchange rate. Another major finding is that different diffuser types, such as round ceiling, plaque face ceiling and square ceiling diffusers positioned at the same mounting position create similar average velocities, as implied by Figure 24 and 25.

Linearly increased average velocity with air exchange rate improves room air motion and would therefore reduce human exposure to pollution in mixing ventilation buildings. A previous study on air distribution in rooms (Bennett et al. 2000) indicates that the effect of air exchange

rate on exposure is linear for both breathing zone and other specific room locations even under incomplete mixing of pollutants, which also implied that indoor velocity could be linearly correlated with air exchange rate.

Table 15 summarizes linear correlations of air exchange rate and indoor air velocity in the occupied zone and above the floor as plotted in Figure 24 and Figure 25. Although the only variable (air exchange rate) is sufficient to generate a relatively strong prediction, it is worthwhile to examine other factors contributing to indoor air velocity. Because room air motion is mainly driven by jets from diffusers/ grilles, the jet momentum could also be an important contributor. The discharge velocity of jets from diffusers / grilles for jet momentum calculation can be determined by the use of diffuser / grille sizes described in Table 6.

This investigation correlates jet momentum with air velocity as described in Table 16. Results show that the overall correlations are a little weaker for momentum than for air exchange rate (shown in Table 15). However, air velocity in the occupied zone and above the floor is linearly rising when correlated with momentum or air exchange rate. The reason for this is that jets produced by high sidewall grilles are less likely to be attached to ceiling or walls and therefore exert a larger influence on the occupied zone and floor region than those produced by ceiling diffusers. Consequently, multiple regressions using both air exchange rate and jet momentum generate better predictions of air velocity as suggested by adjusted R^2 in Table 17. Furthermore, the effect sizes of air exchange rate and jet momentum are analyzed by analysis of variance (ANOVA) summarized in Table 18. Generally, the results show that air exchange rate is a better indicator of indoor velocity than jet momentum in spaces with mixing ventilation. The reason is that jets from diffusers/ grilles are normally designed to be attached to interior surface to reduce draft. Hence, occupied zone is not directly affected by jets.

This investigation provided correlations of air velocity with air exchange rate and jet momentum in a room with the most applicable diffuser types and room loads. These correlations allow an estimation of room air speed using the most achievable variable, air exchange rate.

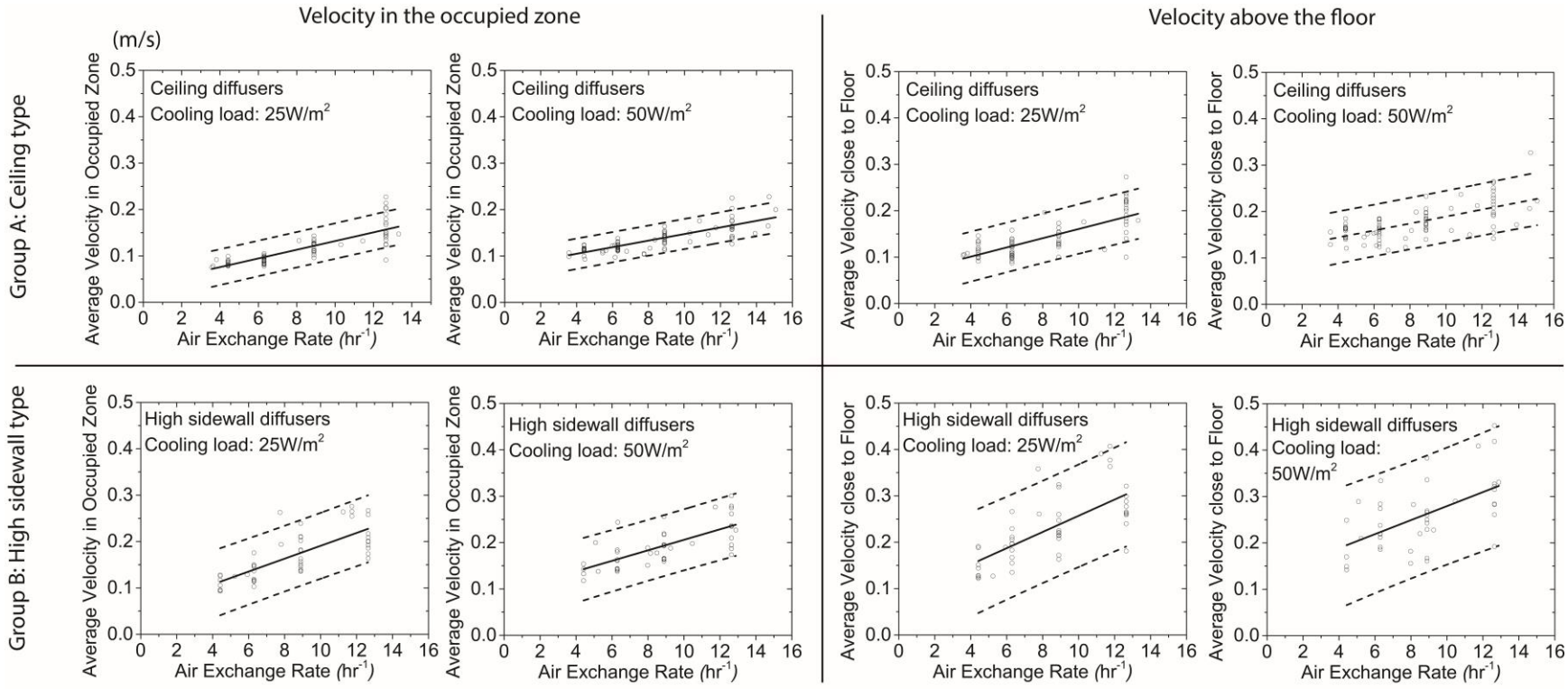

Figure 24: Indoor average air velocity in the occupied zone and close to the floor (0.1m above) under cooling condition; Solid line: linear curve-fitting; Dash line: prediction band of the curve-fitting.

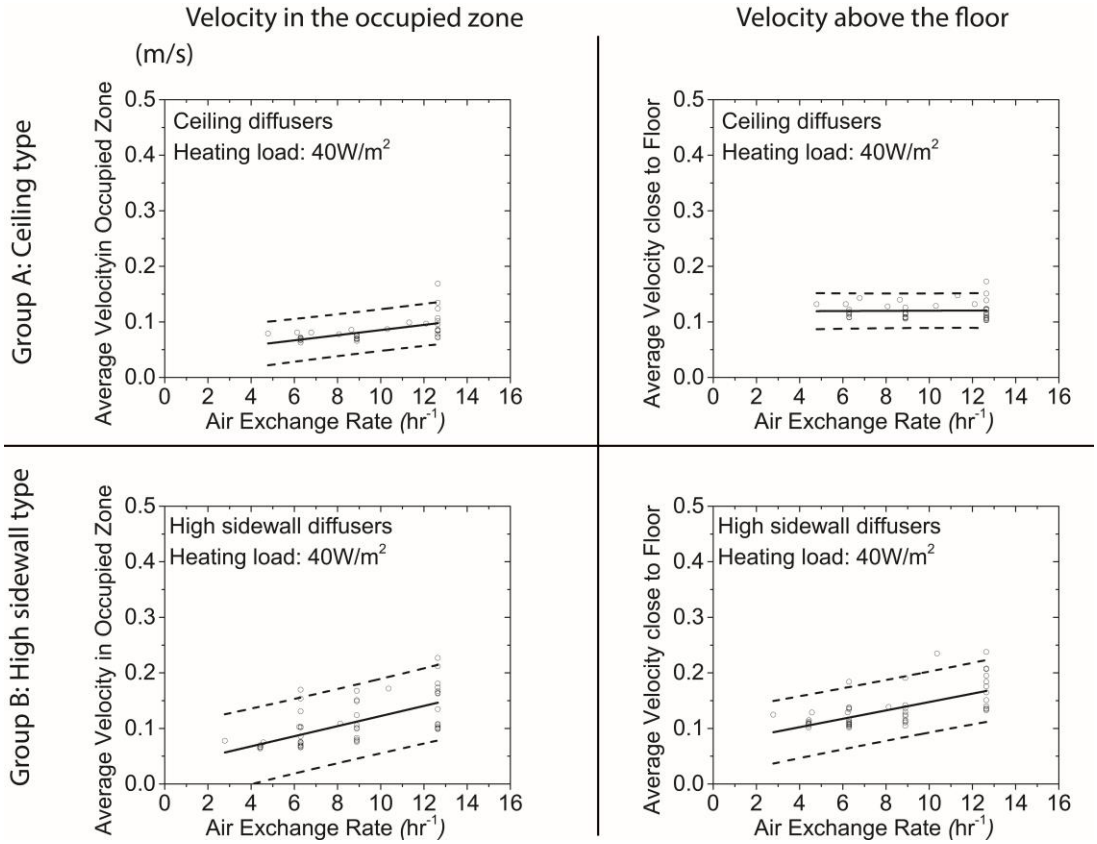

Figure 25: Indoor average air velocity in the occupied zone and close to the floor (0.1m above) under heating condition; Solid line: linear curve-fitting; Dash line: prediction band of the curve-fitting.

Mounting position	Indoor loading (W/m^2)	Average velocity (cm/s) (in the Occupied zone)	Mounting position	Indoor loading (W/m^2)	Average velocity (cm/s) (0.1m above the floor)
Group A: Ceiling type	25 (cooling)	$\bar{V}$=0.99·ACH+3.56 (N=84, adjusted R^2=0.66)	Group A: Ceiling type	25 (cooling)	$\bar{V}$=1.08·ACH+5.67 (N=84, adjusted R^2=0.51)
	50 (cooling)	$\bar{V}$=0.71·ACH+7.63 (N=88, adjusted R^2=0.67)		50 (cooling)	$\bar{V}$=0.75·ACH+11.39 (N=88, adjusted R^2=0.44)
	100 (cooling)	$\bar{V}$=0.69·ACH+10.69 (N=19, adjusted R^2=0.61)		100 (cooling)	$\bar{V}$=0.54·ACH+17.82 (N=19, adjusted R^2=0.18)
	35-40(heating)	$\bar{V}$=0.46·ACH+3.89 (N=41, adjusted R^2=0.29)		35-40 (heating)	$\bar{V}$=0.015·ACH+11.86 (N=41, adjusted R^2=0: almost flat curve)
Group B: High sidewall type	25 (cooling)	$\bar{V}$=1.39·ACH+5.2 (N=49, adjusted R^2=0.57)	Group B: High sidewall type	25 (cooling)	$\bar{V}$=0.75·ACH+8.228 (N=49, adjusted R^2=0.47)
	50 (cooling)	$\bar{V}$==1.13·ACH+9.28 (N=43, adjusted R^2=0.49)		50 (cooling)	$\bar{V}$=0.91·ACH+3.13 (N=43, adjusted R^2=0.31)
	35-40 (heating)	$\bar{V}$==0.91·ACH+3.13 (N=57, adjusted R^2=0.4)		35-40(heating)	$\bar{V}$=0.754·ACH +7.205 (N=57, adjusted R^2=0.4)

Table 15: Summary of correlations of indoor air velocity and air exchange rate (ACH, hr^{-1}) under cooling and heating conditions.

Mounting position	Indoor loading (W/m^2)	Average velocity (cm/s) (in the Occupied zone)	Mounting position	Indoor loading (W/m^2)	Average velocity (cm/s) (0.1m above the floor)
Group A: Ceiling type	25 (cooling)	$\bar{V}$=4.5·M+8.32 (N=84, adjusted R^2=0.61)	Group A: Ceiling type	25 (cooling)	$\bar{V}$=4.71· M+11.01 (N=84, adjusted R^2=0.43)
	50 (cooling)	$\bar{V}$=2.14·M+11.88 (N=87, adjusted R^2=0.33)		50 (cooling)	$\bar{V}$=1.77·M+16.27 (N=87, adjusted R^2=0.12)
	100 (cooling)	$\bar{V}$=0.83·M+16.42 (N=19, adjusted R^2=0.02)		100 (cooling)	$\bar{V}$=-0.36·M+23.11 (N=19, adjusted R^2=0)
	35-40 (heating)	$\bar{V}$=2·M+6.1 (N=41, adjusted R^2=0.51)		35-40 (heating)	$\bar{V}$=0.41·M+11.52 (N=41, adjusted R^2=0.02)
Group B: High sidewall type	25 (cooling)	$\bar{V}$=3.21·M+14.6 (N=48, adjusted R^2=0.39)	Group B: High sidewall type	25 (cooling)	$\bar{V}$=5.01·M+19.38 (N=48, adjusted R^2=0.49)
	50 (cooling)	$\bar{V}$=2.76·M+17.02 (N=41, adjusted R^2=0.39)		50 (cooling)	$\bar{V}$=5.08·M+22.14 (N=41, adjusted R^2=0.49)
	35-40 (heating)	$\bar{V}$=5.85·M+8.16 (N=56, adjusted R^2=0.29)		35-40(heating)	$\bar{V}$=5.85·M+10.95 (N=56, adjusted R^2=0.43)

Table 16: Summary of correlations of indoor air velocity and steady jet momentum (M, $Kg·m/s^2$) under cooling and heating conditions.

Mounting position	Indoor loading (W/m^2)	Average velocity (cm/s) (in the Occupied zone)	Mounting position	Indoor loading (W/m^2)	Average velocity (cm/s) (0.1m above the floor)
Group A: Ceiling type	25 (cooling)	$\bar{V}$=0.62·ACH +2.3·M+4.87 (N=84, adjusted R^2=0.73)	Group A: Ceiling type	25 (cooling)	$\bar{V}$=0.75·ACH+2.04·M+6.83 (N=84, adjusted R^2=0.54)
	50 (cooling)	$\bar{V}$=0.73·ACH-0.12·M+7.56 (N=87, adjusted R^2=0.67)		50 (cooling)	$\bar{V}$=0.95·ACH-1.17·M+10.65 (N=87, adjusted R^2=0.46)
	100 (cooling)	$\bar{V}$=0.80·ACH-0.74·M+10.22 (N=19, adjusted R^2=0.63)		100 (cooling)	$\bar{V}$=0.85·ACH-2.04·M+16.54 (N=19, adjusted R^2=0.32)
	35-40 (heating)	$\bar{V}$=0.05·ACH +1.87·M+5.73 (N=41, adjusted R^2=0.50)		35-40 (heating)	$\bar{V}$=-0.16·ACH+0.8·M+12.65 (N=41, adjusted R^2=0.04)
Group B: High sidewall type	25 (cooling)	$\bar{V}$=1.13·ACH +2.21·M+5.75 (N=48, adjusted R^2=0.74)	Group B: High sidewall type	25 (cooling)	$\bar{V}$=1.31·ACH+3.85·M+9.19 (N=48, adjusted R^2=0.73)
	50 (cooling)	$\bar{V}$=0.93·ACH+2.09·M+9.37 (N=41, adjusted R^2=0.71)		50 (cooling)	$\bar{V}$=1.11·ACH+4.29·M+13.07 (N=41, adjusted R^2=0.65)
	35-40 (heating)	$\bar{V}$=0.70·ACH+3.55·M+3.33 (N=56, adjusted R^2=0.48)		35-40(heating)	$\bar{V}$=0.51·ACH+4.17·M+7.43 (N=56, adjusted R^2=0.58)

Table 17: Summary of multiple regression of indoor air velocity with air exchange rate (ACH, hr^{-1}) and steady jet momentum (M, $Kg \cdot m/s^2$) under cooling and heating conditions.

Mounting position	Indoor loads (W/m2)	ANOVA for velocity in occupied zone					ANOVA for velocity above the floor (0.1m)			
		Variables	Df	Sum of Squares	F value	Significance	Df	Sum of Squares	F value	Significance
Group A: Ceiling type	25 (cooling)	ACH	1	803.09	203.899	<2.2E-16***	1	959.14	92.81	3.96E-15***
		Momentum	1	86.83	22.04	1.06E-05***	1	68.27	6.6	1.20E-02*
		Residuals	82	322.97			82	847.38		
	50 (cooling)	ACH	1	467.66	174.701	<2E-16***	1	524.59	70.7	8.49E-13***
		Momentum	1	0.32	0.12	7.29E-01	1	33.01	4.44	3.79E-02*
		Residuals	85	227.54			85	630.63		
	100 (cooling)	ACH	1	86.58	32.73	2.50E-05***	1	52.835	6.23	2.31E-02*
		Momentum	1	5.54	2.09	1.66E-01	1	41.447	4.89	4.09E-02*
		Residuals	17	44.96			17	143.99		
	35-40 (heating)	ACH	1	60.07	25.25	1.16E-05***	1	60.074	25.25	1.16E-05***
		Momentum	1	41.82	17.57	1.53E-04***	1	41.817	17.57	1.53E-04***
		Residuals	39	92.78			39	92.781		
Group B: High sidewall type	25 (cooling)	ACH	1	795.43	107.865	1.20E-13***	1	1262.59	86.08	4.17E-12***
		Momentum	1	232.46	31.52	1.09E-06***	1	708.21	48.28	1.09E-08***
		Residuals	46	339.22			46	674.7		
	50 (cooling)	CH	1	434.03	70.95	2.60E-10***	1	776.57	39.51	2.08E-07***
		Momentum	1	184.45	30.15	2.63E-06***	1	774.3	39.4	2.14E-07***
		Residuals	39	238.57			39	766.44		
	35-40 (heating)	ACH	1	410.66	43.38	1.93E-08***	1	282.23	54.62	9.54E-10***
		Momentum	1	89.69	9.47	3.27E-03**	1	123.87	23.97	9.23E-06***
		Residuals	54	511.09			54	278.98		

*** $p<0.001$; ** $p<0.01$; * $p<0.05$

Table 18: Analysis of variance (ANOVA) with factors of air exchange rate (ACH, hr^{-1}) and steady jet momentum (M, $Kg \cdot m/s^2$).

Figure 26 summarizes median velocities of all the tested conditions including different air exchange rates, diffuser/ grille mounting positions and room loads. It is observed that the high sidewall type grilles (Group B) generate median velocity 50-70% higher than ceiling type diffusers (Group A) under cooling condition. However, only less than 30% is found under heating mode in Figure 26. Also, this indoor velocity analysis shows that median velocity in the vicinity of the floor (0.1m above) is approximately 30% - 50% greater than that in the occupied zone.

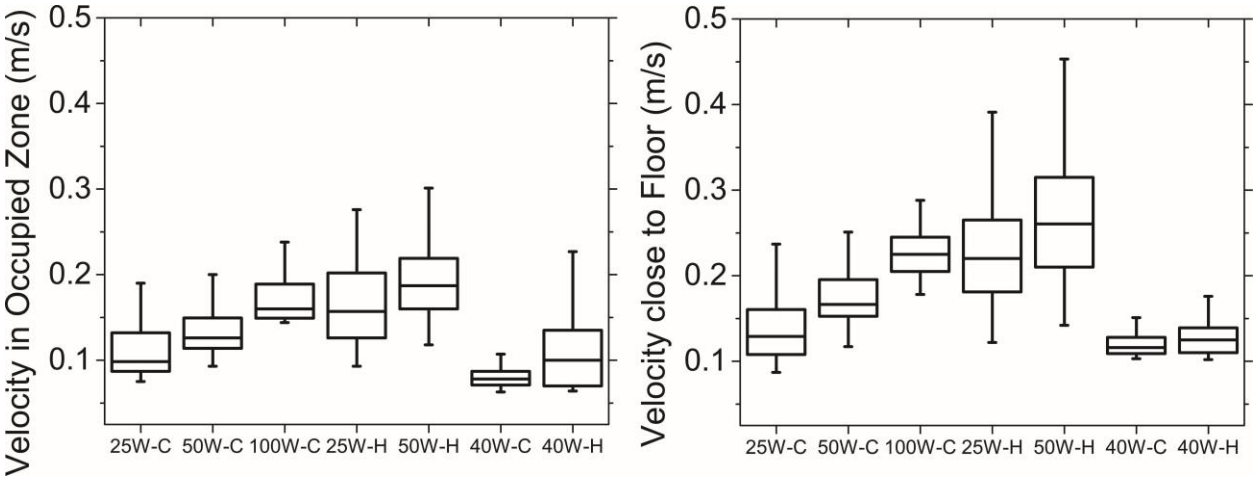

Figure 26: Indoor air velocity above the floor and in the occupied zone (Notation: "C" refers to Ceiling installation; "H" denotes High sidewall installation; 25W, 50W and 100W are cooling loads per square meters of the floor; 40W is the heating load per square meters of the floor).

This investigation presents a systematical analysis of indoor air velocity and will help with future research associated with thermal comfort, pollutant transport and heat transfer. The first implication of this investigation is that air velocity is linearly correlated with air exchange rate for office-type buildings. This enables analytical analysis of particle dynamics, as drag force is a function of air velocity in different conditions. Secondly, this investigation enhances the knowledge of diffuser/grille types affecting air motion; high side wall grilles generate greater air movement and might improve pollutant removal. Lastly, the results of velocity close to the

floor contribute to prediction of indoor heat and mass transfer, as well as particle re-suspension from the floor.

4.2 VELOCITY FIELD IN AN UNSTEADY COUGH JET (INVESTIGATION 2E)

The objective of this investigation is to analytically analyze unsteady jets considering velocity and penetration distance into a quiescent environment. This investigation for unsteady-state jets reports the penetration distance of 6 cough jets with time as described in Table 8 in chapter 3. Also, the velocity variation in a cough jet region is shown in this investigation. Specifically, this section presents the experimental results of penetration distance as a function of time, and velocity field of a cough jet including visualization of the cough jet and correlation of measured axial velocity with the self-preserving scaling law from Equation 10, which verifies the theoretical analysis.

4.2.1 PENETRATION DISTANCE AND VELOCITY FIELD OF A COUGH JET

Snapshot images of a cough jet with a discharge velocity of 6.0m/s at the center and duration of 1s at various times after initiation of the flow are provided in Figure 27. The smoke visualizations of other coughs are not show herein. The snapshots show that the cough jet is broken into a vortex ring at the tip, referred to as the leading tip, followed by the main flow in the first 0.1s. However, the vortex ring decays quickly in 0.15s after triggering the cough jet. Therefore, the penetration distance is measured from the main flow tip instead of vortex ring to the source opening. The turbulent region starts from the transition condition to a turbulent jet. The cough jet transports further than 0.2m during the first 0.1s. Since the jet spreads linearly, the spreading rate of the jet can be obtained via the jet shape of the visible edges. The averaged spreading rate (dr_p/dx_p), is in a range of 0.21-0.26.

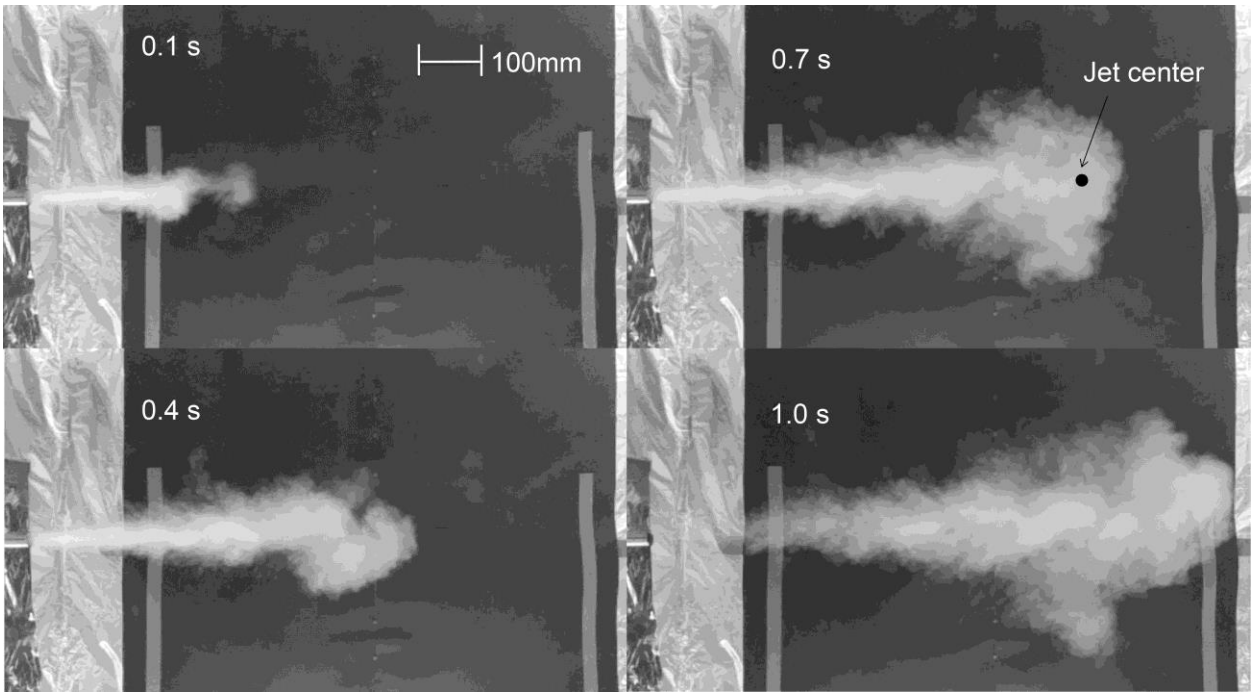

Figure 27: Flow visualization of a cough jet (D=0.024m, U_0=6.0m/s, and Re=9700).

Figure 28 shows the normalized stream-wise penetration distances of the cough jet as a function of normalized time according to the self-preserving scaling of Equation (9), $\frac{S_p - X_0}{D} \sim \left(\frac{U_0 \tau}{D}\right)^n$. The non-dimensional times for the cough (6m/s, 1s) of 0.1s, 0.4s, 0.7s and 1.0s are 25.3 and 101.3, 177.1 and 253 respectively. The curve fit shows that the power n in Equation (9) is 1/2 that is consistent to the study by Sangras et al (2002). In addition, this investigation compares dynamics of the six jets with a real cough reported by Nishimura et al. 2013. The penetration distance in Figure 28 follows the correlation of Equation 9 well in the whole range of dimensionless time investigated in experiments for the six jets and the reported real cough. It is worth noting that the dimensionless penetration distance shown in Figure 28 is horizontal distance from the human volunteer mouth (Nishimura et al. 2013) to the frontal tip of the real cough. The reason is that the real cough is non-isothermal and the buoyancy force will break the conservation of vertical momentum.

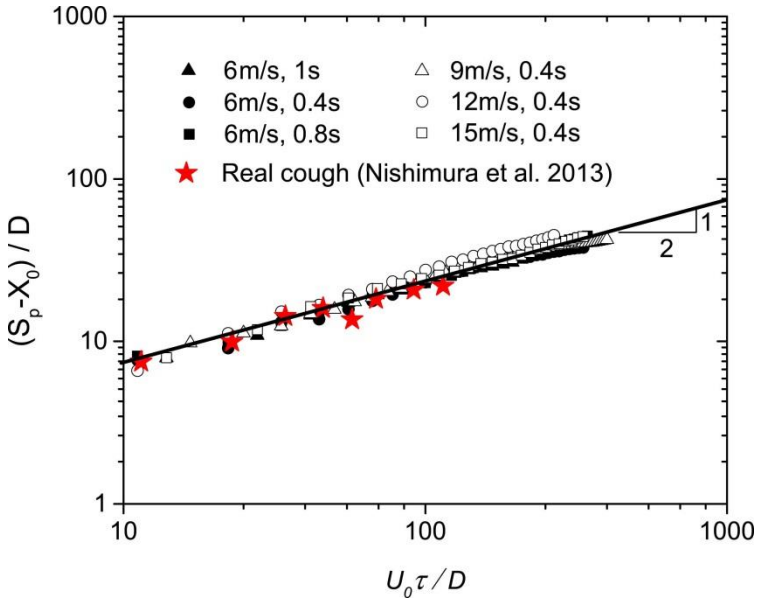

Figure 28: Penetration distance of a cough jet as a function of time.

Self-preserving in Equation 10 shows that the cough jet also has a linear decay of centerline velocity similar to a steady jet. The average centerline velocities of the cough jet (6m/s, 1s) and a steady jet with an identical discharge velocity are plotted in Figure 29a. When the axial distance X>3D, self-similarity is achieved for the cough jet, and the velocity in the jet center reasonably follows the scaling law of Equation 10, with a constant coefficient K_1=0.29. In the region of X<3D where potential core and mixing layer exist, the center velocity is equal to the discharge velocity in the initialization. It is observed that the centerline velocity in the cough jet, maximum velocity, is lower than that of the steady jet at the same location. This indicates that the calculation of particle trajectories of coughed particles employing a steady jet velocity field is not accurate.

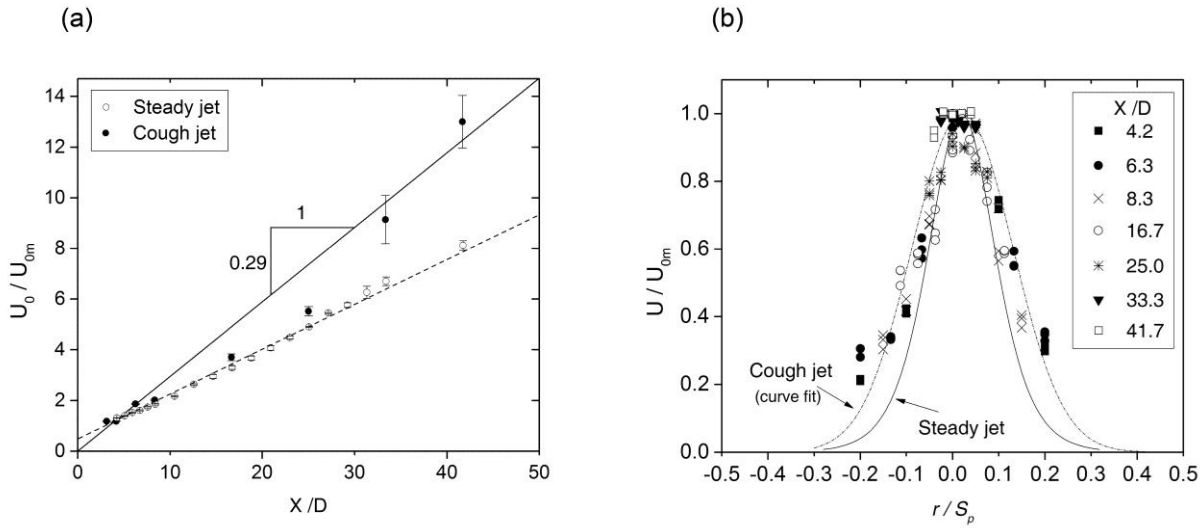

Figure 29: The comparison of velocity fields of a cough jet and steady jet. (a) The centerline velocity of a cough jet and steady jet as a linear function of dimensionless distance; (b) Axial velocity profile through a cough jet center at various *X/D*: 4.2; 6.3; 8.3; 16.7; 25.0; 33.3 and 41.7. Experiments for a steady jet at an identical Reynolds number were conducted by Wygnanski and Fiedler (1969) as described by Equation 12 and 13.

Ghaem-Maghami and Johari (2010) showed that the axial velocity profile through the cough jet center follows a Gaussian function regardless of dimensionless distance, *X/D*. The mean velocity profile for the cough jet is normalized by the velocity at the cough jet center (close to the centerline), U_{0m} and plotted versus radical coordinates, r/S_p in Figure 29b. The axial velocity profiles through the cough jet center follow a Gaussian function Equation 11, $U = U_{0m}\exp(-42.1(r-0.02)^2)$, which is wider than the function for a steady jet with an identical Reynolds number reported by Wygnanski and Fiedler (1969). In other words, the cough jet has a wider radical penetration distance than the steady jet.

Ultimately, this investigation explores the dynamics of unsteady-state cough jets and develops an analytical model of the cough jets concerning velocity field and penetration distance. The results imply that unsteady cough jets, in the ranges of discharge velocities 6-15m/s and the ranges of injection durations 0.3-1s, follow a self-similarity law. The efforts of this investigation about fluid dynamics of a cough jet will help with the prediction of coughed particle transport.

4.3 PARTICLE TRANSPORT ASSOCIATED WITH STEADY-STATE JETS (INVESTIGATION 1D)

This investigation examines the transport of particles inside and outside a steady-state ceiling-attached jet under both cooling and heating conditions. As numerical simulation is powerful tool to simulation indoor particle transmission and provide more detailed information than measurements, this investigation applied both experimental and numerical methodologies. In many situations, indoor particle sources are intermittent, such as particles generated by human activities. Also, air motion driven by supply air jets is very crucial for dispersing particles. A strong air motion surrounding a particle source spreads particles substantially, while a weak one might not transport particles, especially large ones, throughout the room before particle settling. As a result, this investigation presents the results of the concentration distribution of particles in three sizes (0.77, 2.5 and 7μm), when they are released inside and outside of a ceiling-attached jet.

This section is comprised of two main parts: (1) validation of particle simulation using measurements reported in Lu et al. 1996; and (2) Particle transport in a space with steady-state jets created by a ceiling diffuser. This first part provides a validation of RANS-RNG and LES models coupled with Lagrangian particle tracking scheme. The validated models will be applied in the second part, described as follows.

First, the experimental results present the concentration of three sizes of particles (0.77, 2.5 and 7μm) at five locations across the test room with a ceiling-attached jet at cooling condition. The three sizes of particles were released at two locations: inside and outside the jet region. This investigation then compares the measured concentration with numerical predictions using RANS and LES models coupled with Lagrangian-tracking scheme. The purpose of this comparison is to check the performance of the two turbulent models and to validate the capability of Lagrangian-tracking scheme. The last part of this investigation explores the difference of particle transport in the test room when considering the steady-state ceiling-attached jet at cooling mode and heating mode.

4.3.1 The validation of numerical simulation of particles

Since the investigations of particle transport applies CFD numerical simulations, the numerical method conducted in this dissertation was first validated using well established data reported in the literature (Lu et al. 1996). The experimental details were described in the "Methodology" Chapter. Figure 30 shows the comparisons of the mass concentrations in both zones between the numerical simulations and the measurements. The numerical calculation agrees with the experimental data reasonably and indicates that the numerical methodology using RANS and LES in this dissertation is capable of predicting the transport of particles in buildings.

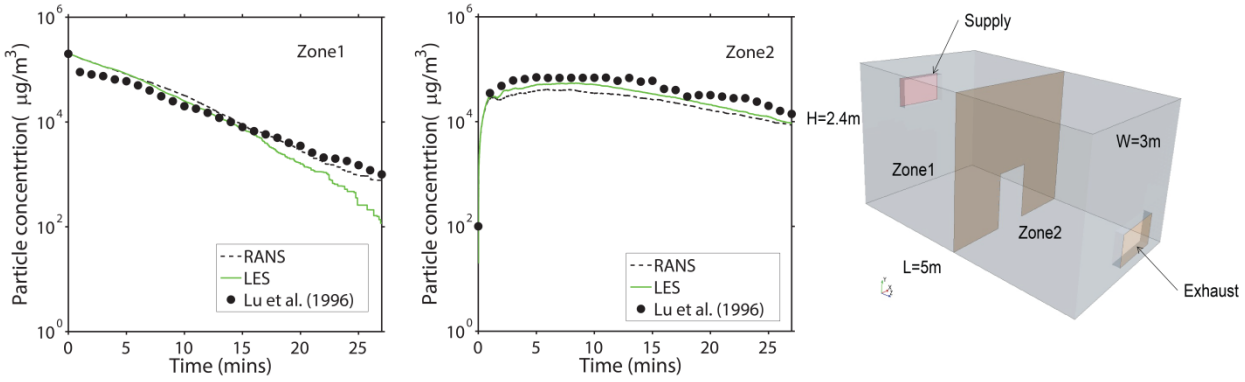

Figure 30: Comparison of measured particle concentration with numerical predictions using RANS-RNG and LES coupled with Lagrangian method.

The validated RANS-RNG-Lagrangian and LES-Lagrangian method were applied to predict particle transport in this investigation related to steady-state jets, as shown in the following sections of numerical simulations.

4.3.2 Transport of particles released from transient sources (Experimental results)

Air motion, particle size and the location of a particle source can affect particle dynamics in a room. The previous sections in this dissertation have discussed air velocity in the full-scale test room with various diffusers/ grilles, and one of the main findings is that specific type of diffusers/ grilles has a small impact on airflow intensity in occupied zone. Therefore, this experimental study of particle distribution with steady-state jets considers only the effects of

particle size and source location. Figure 31 shows the location of the diffuser providing jet and the jet direction, along with 2 source locations and 6 positions for monitoring particle concentration distribution. Source 1 and source 2 are outside and inside the ceiling-attached steady-state jet, respectively. Measurement of particle concentration at 5 locations was repeated at least 3 times and the shade areas around each curve in Figure 31 represent standard deviation calculated based on these repeated measurements. The reference concentration, C_{ref}, refers to the average concentration over 1200 seconds at the exhaust (P2) of the chamber for 0.77μm and 2.5μm particles, while the concentration of 7μm particles was normalized by the instantaneous average concentration, C^*_{ref}, at all the five sampling locations.

When particles were released inside the jet region (Source 2), the concentrations at five locations show a very similar trend for both 0.77 and 2.5μm particles. This implies that the steady-state jet created by diffusers/grilles dominates particle dynamics (PM2.5) when the particle source resides in the jet region. However, gravity settling makes the concentration of 7μm particles to decrease with height. Figure 31 also indicates that the concentration of 0.77 and 2.5μm particles has a more uniform distribution than 7μm particles under cooling condition.

When the particle source resides out of the jet region (Source1), particle concentration mainly depends on the local air motion during the injection period. The example of this air motion during would be a flow driven by human buoyancy. Figure 31 also shows that the concentration at P6 right above the particle source is approximately two orders of magnitude higher than at other locations, especially for 0.77μm particles. Nevertheless, this difference disappears after particle injection period and when the particle cloud gets depressed through the space. This causes all concentration curves to collapse onto one. The results indicates that particle source locations only affect particle transport during the injection period and the relatively short period after it, when diffuser/ grille - created jets provide an acceptable air distribution (ADPI>80%) and well-mixed-air environment.

Additionally, 0.77 and 2.5μm particles approach a relatively uniform concentration in the room shortly after the particle injection finishes. However, the gravitational forces become competing with drag forces for 7 μm particles, leading to a non-uniform concentration distribution in the room (Figure 31).

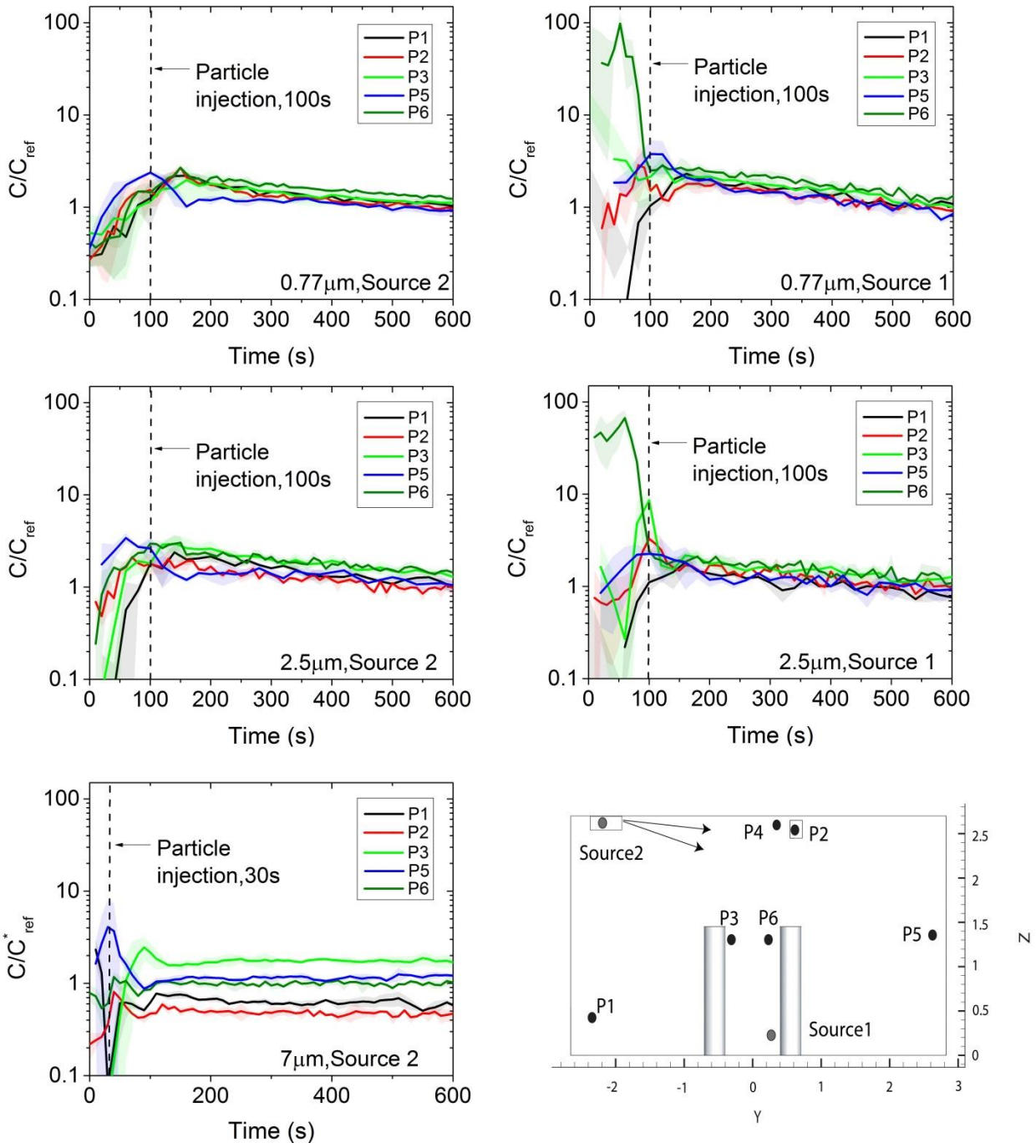

Figure 31: The variation of particle concentration in the full-scale room with a ceiling-attached jet (cooling condition, ACH=3.2 hr^{-1}, exhaust: P1; curve shades represent uncertainty).

The peak concentration during the particle release and particle distribution after the source decay should help with selecting appropriate method for exposure analyses, especially when considering peak and/or cumulate exposure. The results should help with identifying in which situation and for which particles size the assumption of perfect mixing may produce reasonable results, and in which situation the non-uniformity and/or unsteadiness of the concentration filed should be included in the analyses.

4.3.3 Comparison of numerical results using RANS and LES turbulence models

The numerical validation presented in section 4.3.1 shows that RANS and LES predict similar results of particle concentration in a room ventilated by a steady-state jet. The purpose of the comparison of the performance of RANS and LES presented herein is to further examine whether LES is capable to generate way better prediction than RANS-RNG model. The outcome of this effort will offer justification of model selection in the next section 4.3.4 regarding investing particle transport under cooling mode and cooling mode.

Figure 32 provides the experimental results for validation of the numerical simulation of particle modeling when RANS-RNG and LES turbulence models were used. As the concentration at different locations has significant variations primarily during particle injection period, 100s for 0.07 and 2.5μm and 30s for 7μm, Figures 32 and 33 provide comparisons of experimental and CFD results only the first 200 seconds. The transmission of particles released inside the steady-state jet is presented in Figure 32. For 0.77 and 2.5μm particle, there is good agreement between experimental and numerical values of concentration at all locations except for P2, which is attributable to the neglecting of particle deposition on indoor surfaces in the simulations. Comparisons of experimental and numerical concentrations of 2.5μm particles show that the concentration in the strong buoyancy region, P3 and P6, are slightly under-predicted by RANS because the flow fluctuation was not well captured by the RANS model. Also, results show that both LES and RNG predict the concentration of 2.5μm particles relatively well when considering most locations. For the large particles (7μm), numerical simulation under-predicts

concentrations at the location of P3. One possible reason for under-prediction by CFD is deposition of 7μm parcels that was not captured in CFD models due to not sufficiently refined computation mesh at the floor level that caused inaccurate deposition calculation by CFD. Since the experimental validations focused on particle dispersion, however, this discrepancy was not further investigated. As a result, when considering LES and RNG prediction of particle dispersion in well-mixed air environment, there is no obvious advantage in using more computationally intensive LES turbulence model.

When the particle source resides outside of the steady-state jet region, both RANS and LES show reasonable agreement with experimental results as shown in Figure 33. As particles are released in the thermal boundary of a thermal manikin, particles spread unstably in the close proximity to the two manikins, such as P3 and P6. Figure 33 shows that the LES model successfully captures the high level of particle fluctuation in these two locations. In generally, the transport of different size particles can be predicted well using both RANS and LES models.

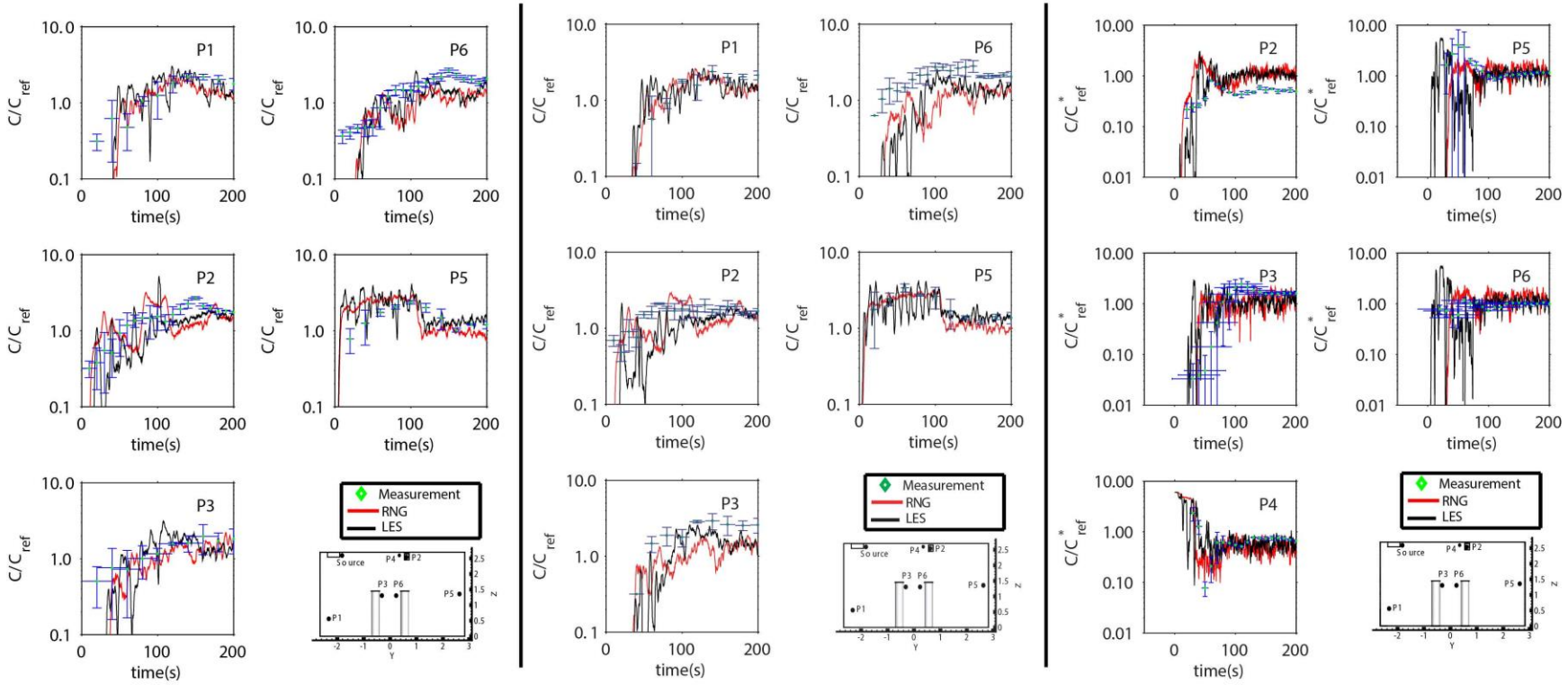

Figure 32: Comparison of experimental and numerical particle (left: 0.77µm; middle: 2.5µm; right: 7µm) concentrations (Source1 inside the steady-state jet at cooling condition); 100s injection of 0.77 and 2.5µm, 30s injection of 7µm.

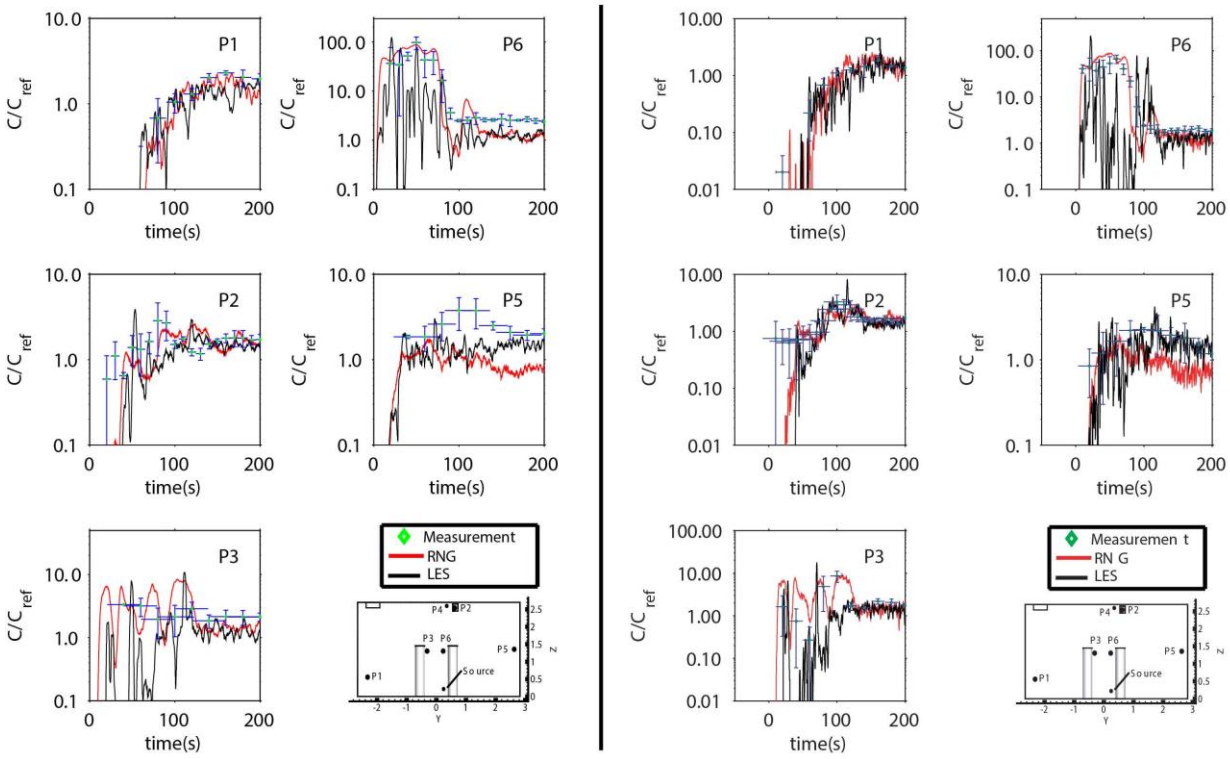

Figure 33: Comparison of experimental and numerical particle (top: 0.77μm; middle: 2.5μm ;) concentrations (Source2 outside the steady-state jet at cooling); 100s injection of 0.77 and 2.5μm.

4.3.4 Comparison of particle transport when a mixing diffuser provides cooling and heating jets

This section offers a further investigation of how a diffuser-created jet affects particle transport under cooling and heating mode. Since a warm jet tends to travel upward because of buoyancy, particles released from a given source might show a different fate from the case under cooling conditions with a cool jet. As the numerical calculation of particle transport in the full-scale room has been validated using experimental results shown in section 4.3.3, this section presents how thermal conditions of the steady-state jets influence the particle transport.

The schematic of the CFD model is illustrated in the methodology section (Figure 13). The thermal back wall in the modeled room provides 320W cooling loads under cooling condition while 320W heating loads under heating condition. Figure 34, Figure 35 and Figure 36

presents the comparison of particle (0.77, 2.5μm and 7um) concentration for the first 6 minutes at 6 locations provide in Figure 31. The results are normalized by the concentration of particles injected in the ceiling-attached jet region (C_{inlet}). Comparison of particle concentrations for the heating and cooling conditions show that a heating/ cooling operation regime matters during the injection period only (<100s for 0.77 and 2.5μm, <30s for 7μm). However, indoor particle concentration tends to achieve relatively uniform after 200 seconds, regardless of the position. In addition, the thermal condition of the supply air jets exerts insignificant effects on particle transport after 200s at all locations. This suggests a relatively small impact of the source location on particle distribution in a space with mixing-type diffusers/ grilles.

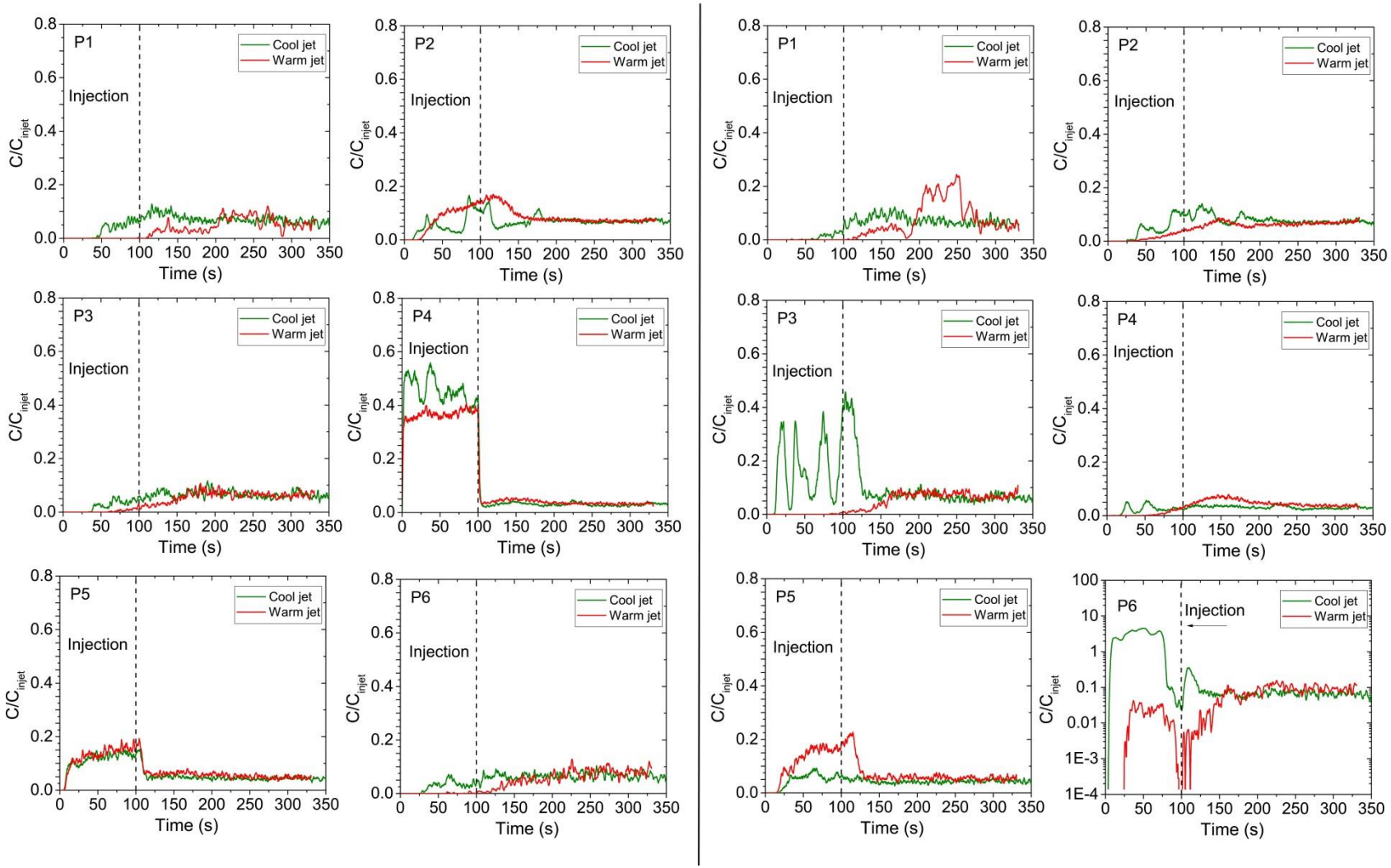

Figure 34: Numerical comparison of particle (0.77μm) concentrations when the full-scale chamber is ventilated at cooling and heating mode; (left): particles are released in the ceiling-attached jet region; (right): particles are released outside the ceiling-attached jet. The positions of sources and sampling locations can be found in Figure 31.

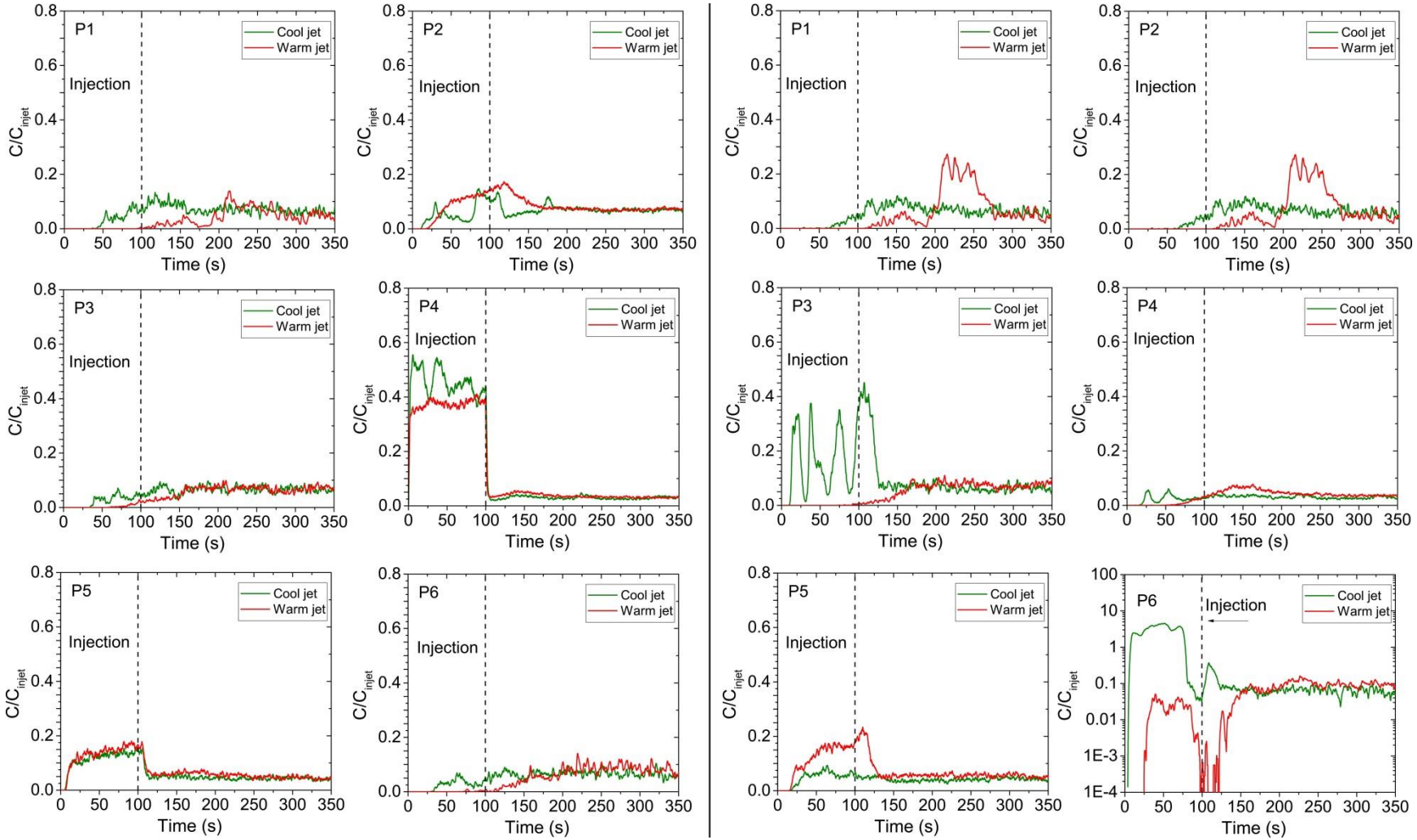

Figure 35: Numerical comparison of particle (2.5μm) concentrations when the full-scale chamber is ventilated at cooling and heating mode; (left): particles are released in the ceiling-attached jet region; (right): particles are released outside the ceiling-attached jet. The positions of sources and sampling locations can be found in Figure 31.

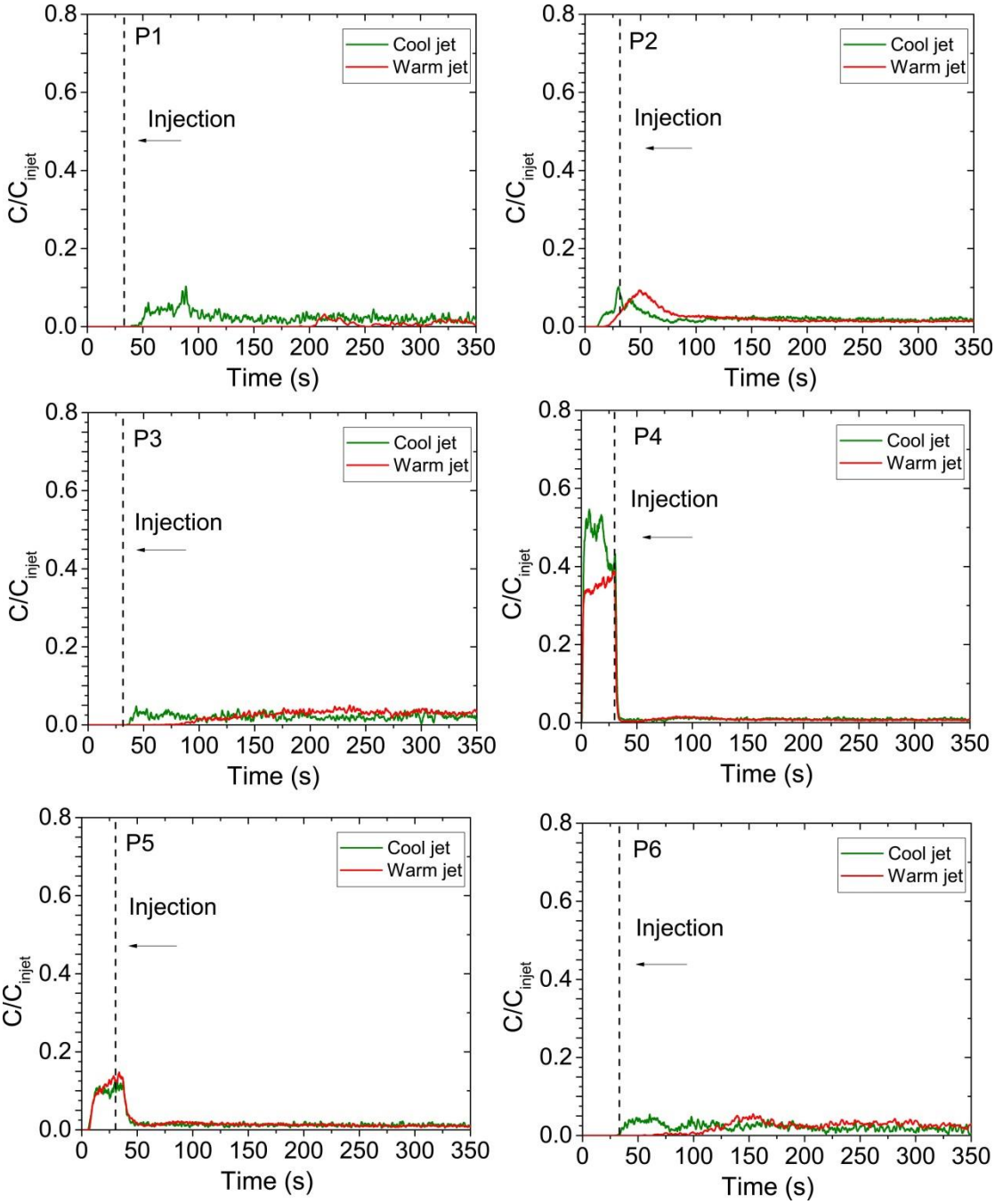

Figure 36: Numerical comparison of particle (7μm) concentrations when the full-scale chamber is ventilated at cooling and heating mode; Particles are released in the ceiling-attached jet region; The positions of sources and sampling locations can be found in Figure 31.

4.4 TRANSPORT OF UNSTEADY COUGHED PARTICLES (INVESTIGATION 2F)

The objective of Investigation 2F is to characterize the transport of particles in various sizes in the cough jet region and surrounding an exposed occupant. The cough jet dynamics dominates the transport of particles in the jet region, while the transport of coughed particles are affected by the interaction of the cough jet and thermal convective flow/ thermal plume of the exposed occupant.

In specific, this investigation compares the trajectories of an individual particle injected by an unsteady-state cough jet and a steady-state jet with the same discharge velocity. In addition, this investigation summaries the concentration of particles of sizes 0.77, 2.5 and 7μm in the vicinity of the exposed occupant as illustrated in Figure 14.

4.4.1 Particle trajectory comparison

This subsection describes the transport/ trajectories of individual particles injected by both the cough jet and room air flow driven by a weak steady-state jet from a floor-level diffuser (ACH=3.5hr^{-1}). Three particle sizes, 0.77, 2.5 and 7μm, were considered, consistent with the sizes used in the transport around the receiver occupant (Figure 14). It should be pointed out that the particles were injected simultaneously with the cough jet. In the potential core and mixing layer the time of particles residing is negligibly small compared to the time spent in the main region (Bocksell 1998). Therefore, the axial velocity in this region was assumed to be identical to the discharge velocity.

Figure 37 shows the trajectories of three size particles following the steady jet and cough jet. It is observed that larger particles have an increased deposition distances than smaller ones. However, the distance even for 7μm particles is only few millimeters, negligible comparing to horizontal penetration. As described in Figure 37(b), the curves

of horizontal penetration for three size particles collapse onto one. The average size of droplet nuclei coughed from healthy subjects is in the range of 0.58-5.42μm (Yang et al. 2007), and the results in Figure 37 suggests that the transport typical size coughed particles are similar in the cough jet region, regardless on their size.

Furthermore, the particles, regardless of size, show a substantial deviation when injected from a steady jet comparing to a cough jet. Overall, the deposition distance of particles in the cough jet is larger than with the steady state jet because of the faster decay of jet velocity (Figure 29) and relatively low velocity magnitude downward the jet. Therefore, particles in the cough jets take longer time to reach a prescribed position. For instance, coughed particles need approximately 1.2s to transport 1.1 meters further away from the jet exit comparing to 0.8s for particles in the steady-state jet.

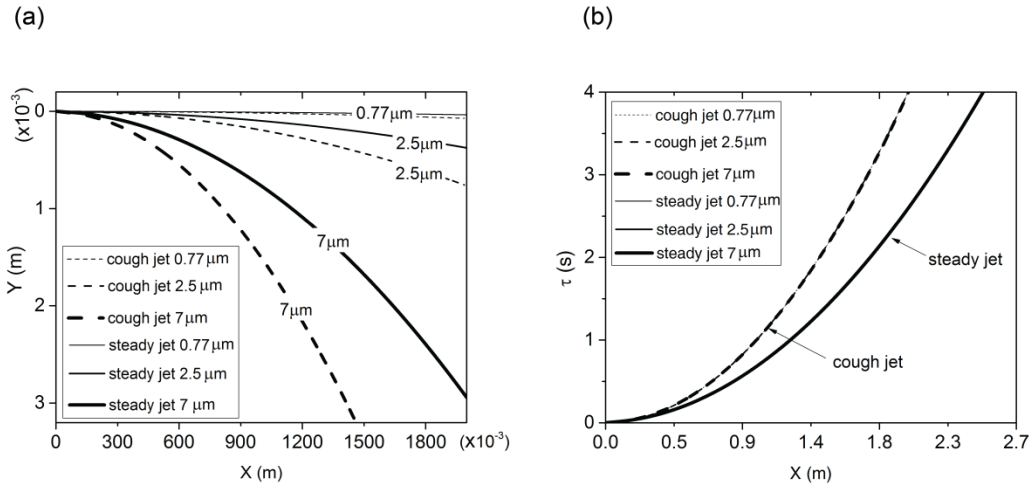

Figure 37: Comparison of trajectories of different size particles following a steady jet and a cough jet (1s duration) with the same discharge velocity, 6m/s; (a) Particle trajectories; (b) The variation of horizontal positions with time.

4.4.2 Human exposure to coughed particles by experimental mesurments

This section provides the concentration of coughed particles injected a cough jet described in last Section 4.4.1 in the vicinity of the receiver occupant (Figure 14). The outcome of this effort will advance the knowledge of human exposure level to coughed particles.

The concentration distribution for particles of three sizes (0.77μm, 2.5μm and 7μm) expelled from a cough jet was measured in the vicinity of the receiver occupant and at the exhaust of the chamber (Figure 14). Figure 38 shows the variation in the normalized distribution of 0.77, 2.5 and 7μm particles emitted by a cough jet. The uncertainties of the concentration (vertical bars) and the concurrence time (horizontal bars) are represented by standard deviations among repeats. Overall, the concentration decays with the increase of particle size in all measured locations around the receiver occupant after the impingement of the cough jet. The results illustrate that different size coughed particles disperse differently in the vicinity of the receiver occupant, unlike in the jet region (cough jet region shown in the smoke visualization in Figure 27). The measured peak concentration of 0.77, 2.5 and 7μm particles in the breathing zone of the receiver occupant, P1, decays to 4.93%, 3.68% and 1.74% of the initial level in the cough box, respectively. It is observed that particle clouds take approximately 1-2 seconds to reach the breathing zone (P1) and rise up to the maximum in 3 seconds for the three size particles. Right above the receiver occupant, P2, the concentration is approximately one order of magnitude lower than that in the breathing zone, P1. This suggests that even 7μm particles can be transported upwards by human thermal plume.

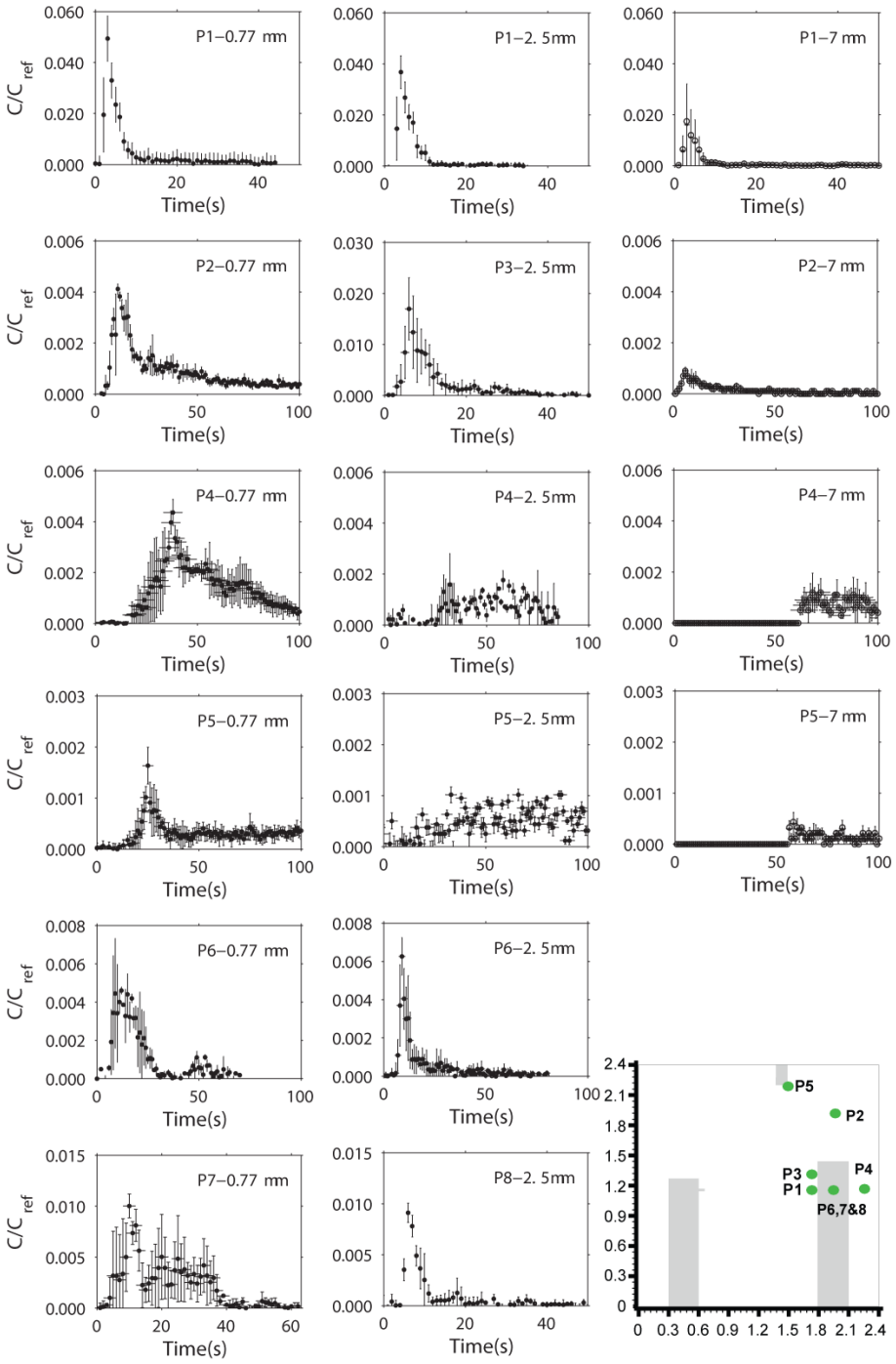

Figure 38: The variation of coughed particle concentration in the vicinity of receiver occupant.

Ultimately, this investigation (2F) about the transport of coughed particles implies that a cough jet presents a similar impact on dispersing particles in the sizes of from 0.77-7μm before the cough jet decays. As the typical size of coughed particle nuclei ranges from 0.58 to 5.42μm (Yang et al. 2007), the outcome of this investigation will advance the state knowledge of coughed particle fate. When the cough jet decays, the exposure level to coughed particles varies substantially with particle size, depending on the interaction of the cough jet with thermal plume. The outcome of this investigation fills the knowledge gaps in person-to-person exposure to coughed particles.

Chapter 5: Conclusions

This dissertation conducted six investigations, addressing the knowledge gaps in air distribution and particle transport associated with steady-state jets created by diffusers/ grilles and unsteady-state coughing jets. Collectively, the six investigations improve the state of understanding of how (1) the steady-state jets above the occupied zone distribute air affecting temperature and velocity filed and transport particles in the occupied zone, and (2) the fluid dynamics of an unobstructed cough together with the thermal plume of a susceptible person affects the distribution of coughed particles.

One of the investigations relates to the development of heating-mode air distribution performance index (ADPI) - a variable that characterizes uniformity of the temperature and velocity field when diffusers/ grilles provide warm jets into a space. In addition, this investigation advances diffuser/ grille selection methodology when the diffuser/ grille operates at cooling mode. The non-dimensional variable characterizing a ratio of jet throw length to the characteristic length of a space ($T_{0.25}/L$), which is employed to define ranges in which diffusers/ grilles provide acceptable air distribution, is determined for all 13 analyzed types of diffusers/ grilles when considering different operation regime (cooling or heating mode) and different room loads. The main finding related to the cooling mode is that for today's typical sensible cooling load in buildings (from 25 to 50 W/m^2) all of 13 types of commercially available diffusers can provide acceptable air distribution (ADPI>80%). The large acceptable ranges of $T_{0.25}/L$ for several of the 13 types of diffusers indicate that they can be more successfully used with variable air volume (VAV) HVAC systems than others; with VAV systems the varying airflow rate results in variation in $T_{0.25}/L$, and the large ranges of $T_{0.25}/L$ in which

ADPI>80% justify the application of VAV-HAVC systems operating at various cooling conditions. Additionally, the main results related to the heating mode operation identify the ranges of $T_{0.25}/L$ resulting in acceptable thermal stratification, providing for the first time diffuser selection guidance under heating condition.

Comparison of thermal sensation regions determined by predicted mean vote (Fanger 1970) with ADPI suggests that ADPI in certain conditions pertains to thermal comfort, and thermal comfort is reflected in the development of ADPI diffuser selection methodology. The implication underlies the understanding of the ADPI method that is mostly regarded as an index representing only indoor thermal uniformity.

The study of indoor air velocity includes a systematic analysis of air speeds from 650 full-scale experiments with various: air diffusers/ grilles (regarding type, manufacturer and sizes), room cooling and heating loads, and supply air flow rates. The spatial average velocities in (1) the occupied zone and (2) the plane above the floor (0.1m) provide correlations that show how these two characteristic velocities vary with operation regime (heating or cooling), diffuser position, and characteristic flow rate defined by air exchange rate (ACH). These correlations are prepared for further application in future studies related to: human thermal sensation, particle removal efficiency, particle re-suspension and gaseous pollutant emission from the floor as well as convection heat transfer analyses. When the cooled air distribution with a ADPI $\geq$ 80%, the median velocities in occupied zone are 0.1m/s - 0.16m/s for ceiling mount diffusers and 0.16m/s - 0.19m/s for side-wall diffusers, depending on the flow rate. However, a smaller median velocity was observed under heating conditions, 0.08m/s for ceiling and 0.1m/s side-wall diffusers. Also, this indoor velocity analysis shows that average velocity

in the vicinity of the floor (0.1m above) is approximately 30% - 50% greater than that in the occupied zone.

To analyze how jets and corresponding air distribution affect particle dispersion, experimental and computational fluid dynamics (CFD) studies were conducted to characterize the transport of particles (0.77, 2.5 and 7μm) released inside and outside of diffuser/ grille jets, under both cooling and heating condition. The results show that 0.77 and 2.5 μm particles injected by intermittent sources (that cover ranges of most common indoor particle sizes) reach relatively uniform spatial concentration shortly after the end of the injection, regardless of indoor thermal condition. This finding suggests that the type and the spatial layout of diffusers/ grilles that satisfy diffuser design criteria (ADPI ≥ 80%) have a relatively small impact on particle distribution when considering intermittent sources of particles.

The study also includes the investigation of unsteady-state jets utilizing an analytical analysis of jet penetration distance for predicting velocity decay and distribution of an unobstructed cough jet. The simple unsteady-state jet has a similar dynamics as a complex human cough when considering traveling in a nearly quiescent environment. Also, the unsteady-state jet, such as cough, has a lower axial velocity but higher expansion rate than a steady one with an identical discharge velocity. Therefore, when compared to particle transport with a steady-state jet, coughed particles take longer time to transport to a specified location in the stream-wise direction. The outcome of this effort provides an analytical model useful to understand cough jet dynamics. The provided model should help with future analyses related to modeling of coughed droplet dynamics including: transmission, settling, evaporation, and coagulation.

The study of coughed particle transport in the vicinity of an exposed person enhances knowledge regarding the interaction of a cough jet with thermal plume of the exposed person and show how this impacts coughed-particles. Even though the trajectories of coughed particles in the jet region imply that the size of typical airborne coughed particles, with the nuclei size 0.35 to 10 μm (Lindsely et al. 2012), has a negligible effect on transmission, different size particles exhibit various transport performances in the vicinity of the recipient occupant. Large particles (e.g. 7μm) have a lower concentration in this zone. The peak concentrations show decreased levels at the position directly above the occupant when compared to the occupant's surroundings, indicating that a cough jet presents a great impact on dispersing particles.

When considering major impacts on building science and engineering, this dissertation provides the update of theoretical and practical knowledge about diffuser performance and design. It helps with improving indoor air distribution and corresponding thermal comfort and air quality parameters. The analytical and numerical models of unsteady cough jet velocity and transport of coughed particles fill the knowledge gap needed for further analyses of disease-carrying particles and human exposure.

Appendices

APPENDIX A: THE EFFECT OF DEFLECTORS ON AIR DIFFUSION PERFORMANCE INDEX (ADPI) OF ADJUSTABLE DIFFUSERS: COOLING CONDITION (RP-1546)

Shichao Liu Atila Novoselac, Ph.D

Student Member ASHRAE *Member ASHRAE*

(Submitted to *HVAC&R*)

Abstract

Diffuser selection guidance listed in ASHRAE Handbook-*Fundamentals* (2009) includes Air Diffusion Performance Index (ADPI) values for horizontal high side-wall grilles and ceiling linear slot diffusers. However, grilles are adjustable at various angles, which generate different airflow patterns in a space and therefore might greatly affect ADPI values. Also, complaints of draft generated by ceiling slot diffusers are common because of inappropriate adjustment of diffuser deflectors. This study measures the ADPI values of three widely used adjustable diffusers - adjustable blade grilles, fixed blade grilles and ceiling linear slot diffusers - at various deflector configurations in a test room with 25W/m^2 (7.9 Btu/hr/ft^2) and 50W/m^2 (15.8 Btu/hr/ft^2) cooling loads. The study explores how deflector adjustments affect diffusers, performance represented by ADPI values. The results show that upward blade deflectors can increase ADPI values greatly for blade grilles. In general, downward jets reduce ADPI values for each adjustable diffuser type operating at cooling conditions. A smoke test can assist in the adjustment of linear slot diffusers to create desired ceiling-attached airflow patterns during commissioning.

Keywords: Diffuser, ADPI, Air Cooling, Deflector angle, Draft

Introduction

Most building Heating, Ventilation and Air Conditioning (HVAC) systems use an all-air delivery method, with the air diffusers/grilles having the task of distributing the conditioned air into the space in a way that provide acceptable thermal comfort for occupants. The current diffuser selection method, described in ASHRAE Handbook-*Fundamentals* (2009), includes 7 types of commonly used diffusers /grilles in the Air Diffusion Performance Index (ADPI) selection guide. Among these types, both high side-wall grilles and ceiling slot diffusers are able to generate various airflow patterns by adjusting the deflectors of the diffusers/grilles (Chow and Wong 1996; Int-Hout 2013). However, the ADPI selection guide is generated based on the studies using standard operation conditions for high side-wall grilles and ceiling slot diffusers: 0^{o} horizontal angle of grille blades and horizontally-opposed adjustment of slot deflectors, respectively (Miller and Nevins 1969, 1970, 1979; Miller 1971; Miller and Nash 1971; Miller and Nevins 1972). The effects of grille deflector angle and slot deflector adjustment are not considered in the ADPI selection guide.

Since an angled-blade grille deflects the supply air from the standard condition, it is expected that the airflow pattern from the grill will deviate from the standard condition as well. Figure A1 illustrates the airflow patterns in an indoor environment with an adjustable blade grille and a fixed blade grille at various blade angles. The adjustable blade grille can be adjusted with an arbitrary angle of blades, while the fixed blade grille has a reversible fixed blade core that can provide an upward or downward jet. Upward blades allow supply air to creep along the ceiling due to Coanda effect before separation

(non-standard condition). Supply air drops into the occupied zone at a shorter distance from the grill with downwards blades (standard condition).

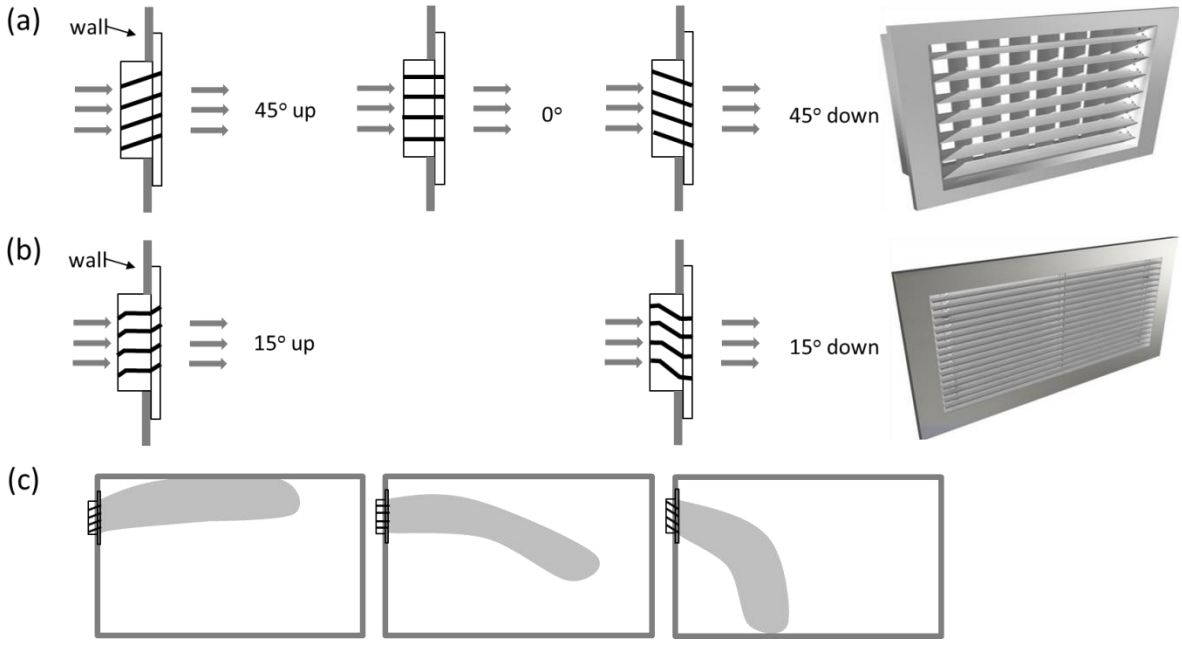

Figure A1: Airflow patterns created by adjustable blade Grilles and fixed blade grilles at various blade angles; (a) Adjustable blade grille; (b) Fixed bladed grille; (c) airflow patterns for upward blades, horizontal blades and downward blades.

Coanda effect occurs when grilles are installed close to the ceiling and the jets from the grilles become attached to the ceiling, allowing them to travel further along the ceiling. The installed distance of the grills from the ceiling affects this attachment phenomenon, thus affecting airflow pattern and consequently ADPI. ASHRAE Standard-70 (2006) recommends a distance of 0.2m (9 in.) to minimize the effect of the ceiling on a grille while testing supply air delivery performance. This measure minimizes the

possible Coanda effect on the performance of the grille. However, ceiling attached jets from grilles are helpful to reduce downward drafts in cooling mode, improving ADPI values.

Linear slot diffusers can also provide various airflow patterns by adjusting slot deflectors at a high level of flexibility. In practice, most diffuser slots should be adjusted to supply jets horizontally along the ceiling. However, it is not unusual for linear slot diffusers to generate indoor air distribution causing draft and cold spots in the occupied zones. One reason for this poor performance is the fact that frequently the slot deflectors (Figure A2) are inappropriately adjusted from vertical to horizontal to provide horizontal airflow along the ceiling (Int-Hout 2013). Our experience shows that an expected horizontal flow pattern is not always created by simply switching the slot deflector from vertical to left or right position, depending on the supply airflow rate and deflector structure. Figure A2 illustrates the reason why the direction of airflow is deflected from horizontal to vertical in operation. In the ideal condition, adjusting two deflectors ("ice tong") at horizontal-vertical combination for each slot allows supply air delivered through only one half of slot section, deflecting airflow along the ceiling. However, air bypass through the left or right deflector described in Figure A2 collides with the main flow and forms an angular down jet instead.

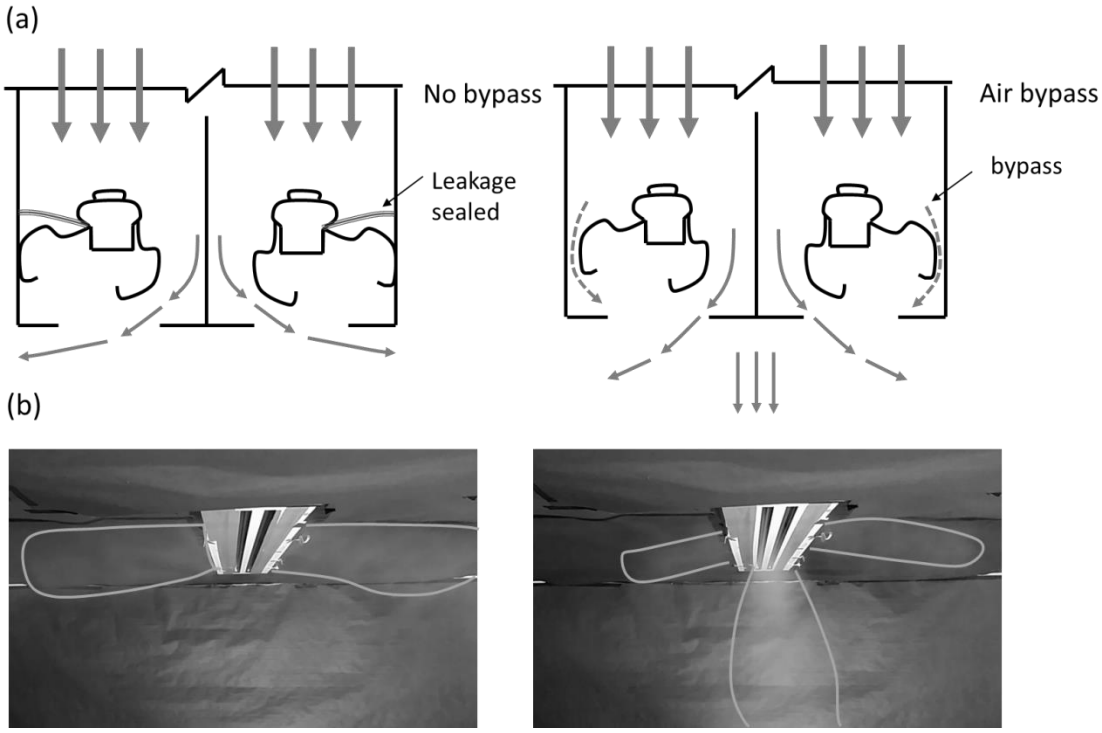

Figure A2: Smoke testing of two-way opposite airflow patterns for linear slot diffusers; (a) horizontal jets when air bypass is sealed; (b) downward jets when air bypass exists.

Since the adjustment of diffuser deflectors affects the flow pattern of supply air, as illustrated in Figure A1 and Figure A2, indoor temperature and velocity distribution will also vary with the deflector adjustment of adjustable blade grilles, fixed blade grilles and ceiling linear slot diffusers. As a result, the design guideline in ASHRAE Handbook-*Fundamentals* (2009) has difficulties to describe air performance of the three diffusers at non-standard configuration.

This paper examines how ADPI values change for deflectors with adjustable diffusers adjusted away from standard conditions described in ASHRAE Handbook-*Fundamentals* (2009). Specific objectives include investigation of ADPI values in a test

room installed with three types of diffusers- adjustable blade grilles, fixed blade grilles and ceiling linear slot diffusers- at various deflector configurations. The adjustable blade grilles are tested with blade angles of upwards 45^{o}, horizontal 0^{o} and downwards 45^{o}, while fixed blade grilles are measured at upwards 15^{o} and downwards 15^{o} conditions as illustrated in Figure A1. In addition, this study compares the performance of linear slot diffusers when slot deflectors are appropriately adjusted ("no bypass") with the inappropriately adjusted cases ("air bypass") (Figure A2). Moreover, this study examines the effect of indoor cooling loads on ADPI values using two cooling loads: $25W/m^2$ (7.9 $Btu/hr/ft^2$) and $50W/m^2$ (15.8 $Btu/hr/ft^2$).

The paper is organized as follows: (1) "Methodology" describes the experimental setups in the test chamber; "Results" shows the ADPI profiles for the three diffuser type with different adjustments; "Discussion " discusses potential practical application; and we conclude in "Conclusion" section.

Methodology

This section describes the experimental facility and our measurements for ADPI values for the three types of diffusers over a range of airflow rates. Each type of diffusers was provided by three to four different manufacturers in two different sizes; variation and result uncertainty caused by the use of different manufacturers or diffuser sizes are assessed using 95% confidence intervals.

The study measured ADPI values for all diffusers in an environmental chamber with geometries of 5.2 m (205 in.) × 4.5 m (236 in.) × 2.4 m (94 in.). The chamber was ventilated with a sophisticated HVAC control system that can supply a large range of

airflow rates into the chamber with Air Change Rates (ACH) from approximately from 3.5 to 14 hr^{-1}. More information about the chamber and the control system can be found in the literature (Liu and Novoselac 2014). The chamber allowed airflow supplied by high side-wall grilles and ceiling linear slot diffusers as described in Figure A3. One high side-wall grille was mounted at the top region of one wall with the grille's upper frame 0.1m from the ceiling. In addition, this paper applied two linear slot diffusers evenly spaced at the center of the chamber ceiling. The supply airflow rate for each slot diffuser was held to a maximum difference within 10%. To generate different cooling loads, adjustable electric heaters simulated indoor occupants, computers, lamps and floor heat gains in the chamber. Table A1 shows the apportionment of the cooling loads. The two loads, 25W/m^2 (7.9 Btu/hr/ft^2) and 50W/m^2 (15.8 Btu/hr/ft^2) were selected to represent typical cooling loads of an office space (ASHRAE Handbook-*Fundamentals* 2009*;* Huang and Zhang 1999). The room control temperature in the experiments was maintained at nearly 23±0.5 ^oC. The insulation of the test chamber minimized outdoor impact and the heat loss through the chamber's envelop was within 3% of the total cooling load.

Heaters	Room Loads	
	25 W/m^2 (7.9 Btu/hr/ft^2)	50 W/m^2 (15.8 Btu/hr/ft^2)
Lamps	100W (341 Btu/hr) ×4	100W (341 Btu/hr) ×4
Box heaters	47W(160 Btu/hr) ×2	100W (341 Btu/hr) ×2
Cylinder heaters	47W(160 Btu/hr) ×2	100W (341 Btu/hr) ×2
Floor heater	0W(0 Btu/hr) ×1	370W (1262 Btu/hr) ×1

Table A1: Heat simulators for two cooling loads.

Twelve hot-sphere anemometers with an accuracy of 0.03m/s (5.9 fpm) and 0.1^{o}C (0.2^{o}F) monitored velocity and temperature at 60 locations in the occupied zone at four heights above the floor - 0.1m (3.9in.), 0.6m (23.6in.), 1.1 (43.3in.) and 1.7m (67in.) – in accordance with ASHRAE Standard-113: Method of Testing for Room Air Diffusion. Figure A3(b) describes the positions of the 60 sampling sensors at 15 horizontal locations evenly distributed across the floor and one reference point (1.1m (43.3 in.) above the floor). To obtain data at sixty locations with 12 available sensors, the study repeated each experiment five times by moving three tripod-stands with each containing 4 sensors along five specific locations. Among all five repeats, the temperature varied within 1^{o}C (1.8^{o}F) and the measured local temperatures for different repeats were corrected using the temperature data at the reference point (1.1m (43.3in.)) according to ASHRAE Standard-113 (2009). This measure ensured compensation for temperature variation among different repeats.

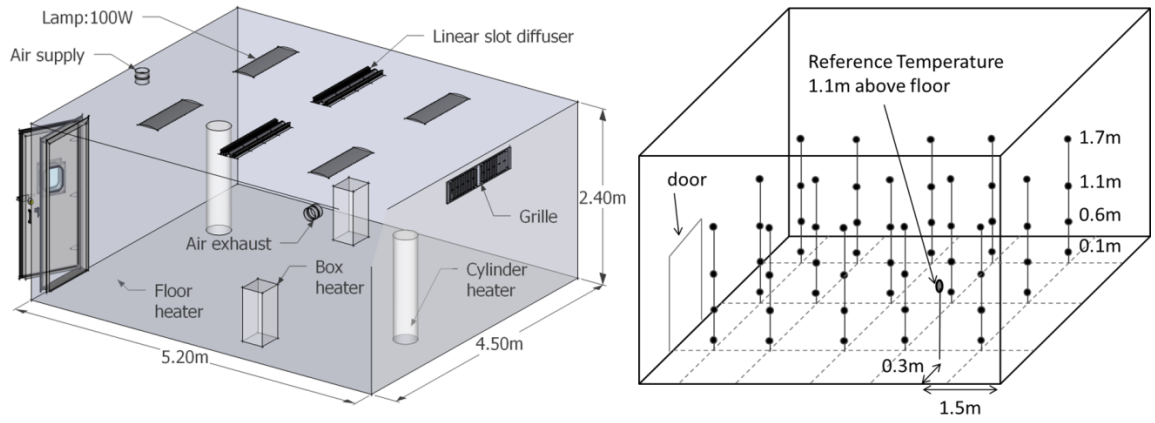

Figure A3: Chamber geometry and sensor positions.

The study analyzed three diffuser types, adjustable blade grilles, fixed blade grilles and ceiling linear slot diffusers. To include the uncertainly of ADPI values due to manufacturer variations, this study selected randomly three to four manufactures for each diffuser type. The impact of size was also considered by testing two sizes for each diffuser type. Table A2 shows the description of test diffusers and the deflector adjustment for each diffuser type as illustrated in Figure A1 and Figure A2.

#	Diffuser type	Size	Manufacturer[§]	Deflector adjustment
1	Adjustable blade grille	41×15cm (16×6in.) & 61×15cm (24×6in.)	A, B & D	45° upward 0° horizontal 45° downward
2	Fixed blade grille	41×15cm (16×6in.) & 61×15cm (24×6in.)	A, B, C & D	15° upward 15° downward
3	Linear slot diffuser	2 slots & 4 slots, 120cm (48in.) long	A, B & D	No bypass Air bypass

[§] A: Krueger; B: Price; C: Titus; D: Nailor;

Table A2: Description of the three types of diffusers.

Each diffuser generates a jet with a particular throw length for a given airflow rate. Throw is defined as the distance from a diffuser to the point where the maximum velocity in the stream cross section has been reduced to a selected terminal velocity, typically 0.25m/s (49fpm) (ASHRAE Standard-70 2006). ADPI values for each diffuser type are usually presented as a function of the ratio of isothermal throw length to the room characteristic length (Miller 1971; Miller and Nash 1971; Miller and Nevins 1972). ASHRAE Standard-70 (2006) requires manufactures to report the isothermal throw length for each diffuser over a range of airflow rates. The isothermal throw length ($T_{0.25}$) of each diffuser for the terminal velocity of 0.25m/s (49fpm) can be found in the diffuser manufacturer catalog along with the airflow rate. The characteric length (L) of the test chamber in this study for the adjustalbe blade grilles, fixed blade grilles and ceiling linear slot diffusers are 2.6 m (102 in.), 2.6m (102 in.), and 5.2m (205 in.), respectively.

By measuring velocity and temprature distribution at a given $T_{0.25}/L$, the ADPI value can be calcuated using Effective Draft Temperature (EDT) (ASHRAE Standard-113 2009). EDT is a calculated temperature difference that combines air temperature difference and air speed. The EDT was first introduced by Rydberg et. al. (1949) and then modified by Straub in a discussion of the paper by Koestel and Tube (1955), as shown in Equation A1:

$$\text{EDT} = T_i - T_a - 8.0(V_i - 0.15)\ ^oC \tag{A1}$$

where T_i is air temperature at the test point, i; T_a is spatial average air temperature in the occupied zone and V_i is local air speed. The criterion's range of EDT is between -1.7 ^{o}C (-3 ^{o}F) and 1.1 ^{o}C (2 ^{o}F) with an air speed less than or equal to 0.35 m/s (69 fpm). Using measured EDT values, ADPI can be calculated as the percentage of occupied zone falling into the acceptable velocity and temperature region determined by measuring EDT.

The uncertainty of the proposed diffuser selection methodology depends on several factors. Specifically, the measurement uncertainty depends on the accuracy of the instruments used and factors relates to experimental set-up, such as diffuser installation, and flow adjustment and balancing. Other factors, such as variation in the geometry of diffusers produced by different manufacturers, as well as variations in diffuser size for the same diffuser type, introduce additional different levels of uncertainty. Because of the high accuracy of velocity and temperature sensors used (±0.03m/s (5.9 fpm) and ±0.1^{o}C (±0.2^{o}F), respectively) in this study, the error propagation analysis showed that the uncertainty caused by instrumentation had a small impact on calculated effective draft

temperature. Therefore, the largest impact could be caused by the variation in diffuser sizes, and in the geometries of diffusers produced by different manufacturers. Consequently, this study reports uncertainties caused by different manufactures and diffuser sizes expressed by 95% confidence interval on the mean.

Results

This section presents ADPI values as a function of $T_{0.25}/L$ for different adjustments of each diffuser type at two cooling loads. Using the measured ADPI data, a diffuser selection guide specifies the range of $T_{0.25}/L$ in which ADPI values of selected diffuser are higher than 80%. The selection guide enables designers to select diffuers to achieve the maximum occupant comfort.

Figure A4 shows measured ADPI values of adjustable blade grilles at a range of $T_{0.25}/L$. At a given airflow rate, upward or downward blade deflections have a shorter throw length than horizontal deflector blades. Due to buoyancy, cool jets from the diffusers tend to travel downward and cause drafts in the occupied zone. This is particularly true for downward deflectors. In Figure A4, when blade deflectors are at a 45^o downward angle, almost all tested adjustable blade grilles fail to create indoor air distribution with ADPI values greater than 80% for both $25W/m^2$ (7.9 $Btu/hr/ft^2$) and $50W/m^2$ (15.8 $Btu/hr/ft^2$). However, 45^o upward angled blades cause suppy air jets to travel along the ceiling before moving downward along a side-wall. As a result, the occupied zone is less exposed to cold jets, which produces an indoor air distribution with a higher ADPI value (almost as high as 90%) created using 45^0 upwards blade grilles, as shown in Figure A4. In addition, ADPI values increase with a decrease of indoor

cooling load, especially for lower supply airflow rates or $T_{0.25}/L$ values. Figure A4(b) shows that ADPI values, for the cases of downward and horizontal defelctors, at $T_{0.25}/L$ of smaller than 1 are lower than 60% when cooling load is 50W/m^2 (15.8 Btu/hr/ft^2).

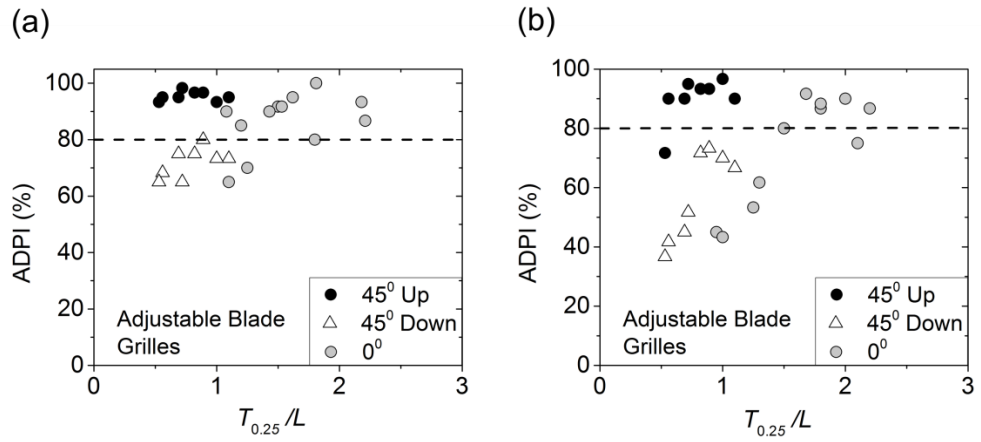

Figure A4: ADPI values for adjustable blade grilles. (a) 25W/m^2 (7.9 Btu/hr/ft^2); (b) 50W/m^2 (15.8 Btu/hr/ft^2).

In Figure A5, fixed blade grilles have similar ADPI responses with deflector configuration as adjustable blade grilles: downward deflectors cause lower ADPI values while upward deflectors result in greater ADPI values. However, the deflector adjustments for fixed blade grilles exert less impact on ADPI values than adjustable blade grilles because the deflector angle of the fixed blade grilles is only 15^0. This illustrates that deflector angles can improve diffuser performance greatly if the deflectors are appropriately adjusted. Lower cooling loads are always favorable for ADPI values over a large range of $T_{0.25}/L$. Figure A5(a) shows that fixed balde grilles can create air distribution with an ADPI value higher or slightly lower than 80% for upward or downward deflectors at a lower cooling load of 25W/m^2 (7.9 Btu/hr/ft^2). The adjustment

of deflectors is less sensitive to deflector configuration at this cooling load. Neverthelss, downward deflectors cause a strong draft in the occupied zone when $T_{0.25}/L$ is smaller than 1.5 for the cases of 50 W/m^2 (15.8 Btu/hr/ft^2) as observed in Figure A5(b). In general, Figure A5 and Figure A6 imply that design engineers or installation contractors are able to improve the performance of blade grilles by adjusting blade deflectors slightly upward instead of keeping them horizontally.

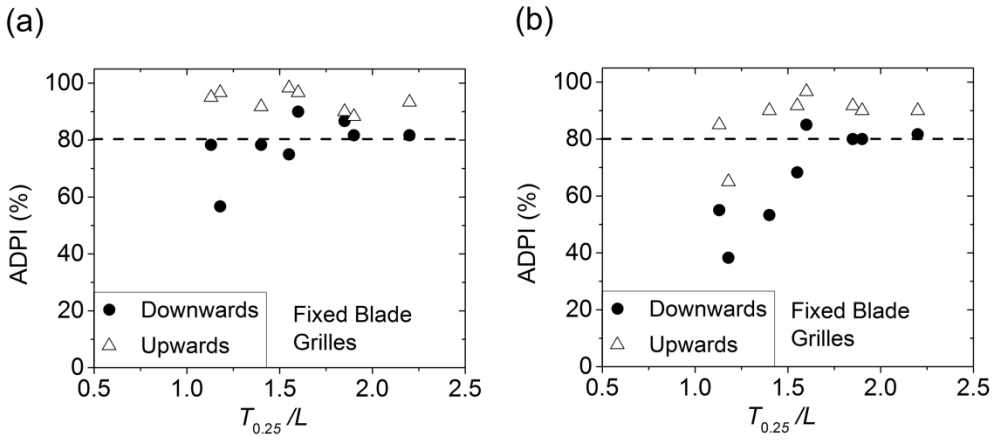

Figure A5: ADPI values for fixed blade grilles. (a) 25W/m^2 (7.9 Btu/hr/ft^2); (b) 50W/m^2 (15.8 Btu/hr/ft^2).

Linear slot diffusers are associated with draft issues because of adjustment flexibility and geometry complex. As described in Figure A2, the airflow patterns created by linear slot diffusers are not always attached to the ceiling as expected even though the deflectors are adjusted according to diffuser specifications. The unexpected airflow pattern usually results in downward jets in the occupied zone. Figure A6 compares the ADPI values of linear slot diffusers in an "air bypass" configuration with

those at a "no bypass" configuration. As expected, the horizontal airflow pattern in the "no bypass" configuration shows a higher ADPI value than those in the "air bypass" case. This appears to be the results of the "air bypass" configuration generating a vertical downward jet in the occupied zone. This may explain why indoor environments employing linear slot diffusers are usually uncomfortable and drafty as described in the literature (Int-Hout 2013). Figure A6 presents that linear slot diffusers in the "no bypass" configuration can improve ADPI values up to and greater than 90% for almost all $T_{0.25}/L$ values, regardless of cooling loads. However, ADPI values are typically lower or slightly higher than 80% for the "air bypass" configuration. The situation becomes even worse for a higher cooling load. Failure to adjust slots usually causes cold air being directed down on occupants. To avoid downward jets, smoke tests are recommended for the whole range of operational airflow rates during commissioning.

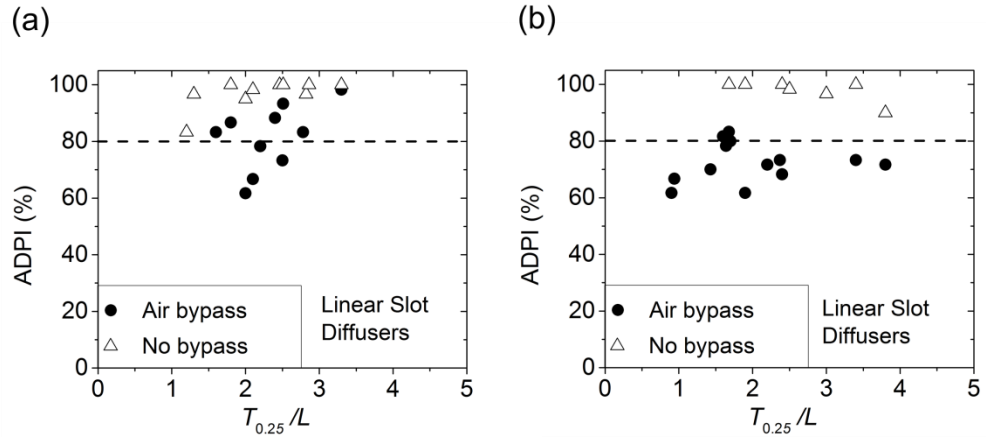

Figure A6: ADPI values for linear slot diffusers. (a) 25W/m^2 (7.9 Btu/hr/ft^2); (b) 50W/m^2 (15.8 Btu/hr/ft^2).

Table A3 shows the maximum ADPI values and $T_{0.25}/L$ ranges in which ADPI values are greater than 80% for the three adjustable diffuser types at various deflector configurations. Overall, upward deflectors can generate greater ADPI values than horizontal deflectors as shown in ASHRAE Handbook-*Fundamentals* (2009). The downward deflector configuration for blade grilles should be avoided because the occupied zone will likely be exposed to cold drafts. Linear slot diffusers are the least sensitive to $T_{0.25}/L$ for creating an indoor air environment with ADPI values greater than 80% if the diffusers are properly adjusted. Under such conditions, ADPI values can be as high as 100% for linear slot diffusers as shown in Table A3. When the linear slot diffusers are inappropriately adjusted, however, the maximum ADPI value is only 75% on average for loads of 50W/m^2 (15.8 Btu/hr/ft^2). Consequently, it is necessary to conduct smoke tests to ensure the airflow patterns generated by linear slot diffusers are attached to the ceiling.

Terminal Device	Cooling load	Deflector adjustment	$T_{0.25}/L$ for Max. ADPI	Maximum ADPI (95% confidence interval)	$T_{0.25}/L$ range (ADPI>80%)
Adjustable Blade Grilles	25W/m^2 (7.9 Btu/hr/ft^2)	Upwards 45^o	0.8	97±1%	0.5-1.1
		Horizontal 0^o	1.8	93±6%	1.2-2.2
		Downward 45^o	0.9	75±4%	-
	50W/m^2 (15.8 Btu/hr/ft^2)	Upwards 45^o	0.9	96±4%	0.6-1.1
		Horizontal 0^o	2	87±6%	1.7-2.2
		Downward 45^o	1	70±8%	-
Fixed Blade Grills	25W/m^2 (7.9 Btu/hr/ft^2)	Upwards 15^o	1.1	95±5%	1.1-2.2
		Downward 15^o	1.9	85±9%	1.6-2.2
	50W/m^2 (15.8 Btu/hr/ft^2)	Upwards 15^o	1.9	92±8%	1.2-2.2
		Downward 15^o	1.9	81±10%	1.9-2.2
Linear Slot Diffusers	25W/m^2 (7.9 Btu/hr/ft^2)	No bypass	2.8	100	1.2-3.3
		Air bypass	3.3	100	1.6-3.3
	50W/m^2 (15.8 Btu/hr/ft^2)	No bypass	>1.9	100	1.7-3.8
		Air bypass	2.4	75±5%	-

Table A3: ADPI Selection Guide for adjustable diffusers at cooling condition.

Discussions

This study measures the ADPI values of the three adjustable diffusers in an office-like room with a ceiling height of 2.4m (94in.). Upward deflectors for adjustable blade grilles and fixed blade grilles direct supply air jets shooting at the ceiling, which results in greater ADPI values as shown in Table A3. However, the findings in this study might not be generalized to high space buildings such as airport terminal, auditorium and hotel lobby. In addition, the installation height of side-wall diffusers is an important factor related to ADPI values. When supply jets are generated at a much higher level than the occupied zone, downward cold jet drafts can be warmed by mixing with the upward thermal plume from the occupied zone.

Complaints of drafts in a space using ceiling linear slot diffusers are very common if the diffusers are inappropriately adjusted. In the extreme, as experienced during this study, the adjustment of deflectors according to product specifications may not guarantee a ceiling-attached airflow pattern. A relatively simple smoke test (with injection in the supply air or at the edge of the diffuser) could be fine too to avoid undesired downward jets due to improper blade adjustment. Our experience from using the smoking tests indicates that sealing the slot deflectors from the back could eliminate downward influences on the jets from bypass airflows, resulting in horizontal ceiling-attached jets from the diffusers (Figure A2).

The presented study has certain limitations. For example, the number of diffusers for each type may not be sufficient to represent all diffusers on the market. Although several repeated tests at specific $T_{0.25}/L$ ratios show that manufacture and size might be an important contributor to uncertainty of ADPI, the limited data points prohibit

calculating a meaningful value for the average variations of ADPI with $T_{0.25}/L$ for each diffuser type. A statistical sensitivity analysis or a larger pool of sample diffusers will be necessary in future studies.

Conclusions

This paper investigates how the adjustment of deflectors affects adjustable diffusers' performance at different indoor cooling loads. By measuring air temperature and speed in the occupied zone of a test room, the study calculates ADPI values of three adjustable diffusers- adjustable blade grille, fixed blade grille and linear slot diffuser-at various deflector configurations.

The results show that upward blade deflectors increase air diffusers' performance represented by ADPI values regardless of cooling load intensities, while the effects reverses for downward deflectors. The ADPI values in the cases with upward blade deflectors exceed 80% for almost the whole range of $T_{0.25}/L$ values applied in the experiments. Adjustable blade grilles and fixed blade grilles should avoid downward jets resulting from improperly-configured diffusers because of low ADPI values (<80%). The study also explains how linear slot diffusers can cause drafts in the occupied zone as a result of improper adjustment of diffuser deflectors, allowing undesired air bypass that causes downward jets. Without air bypass, linear slot diffusers present the greatest robustness to create an air distribution with ADPI greater than 90% over a large range of airflow rates. Since adjustment of linear slot diffusers is crucial to create ceiling-attached airflow pattern and therefore high ADPI values, this paper highly recommends

smoke testing during commissioning to ensure proper operation of diffusers. In general, downward jets should be avoided for all three diffuser types in the cooling condition.

APPENDIX B: AIR DIFFUSION PERFORMANCE INDEX (ADPI) OF DIFFUSERS FOR HEATING MODE

Shichao Liu Atila Novoselac, Ph.D

(Submitted to *Building & Environment*)

Abstract

This paper proposes an Air Diffusion Performance Index (ADPI) model for diffuser selection when considering the operation in all-air heating mode. The model uses the Predicted Mean Vote (PMV) Index (Fanger 1970) adopted by ANSI/ASHRAE Standard-55 to develop the relation between indoor air temperature and velocity. This paper also generates an ADPI selection guide for the application of 11 types of widely used ceiling, high sidewall and linear slot diffusers. The selection guide is developed based on 81 experiments in a full-scale environmental chamber by measuring the ADPI as a function of two factors: (1) the ratio of throw length of jets from diffusers to room characteristic length, and (2) diffuser types. Moreover, the measurements consider different diffuser sizes and manufactures. The selection guide discusses possible thermal stratification occurring at heating mode conditions and incorporates this factor into the proposed ADPI model. Overall, the measurements show that all 11 types of diffusers can generate ADPI greater than 80% when they are properly used. However, some diffusers are less sensitive to the variation of supply airflow rate than others. Linear bar grilles and round ceiling diffusers are the most suitable for application when supply flow varies during HVAC operation.

Keywords: Diffuser, ADPI, Air Heating, Effective Draft Temperature, PMV index, Thermal stratification

Practical implications

The current Air Diffusion Performance Index (ADPI) method is suitable for diffuser selection and positioning only when diffusers are used in cooling mode. However, diffusers in all-air Heating, Ventilation and Air Conditioning (HVAC) systems are used in both cooling and heating modes. HVAC operation in heating mode could cause thermal discomfort and/or temperature stratification if diffusers are chosen solely for their cooling-mode performance. The updated ADPI method and new diffuser selection guide for heating mode provide a useful tool for designers to select and layout diffusers in a way that allows the HVAC system to provide an effective air distribution for both cooling and heating mode operation.

Introduction

Many commercial buildings use all-air delivery systems as a part of Heating, Ventilation, and Air Conditioning (HVAC) systems. The air distribution in an indoor space is created by terminal diffusers, ranging from simple-geometry grills to complicated swirl diffusers. The selection and positioning of diffusers depend on many factors, such as building function, aesthetic requirements and occupant comfort. However, the main task of air diffusers is to distribute supply air, and to remove indoor cooling or heating loads while providing air velocity and temperature distribution that can

achieve occupant comfort. The widely accepted and applied design index that quantifies the performance of diffusers when considering the spatial uniformity of air velocity and temperature and their contribution to thermal comfort is Air Diffusion Performance Index (ADPI) (Miller and Nash 1971). ADPI is defined as the percentage of occupied zone falling into the acceptable velocity and temperature region determined by measuring local Effective Draft Temperature (EDT); EDT is a calculated temperature difference that combines air temperature difference and air speed (ANSI/ASHRAE Standard-113 2009). ADPI also defines the maximum acceptable velocity in the occupied zone.

ADPI primarily quantifies ETD distribution (function of air temperature and velocity) and the acceptable maximum air speed in the occupied zone, as it relates to thermal comfort. However, thermal comfort also depends on other important factors such as relative humidity (RH), mean radiant temperature, metabolic rate and clothing insulation (Fanger 1970; ANSI/ASHRAE Standard-55 2010). Even though the thermal comfort model is a more comprehensive tool for the holistic evaluation of a wide range of influencing parameters, ADPI-based diffuser selection assesses uniformity of effective draft temperature field in the occupied part of the room.

The ADPI method considers two main thermal comfort variables (air temperature and velocity) and a set of design variables characterizing a diffuser: diffuser air jet throw (T_v) for a given terminal velocity (v), room geometry represented by a characteristic length (L), and types of heating/cooling loads as well as load intensity. Throw is defined as the distance from a diffuser to a point where the maximum velocity in the stream cross section has been reduced to a selected terminal velocity (ANSI/ASHRAE Standard-70 2006). This standard also requires manufactures to report the isothermal throw length for

each produced diffuser at a range of airflow rates. By employing the ratio of isothermal throw length ($T_{0.25}$ – distance at which jet velocity decreases to 0.25 m/s) to the room characteristic length (L – typically defined as a distance from the diffuser to a wall perpendicular to jet or to the closest wall), a designer can select appropriate diffuser type and positioning layout that create acceptable comfort (ADPI>80%) according to the range of $T_{0.25}/L$ described in ADPI selection guide (ASHRAE-Handbook *Fundamentals* 2009). The ADPI values and diffuser selection guide are intended to be used in the design stage of a building before other more elaborate thermal comfort indexes can be applied. Employing the ADPI selection guide in ASHRAE-Handbook *Fundamentals* (2009), designers have been more or less successfully designing air diffusion systems for cooling mode since the 1970s (Miller and Nevins 1969; Miller and Nash 1971).

When the first ADPI-based diffuser selection guide was developed, HVAC systems for delivering warm air in heating mode were uncommon. Nowadays, however, the operation of HVAC systems for heating has been much more popular than before, and HVAC systems have to meet both heating and cooling requirements in most climates (Krarti 2008; Platt et al. 2010; Vakiloroaya et al. 2014). Even though ANSI/ASHRAE Standard-113 (2009) states that "the ADPI method for mixing systems should be applied to traditional overhead air distribution systems under cooling operation only", the same diffusers are used for heating in the winter. The lack of ADPI method for heating mode often causes underperformance of all-air delivery systems when used for heating. When diffusers supply air at a low airflow rate but a high temperature, the thermal stratification causes not only thermal comfort issues but also stagnant air in the occupied zone resulting in low ventilation effectiveness (Novoselac and Srebric 2003; Krajčík et al.

2012; Tomasi et al. 2013). Therefore, further development of the ADPI method is required for applications in heating mode.

The general objective of this study is to propose an ADPI diffuser selection method for heating mode. Specifically, the study uses the established thermal comfort model (Fanger 1970) to develop EDT for heating and then uses this EDT and experimental data to obtain the ranges of $T_{0.25}/L$ during which at least 80% ADPI can be achieved in a space using various types of diffusers. The next section reviews the relevant ADPI method for cooling mode, followed by a "Theoretical Background" section that proposes a heating mode EDT in terms of the Predicted Mean Vote (PMV) index from the thermal comfort model. The "Methodology" section describes the experimental apparatus and measurement protocol for 81 experiments using 11 diffuser types. Next, the "Results" section shows ADPI values for each diffuser type at various $T_{0.25}/L$ by which an ADPI selection guide will be generated for heating mode. Finally, "Discussion" and Summary" discusses factors affecting heating ADPI model and summarizes the major findings, respectively.

Previous research on ADPI

The currently used ADPI method for cooling mode developed by Miller and Nash (1971) was derived from the subjective response to draft (air temperature difference and velocity) obtained by Houghen et al. (1938) and the work of Rydberg and Norback (1949). The ADPI is an indicator of air thermal diffusion performance of a diffuser at a specific air delivery rate and space load (ANSI/ASHRAE Standard-113 2009). It is determined based on only air speed and effective draft temperature (EDT). The EDT

was first introduced by Rydberg et al. (1949) and then modified by Straub in a discussion of the paper by Koestel and Tube (1955), as shown in Equation B1:

$$EDT\ (\theta) = T_i - T_a - 8.0(V_i - 0.15)\ ^oC \quad \text{(B1)}$$

where T_i is air temperature at the test point, i; T_a is spatial average air temperature in occupied zone and V_i is local air speed.

The criterion's range of EDT is between -1.7 ^{o}C and 1.1 ^{o}C with an air speed less than or equal to 0.35 m/s. The lower boundary of EDT (-1.7^{o}C) shows a good agreement with Houghten's data for 80% of the occupants reporting comfort (Nevins and Miller 1972). Koestel and Tuve (1955) indicated that the upper limit of EDT=1.1^{o}C is satisfactory. Furthermore, the velocity 0.15m/s in the EDT Equation B1 represents the effect of human buoyancy. Additionally, the maximum acceptable velocity of 0.35m/s that occupants can tolerate was recommended by Nevins and Miller (1972). The range derived from subjective thermal sensation defines the variation in EDT with air temperature difference and speed.

Previous studies of ADPI for cooling mode have shown that ADPI primarily depends on $T_{0.25}/L$ and then on the intensity of cooling loads (Miller and Nash 1971). The design guidance for ADPI>80% is based on ADPI versus $T_{0.25}/L$ graphs such as the one presented in Figure B1(a). Most studies for cooling loads have shown that (1) curves have a concave-like shape as illustrated in Figure B1(a), (2) that the ADPI is low for small and large $T_{0.25}/L$ ratios, and (3) that in-between is a point with the maximum ADPI (Miller and Nevins 1970; Miller 1971, Miller and Nevins 1972; Nevins and Miller 1972; Miller 1979). At a small $T_{0.25}/L$ ratio, jet momentum is too weak to disperse cool supply

air into occupancy zone, which causes thermal stratification and cold spots in this zone. In contrast, the local air speed might be out of ADPI criteria for the maximum acceptable value (0.35m/s) at a large $T_{0.25}/L$ ratio. For each type of diffusers, there is a different $T_{0.25}/L$ range for ADPI >80% and a specific $T_{0.25}/L$ for the maximum ADPI within the range.

Nevertheless, ADPI versus $T_{0.25}/L$ curves maybe different for heating mode. Warm supply air tends to stay in the upper region of a space because of buoyancy force. This introduces complexities in ADPI curves for heating mode and Figure B1(b) shows four scenarios with each corresponding to ADPI variations with $T_{0.25}/L$. At low $T_{0.25}/L$ ratios, warm supply would create two different phenomena: (1) "stagnant flow" when supply air stagnates above the occupied zone, and (2) "thermal stratification" when supply air reaches the occupied zone but create great vertical temperature difference in the zone (often called "warm head-cool feet"). The reason why the "stagnant flow" still generates a high ADPI value is that hot air concentrates at top of the room and the occupied zone below is less affected by supply air and therefore has a relatively uniform velocity and temperature distribution. When $T_{0.25}/L$ increases, warm supply air exerts various effects on the air speed in the occupied zone. Some diffusers delivering a large amount of air lead to (3) unacceptable air speed in the occupied zone ("some impact on air speed") while other diffusers supply only less air at the same $T_{0.25}/L$ ratio resulting in (4) "no impact of high speed" curve in Figure B1b. Due to the four possible regimes of ADPI, it is expected that heating mode ADPI curves will present great variations among different diffuser types.

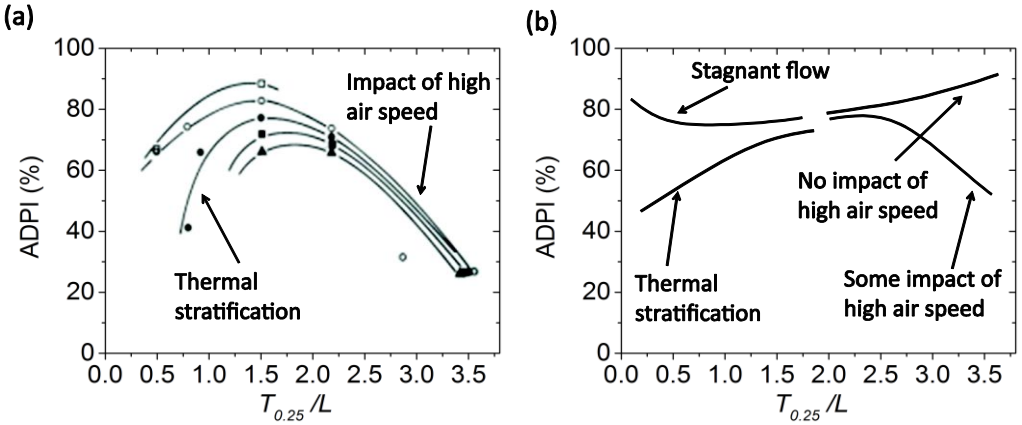

Figure B1: General ADPI profiles as a function of $T_{0.25}/L$; (a) Cooling mode, symbols are real data of high sidewall grilles from Miller and Nash at different cooling loads (1971); (b) Heating mode, solid line: thermal effect dominant; Dash line: air movement dominant.

Theoretical Background

This section analyses the Effective Draft Temperature (EDT) in heating mode by (1) comparing the region of EDT in the ADPI method to the region of 80% thermal comfort in the PMV index; (2) deriving a heating mode EDT; and (3) proposing an ADPI method in terms of the derived EDT for heating mode. The proposed method for heating mode is then applied to calculate ADPI and to generate a selection guide for 11 types of diffusers.

The ADPI method specifies EDT range and the maximum air speed. The method considers only air temperature and velocity. However, PMV index involves four additional factors including (1) mean radiant temperature, (2) relative humidity, (3) metabolic rate, and (4) clothing insulation. When considering mean radiant temperature, Int-Hout(1983) compared the mean radiant temperature and air temperature with

common overhead air distribution systems and found that in many cases radiant temperature is relatively close to room air temperature, suggesting a small impact of radiation when included in comfort calculations. When considering the metabolic rate (Unit: Met.), an office worker normally has a rate ranging from 1.0 to 1.3 Met. The clothing insulation (Unit: Clo.) is typical 0.5 Clo. for an office environment in summer and 1.0 Clo. in winter (ANSI/ASHRAE Standard-55 2010). The only variable that may vary significantly in commercial buildings is relative humidity (RH) and it may have a significant effect on thermal comfort; because the EDT doses not take into account RH, this study adopts a most desirable RH of 50% for summer and winter conditions. When considering difference between heating and cooling mode and the impact on EDT, one can find that clothing insulation is an important contributor along with velocity and temperature. The significant difference between cooling and heating modes suggests that designers will need two different ADPI models for summer and winter operation. The following section will discuss an 80% thermal acceptance region for EDT in cooling mode based on PMV during summer conditions, then derive a heating mode EDT according to an 80% thermal acceptance region based on PMV in winter condition.

Thermal acceptance regions of PMV and EDT for cooling mode

The range of EDT in cooling mode for Equation B1 illustrates a region of the relationship between velocity and air temperature difference shown in Figure B2(a). Zero EDT (θ=0) represents a neutral thermal sensation. Figure B2(b) shows the PMV range from -0.5 to 0.5 in a plot of air velocity versus temperature for a typical office space in summer (cooling mode) assuming metabolic rate of 1.15 Met., clothing insulation of 0.5

Clo. and relative humidity of 50%. The plot was generated using PMV index according to ANSI/ASHRAE Standard-55 (2010). The region of PMV in this study is limited to air speeds below 0.2m/s as described in the Standard. Neutral thermal sensation is achieved when PMV is equal to zero. Since both EDT =0 and PMV=0 represent the condition of neutral thermal sensation, Figure B2(c) shifts the PMV region (-0.5 to 0.5) in Figure B2(b) to collapse PMV=0 to EDT=0 in Figure B2(a). It shows that the boundaries of PMV region -0.5 and 0.5 overlap with the EDT's boundaries of -1.7 ^{o}C and 1.1 ^{o}C, respectively. This suggests that the PMV index for 80% thermal acceptance agrees with Houghen's 80% thermal acceptance proposed in 1938 (Houghten et al. 1938). This also indicates that occupant's thermal acceptance has not been changed significantly.

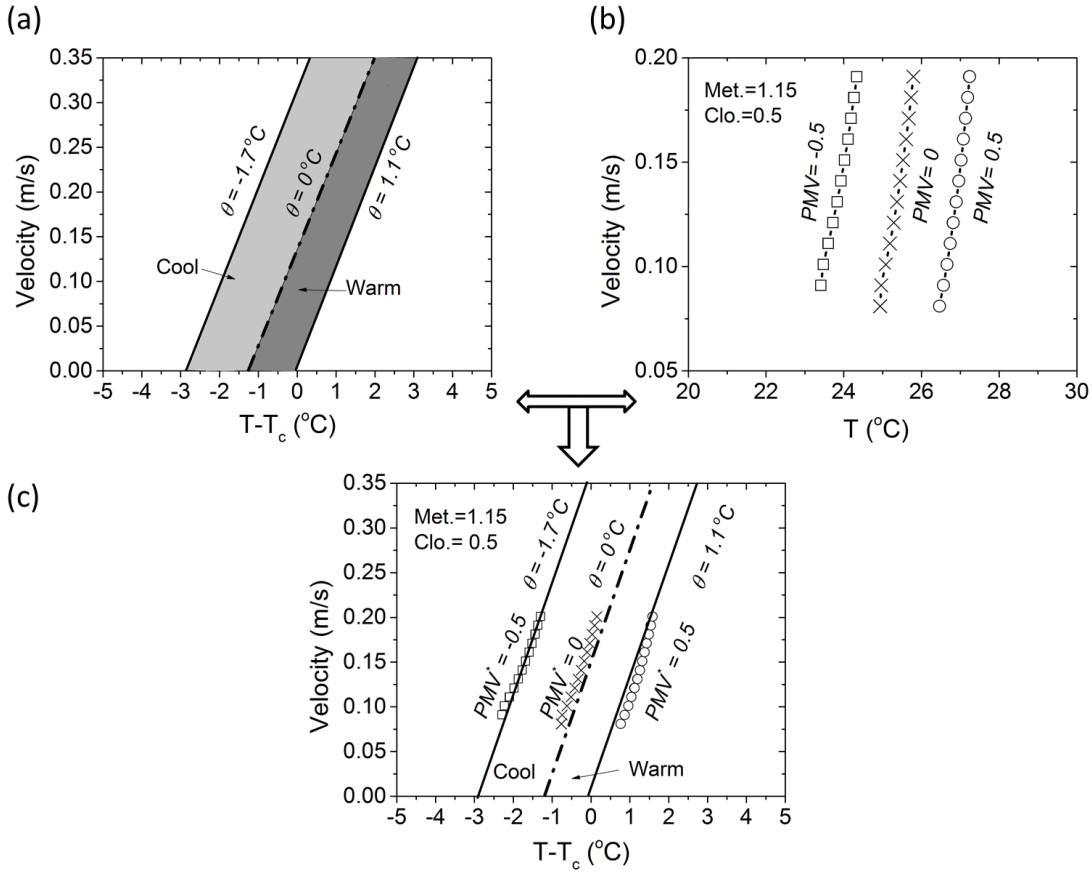

Figure B2: ADPI and PMV as a function of air temperature and velocity for cooling mode (Metabolic activity: 1.15Met., Clothing condition: 1 Clo., and Relative humidity: 50%); (a) The range of 80% comfort acceptance using EDT; (b) The range of 80% comfort acceptance using PMV; (c) Comparison of the comfort ranges of EDT and PMV.

By employing the same manner as the cooling mode, Figure B3(a) plots the 80% comfort acceptance region calculated using PMV index for heating mode. Because EDT is a function of local air temperature difference and air velocity, EDT for heating mode should have a format of Equation (B2):

$$\theta_1 < EDT\ (\theta) = T_i - T_a - k(V_i - 0.15)\ ^oC < \theta_2 \quad \text{(B2)}$$

where θ_1 and θ_2 are the boundaries of EDT's range for heating mode, and k is a coefficient connecting temperature difference to air speed while considering thermal sensation.

Thermal acceptance regions of PMV and EDT for heating mode

The heating mode ADPI method can be resolved if the coefficient k and two boundaries (θ_1 and θ_2) are determined. Due to the consistence of EDT and PMV regions for 80% thermal acceptance, one can derive the heating mode EDT by curve fitting EDT boundaries with those of PMV. Figure B3(b) shows the best curve fitting of EDT's range according to PMV regions, which gives k=*9.1,* θ_1 =*-2.2* and θ_2 =*2*. Therefore, the heating mode EDT can be written as Equation B3:

$$EDT\ (\theta) = T_i - T_a - 9.1(V_i - 0.15)\ ^oC \quad \text{(B3)}$$

The criterion's range of EDT (Equation B3) is between -2.2 ^{o}C and 2 ^{o}C. Similar to cooling mode EDT, the velocity of 0.15m/s in Equation B3 stands for the velocity of human thermal plume. This study keeps the criterion of air speed less than or equal to 0.35 m/s because occupants generally accept air speed greater than 0.2m/s for warm air circumstances as stated in ANSI/ASHRAE Standard 55 (2010). Another important criterion is the vertical air temperature difference and thermal stratification. ANSI/ASHRAE Standard 55 (2010) allows the maximum vertical air temperature of 3^{o}C between head (1.1m) and ankles (0.1m). In addition, higher vertical temperature gradient

prohibits an efficient air mixing in the room. Therefore, this study adds an additional thermal stratification criterion to the ADPI method for heating mode and the significance of this criterion is illustrated in the "Results" section of the paper. In general, the heating mode ADPI method consists of three criteria: (1) EDT (Equation B3) ranging from -2.2^{o}C to 2^{o}C; (2) local air speed less than or equal to 0.35 m/s; and (3) Overall vertical temperature gradient lower than 3^{o}C/m, and local maximum temperature difference between 0.1m to 1.1m of less than 3 ^{o}C.

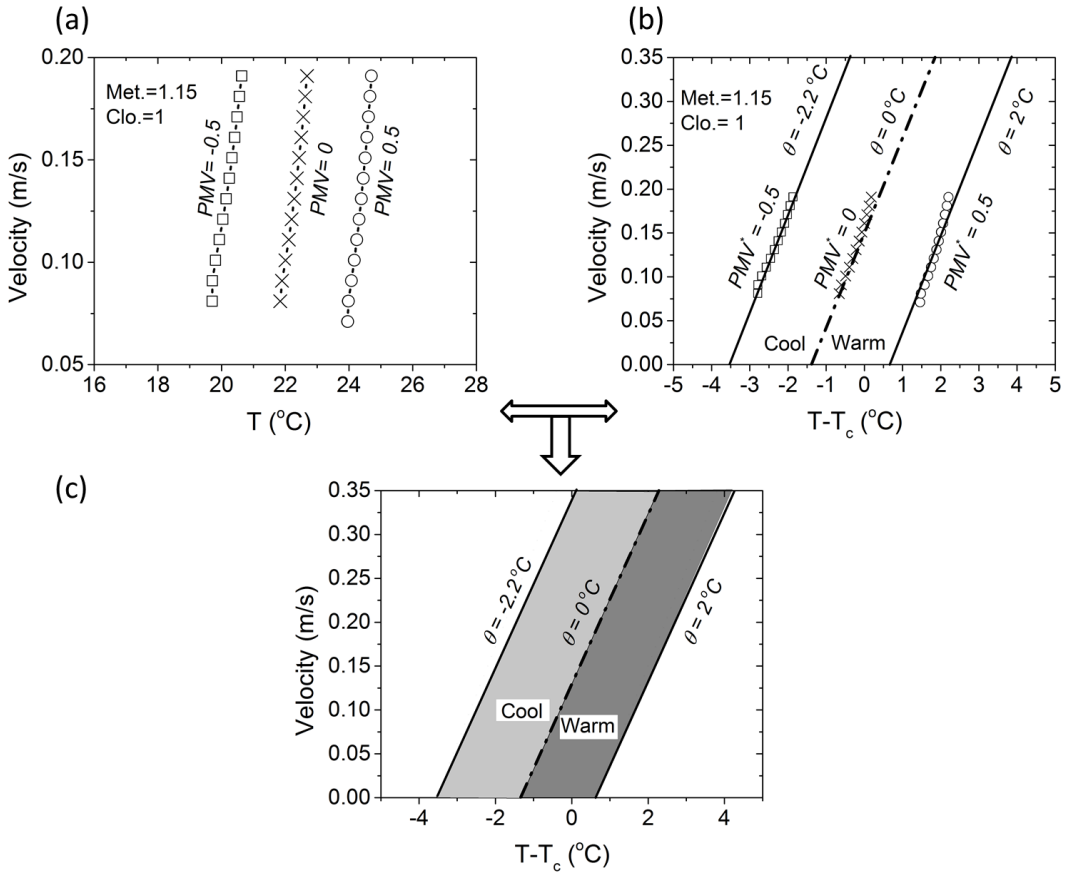

Figure B3: ADPI and PMV as a function of air temperature difference and velocity for heating mode (Metabolic activity: 1.15Met., Clothing condition: 1Clo., and Relative humidity: 50%); (a) The range of 80% comfort acceptance using PMV; (b) EDT boundaries collapsing to those of PMV for 80% comfort acceptance. (c) The range of 80% comfort acceptance using EDT.

Methodology

This section describes the measurements for heating mode ADPI as a function of $T_{0.25}/L$ for 11 types of diffusers available on the market. Each type of diffuser was

provided by three to four manufacturers with two different sizes. Moreover, this section presents a way to assess measurement uncertainty.

This study carried out all the experiments in a test chamber 6m × 4.5m × 2.7m (73m^3) with a sophisticated HVAC control system. More information about the chamber and the control system can be found in the literature (Liu and Novoselac 2014). The experimental set-up allowed testing three diffuser mounting positions: (1) ceiling position for ceiling diffusers; (2) ceiling position for linear slot diffusers; and (3) high sidewall position for grilles. Figure B4(a) shows the chamber geometry and three configurations for diffuser installation. Position 1 and 2 used two identical diffusers while position 3 employed only one grille. The two diffusers for position 1 (or 2) were balanced to have the maximum airflow rate difference within 10%. The experiments employed a plenum box at each duct terminal to ensure that the airflow was uniformly distributed by a diffuser in relevant directions (ANSI/ASHRAE Standard-70 2006). The characteristic length (L) of the test chamber for ADPI calculation for the three configurations was 1.4 m, 2.6m and 5.2m, respectively.

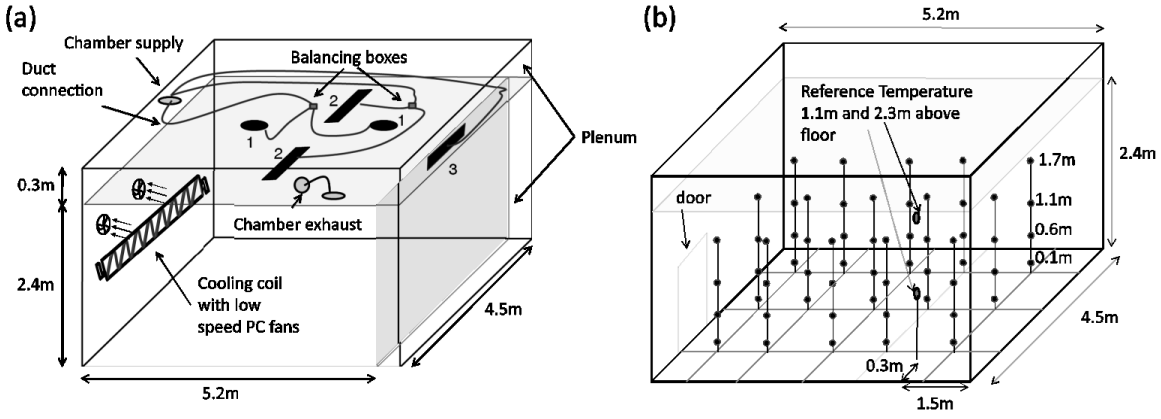

Figure B4: Chamber geometry and sensor positions; (a) Ductwork for three installation configurations 1: Ceiling diffusers, 2: Ceiling linear slot diffusers and 3: High sidewall grilles or nozzles (0.1m from the upper frame to the ceiling); (b) The locations of sixty sampling positions.

To simulate indoor heating load, the chamber employed a cooling water coil attached with very low speed fans circulating air towards a chamber wall (Figure B4(a)). The low velocity provided no disturbance in the occupied zone while cooling down the wall surface. This cold chamber wall modeled a typical window and exterior wall in wintertime causing a specific heating load in the range of 35-40W/m^2. This load was selected to represent a typical heating load of an office space (Huang and Zhang 1999; ASHRAE Handbook *Fundamentals* 2009). The room control temperature in the experiments was maintained at nearly 23±0.5^{o}C. The insulation of the test chamber minimized outdoor impact and the heat loss through the chamber's envelop was within 3% of the total heating load.

Twelve hot-sphere anemometers with an accuracy of 0.03m/s and 0.1^{o}C monitored velocity and temperature at 60 locations in the occupied zone at four heights above the floor (0.1, 0.6, 1.1, and 1.7m) according to ANSI/ASHRAE Standard-113

(2009). Figure B4(b) describes the positions of the 60 sampling sensors at 15 horizontal locations evenly distributed across the floor and two reference points (1.1 and 2.3m above the floor). To obtain data at sixty locations with 12 available sensors, the study repeated each experiment five times by moving three tripod-stands with each containing 4 sensors along five specific locations. Among all five repeats, the temperature varied within 1^{o}C and the measured local temperatures for different repeats were corrected using the temperature data at the reference point (1.1m) according to ANSI/ASHRAE Standard-113 (2009). This measure ensured compensation for temperature variation among different repeats. In order to identify temperature stratification, furthermore, the temperature gradient was calculated based on five vertical locations by using the average temperature at the same height of 0.1, 0.6, 1.1 and 1.7m, and the temperature of the reference point at 2.3m.

This study analyzed 11 types of common diffusers for HVAC designers and diffuser manufacturers. To include the uncertainly of ADPI due to manufactures, this study selected randomly three to four manufactures for each diffuser type. The impact of sizes was also considered by testing two sizes for each of 11 types. The specific sizes were selected based on the diffuser's airflow rate delivery capacity and the chamber size. Unsuitably large diffusers would provide weak jets to mix the occupied zone well, leading to a stagnant zone as illustrated in Figure B1(b), while too small sizes would cause great pressure resistance of diffusers. Therefore, the range of $T_{0.25}/L$ reported in "Results" section is based on only realistic selections instead of a whole range from zero to a very high value. Each diffuser at the selected $T_{0.25}/L$ range supplied air into the chamber with Air Change Rates (ACH) from approximately 3.5 to 14 hr^{-1}. Table B1

shows the description of the 11 diffuser types. This work obtained 81 data points of ADPI as a function of $T_{0.25}/L$ for the 11 diffuser types.

#	Diffuser type	Size (cm)	Manufacturer[§]	Installation location
1	Adjustable blade grille	41×15 & 61×15	A, B & D	High sidewall
2	Fixed blade grille	41×15 & 61×15	A, B, C & D	High sidewall
3	Linear bar grille	41×15 & 61×15	A, B, C & D	High sidewall
4	Nozzle	13[*]& 15[*]	A, B & C	High sidewall
5	Round ceiling diffuser	15[*]& 25[*]	A, B, D & E	Ceiling
6	Square ceiling diffuser	15[*]& 20[*]	A, B & C	Ceiling
7	Perforated diffuser-Round pattern	15[*]& 20[*]	A, B & C	Ceiling
8	Perforated diffuser-Directional pattern (4-way)	15'[*]& 20[*]	A, B, C & D	Ceiling
9	Louvered face diffuser[†]	15[*]& 23[*]	A, B & C	Ceiling
10	Plaque face diffuser	15[*]& 20[*]	B, C & D	Ceiling
11	Linear slot diffuser	2-slots & 4-slots, 122cm long	A, D &E	Ceiling slot

[§] A: Krueger; B: Price; C: Titus; D: Nailor; E: Metalaire

[*] Size in duct diameter

Table B1: Description of the 11 types of diffusers on the market.

The isothermal throw length ($T_{0.25}$) of each diffuser for the terminal velocity of 0.25m/s can be found in the diffuser manufacturer catalog in accordance with the airflow rate. By employing the EDT (Equation B3) for heating mode, the ADPI value can be calculated using the measured velocity and temperature data.

The uncertainty of the proposed diffuser selection methodology depends on several factors. Specifically, the measurement uncertainty depends on the accuracy of the instruments used and factors relates to experimental set-up, such as diffuser installation, and flow adjustment and balancing. Other factors, such as variation in the geometry of

diffusers produced by different manufacturers, as well as variations in diffuser size for the same diffuser type, introduce different levels of uncertainty. Because of the high accuracy of velocity and temperature sensors used (±0.03m/s and ±0.1^{o}C respectively) in this study, the error propagation analysis showed that the uncertainty caused by instrumentation had a small impact on calculated effective draft temperature with a range of -2.2 to 2^{o}C, and consequently even smaller influence on ADPI compared with the impacts caused by the variation in the experimental set-ups. The uncertainty caused by the experimental set-up was evaluated by repetitions of experiments for the same diffuser at various stages of the project. The result showed that uncertainty caused by experimental set-ups generated a variation in ADPI of roughly ±2.7% (absolute value, 95% confidence interval). When considering the variation in ADPI versus *T/L* curves (illustrated in Figure B1), however, the largest impact is caused by the variation in diffuser sizes, and in the geometries of diffusers produced by different manufacturers for most of the 11 diffuser types. In the result table, the uncertainty caused by different manufactures and diffuser sizes are expressed by 95% confidence interval for the maximum ADPI.

Results

This section first exemplifies possible thermal stratification issues when $T_{0.25}/L$ ratio is small, then shows ADPI data for the 13 types of diffusers. Moreover, an ADPI selection guide for heating mode is presented using the measured ADPI data for the 13 diffuser types in the same manner as the cooling mode described in ASHRAE Handbook *Fundamentals* (2009).

Figure B5 illustrates two examples of average vertical temperature distributions in the test chamber using round ceiling diffusers at two different supply airflow rates. The two cases both have an ADPI nearly 95% in terms of the heating ADPI model. The diffuser for the high thermal stratification case shown in Figure B5(a) has a low $T_{0.25}/L$ of 0.75. Hence, the warm air provides a decreased momentum to mix with the air in the occupied zone and stagnates above due to buoyancy force. A greater temperature gradient can be observed in the upper region. As a result, the ventilation strategy might be flawed for pollutant removal effectiveness even though the calculated ADPI is as high as 95%. In contrast, the second example presented in Figure B5(b) shows a low thermal stratification in the whole space because of a greater $T_{0.25}/L$ of 2.1 and as a result of a stronger mixing effect. Figure 5B implies that a low $T_{0.25}/L$ in the diffuser selection and layout may result in poor indoor air quality even though ADPI is high in the occupied zone.

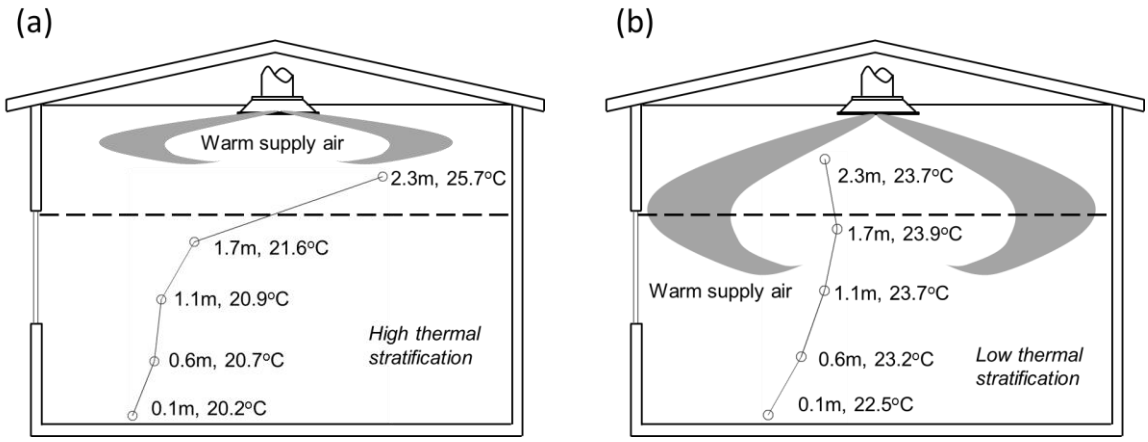

Figure B5: Examples of thermal stratifications in the chamber using round ceiling diffusers; (a) High thermal stratification; (b) Low thermal stratification.

The ADPI as a function of $T_{0.25}/L$ for the 13 diffuser types is shown in Figure B6. The results for each diffuer type aggregate measured ADPI for different diffuser sizes and manufactures. The second-order polynomial curve fitting is applied to generate ADPI profiles described in the illustration of Figure B1. In Figure B6**,** the ADPI of the adjustable blade grilles statistically increases gradually with $T_{0.25}/L$ because a greater $T_{0.25}/L$ can create better mixing while maintaining an acceptable air speed. In the range of $T_{0.25}/L$ from 0.5 to 2.2, ADPI is higher than 80% except for the point with the largest $T_{0.25}/L$. The reason is that the grille used in the measurement of this point has a smaller net area. This results in the jet from the grille having an air speed exceeding 0.35m/s at more regions in the occupied zone. It should also be noted that high thermal stratification occurs when $T_{0.25}/L$ is less than 1.1 resulting in the warm supply air stagnating in the upper region of the room and leaving the occupied zone poorly ventilated. Consequently, ventilation designs for heating mode should avoid this lower $T_{0.25}/L$ range.

The highest ADPI for round ceiling diffusers occurs in the lower and higher $T_{0.25}/L$ ratios. However, when $T_{0.25}/L<1.4$, warm air stays above the occupied zone and most locations in the occupied zone fall into the EDT comfort region only because of low air movement. However, the temperature gradient in this range of $T_{0.25}/L$ exceeds the ADPI criterion (3^{o}C per meter vertically), so this range should be avoided.

The airflow delivered by plaque face diffusers has an increased Coanda effect because of a small opening height (~1 to 2cm). Hence, the airflow from these diffusers tends to be attached to the ceiling especially for heating mode conditions. To overcome possible thermal stratification, $T_{0.25}/L$ needs to be at least as large as 2.1 as demonstrated

in Figure B6**.** The linear slot diffuser shows ADPI values greater than 80% at a large $T_{0.25}/L$ range of 1.3-3 without thermal stratification issues.

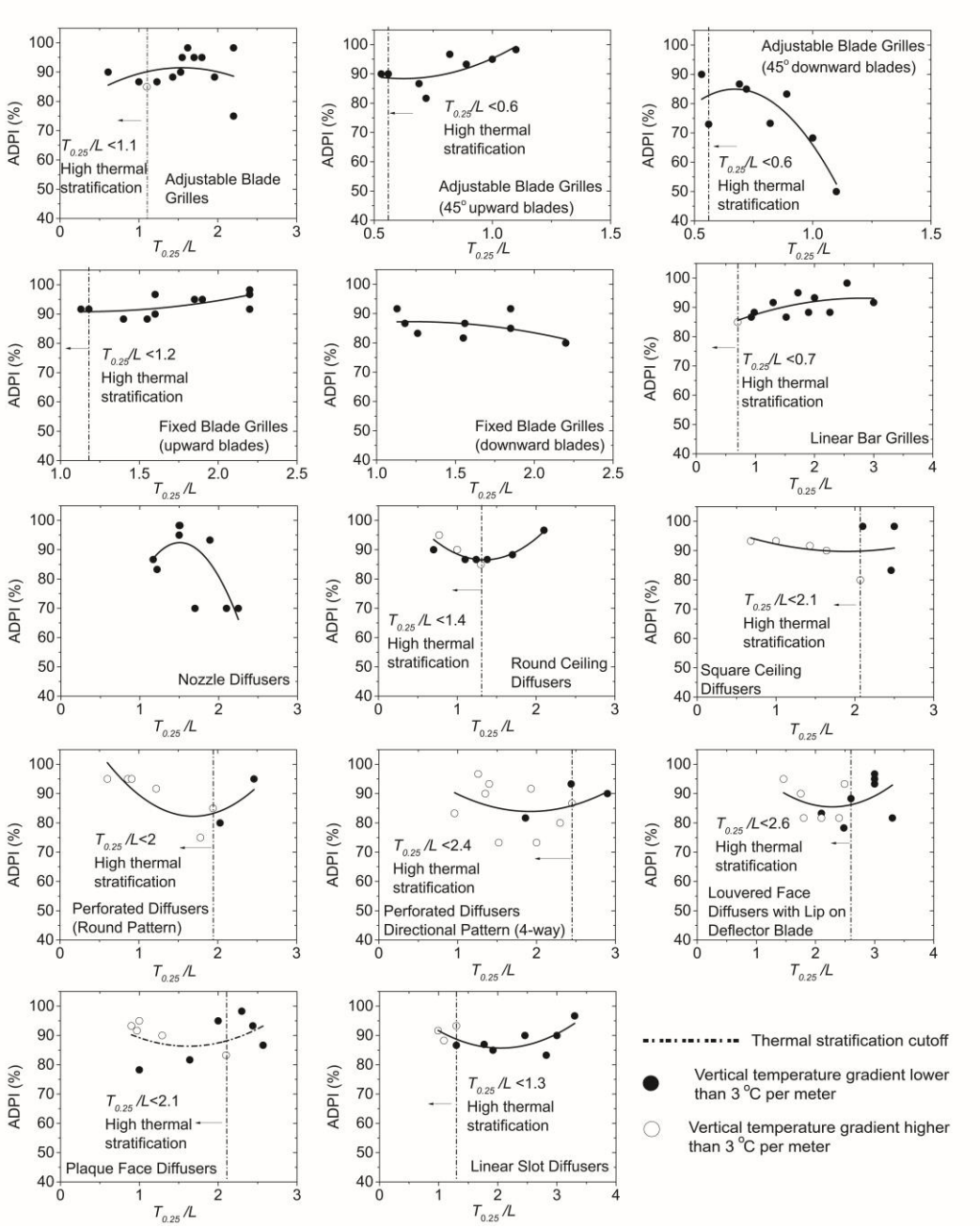

Figure B6: ADPI values vs. $T_{0.25}/L$ for diffusers/grilles under heating condition.

Figure B6 shows that a larger $T_{0.25}/L$ could reduce thermal stratification for all types of diffusers/ grilles. The reason is that jet momentum will be increased and therefore exert greater impact on the jet than buoyant effect. The comparison of buoyant effect and jet momentum (inertial) effect can be represented by Archimedes number. A smaller Archimedes number denotes a lower effect of buoyancy force due to temperature difference, leading to a higher ADPI value. Even though Archimedes number might be an indicator of ADPI for heating mode, it is not directly linked as $T_{0.25}/L$ to diffuser/ grille properties. The Archimedes number is also very useful to characterize the impact of the height of the room on the buoyancy effect under heating condition. Nevertheless, this investigation considers a fixed room height and therefore the Archimedes number is a function of only temperature difference between supply and room air, and also jet momentum rather than room size. To use Archimedes number as a design parameter in diffuser/ grille selection procedure, an HVAC designer needs more input variables; among them is the jet discharge velocity that is not often provided in the diffuser/ grille manufacturer catalogs. Consequently, this dissertation reports ADPI as a function of $T_{0.25}/L$ rather than Archimedes numbers.

By summarizing the ADPI data for diffusers in Figure B6, the paper provides an ADPI selection guide for heating mode when using one of the 11 diffuser types presented in Table B2. The selection guide provides the maximum ADPI for each diffuser type and the range of $T_{0.25}/L$ that can create an ADPI greater than 80%. The linear bar grilles and round ceiling diffusers have larger ranges of $T_{0.25}/L$ ratios (0.7-3 and 1.4-2.1) that generate a large ADPI (>80%) for high sidewall and ceiling diffusers, respectively. The ceiling slot diffusers have a range from 1.3 to 3 for ADPI higher than 80%. The large ranges indicate the robustness of diffusers for variable air volume (VAV) systems.

Terminal Device	$T_{0.25}$ / L for Max. ADPI	Maximum ADPI (95% confidence interval)	$T_{0.25}/L$ range (ADPI>80%)
Adjustable Blade Grilles (High Sidewall installation)	1.6	91±4%	1.1-2.2
Fixed Blade Grills(High Sidewall installation)	2.2	92±6%	0.6-2.2
Linear Bar Grilles (High Sidewall installation)	2.5	93±3%	0.7-3
Nozzles(High Sidewall installation)	1.5	92±7%	1.2-1.9
Round Ceiling Diffuser	2.1	96±3%	1.4-2.1
Square Ceiling Diffuser	2.5	91±9%	2.1-2.5
Perforated Diffusers-Round Pattern	2.5	91±9%	2-2.5
Perforated Diffusers- Directional Pattern (4-way)	2.4	90±10%	2.4-2.9
Louvered Face Diffusers-with Lip on Deflector Blade	3	93±6%	2.6-3.3
Plaque Face Diffusers	2.3	90±6%	2.1-2.6
Linear Slot Diffusers	3	91±8%	1.3-3

Table B2: ADPI Selection Guide for Heating Mode (35-40W/m^2).

Discussion

This work builds the connection between ANSI/ASHRAE Standard-55 and the ADPI method described in ANSI/ASHRAE Standard-113 by comparing 80% thermal acceptance using the PMV index and cooling mode ADPI based on Houghten's 80%

acceptance. Employing the same technique, a heating mode ADPI is developed and shows compliance to PMV as well. The ADPI method only considers two variables: air temperature and local air speed. Besides these two variables, however, PMV involves four additional factors involving environmental effects and human behavior: radiant temperature, humidity, metabolic rate and clothing insulation. This paper compares PMV and ADPI by fixing the four factors at values for a typical office environment in summer or winter and for only a sedentary office-worker condition. However, indoor relative humidity might be much different in summer and winter. Therefore, the PMV region for 80% thermal acceptance could be different from that in Figure B2 and Figure B3. Under such conditions, the ADPI method might show less compliance to the PMV index if indoor thermal environment or occupant behavior deviates from the standard office condition used in this study. However, one can modify ADPI method according to PMV using the same manner presented in this paper if needed.

The heating mode ADPI in Table B2 was obtained using a constant cooling source of 35-40W/m^2. When the heating load is decreased, supply air will be affected by a lower level of buoyancy, providing better mixing effects in the occupied zone as $T_{0.25}/L$ ratios decrease. It is expected that a low heating load would create an environment approaching isothermal condition. Therefore, the ADPI value might be higher than that determined in this study when a lower heating load is encountered. This improvement of ADPI at a lower indoor thermal load for heating mode is consistent with cooling mode behavior reported in previous studies (Miller and Nash 1971; Miller and Nevins 1972). At a higher heating load, however, ADPI values would be reduced due to increasing buoyancy force. Finally, the number of diffusers tested in this study may not be sufficient

to represent all diffusers on the market. Although several repeated test at specific $T_{0.25}/L$ ratios show that manufacture and size might be an important contributor to uncertainty of ADPI, the limited data points prohibit calculating a meaningful value for the average variations of ADPI with $T_{0.25}/L$ for each diffuser type. A statistical sensitivity analysis or a larger pool of sample diffusers will be necessary in future studies.

Summary

This paper proposes an ADPI method for heating mode in terms of PMV index described in ASHRAE Standard-55. The proposed ADPI model considers thermal stratification as well as the range of effective draft temperature and maximum local air speed. Furthermore, this work generates an ADPI (>80%) selection guide for heating mode by measuring ADPI as a function of the ratio of throw length to characteristic room length for 11 types of diffusers on the market in a test chamber. The diffusers are selected from three to four manufacturers and with two sizes of each type. The measurements show that each diffuser type in this study is able to generate the maximum ADPI of greater than 80%. In addition, it is found that linear bar grilles and round ceiling diffusers are more robust and generate ADPI values of greater than 80% over a large range of $T_{0.25}/L$ ratios.

Acknowledgement

Financial support for this work was provided by the American Society of Heating, Ventilation, and Air Conditioning Engineers (ASHRAE RP-1546). The authors wish to thank Krueger, Metalaire, Nailor, Price and Titus for their generous donation of diffusers.

APPENDIX C: MODELING OF PARTICLE DISPERSION IN INDOOR ENVIRONMENT: COMPARISON OF THE LAGRANGIAN METHOD COUPLED WITH RANS AND LES TURBULENCE MODELING (RP-1512)

Shichao Liu — *Student Member ASHRAE*

Atila Novoselac, Ph.D — *Member ASHRAE*

(Published in *HVAC&R*)

Abstract

Indoor particulate contaminants can be generated in many ways, commonly from human activities, infiltration of HVAC systems, or resuspension from indoor surfaces. Most of these sources are transient and generate non-uniform particle distribution in the space. This study used experimental and numerical methods to investigate the dispersion of three different particle sizes (0.7, 2.5 and 7 micrometers) emitted from typical source positions. A test room and simplified thermal manikins were employed to mimic a realistic indoor environment, and experimental data were compared with particle modeling using the Lagrangian method coupled with Reynolds Averaged Navier-Stokes (RANS) and Large Eddy Simulation (LES) Computational Fluid Dynamics (CFD) turbulence models. Particle dispersion was studied for two ventilation patterns: buoyancy-driven ventilation and well-mixed ventilation. The results provided a comparison of Lagrangian-RANS particle modeling, Lagrangian-LES particle modeling, and experimental data considering non-uniform temporal and spatial particle concentrations. Experimental and modeling results were evaluated with three different metrics: peak normalized concentration at various locations, peak-concentration occurrence time, and mean exposure defined as the averaged concentration in the

occupant's breathing zone. The results show that Lagrangian-LES more accurately predicts concentration fluctuation during particle emission. Considering long-term exposure, however, both methods show similar results.

Keyword: Particle modeling, Indoor environment, Lagrangian, LES

Introduction

Prediction of particle dynamics in a building environment is very important for designing and maintaining a healthy indoor environment. Human exposure to particles is determined by processes that include particle dispersion around sources, their transport through the space, as well as their distribution in the vicinity of an occupant. Research studies have shown that a 'perfect mixing' assumption can underestimate the human exposure to particulate pollutants (Melikov and Kaczmarczyk 2007; Rim and Novoselac 2009), and pointed out a need for reliable and affordable modeling methods that can simulate particle dynamics in indoor environments. Since particle dispersion depends on the airflow field, particle modeling can be considered as an extension of Computational Fluid Dynamics (CFD) modeling. Generally, the particle modeling can be conducted by Eulerian or Lagrangian methods. Both methods can accurately predict the steady-state particle concentration distribution. However, particle sources in indoor environment are often unsteady, and previous studies showed that the Lagrangian method is often more suitable than Eulerian for modeling a particle cloud in typical indoor environments (Zhang and Chen 2007).

There are two commonly used CFD methods coupled with the Lagrangian particle tracking model: Reynolds-Averaged Navier Stokes (RANS) modeling and large eddy simulations (LES). The RANS modeling requires less computing time than LES. However, it requires more modeling work related to implementation of the effect that turbulence has on particle diffusion than LES. The effect of turbulence is implemented into the Lagrangian particle tracking model by the use of a discrete random walk (DRW) model. Since the LES model resolves the velocity field in large eddies and only models small-scale eddies, it is questionable if the LES coupled with Lagrangian particle tracking actually improves particle diffusion modeling.

Many studies of particle dispersion in indoor environment use RANS-Lagrangian particle modeling. A significantly lower number of studies use LES-Lagrangian particle modeling. The RANS-Lagrangian modeling of indoor environment method has mainly been used to predict the temporal development of mean concentration (Lu et al. 1996; Rim and Novoselac 2009), the personal exposure to particulate contaminants (Rim and Novoselac 2009; Lai and Wong 2010; Lai and Wong 2011), air cleaning effectiveness (Novoselac and Siegel 2009; Gao and Zhang 2010), and particle deposition in public transportation systems (Zhang et al. 2009; Zhu et al. 2012). While LES has been successfully applied to airflow simulations in buildings, LES was coupled with the Lagrangian particle tracking in buildings and airplane cabins only in a few studies (Emmerich 1998; Liu et al. 2012; Chen et al. 2013). All these previous analyses indicate lower computational cost as the main reason for the more common use of RANS-Lagrangian models than LES-Lagrangian. However, it is not clear how different the

simulation results are when considering peak cumulative exposure from unsteady particle clouds.

Several previous studies used experimental data for the validation of Lagrangian particle modeling. Some of these studies focused on particle dispersion in the bulk air (Lu et al. 1996; Chung 1999; Bouilly et al. 2005; Richmond-Bryant et al. 2006; Zhang and Chen 2006) while others focused on the emission characteristics and concentrations in the vicinity of an occupant (Rim and Novoselac 2009; Lai and Wong 2010; Lai and Wong 2011) and human breathing zones (Spitzer et al. 2010). These studies provide valuable information about the accuracy of Lagrangian particle modeling, but the two major drawbacks of these previous experimental validation studies are (1) the particle size resolution or poorly defined particle sizes, and (2) the absence of transient sources.

The study presented in this paper investigates the impact of two turbulence models (RANS-RNG and LES) on modeling of particle diffusion and dispersion considering different particle sizes. It focuses on the dispersion from transient particle sources and evaluates the accuracy of the two models.

Methodology

This study used experimental and numerical methods. It evaluated the dispersion of three size particles: 0.7μm, 2.5μm and 7μm emitted from two transient sources in the vicinity of (1) occupant feet and (2) supply air. A test room and simplified thermal manikins were employed to mimic a realistic indoor environment, and state-of-the-art instruments recorded the temporal and spatial concentration changes in the room. CFD models were generated for modeling initial particle dispersion and particle cloud

dynamics by RANS-Lagrangian and LES-Lagrangian modeling methods. The following two subsections provided details about the experimental and numerical methods in this study.

Experimental apparatus and measurements

A full-size test chamber with dimensions of 6m (236 in.)×4.5m (177 in.)×3m (118 in.) with a sophisticated control system (HVAC) was used as a test room (Figure C1). The chamber can be used to generate various ventilation patterns by changing the ventilation configuration. The surface temperature of the chamber was controlled and adjusted to mimic a thermal source such as a window, and the heat from transmitted solar radiation and heat conduction. To increase the accuracy of experiments, the background particle concentration was minimized by the use of a HEPA filter in the air supply duct. Moreover, the background concentration was subtracted from the concentration measured after a cough, and the graphs in the result section show the particle concentration increase due to the cough or other particles injected into the chamber during the experiments.

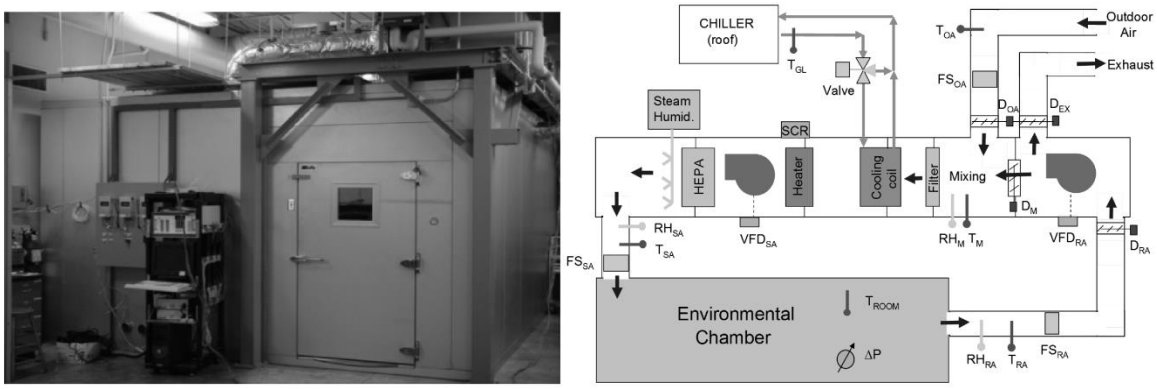

Figure C1: Test chamber used to mimic indoor environment (left) with the HVAC system for environmental control (right).

Indoor particles have sizes ranging from smaller than 1μm to larger than 10μm. This study used 0.7μm particles to study smaller particles (<1μm). For short-lived transient particle sources, the turbulent dispersion of small particles (<1μm) has a larger impact on particle transport than the diffusion caused by Brownian motion (Rim and Novoselac 2009). For this reason, it was assumed that particles smaller than 1μm behaved similarly to larger particles with regard to dispersion, but not with regard to deposition. Also, it has been shown that ventilation has a much larger impact on the small particle removal than the deposition for typical airflow rates in indoor environments (Waring and Siegel 2008). The behavior of large particles was studied using 7μm particles. Since gravitational settling has an increased impact on airflow dynamics for particles larger than 3μm, 2.5μm particles were used to represent medium-sized particles (Rim and Novoselac 2010). Latex spherical mono-dispersed particles (size variation coefficient, 1%-3%) with a density of 1050kg/m^3 were used to generate small and medium particles, while Arizona Test Dust (ATD, nominal 5-10μm, Powder Technology, Inc) was used to

produce large particles. All particle concentrations were measured with Aerotrak particle counters (TSI). Table C1 gives a summary of particle characteristics.

Size, (μm)	Material	Density, (kg/m^3)	Slip correction	Generator
0.77	Latex	1050	1.22	Collison Nebulizer
2.5	Latex	1050	1.07	Collison Nebulizer
7	ATD	2650	1.02	ATD generator

Table C1: The characteristics of particles in the experiment.

Two occupants were simulated with two simple-geometry cylinders, which had a diameter of 0.3m (11.8 in.) and a height of 1.5m (59 in.). At the bottom of the first cylinder was a particle source (index occupant) and the concentration was measured in the breathing zone of the second cylinder (target occupant). Both cylindrical manikins were fully coated with electric heaters, which generated a constant heat flux of 90W. The heaters were coated with aluminum foil, minimizing radiation to a negligible level and defining convective heat flux thermal boundary conditions for the CFD models. Beside the two thermal manikins, two unheated boxes and tables were placed against two walls to represent furniture.

The indoor airflow pattern, the source position relative to the main airflow pattern, and the occupants substantially affect the particle dispersion and occupant exposure. In residential buildings, buoyancy driven ventilation (BDV) is a dominant air and pollutant transport mechanism. Well-mixed ventilation (WMV) is common for

commercial buildings and residences where the air conditioning system operates. BDV and WMV are two widely utilized schemes and are also well-studied in previous literature (Yin et al. 2009; Lai and Wong 2010). Therefore, these two ventilation schemes were applied in the experimentation. The airflow pattern typically for BDV was achieved by use of a diffuser providing "low-momentum displacement ventilation", while airflow typically for WMV was produced by a high-momentum supply diffuser at the ceiling level (Figure C2).

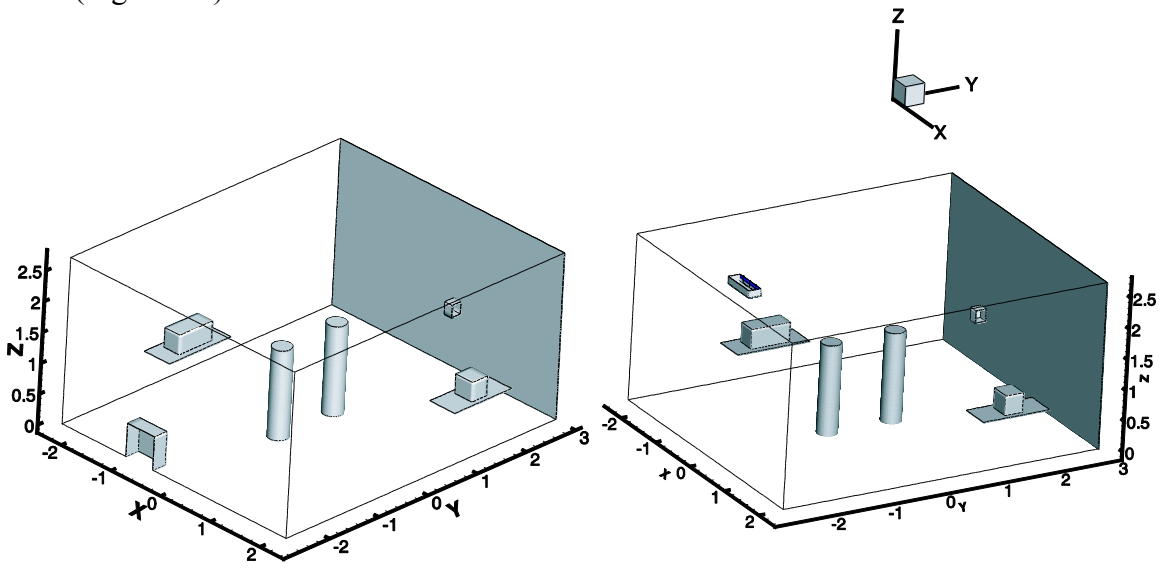

Figure C2: Schematic of two set-ups. Left: BDV scheme generated by the displacement ventilation diffuser at floor; Right: WMV scheme produced by the side diffuser at the ceiling level.

For each ventilation scheme, particles were generated from two different positions to mimic different particle sources. For the cases with position 1, particles were injected in the diffusers, which mimics outdoor particles (and indoor particles recirculated by return diffusers) that spread through the ventilation system. For the cases with particle position 2, a particle source was positioned near the index thermal manikin

(0.02m (0.79in) from the cylinder and 0.3m (11.8in.) above the floor). The mimicked particles from this source were resuspended by various occupant activities from the floor. Another situation can develop where the particle cloud is captured and carried by the occupant's thermal plume. Four scenarios, two ventilation systems, and two sources are considered and listed in Table C2. In scenarios where the source was the supply air, particles were emitted into the ventilation ducts at least one meter upstream of the supply diffusers, which enabled particles to be uniformly distributed upon leaving the supply diffuser. In scenarios with the source in the vicinity of the cylindrical thermal manikin, particles were injected by a Collison nebulizer at a low velocity <0.1m/s to minimize the disturbance of the injection on local particulate plumes. However, the ATD generator generated large particles at a high airflow rate. Hence, it prevented particles from being injected into the low momentum region near the feet of the index manikin. Considering this, ATD was only emitted in the high momentum region, the supply air duct, in this study. The injection period for 0.7μm and 2.5μm particles was 100 seconds, while the large particles (or ATD) were injected for only 30 seconds due to the high injection rate.

Scenario	Ventilation Pattern	Source location	Particle sizes
A	BDV	Air supply duct	0.7μm, 2.5μm and 7μm
B	BDV	Feet region	0.7μm and 2.5μm
C	WMV	Air supply duct	0.7μm, 2.5μm and 7μm
D	WMV	Feet region	0.7μm and 2.5μm

Table C2: Scenarios for the particle transmission in the large chamber.

For particle concentration measurements, five Aerotraks were used. They monitored the variation of particle concentration in the breathing zones (near the heads) of the two thermal manikins, at the room exhaust, and three other characteristic positions in the space. During the experiments, five of six locations were monitored for each scenario. The five Aerotraks were calibrated side-by-side before the measurements. It was observed that the maximum discrepancy in transient particle concentration was about 12%.

Figure C3 and Table C 3 provide details about these locations. Due to space limitations, this paper primarily focuses on the particle concentration in the breathing zone of the target occupant, P3. The particle concentration measured at this location provides good validation data for particle modeling, considering the particle transport by the advection along the buoyancy-driven flow and turbulent diffusion that is the main contributor to horizontal particle transport (i.e., normal to the main buoyancy flow). The particle concentrations were recorded for a period of 1200 seconds. Nevertheless, high particle concentration variations occurred during the first 200 seconds. Therefore, this paper only presents the results for a short period. The experiments of the particle transmission were repeated three times for all four scenarios. Again, the background concentration was subtracted from all the values of the concentration.

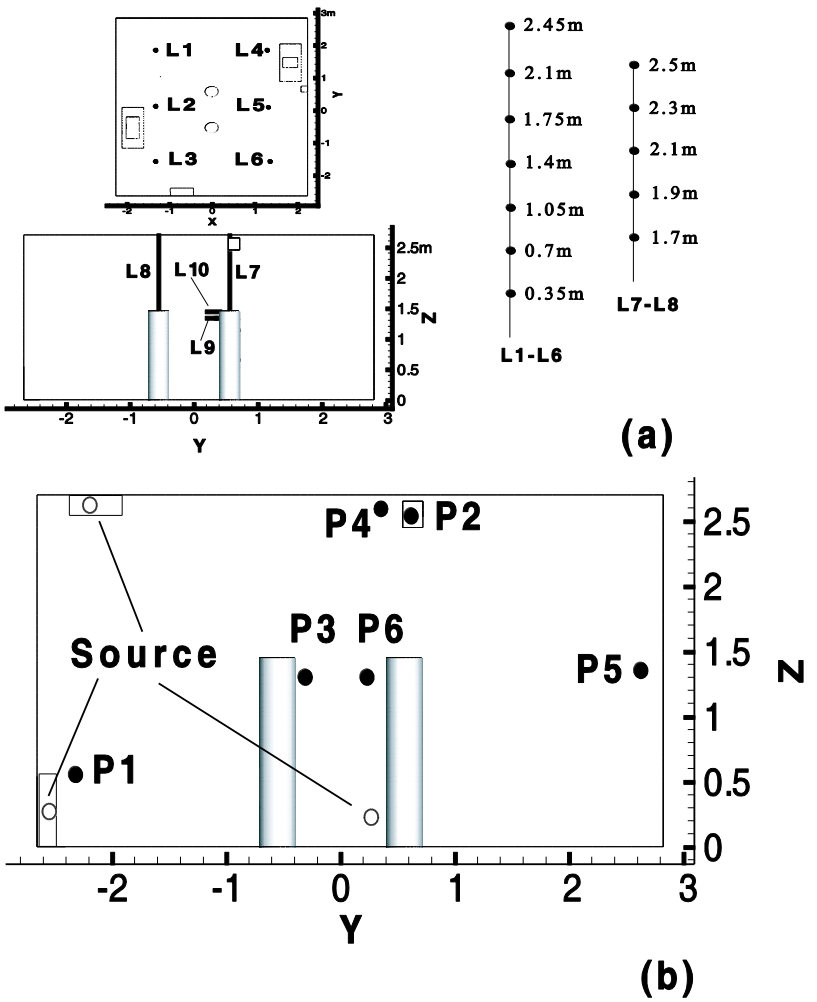

Figure C3: The sampling positions of (a) temperature, velocity and (b) particle concentration.

Samples	X, m	Y, m	Z, m
1	0(0 in.)	-2.35(-92.5 in.)	0.59(23.2 in.)
2	2.05(80.7 in.)	0.63(24.8 in.)	2.55(100 in.)
3	0(0 in.)	-0.35(-13.8 in.)	1.3(51.2 in.)
4	0(0 in.)	0.55(21.7 in.)	2.65(104.3 in.)
5	0(0 in.)	2.72(107 in.)	1.3(51.2 in.)
6	0(0 in.)	0.35(13.8 in.)	1.3(51.2 in.)

Table C3: Sample positions of the particle concentration.

Since the local airflow significantly affects the particle concentration distribution, the study also measured the local air velocity and temperature throughout the chamber and in the vicinity of the thermal manikins (0.025m (0.98 in) from the surface). The velocity and temperature were monitored using hot sphere anemometers (HT-400, SENSOR, Poland) with an accuracy of 0.03m/s for velocity and 0.3^{o}C for temperature. The presented velocities and temperatures were averaged over three minute measurements with a frequency of 0.5Hz (2 seconds for each sample). The detailed positions are shown in Figure C3.

Modeling and Numerical Analysis

Both a Reynolds Average Navier-Stokes (RANS) and a Large Eddy Simulation (LES) turbulence model with a dynamic Smagorinsky Subgrid Scale model (SGS) were used to simulate the three dimensional turbulent airflow fields in the chamber. An

Eulerian approach was used to simulate the airflow field in the chamber and then particle trajectories were calculated with a Lagrangian method.

As recommended by previous studies (Chen 1995; Rim et al. 2008), the RNG k-ε model generally performs better for indoor airflows and buoyancy-driven flows than other eddy-viscosity models. The governing equations can be generalized as:

$$\frac{\partial \emptyset}{\partial t} + \sum_{i=1} \frac{\partial}{\partial X_i}(U_i \emptyset) = \sum_{i=1} \frac{\partial}{\partial X_i}\left(\Gamma_\emptyset U_i \frac{\partial \emptyset}{\partial X_i}\right) + S_\emptyset \quad \text{(C1)}$$

where Φ can represent a velocity component *u, v, w,* turbulent kinetic energy, *k*, turbulent dissipation rate, ε and air temperature, *T*. Γ_Φ is the effective diffusion coefficient. S_Φ is the source term of the equation. The effect of buoyancy in the momentum equation was calculated with the Boussinesq approximation.

LES has recently attracted attention for its use in the simulation of indoor environments. In LES, the large-scale eddies are solved directly, like Direct Numerical Simulation (DNS) and the small eddies are modeled using sub-grid scale models (SGS). A spatial filtering operation is used to separate the large and small eddies, which results in filtered continuity and momentum equations in a similar form to the RANS equations:

$$\frac{\partial \overline{u_\iota}}{\partial x_i} = 0 \quad \text{(C2)}$$

$$\frac{\partial\, \overline{u_\iota}}{\partial t} + \overline{u_J} \frac{\partial\, \overline{u_\iota}}{\partial x_j} = \frac{1}{\rho} \frac{\partial\, \bar{p}}{\partial x_j} + \nu \frac{\partial^2 \overline{u_\iota}}{\partial {x_j}^2} + \frac{\partial\, \tau_{ij}}{\partial x_j} \quad \text{(C3)}$$

where the over-bar represents a spatial filtering operation, and $\overline{u_i}$ and $\bar{p}$ are the filtered velocity and pressure, respectively. The additional stress terms τ_{ij} are attributable to convective momentum transport due to interactions between the unresolved or SGS eddies. These terms are commonly termed the sub-grid-scale stress. The SGS viscosity can be evaluated as follows:

$$\mu_{SGS} = \rho(C_{SGS}\Delta)^2|\bar{S}| = \rho(C_{SGS}\Delta)^2\sqrt{2\overline{S_{ij}S_{ij}}} \tag{C4}$$

where C_s is the Smagorinsky constant dependent on flow characteristics, Δ is filter cutoff width and S_{ij} is the strain rate. Lilly (1992) suggested a least-squares approach to evaluate the local values of C_{SGS} shown below:

$$C^2{}_{SGS} = \frac{< L_{ij}M_{ij} >}{M_{ij}M_{ij}} \tag{C5}$$

where L_{ij} and M_{ij} are the resolved stress tensor, and the angular bracket < > indicate an average processing over the homogeneous direction.

A Lagrangian model method solves the particle momentum equation for each individual particle. Solving the force balance equation for each particle enables the calculation of the trajectory for each particle in the simulation domain. By equating particle inertia with external forces, the momentum equation for a single particle has the following form:

$$\frac{d\overrightarrow{u_p}}{d\tau} = \overrightarrow{F_G} + \overrightarrow{F_D} + \overrightarrow{F_B} + \overrightarrow{F_L} + \overrightarrow{F_{Th}} \quad \text{(C6)}$$

where $\overrightarrow{u_p}$ is particle velocity, τ is time, and $\overrightarrow{F_G}$, $\overrightarrow{F_D}$, $\overrightarrow{F_B}$, $\overrightarrow{F_L}$, $\overrightarrow{F_{Th}}$ are Gravitational, Drag, Brownian, Lift, and Thermophoretic forces (per unit of mass), respectively. In the simulation, the study only considered drag and gravity forces since the others are negligibly small.

With the Lagrangian particle transport method, the velocity fluctuation (u') is calculated based on turbulence kinetic energy (k) and a normally distributed random number (ξ) obtained from a random number generator:

$$\overline{u'} = \xi \sqrt{\frac{2}{3}k} \quad \text{(C7)}$$

Also, the turbulence kinetic energy (k) contains only the kinetic energy of eddies smaller than the resolved size for LES.

The simulations were performed with a commercial CFD software, ANSYS FLUENT (version 12.1) using a hexahedral grid. The cells were refined gradually with a ratio of roughly 1.4 (247,000, 500,000 and 1,000,000) to generate grid-independence results for RANS simulation. The study found that the predicted velocity and temperature changed at a negligible level for the three meshes. Considering LES simulation, the decreasing cell size reduces the effects of sub-grid model and enables the calculation to approach DNS. Therefore, the grid independence was not performed for LES.

In this study, the same mesh (500,000 cells) was utilized for the RNG and LES model in order to compare their performance. All of the discretizations followed a

second-order upwind scheme except for the momentum equation of the LES, which used a bounded central differencing scheme. The PISO algorithm was used as the pressure-velocity coupling method. The staggered scheme, PRESTO!, was employed for the pressure interpolation concerning the buoyancy flow. Due to the low particle load in the bulk environment, the particle simulation used one way coupling of airflow and particles. The convergence criteria were assumed to have been met when the iteration residuals became less than 10^{-6} for the energy equation, and 10^{-4} for the other parameters in all simulations. Table C4 summaries the information of simulation in this study.

Set-up	BDV	WMV
Chamber volume(m^3)($in.^3$)	$67(4.1\times10^6)$	$67(4.1\times10^6)$
Ventilation Patten	Buoyancy driven	Mixing
# of cells	496650	500,086
Cell geometry	Hexahedral	Hexahedral
Minimum cell volume(m^3) ($in.^3$)	$2.86\times10^{-7}(0.017)$	$3.43\times10^{-7}(0.02)$
Maximum cell volume(m^3) ($in.^3$)	$9.97\times10^{-4}(60.8)$	$1.07\times10^{-3}(65.3)$
Maximum aspect ratio	29	23
Supply velocity distribution	Measured	Measured
Air exchange rate(hr^{-1})	3.2	3.2
Diffuser modeling	Momentum method (Chen Q. 1991)	N/A
Turbulence intensity	5%	5%
Hydraulic diameter of openings(m)(in.)	0.54 (21.3)	0.15(5.9)
Momentum added($kg\bullet m/s^2$)	0.173	N/A
Supply air temperature(^oC)	17.36	17.57
Total heat rate(W)	462	500
Number of particles injected(#)	600,000	600,000
Time step size (s)	0.05	0.05
Minimum CFL number	0.9	1.8
Physical time(s)	>1200	>1200
Particle deposition on surfaces	No	No

Table C4: Summary of numerical simulations adopted in the four setups.

Data processing

In this study, volume averages were employed to calculate the particle concentration at a certain point in the chamber. The approach defined a group of locations of interest using volumes that were spherical, cubic, or cylindrical, depending on the local airflow pattern and particle transmission characteristics. The particles generated were tracked in order to determine the particle number that resided in each prescribed control volume at each time step. The method is not complex, but care must be taken in selecting the control volume to obtain reliable results. Theoretically, the particle number concentration can be described as:

$$C_p = \lim_{V \to 0} \frac{N_p}{V} \tag{C8}$$

where C_p is the particle number concentration at a certain position, and N_p is the particle number in the control volume, and V is the volume around the defined position.

The volume needed to calculate the particle number concentration was determined by considering resolution requirements and the sampling airflow rate of particle counters. The volume size should be small enough to obtain the concentration at a specific location. On the other hand, the sampling volume size has to be larger than the zone of which a particle counter analyses the air. For example, the airflow rate of an Aerotrak is 2.83L/min in this study. In other words, the Aerotrak pulls 2.83 liters of surrounding air per minute. If the intake air is a sphere with a diameter of 0.05m (1.96 in.), the velocity at the boundary of the sphere is 0.006m/s, which is lower than typical indoor air velocities. This implies that a spherical volume of diameter 0.05m is large enough to enable the

movement of particles outside the volume to be negligibly affected by the airflow of the instrument. This study uses the calculation volumes of 0.05m (1.96 in.) in diameter at all locations.

Since unsteady RANS and LES simulate instantaneous flows, the particle concentration tends to present high fluctuations, especially for LES simulation. In order to "smooth" the fluctuations for better comparison, the study used a moving average approach to process the results. For a given series of variables, the first moving average is calculated by taking the average of the initial fixed subset of a variable series. Then the subset is modified by "shifting" forward, which excludes the first number of the series and includes the next number following the original subset in the series. The process is repeated over the entire data series. Equation (C9) shows the calculation for the moving average approach:

$$C_{average}\,(i) = \sum_{i}^{n=m+i} \frac{C(i)}{m} \tag{9}$$

where m is the number of variables being averaged (m=20 in this study) n is a dummy variable, and i is the ith element of the processed data.

To facilitate the comparison of experimental and calculated particle concentrations for different scenarios, all measurement results were normalized by a reference value. The ideal reference value is the particle emission concentration. However, the injection concentration of the particles was difficult to measure because of the unsteady emission rate, especially in the case of large particles. This was proved by a

concentration decay test that showed the decay rate of the small and medium size particles was mainly dominated by the ventilation. Particle deposition loss, however, tends to be of importance for the large particles such as 7μm particles. Therefore, for 7μm particles, the particle concentration was normalized by the instantaneous average concentration throughout the entire room. This instantaneous average concentration, C^*_{ref}, was calculated by taking the average concentration at the six locations for simulations and five locations for experiments during each individual sampling interval. The normalized value of this method reflects the extent to which the local concentration was higher or lower than average.

From the variation of particle concentrations at each measured location, three different metrics were calculated: (1) peak normalized concentration, (2) peak-concentration occurrence time and (3) mean exposure level. The peak normalized concentration provides insight into the maximum level of exposure. Furthermore, human respiratory activities, like coughing and sneezing, enhance the spread of epidemics which spread through air movement. This study calculated the peak-concentration occurrence time, or the time for a particle cloud to reach maximum concentration at a certain position from the time of particle emission. Finally, the mean exposure level was evaluated at each position for each scenario. This value was calculated by taking average particle concentrations over the entire sampling period (20 minutes) at a certain location.

Results and discussion

Velocity and temperature distribution

Figure C4 shows the background flow field and thermal distribution in the large chamber with buoyancy-driven ventilation. Generally, RNG and LES under-predict the thermal stratification in the lower region of the chamber with BDV. The major reason is the failure of the momentum method to mimic the entrainment of the airflow in the vicinity of the diffuser due to momentum loss (Cehlin and Moshfegh 2010). The results of LES show slightly larger discrepancies in temperature from the experimental data than RNG.

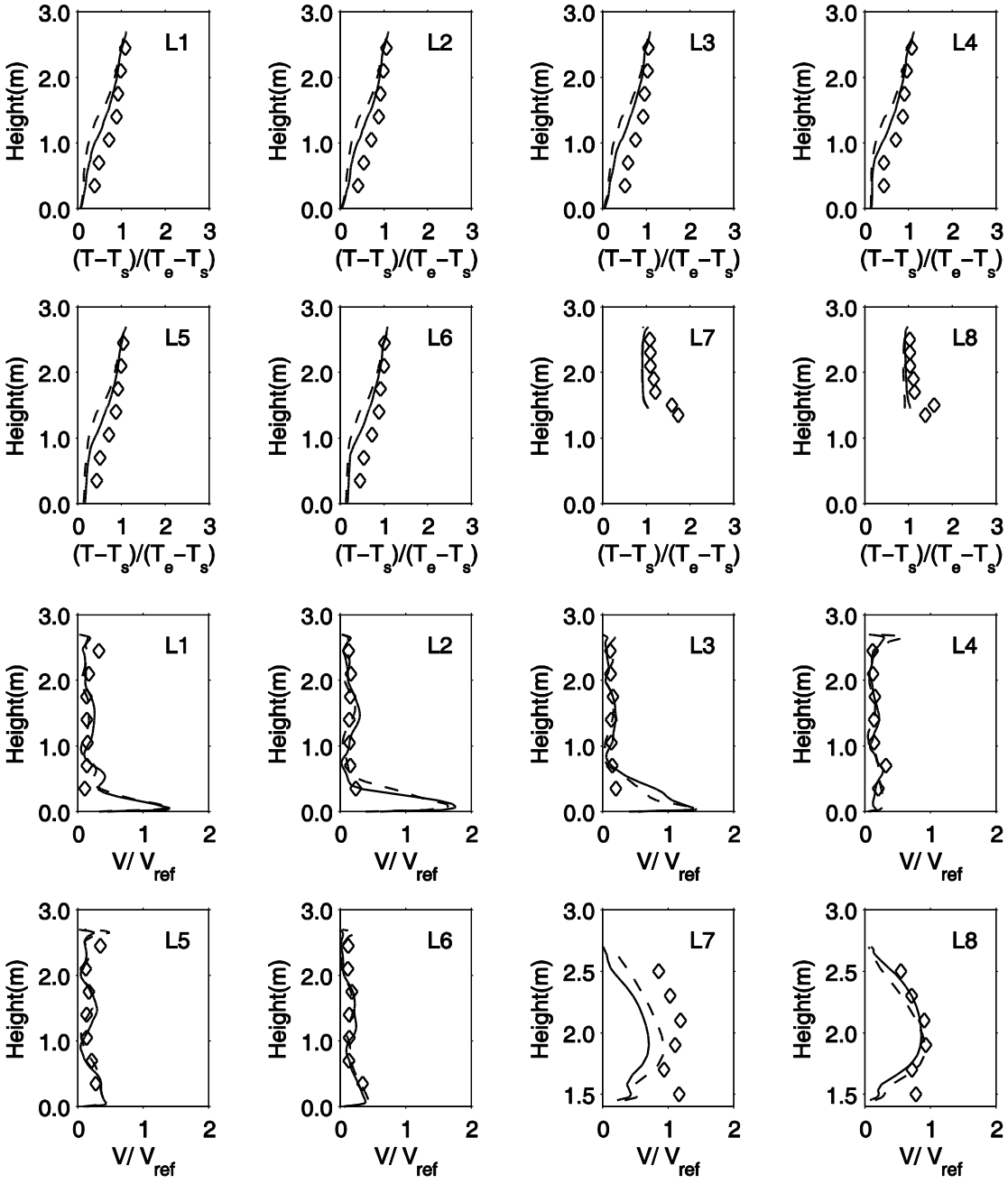

Figure C4: The comparison of velocity and temperature distribution in the large chamber (BDV). Symbol: Measurement; Solid line: RNG model; Dashed line: LES model.

For the velocity, both LES and RNG present good agreement with the experiments except for at L7 which is located in the high buoyancy region. The human thermal plume has high velocity fluctuation and RANS is lacking in its ability to capture the fluctuations. LES shows slightly better results in this thermal plume region.

Since the chamber with mixing ventilation has weak thermal and velocity gradients, the numerical results tend to have a better agreement with the experimental data as shown in Figure C5. The temperature distribution is inclined to be uniform except for in the occupants' thermal region, like L7, L8, L9 and L10. In mixing ventilation, LES tends to make a better prediction than RNG concerning both temperature and velocity distribution. However, both the LES and RNG models over-predict the velocity in the upper region of thermal plume above the occupants, L7 and L8.

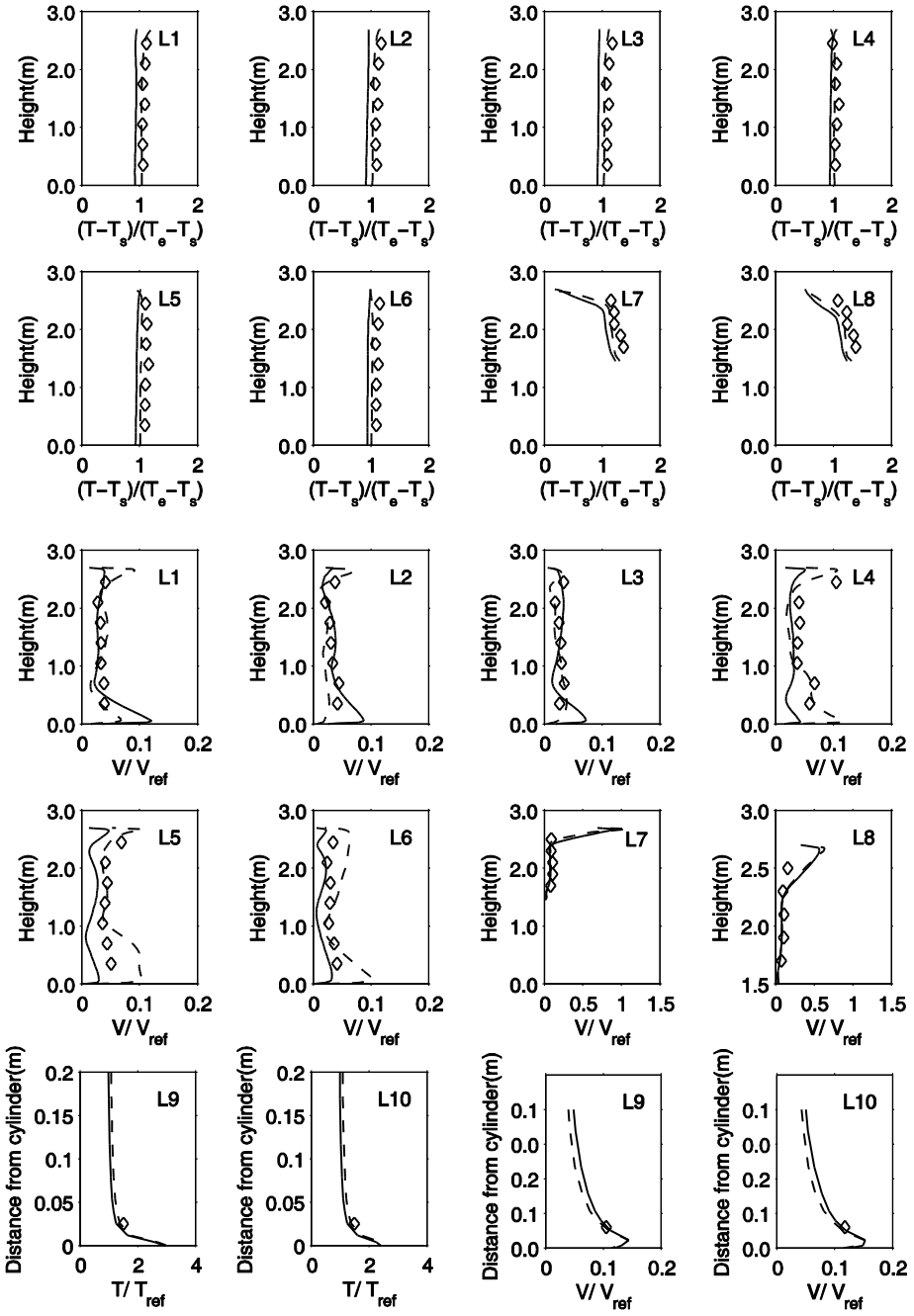

Figure C5: Comparison of the velocity and temperature distributions in the large chamber (WMV). Symbol: Measurement; Solid line: RNG model; Dashed line: LES model.

Particle concentration

This section describes the variation of particle concentration at the location of P3 for the four scenarios in the chamber. In Figure C6, the results of LES and RNG show a similar trend but under-predict the peak concentration of 0.7μm and 2.5μm particles in the breathing zones (P3) because the deposition effect was not considered in the simulation. Another reason is that, as a result of using the momentum method, the airflow entrainment is under-predicted around the diffuser which leads to higher airflow momentum and can subsequently overcome part of the thermal plume. This effect makes the thermal plume unable to entrain these two particle sizes and drives them into the breathing zone. For large particles (7μm), the normalized concentration (the ratio of local concentration to instantaneously average concentration) was over-predicted by the LES model during the particle injection period (30s). The major discrepancy between RNG and LES occurs in the injection period for all particle sizes. The prediction by using LES shows an elevated fluctuation of particle concentration compared to that of RNG. Particles of 2.5μm in size present higher concentrations at P3 in comparison to particles 0.7μm in size. It should be pointed out that experimental particle concentration is not reported when the value is lower than 0.001.

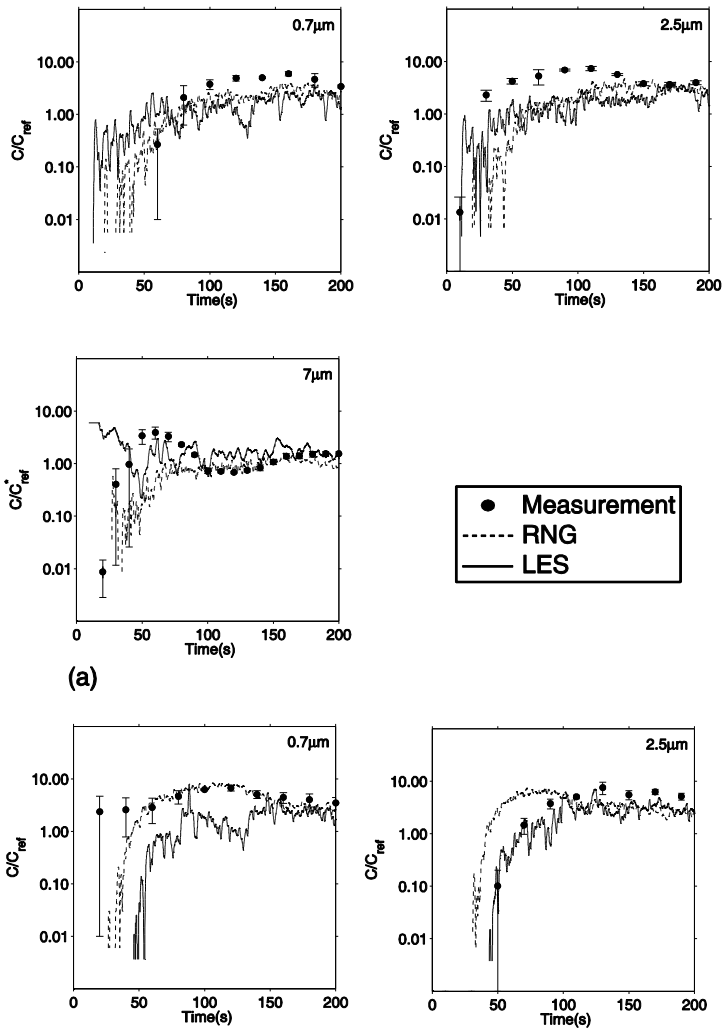

Figure C6: Comparison of experimental and numerical particle concentrations of the BDV scheme.

In Scenario B, the particles are generated in the index occupant's feet region with a high buoyancy effect, which drives particles upwards around the index occupant. Some particles travel directly to the exhaust, 'short-circuiting' the chamber, while others mix into the bulk flow and are carried with the air out of the chamber. Figure C6 shows the particle variation at the breathing zone of the target occupant for this scenario. For small

particles, the prediction of RNG is in good agreement with the experiments at location P3. Conversely, LES performs better in modeling the medium-sized particle concentration at the same position. More precisely, results show that LES under-predicts the initial concentration of 0.7um particles, which was not observed for 2.5μm particles. This could be attributed to the inaccuracy of the airflow prediction. Results in Figure C6 suggest that the discrepancy in the prediction of the airflow with LES affects the dispersion of small particles (0.7μm) more than medium size particles (2.5μm).

Comparing results in scenarios A and B, it is observed that small particles disperse instantaneously to the breathing zone, resulting in an enhanced human exposure. Relative to Scenario A, in Scenario B the uncertainty associated with small particle concentrations increases because the small particles followed the oscillating flows of the thermal plume and then dispersed to P3. However, it is observed that the normalized concentration of 2.5μm particles is lower than 0.01 for the first 50s, which is not case in Scenario A.

The WMV scheme enables the particles to disperse more uniformly in the chamber, as described in Scenarios C and D. In this condition, the particle concentration gradients tend to be reduced, and it can be less challenging for CFD to predict the particle variation. Figure C7 shows the transmission of particles emitted from the diffuser together with the supply air. For all particle sizes, there is a good agreement between experimental and numerical values of the concentration at all locations except for first 80 seconds for large particles. High particle fluctuations are observed during the particle emission period. Comparisons of experimental and numerical values of medium particle concentrations show that the concentration in the strong buoyancy region, P3, is slightly

under-predicted by RNG because the flow fluctuation is not captured by the RNG method. This implies that LES simulation provides an advantage in predicting transient particle sources. In the WMV scheme, the particles have a longer average residence time since particle removal efficiency is lower than that in the BDV scheme (Wan and Chao 2007).

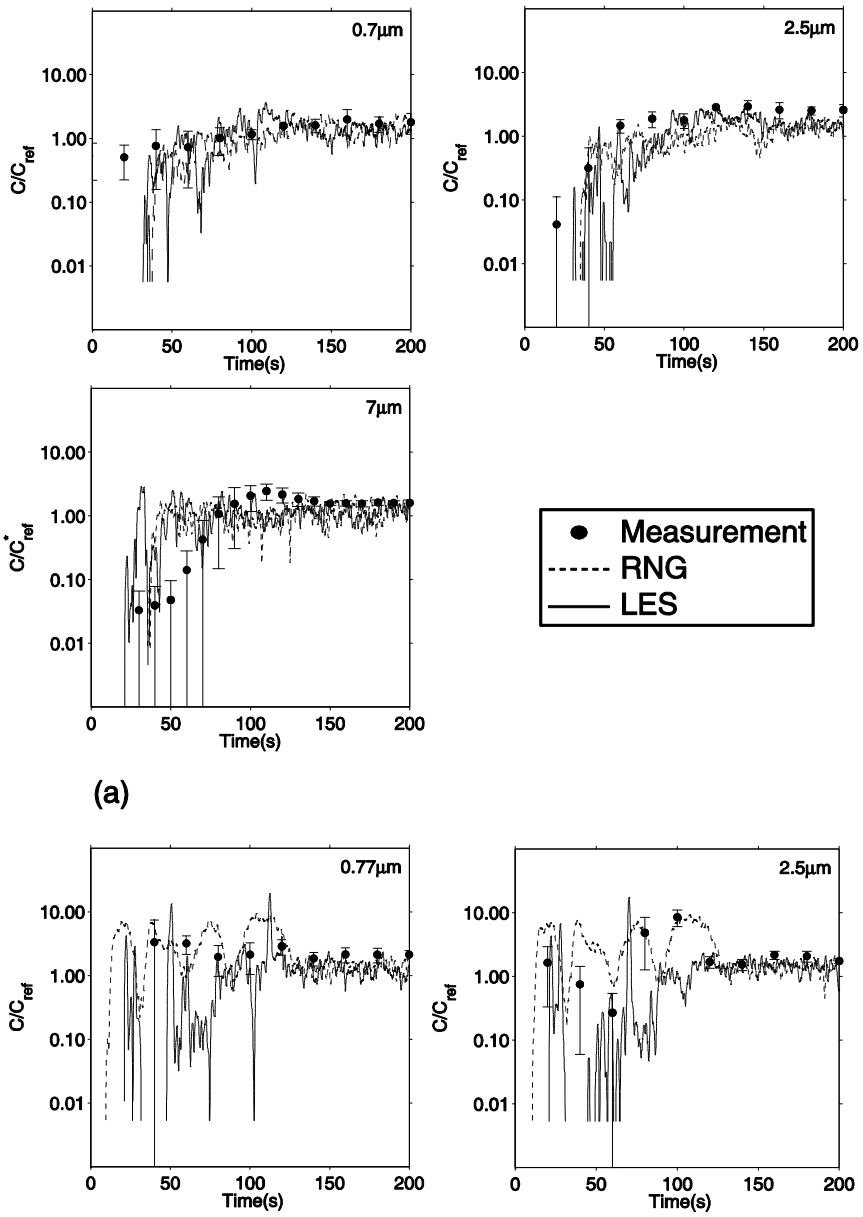

Figure C7: Comparison of experimental and numerical particle concentrations of the WMV.

In Scenario D, the particles are injected from the index occupant's feet region, as shown in Figure C7. When comparing LES and RNG, it is observed that both models

show reasonable agreements with measurements for the small and medium particles. Compared with the experimental results, the concentration uncertainties are better predicted by LES.

In the following section, normalized peak concentration and peak-concentration occurrence time for experimental and numerical results at different locations are presented for all four scenarios. Figure C8 shows the comparison of three metrics (normalized peak particle concentration, peak-concentration occurrence time and average normalized particle concentration) for Scenario A, considering various particle sizes. Results show that both RNG and LES are in reasonably good agreement with experimental results for normalized peak concentration at all locations except positions P1 and P5. Comparing the performance of RNG and LES, LES better predicts the peak concentration at location P1 but worse at P5 for small particles. Little difference is observed in the peak concentration between the two models in other locations. At P5, the simulation under-predicts the peak-concentration occurrence time for the small and large particles, while over-predicts the values at locations P1 for large particles. Both RNG and LES are in good agreement with the experimental results for peak-concentration occurrence time of the medium particle size. The major difference is the prediction of peak-concentration occurrence time for large particles. Figure C8 shows that LES gives better predictions, while RNG fails to predict the peak-concentration occurrence time, at locations P2 and P3.

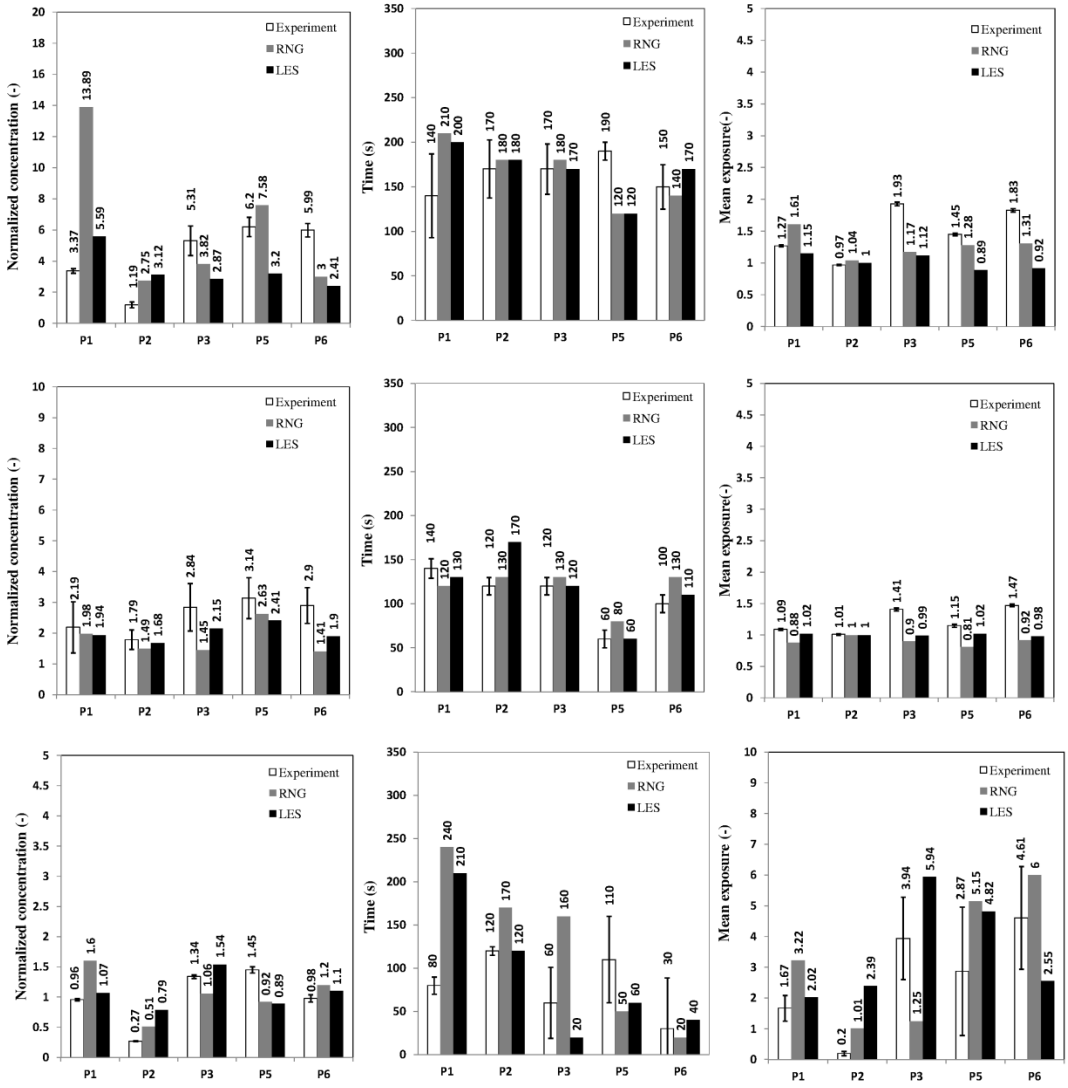

Figure C8: Comparison of normalized peak particle concentrations, peak occurrence time and average normalized particle concentration in 20min (Scenarios-A); top, 0.7μm; middle, 2.5μm; bottom, 7μm.

Neither LES nor RNG shows good agreement with measurements for the mean exposure at P3 for small particles. However, RNG shows slightly better prediction than LES for various locations. RNG also tends to be better in predicting the mean exposure at P2 and P6 for large particles, while LES presents more satisfactory results at other positions. Generally, the prediction of mean exposure by RNG and LES models is in reasonably good agreement with the experiments, especially for the medium size particles.

From Scenario B, as illustrated in Figure C9, no obvious peak normalized concentration and peak-concentration occurrence time are observed at P5 and P6 for LES, and at P6 for RNG. This is due to the gradual change in particle concentration at these locations. However, Figure C9 shows that both LES and RNG agree reasonably well with the experimental results in general. For the small and medium particles, LES predicts more accurate peak concentrations at all locations except for P3. Additionally, the peak-concentration occurrence times are better predicted by the LES model for both small and medium particles, except at P6. The position, P6, is located in the high buoyancy region, and LES shows that the particle cloud reaches this point faster than experiments. Although the simulation predicts lower mean exposure at locations P1 and P6, the prediction at other locations is still in good agreement with the experiments.

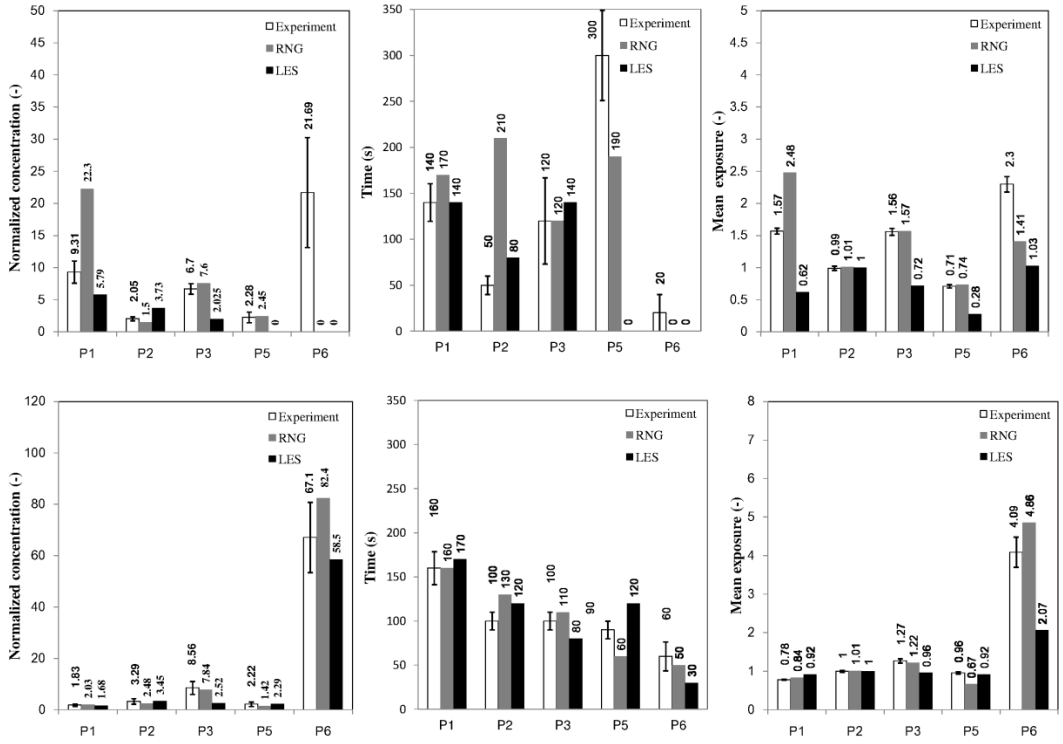

Figure C9: Comparison of normalized peak particle concentrations, peak occurrence time and average normalized particle concentration in 20min (Scenarios-B); top, 0.7μm; bottom, 2.5μm.

When the particles are injected from the diffuser in the MV scheme (Scenario C), both LES and RNG show good agreements with experimental results for small particles concerning the three parameters described in Figure C10. However, the simulation fails to predict the peak concentration at P1 and P3, and the peak-concentration occurrence time at the exhaust (P2) for the medium particles. In the simulations, the particle clouds reach the exhaust earlier than in experiments, and the mean exposure concentration, at P3 and P6, are lower than those in the experiments for medium particles. As for large particles, the prediction is in good agreement with the measurements. However, the

calculation of the peak concentration at location P1 for medium particles by the RNG model is poor. Nevertheless, LES fails to predict the peak concentration at location P6. For all particle sizes, both LES and RNG are in reasonably good agreement with the experimental data concerning mean exposure.

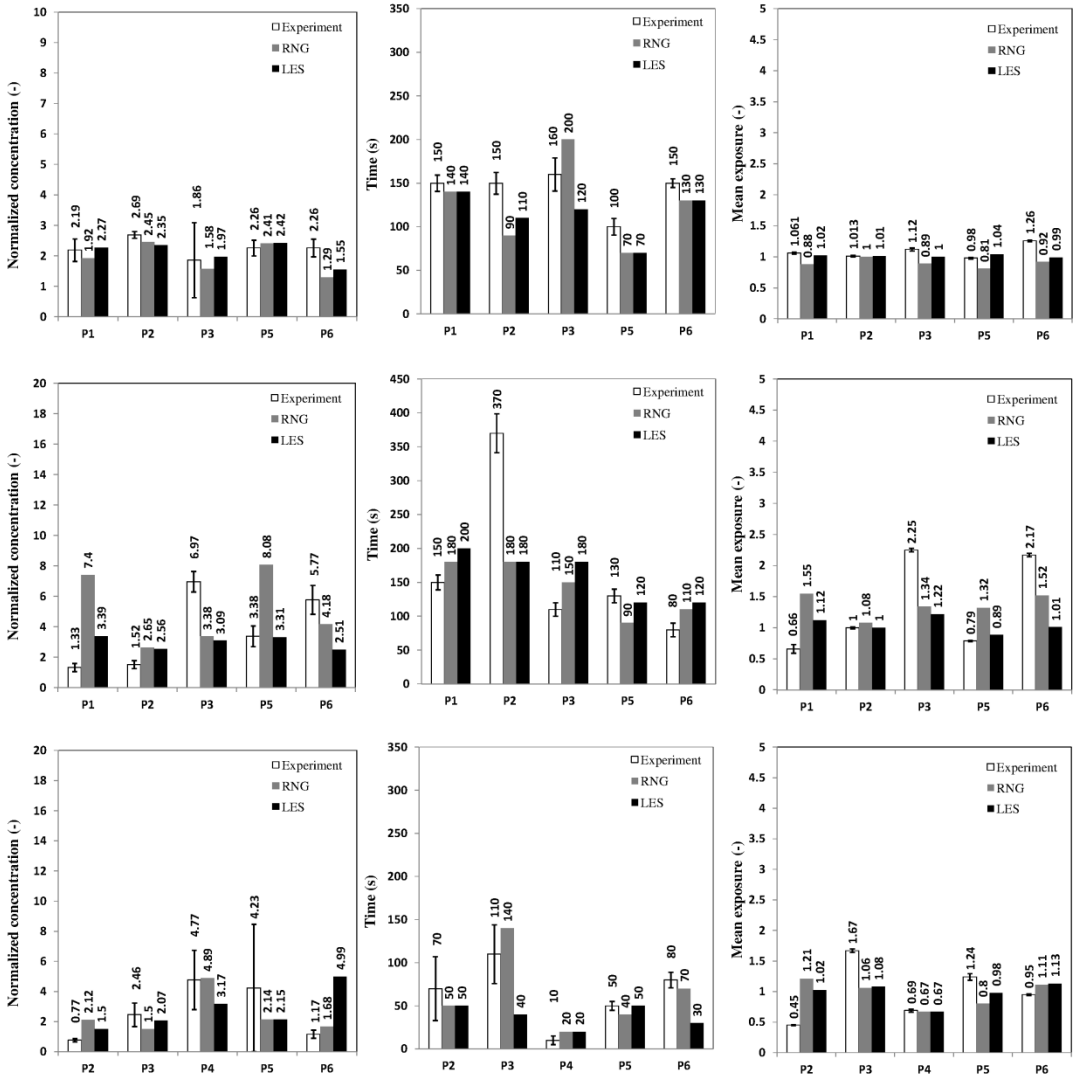

Figure C10: Comparison of normalized peak particle concentrations, peak occurrence time and average normalized particle concentration in 20min (Scenario-C); top, 0.7μm; middle, 2.5μm; bottom, 7μm.

As shown in Figure C11, location P6 shows much higher concentration than that of other locations for Scenario D. The peak concentration for the small particles predicted by RNG and LES agree reasonably with the measurements except at location P6 where LES fails to predict the peak concentration and mean exposure level. It is also observed that the simulation over-predicts the peak-concentration occurrence time at the exhaust (P2) for small particles. For medium particles, however, LES performs better in predicting the peak concentration at P1 and P6, and peak-concentration occurrence time at locations P2 and P5 than the RNG model. As for mean exposure, RNG performs better for small particles. With respect to medium particles, neither LES nor RNG shows a good agreement for mean exposure at P1 and P5.

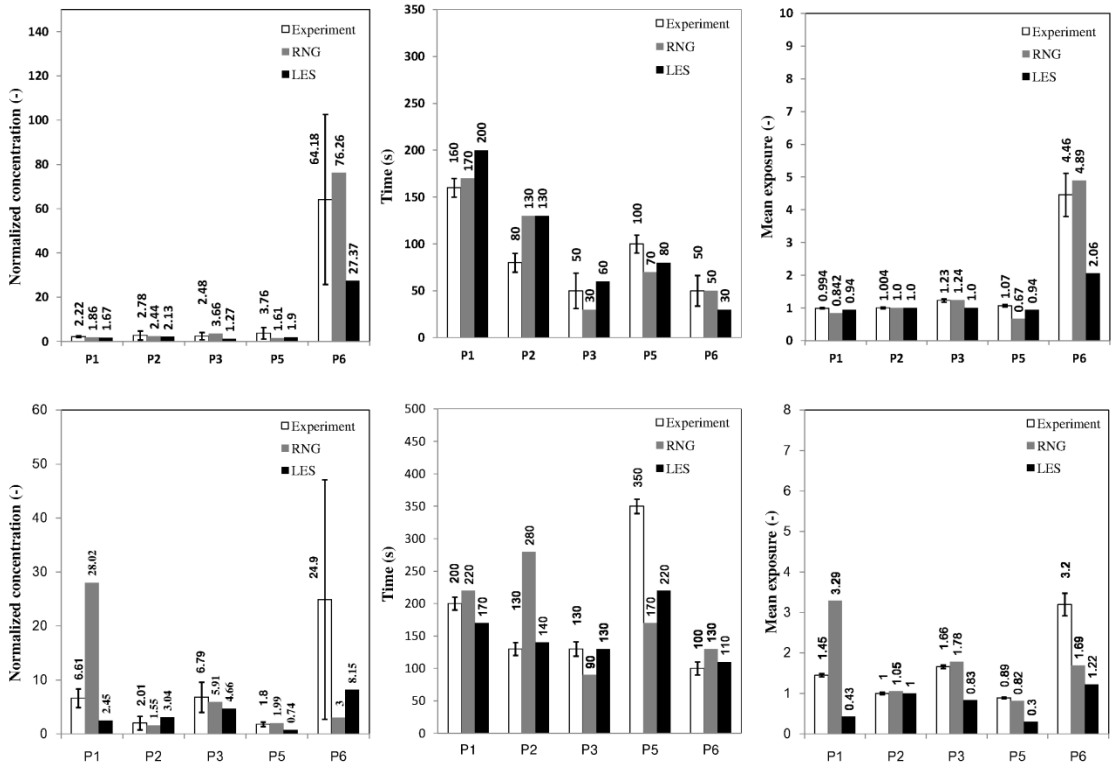

Figure C11: Comparison of normalized peak particle concentrations, peak occurrence time and average normalized particle concentration in 20min (Scenarios-D); top, 0.7μm; bottom, 2.5μm.

The measured exposure in the entire chamber and the breathing zones for different schemes are summarized in Table C5. The overall exposure and the local exposure in the breathing zones, P3 and P6, are evaluated by taking the average of the concentration over 20min at five locations and two breathing zones, respectively. Table C5 shows that when the particles are generated from diffusers, the BDV scheme results in increased overall and local breathing-zone exposure levels for small particles. The exposure in the breathing zone tends to be higher in the WMV scheme, although the overall exposure is lower for the medium particles. When particles are injected in the feet

region of the index occupant, however, the average exposure level in the chamber tends to decrease in the BDV scheme. It is illustrated that BDV has better particle removal if the particles are generated in the vicinity of the occupant. It should be pointed out that the decreased exposure averaged over 20mins does not necessary mean a lower peak concentration in the breathing zone. For example, the peak concentration at P3 is higher in BDV than WMV scheme when particles are generated at the feet region. However, the exposure level in the breathing zone is much more dependent on particle size and position. In the breathing ozone of the target occupant (P3), the higher local exposure occurs for small particles under the BDV scheme and for medium particles under the WMV scheme, while the index occupant (P6) presents an opposite trend.

Particle source	Particle size	Overall exposure		P3		P6	
		BDV	WMV	BDV	WMV	BDV	WMV
Diffuser	0.7μm	1.49	1.09	1.93	1.12	1.83	1.26
	2.5μm	1.37	1.23	1.41	2.25	1.47	2.17
	7μm*	1	1	1.34	1.67	0.98	0.95
Feet	0.7μm	1.43	1.75	1.56	1.23	2.3	4.46
	2.5μm	1.64	1.62	1.27	1.66	4.09	3.2

*: The concentration was normalized by C^*_{ref}

Table C5: Overall and breathing zone exposure levels in the four scenarios.

Summary

This study investigates the dispersion of three different size particles emitted from two transient sources in the chamber with two ventilation patterns. The human exposure at the breathing zone and throughout the chamber is examined considering normalized peak particle concentrations, peak-concentration occurrence time and average normalized particle concentration.

Results show that the LES model generally provides a better prediction of particle variations during the period of the particle generation due to the unstable flow and therefore unstable particle emission. RNG and LES, however, performed similarly well in predicting the particle concentration thereafter.

Overall, the results of LES obtain a better agreement with experimental results than RNG at most locations for normalized peak particle concentration, peak-concentration occurrence time, and average normalized particle concentration. The major advantage of LES is observed in the prediction of normalized peak particle concentration which can be the critical metric for highly pathogenic bio-aerosols.

When particles were emitted by supply diffusers, buoyancy-driven ventilation (BDV) caused a reduced average particle exposure level (over the period of 20mins) when compared to well-mixed ventilation (WMV). However, the WMV scheme has better performance when the sources are located at the feet region. Considering the local breathing zones of the two occupants, the BDV scheme tends to increase the exposure for small particles but decrease exposure for medium particles when the particles are generated from supply diffusers.

APPENDIX D: TRANSPORT OF AIRBORNE PARTICLES FROM AN UNOBSTRUCTED COUGH JET

Shichao Liu and Atila Novoselac

(Published in *Aerosol Science & Technology*)

Abstract

This paper presents analytical and experimental results for the velocity distribution and transport of expiratory particles from an artificial cough. The stream-wise penetration distance and velocity field of the cough jet were determined through a combination of dimensionless analysis and experimental techniques. The experiments were conducted in a well-controlled environmental chamber with simplified thermal manikins to simulation human coughs and buoyant thermal plumes, and involved flow visualization, velocity measurements employing high and low velocity hot-wire anemometers, and particle size and concentration measurement. The study analyzed three particle sizes - 0.77, 2.5 and 7μm - to examine the impact of particle size on particle transport in the cough jet region and in the vicinity of a receiver occupant positioned in close proximity to the coughing source. The results indicate that the cough jet has a lower axial velocity but higher span-wise expansion rate than a steady jet with an identical discharge velocity. The particles of three sizes have a similar trajectory when considering the transport in the cough jet region. However, particle concentration distributions of the three size particles show that size is an important factor for particle transport in the vicinity of the receiver occupant where airflow velocity decays to the room background air velocity. Furthermore, the results suggest that a cough jet is able to overcome the

buoyant human thermal plume and travel further ahead in the region behind the receiver occupant.

Keywords: Cough, transient jet, particle transport, human thermal plume

Introduction

Epidemic diseases are believed to be related to respiratory airborne transmission (Roy and Milton 2004), and human coughing promotes the spread of human released particles. By discharging a large quantity of airborne particles with a high discharge velocity, coughing releases particles with a higher concentration than breathing or talking. Lindsley et al. (2012) found that the average number of particles expelled by each cough ranges from 900 to 302,200. For an influenza-infected subject, it is very likely for a cough jet to contain pathogens and spread airborne diseases that can be inhaled into the respiratory tracts of other individuals. Furthermore, coughed particles have a wide range of sizes, with different transport characteristics. Lindsley et al. (2012) also observed that coughed particles have a size range of 0.35 to 10μm and Yang et al. (2007) pointed out that the entire average size distribution of the coughed droplets was 0.62-15.9μm with nuclei sizes of 0.58-5.42μm. An extensive review conducted recently by Gralton et al. (2011) summaries the size range of coughed particles from a large quantity of studies and concludes that the size scale of particles ranges from 0.1 to 100μm for individuals prior to and after 1979. Without conducting another review about particle size, this paper focuses on the airborne phase particles as they stay longer before deposition and have a higher potential for a long-term transmission. World Health

Organization (2007) employs a 5μm cut-off to delineate between droplet (>5μm) and airborne (≤ 5μm) transmission. Due to the large size range of and possibly long-term transmission of airborne coughed particles, it is of importance to comprehend the dynamics of coughed particles with different sizes for understanding interpersonal exposure mechanisms.

A cough jet dominates the transport and dispersion of released coughed particles. The velocity field of human coughs has been extensively examined using various experimental methods, including Particle Image Velocimetry (PIV) (Zhu et al. 2006; Chao et al. 2009; VanSciver et al. 2011; Nishimura et al. 2013) and Schlieren imaging (Tang et al. 2009). A typical cough has a peak velocity in a range of 6-22 m/s with a duration ranging from 0.25s to 0.8s (Zhu et al. 2006; Gupta et al. 2009). A theoretical analysis of coughed droplets analyzed the trajectories of different size droplets driven by a cough jet assuming the cough jet was steady (Xie et al. 2007). Although this analysis is very helpful to understand the dynamics of different size droplets in a jet, the simplification related to the steady state jet limits the findings from being generalized to real cough conditions. Kouros et al. (1993) found that an unsteady-state jet, such as puff, has significantly different properties from a steady-state jet with the same inlet velocity. Another study has shown that the momentum of a puff is constant in time and flow, and self-persevering (self-similarity) can be achieved downstream from the puff source (Kovasznay et al. 1975). The short duration of a cough jet classifies it as a puff and using a puff theory helps the theoretical analysis of the velocity field of a cough, and consequently the trajectories of various size particles within a cough jet.

There are numerous numerical and experimental studies that consider the dispersal of airborne particles expelled from a cough in different indoor environments. Yin et al. (2011) presented the spatial distribution of particles coughed and breathed out by a recumbent patient in a medical ward with two ventilation modes. They concluded that the difference in particle distribution between two cases of coughing and breathing was insignificant only for mixing ventilation. A numerical simulation of an airline cabin showed that the expelled particles from a subject are predominately affected by the bulk airflow (Gupta et al. 2011). Modeling of coughs in railway cabins showed that the transmission of particles expelled from a 0.4s cough contains two sets of events: particles generated in the first 0.2s escaping from the body plume, and particles generated in the next 0.2s following the upward body plume (Zhang and Li 2012).

While the previously mentioned studies concerned the dispersion of coughed particles in indoor environments, Lai et al. focused on the interpersonal transport of expiratory particles in scaled and full-scale chambers (Berrouk et al. 2010; Lai and Wong 2010; Seepana and Lai 2012). In these studies, coughs were simulated by using a spray gun with the results providing fundamental data regarding interpersonal transmission of coughed particles. However, further improvement of experimental studies regarding interpersonal transport is possible, especially when considering the size of the discharge opening ("human mouth") and more details on discharge concentration. The discharge concentration of a cough allows an analysis of to what extent expiratory particle concentration decays during particle transport. Furthermore, much less is known about the effect of particle size on coughed particles transporting in the jet and vicinity of a receiver occupant. Most particle sampling instruments, e.g. Optical Particle Counters

(OPC) and Aerodynamic Particle Sizes (APS), have a minimum response time not less than 1s. This prevents the measurement of particle concentration in the cough jet region where coughed particles pass through a position quickly, especially when the cough velocity is high. This may explain why previous studies measured only long-duration and low-discharge-velocity coughs (Lai and Wong 2010; Seepana and Lai 2012; Chen et al. 2013). Detailed studies about the transport of particles expelled from a typical cough are very scarce.

To address the challenges and knowledge gaps identified by previous research on human coughs, this paper provides an empirical analysis of an unobstructed coughed jet regarding penetration distance and velocity field. The unobstructed cough refers to a cough that is not covered by hand, tissue or other covering cases. Even though most people attempt to cover their mouth while coughing, a survey conducted at a train station, a shopping mall and a hospital shows that approximately one in four people uncover their mouths when coughing or sneezing (Barry et al. 2009). This study focuses on the unobstructed cough jet, since it has a larger penetration distance and particle dispersion than an obstructed jet. The general objective of the present work is to explore the transport of coughed particles in the cough jet region and the vicinity of a receiver occupant. Specific objectives are the following: (1) analyze the velocity field of a cough jet; (2) evaluate the transport of particles expelled from both a cough jet and steady jet with an identical discharge velocity; (3) examine the transport of coughed particles affected by an occupant's thermal plume; (4) and explore the impact of particle size. To fulfill these objectives, the paper discusses the relation of cough penetration distance and time using dimensionless analysis and flow visualization. They characterize the cough

jet's velocity field as measured further by anemometers. Moreover, this work measures and analyzes the interpersonal transport of coughed particles while considering different particle sizes.

The following sections of the paper provide the theoretical background in which a similarity analysis is used to analyze flow dynamics of a cough jet and the governing equations for the trajectories of coughed particles. Since flow dynamics becomes much more complicated when the cough jet reaches the region of human thermal plume, it is difficult to predict particle transport in such region by employing an analytical method. Therefore, this work applies experimental methods to investigate particle distribution in this region and to validate the results for the analytical analysis. The methodology section describes experimental facilities and setup. And the results and discussion section presents the cough jet velocity findings, and the transport of coughed particles as obtained by theoretical analysis and measurements.

Theoretical background

This section provides a mathematical description of the penetration distance and velocity field of a cough jet, and the trajectories of particles driven by the jet. As the short duration of a cough prevents detailed measurements of particle dynamics due to the limited capabilities of particle counters, theoretical or numerical analysis are the alternatives. In this study, analytical methods were applied to analyze the flow and particle dynamics in the *cough jet region* where the airflow was dominated by the jet. In this jet-dominant region, particles especially fine ones (PM 2.5), strictly follow jet streamlines because of the high discharge velocity. The dispersion of particles is mainly

driven by drag force for fine particles and by gravity for coarse ones. When the cough jet decays and travels to another occupant, the body's thermal plume may affect dispersion. Other factors, such as receiver occupant's movement and respiratory activities, might also impact the transport and dispersion of coughed particles. The influence level of these factors depends on the characteristics of a cough jet.

Most coughs last 1 second or less with a velocity of 6m/s or higher (Gupta et al. 2009; Nishimura et al. 2013). For a commonly used particle sampler, e.g. OPC or APS, it is improbable that the sampler will have enough time to measure particle dispersion accurately in the cough jet region. Fortunately, momentum conservation allows a parameter analysis in the jet region before the jet decays to room background (Kovasznay et al. 1975). In the vicinity of a receiver occupant, including the breathing zone, the momentum conservation of the cough jet is broken by additional buoyancy force due to the body thermal plume. In such region, flow and particle dynamics become increasingly complex and limit the theoretical analysis.

The characteristics of an unsteady cough jet are strongly related to: injected volume flow rate and duration of the jet besides the parameters defining a steady jet such as discharge velocity and inlet geometry. Due to the self-preserving (or momentum conservation) of a cough jet flow in the downstream region, the penetration distance S_p referring to the distance from injection source to jet frontal tip, can be written as Equation D1:

$$S_p = f(U_0, D, \tau) \tag{D1}$$

where U_0 is discharge velocity, τ is time, and D is the diameter of jet source. The volume flow rate of the jet is $\pi U_0 D^2/4$. A dimensionless analysis results in a relationship for the jet at a constant discharge velocity U_0,

$$\frac{S_p - X_0}{D} \sim \left(\frac{U_0 \tau}{D}\right)^n \tag{D2}$$

where X_0 is the virtual origin. The power n (n=1/2) reflects the relationship between penetration distance with time, which varies in different studies (Lee and Chen 1998; Sangras et al. 2002; Song and Abraham 2003). It is worthy noted that Equation (D2) is valid for the case of a jet with a constant discharge velocity.

After taking the derivative of the penetration distance, S_p, with respect to time, τ, we arrive at Equation (D3),

$$\frac{U_{0m}}{U_0} = K_1 \left(\frac{S_p - X_0}{D}\right)^{-1} \tag{D3}$$

where U_{om} is the maximum centerline velocity at the jet tip with a penetration of S_p. U_{om} can also refer to the peak average velocity at the cough jet center following the tip. The cough jet center is defined as a location of maximum velocity. Equation (D3) shows that the tip velocity of a cough jet has a similar relationship with the dimensionless distance, S_p/D, as a steady jet (Chen and Rodi 1980). The coefficient K_1 is a constant value that can be determined via experiments.

Ghaem-Maghami and Johari (2010) reported that the axial velocity profile through a puff center follows a Gaussian function similar to a steady jet as described in Equation (D4),

$$\frac{U}{U_{0m}} = \exp(-K_2(r^* - r_0^*)^2) \quad \text{(D4)}$$

where $r^*=r/S_p$, $r_0^*= r_0/S_p$, and r is the vertical distance from the cough jet center. r_0^* is used because the cough jet center may be slightly off-center.

Furthermore, the velocity profiles of a steady jet with an identical Reynolds number as the cough jet in the literature were used for comparison with the cough jet (Wygnanski and Fiedler 1969; Bocksell 1998),

$$\frac{U_{0m}}{U_0} = B\left(\frac{S_p}{D}\right)^{-1} \quad \text{(D5)}$$

$$\frac{U}{U_{0m}} = \text{sec}h^2(\sigma r^*) \quad \text{(D6)}$$

where B is velocity-decay constant, 5.5 , and σ is 10.4 through curve- fitting.

Once the velocity field is determined, the trajectory of a particle injected with a cough jet can be obtained according to Newton's second law of momentum conservation. Because the particle sizes concerned in this study were in the range of 0.35-10μm and the density of coughed particles is approximately equal to water liquid (Havel et al. 1955),

only drag, buoyant and gravity forces dominate particle momentum. For the unobstructed cough and particle sizes considered in this study, these forces are several orders of magnitude greater than Brownian force, thermophoresis force and lift force (Talbot et al. 1980; Li and Ahmadi 1992). It is worth noting that this study focuses on an isothermal cough jet. This phenomenon can be reflected by r_0^* in Equation (D4). Furthermore, the particle momentum and displacement equations can be written as follows:

$$\frac{\mathrm{d}\,\overrightarrow{U_p}}{\mathrm{d}\tau} = \frac{3C_d\rho_a}{8\rho_p r_p}\left|\overrightarrow{U_a} - \overrightarrow{U_p}\right|\left(\overrightarrow{U_a} - \overrightarrow{U_p}\right) + \vec{g}\left(1 - \frac{\rho_a}{\rho_p}\right) \tag{D7}$$

$$\frac{\mathrm{d}\,\overrightarrow{X_p}}{\mathrm{d}\tau} = \overrightarrow{U_p} \tag{D8}$$

where $\vec{U}$ is velocity, ρ is density, r_p is particle size and $\vec{g}$ refers to gravitational acceleration. The subscript, *p* and *a*, represents particle phase and air phase, respectively. C_d is the drag coefficient represented by a general function of particle Reynolds number, *Re,* as shown in Equation (D7),

$$C_d = \mathrm{a}_1 + \mathrm{a}_2 Re^{-1}\mathrm{a}_2 + \mathrm{a}_3 Re^{-1} \tag{D9}$$

where a_1, a_2 and a_3 are constants that apply to spherical particles over a large range of *R*e (Morsi and Alexander 1972).

In terms of Equations (2)-(9), the trajectory of a single particle in a cough jet or steady jet can be determined. In this study, the fourth-order Runge-Kutta method was

employed to numerically solve the differential equations. The calculation applied the same initial condition as experiments described in next section.

Methodology

The impact of particle sizes (0.77μm, 2.5μm and 7μm) was examined by comparing their trajectories in the high velocity jet region. In addition, the transport of coughed particles of the three sizes, released by a source occupant, in the vicinity of a receiver occupant was examined and compared to the results in the cough jet region regarding the influence of particle sizes. The receiver occupant was positioned in a further region of the source where velocity decayed to a low level. Experimental setup and instrumentation are described in the following four methodology subsections that provide specifics about a cough generator, velocity measurement at various locations in the cough jet region, stream-wise penetration distance and the concentration of coughed particles of three sizes surrounding the receiver occupant. The velocity field in the jet region and particle concentration distribution at the locations further from the jet source will be experimentally validated in the result section.

Cough box/ generator

A cough box/ generator depicted in Figure D1, was constructed to model a human cough. The cough box has dimensions of 0.25m×0.25m×0.25m (15.6L), and a cough jet was released by injecting pressurized air into the box. The coughed flow was controlled by a fast-response solenoid valve actuated in an "on-off" (square wave) manner. An airflow straightener was built inside to create a piston-like unidirectional flow. In ideal

conditions, the unidirectional flow in the box carries particles at a low deposition rate. When the particle generator was turned on, a pump connected to the box drew air to maintain a slightly negative pressure inside the box. This prevented particles from leaving the box before coughing. Additionally, a small computer fan was placed at the center bottom to create a well-mixed condition. The cough box used a 6cm long stainless steel tube with an inner diameter of 2.4cm as the discharge opening to simulate a human mouth, 4cm^2 (Gupta et al. 2009). In this study, the cough jet was adjusted to have a discharge velocity of 6.08m/s (Reynolds number 9700), and turbulence intensity 4.25% at the center of the tube opening. The duration of the cough jet was 1 second.

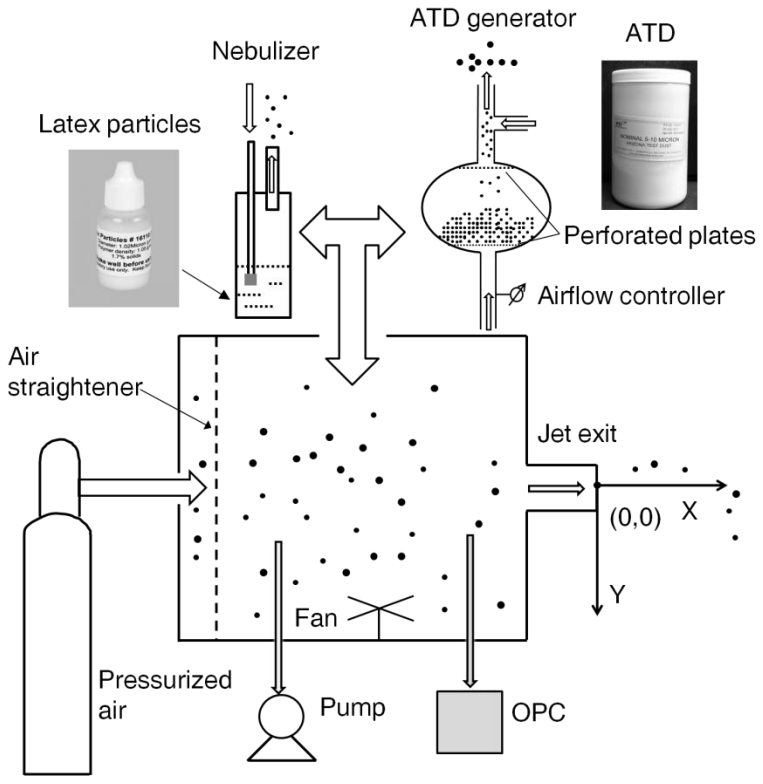

Figure D1: Schematic of the cough box/ generator and the particle generators.

Particle sizes of 0.77μm, 2.5μm and 7μm, were employed in this study. For 0.77 and 2.5μm particles, a Collison nebulizer sprayed particle solution into the box. The solution contained latex spherical mono-dispersed particles (coefficient of size variation 1%-3%) with a density of 1.05g/cm^3. Careful attention was paid to ensure that all solution except particle nuclei was evaporated in the box before coughing. Such mono-dispersed particles can be monitored without size categorization issues if the background concentration is negligibly low. However, the Collison nebulizer had difficulties generating enough mono-dispersed 7μm particles. Therefore, in this study we developed a large-particle disperser that can generate a large quantity of Arizona Test Dust (ATD) (nominal 5-10μm) particles (Figure D1).

Axial velocity field in the cough jet region

A one-dimensional hot-wire anemometer and a hot-sphere anemometer measured axial velocity in the center-section plane (76 positions) downstream the cough jet. The hot-wire anemometer measured high velocities (>0.1m/s), while the hot-sphere anemometer measured velocities between 0.05m/s to 0.1m/s. The hot-wire anemometer was calibrated using a Pitot-static system with a pressure transducer (0.1Pa resolution). The measurement at each position was repeated three times. Furthermore, flow visualization offered an illustration of a cough jet penetrating into an environment. The penetration distance of a cough jet as a function of time and the spreading rate can be easily obtained from visualization. The visualization was created by using a water based fog machine (Model EF-1000, Eliminator Lighting, Los Angeles, CA, USA) that atomizing unscented water based fog juice (density of 1.043×10^3 kg/m^3 at temperature

23.0 °C) into particles with 60% in number smaller than 1.0μm and 99% smaller than 2.5μm.It is believed that the cough jet profile was captured by such smokes. The smoke temperature was only slightly higher than background yielding a nearly isothermal turbulent cough jet. The visualization video was recorded by a camera at 60 fps (frames per second).

Particle dispersion in the vicinity of a receiver occupant

To examine how different size particles from coughing dispersed around a receiver occupant, this study carried out experiments of interpersonal transport of coughed particles in a stainless-steel chamber with two thermal manikins insides as shown in Figure D2. The chamber had a ventilation rate of approximately $3.5hr^{-1}$ and supply air was filtered with a high efficiency filter. The temperatures of supply air and exhausted air were 21.6-21.9^{o}C and 24.2-24.6^{o}C during the experiments, respectively. Thermal plumes were created by two thermal manikins, referred to as source and receiver, which were coated with electric heater sheets generating 45W convective heat each. We compared the velocity 0.25m above the cylindrical manikin with that in our previous study using a full-scale manikin. It was observed that 45W heat can generated a thermal plume with a velocity of 0.19m/s at the region of 0.25m above the head which was consistent to that for the full scale thermal manikin ((Rim and Novoselac 2009). In order to decrease the radiant heat transfer between the manikins and interior surfaces of the chamber, aluminum foil with very low emissivity was used to cover the exterior surfaces of the manikins.

(a)

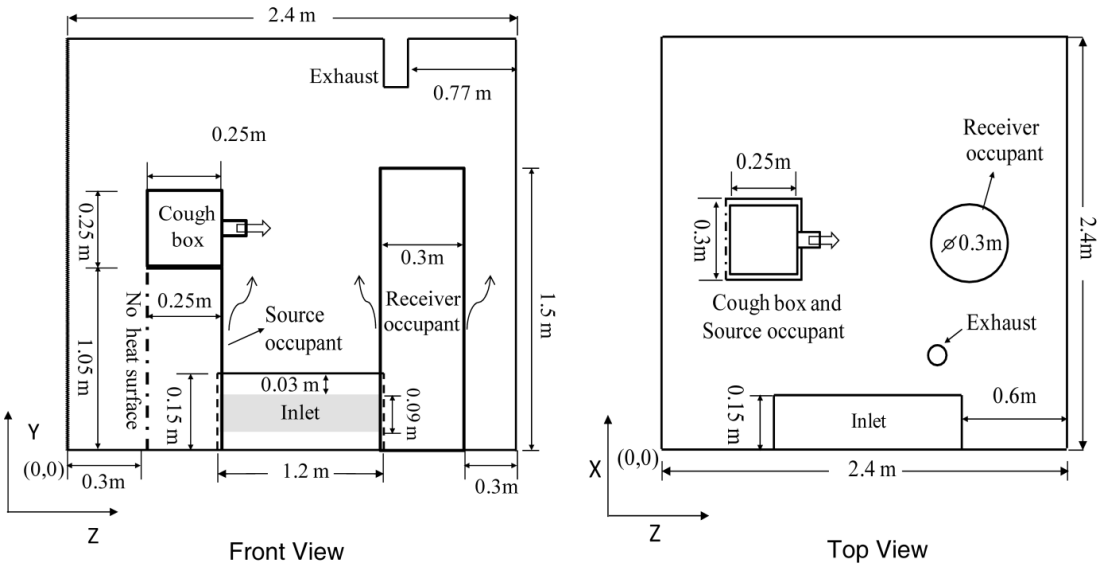

(b)

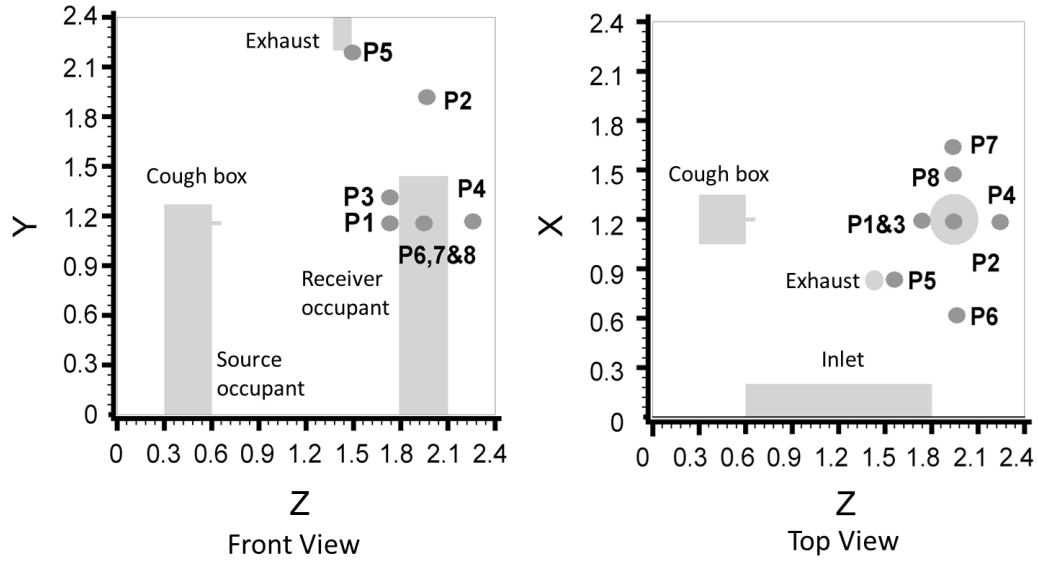

Figure D2: (a) Schematics of the experimental setup; and (b) measurement locations of particle concentration.

Two particle sensors sampled particles in the chamber and cough box, respectively. An APS is capable of measuring the concentration of particles from 0.5 to 20μm using a sophisticated time-of-flight technique which enables high resolution sizing over the entire particle size range. Due to its "high" sampling frequency (up to 1Hz), the APS was used to monitor the dispersed particles in the surrounding of the receiver occupant as depicted in Figure D2, whereas an OPC sampled particles in the cough box to measure the injection concentration of a cough. The performance of two particle sensors was calibrated side-by-side before experiments. Before tracking the particle dispersion of an individual cough, the chamber was stabilized and cleaned by ventilation to minimize background concentration. In the data interpretation, the background concentration in the chamber was subtracted in the "Results and Discussion" section (Liu and Novoselac 2014). Table DS1 shows the coordinates of sample locations of coughed particles. Although the concentration at other locations in the vicinity of the receiver occupant was also measured, the readings were too low to achieve statistically reliable results. The measurements at each location were repeated at least three times; for example, measurements at P1 were repeated thirteen times for 0.77μm particles. To faciliate the comparison of number concentrations of different size particles, all experimental results were normalized by the injection concentration in the cough box.

Results and Discussion

This section presents the experimental results of penetration distance as a function of time, and velocity field of a cough jet including visualization of the cough jet and correlation of measured axial velocity with the self-preserving scaling law from Equation

(D2)-(D4), which verifies the theoretical analysis. Next, the trajectories of three single particles of size 0.77, 2.5 and 7μm were calculated in terms of cough flow velocity. Finally, the variation of normalized concentrations of three size particles at different locations is discussed.

Penetration distance and velocity field of a cough jet

The hot-wire anemometer measured the velocity profile of the cough jet with a discharge velocity of 6.08m/s at the center of the source opening. The velocity distribution across the source opening follows the velocity profile of a fully developed turbulent pipe flow. Figure D3(a) compares the area-weighted average velocities of the cough jet varying with time in this paper with those reported in three previous studies by Khan et al. (2004), Gupta et al. (2009) and Nishimura et al. (2013), respectively. The velocity profile in the paper of Gupta et al. (2009) is calculated according to recommended regressed models by assuming a standard male occupant with a height of 1.7m and weight of 70Kg. Real cough jets have a large uncertainty in velocity profile, and the peak velocity ranges from approximately 5.5m/s to 21m/s. The artificial cough jet in this paper has a simple square wave manner profile that is much different from a real one as shown in Figure D3(a). The total air volume of a cough presented in Figure D3 (b) shows that a cough can generate 0.15-2.2 liters of air.

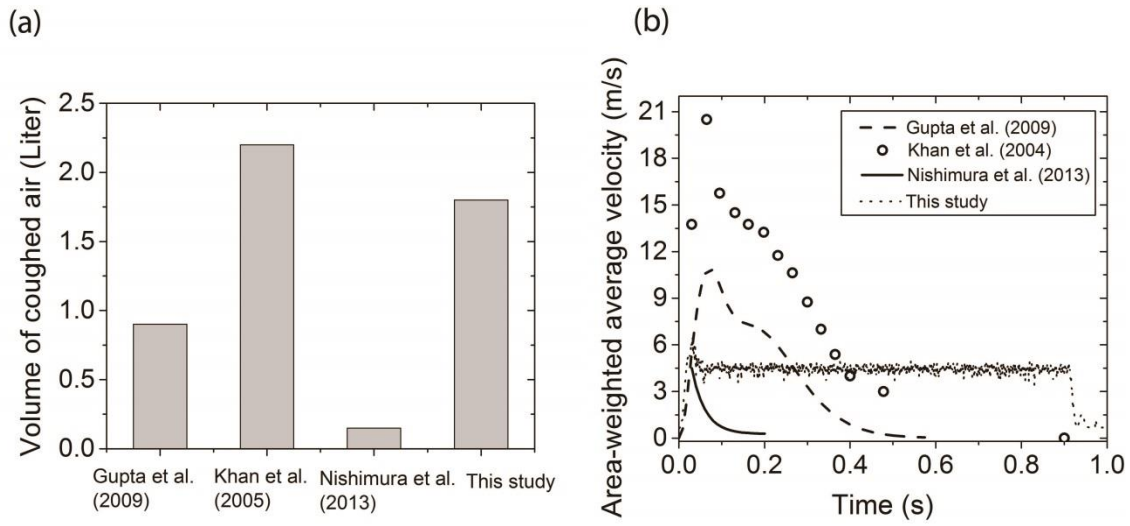

Figure D3: Velocity profiles and total air volume of different cough jets; (a) Velocity profile; (b) Volume of coughed air.

Snapshot images of a cough jet with a discharge velocity of 6.08m/s at the center and duration of 1s at various times after initiation of the flow are provided in Figure D4. The snapshots show that the cough jet is broken into a vortex ring at the tip, referred to leading tip, followed by the main flow in the first 0.1s. However, the vortex ring decays shortly in 0.15s after triggering the cough jet. Therefore, the penetration distance is measured from the main flow tip instead of vortex ring to the source opening. The turbulent region starts from the transition condition to a turbulent jet. The cough jet transports further than 0.2m during the first 0.1s. Since the jet spreads linearly, the spreading rate of the jet can be obtained via the jet shape of the visible edges. The averaged spreading rate (dr_p/dx_p), is in a range of 0.21-0.26.

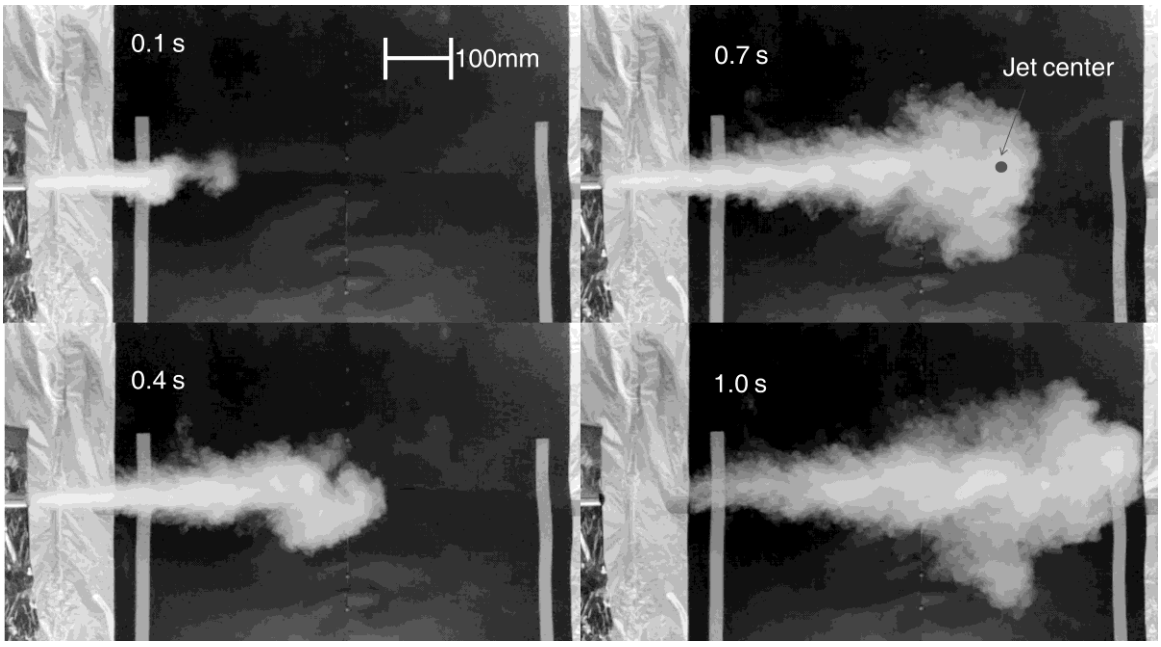

Figure D4: Flow visualization of a cough jet (D=0.024m, U_0=6.08m/s, and Re=9700).

Figure D5 shows the normalized stream-wise penetration distances of the cough jet as a function of normalized time according to the self-preserving scaling of Equation (D2), $\frac{S_p - X_0}{D} \sim \left(\frac{U_0 \tau}{D}\right)^n$. The non-dimensional times for 0.1s, 0.4s, 0.7s and 1.0s in Figure D4 are 25.3 and 101.3, 177.1 and 253 respectively. The curve fit shows that the power n in Equation (D2) is 1/2 that is consistent to the study by Sangras et al (2002). The virtual origin X_0 is approximately 5.1 times jet exit diameter. The penetration distance in Figure D5 follows the correlation of Equation (D2) well in the whole range of dimensionless time investigated in experiments.

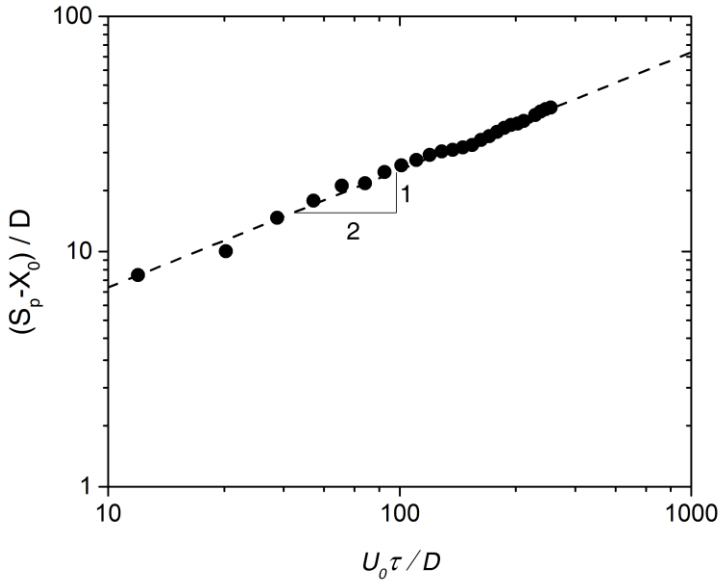

Figure D5: Penetration distance of a cough jet as a function of time.

Self-preserving in Equation (D3) shows that the cough jet also has a linear decay of centerline velocity similar to a steady jet. The average centerline velocities of the cough jet and steady jet with an identical discharge velocity are plotted in Figure D6(a). When the axial distance X>3D, self-similarity is achieved for the cough jet, and the velocity in the jet center reasonably follows the scaling law of Equation (D3), with a constant coefficient K_1=0.29. In the region of X<3D where potential core and mixing layer exist, the center velocity is equal to the discharge velocity in the initialization. It is observed that the centerline velocity in the cough jet, maximum velocity, is lower than that of the steady jet at the same location. This indicates that the calculation of particle trajectories of coughed particles employing a steady jet velocity field is not accurate.

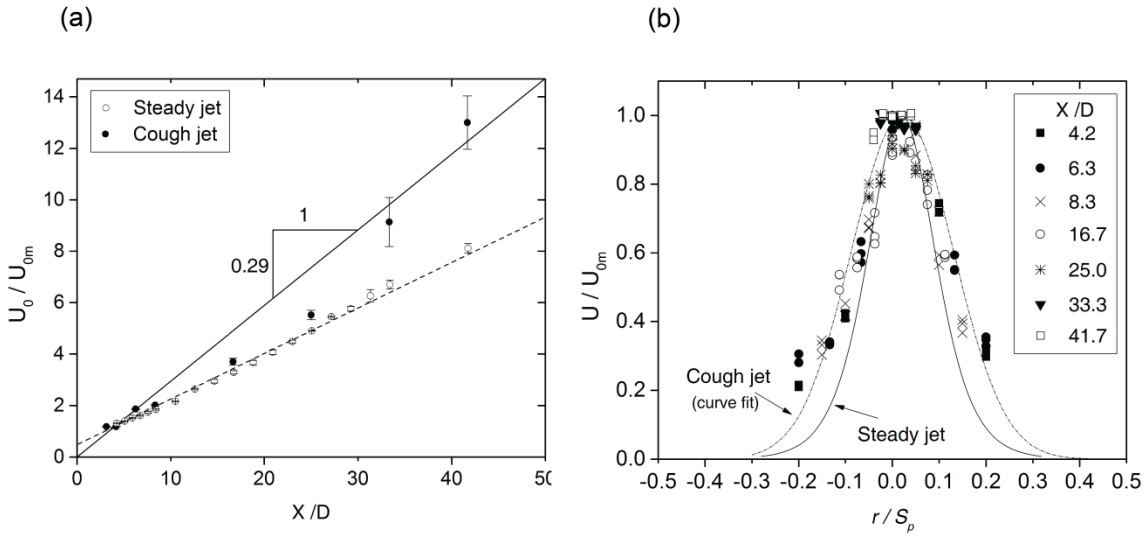

Figure D6: The comparison of velocity fields of a cough jet and steady jet. (a) The centerline velocity of a cough jet and steady jet as a linear function of dimensionless distance; (b) Axial velocity profile through a cough jet center at various *X/D*: 4.2; 6.3; 8.3; 16.7; 25.0; 33.3 and 41.7. Experiments for a steady jet at an identical Reynolds number were conducted by Wygnanski and Fiedler (1969) as described by Equation (D5) and (D6).

Ghaem-Maghami and Johari (2010) showed that the axial velocity profile through the cough jet center follows a Gaussian function regardless of dimensionless distance, *X/D*. The mean velocity profile for the cough jet is normalized by the velocity at the cough jet center (close to the centerline), U_{0m} and plotted versus radical coordinates, r/S_p in Figure D6(b). The axial velocity profiles through the cough jet center collapse onto a Gaussian function Equation (D4), $U = U_{0m}\exp(-42.1(r - 0.02)^2)$, which is wider than the function for a steady jet with an identical Reynolds number reported by Wygnanski and Fiedler (1969). In other words, the cough jet has a wider radical penetration distance than the steady jet.

Particle transport in the cough jet region

This subsection describes the transport/ trajectories of individual particles injected by both the cough jet and steady jet. Three particle sizes, 0.77, 2.5 and 7μm, were considered, consistent with the sizes used in the transport around the receiver occupant (Figure D2). It should be pointed out that the particles were injected simultaneously with the cough jet injection. In the potential core and mixing layer, additionally, the time of particles residing is negligibly small compared to the time spent in the main region (Bocksell 1998). Therefore, the axial velocity in this region was assumed identical to the discharge velocity.

Figure D7 shows the trajectories of three size particles following the steady jet and cough jet. It is observed that larger particles have an increased deposition distances than smaller ones. However, the distance even for 7μm particles is only few millimeters, negligible comparing to horizontal penetration. As described in Figure D7(b), the curves of horizontal penetration for three size particles collapse into one. This suggests that the transport characteristics of coughed particles in the range of 0.58-5.42μm are very similar in the cough jet region. The range of 0.58-5.42μm is the average size of droplet nuclei coughed from healthy subjects (Yang et al. 2007).

Furthermore, the particles-regardless of size-show a substantial deviation when injected from a steady jet comparing to a cough jet. Overall, the deposition distance of particles in the cough jet is larger than the steady jet because of relatively low velocity magnitude. Therefore, particles in the cough jets take longer time to reach a prescribed position. For instance, coughed particles need approximately 1.2s to transport 1.1 meters further away from the jet exit comparing to 0.8s for particles in the steady jet.

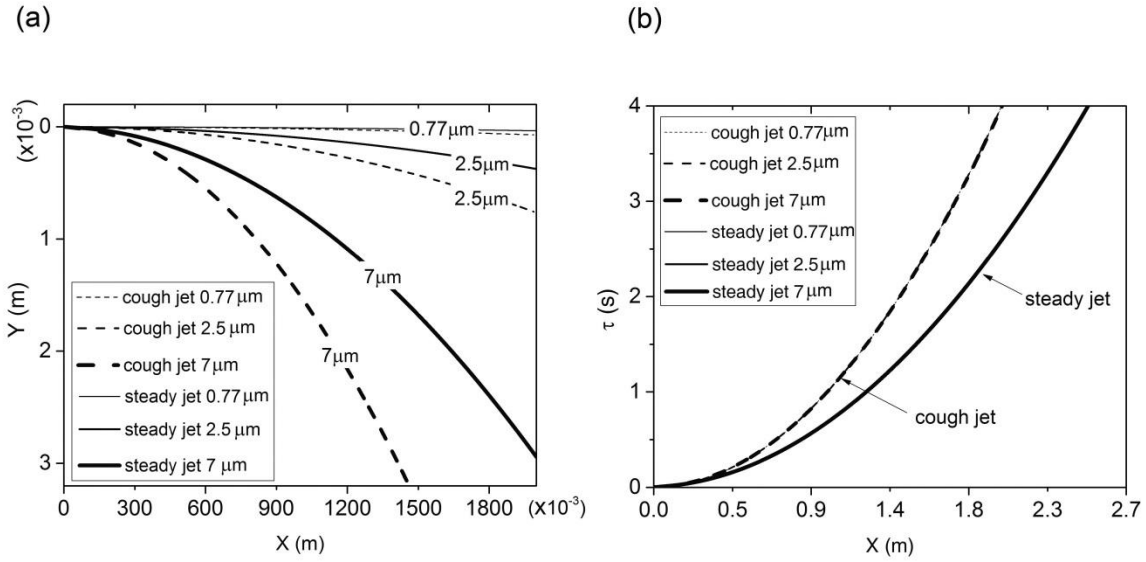

Figure D7: Comparison of trajectories of different size particles following a steady jet and a cough jet with the same discharge velocity. (a) Particle trajectories; (b) The variation of horizontal positions with time.

Particle transport in the vicinity of the receiver occupant

The concentration distribution for particles of three sizes (0.77μm, 2.5μm and 7μm) expelled from a cough jet was measured in the vicinity of the receiver occupant and at the exhaust of the chamber (Figure D2). Figure D8 shows the variation in the normalized distribution of 0.77, 2.5 and 7μm particles emitted by a cough jet. The uncertainties of the concentration (vertical bars) and the concurrence time (horizontal bars) are represented by standard deviations among repeats. Overall, the concentration decays with the increase of particle size in all measured locations around the receiver occupant after the impingement of the cough jet. It illustrates that coughed particles with various sizes in the vicinity of the receiver occupant perform different transport

characteristics as in the cough jet region shown in Figure D7. The measured peak concentration of 0.77, 2.5 and 7μm particles in the breathing zone of the receiver occupant, P1, decays to 4.93%, 3.68% and 1.74% of the initial level in the cough box, respectively. It is observed that particle clouds take approximately 1-2 seconds to reach the breathing zone (P1) and rise up to the maximum in 3 seconds for the three size particles. Right above the receiver occupant, P2, the concentration is approximately one order of magnitude lower than that in the breathing zone, P1. This suggests that even 7μm particles can be transported upwards by human thermal plume.

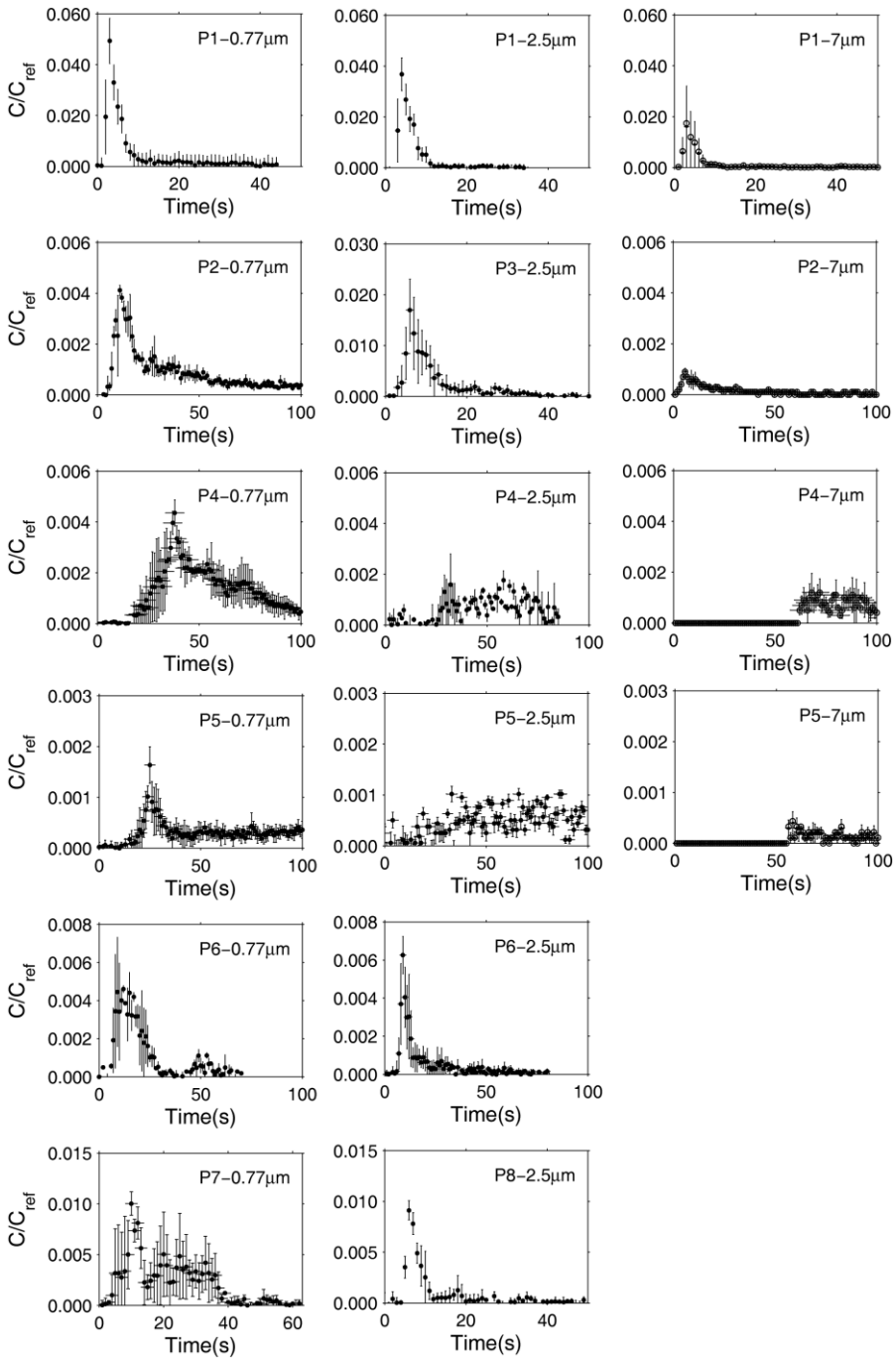

Figure D8: The variation of coughed particle concentration in the vicinity of receiver occupant.

Two side-locations (P6 and P7) that are 0.3m away from the receiver occupant on the side have slightly higher concentrations for 0.77μm particles than the position above (P2). However, the concentrations of 2.5 and 7μm particles were too low to be detected at the two side locations. The reason is that large particles disperse a shorter distance in the span-wise direction due to increased inertia. The study also measured the concentration of three size particles behind the receiver occupant, P4. The result shows a concentration equivalent to that above the receiver occupant (P2) for both 0.77 and 2.5μm particles. The results of the particle concentration indicate that the cough jet is still strong enough in the zone behind the occupant to overcome the thermal plume. The level of exhaust concentration (P5) demonstrates particle removal by both ventilation and deposition that increases with particle size. Figure D8 shows that peak normalized exhaust concentrations of three size particles are approximately 0.16%, 0.10% and 0.042%, respectively. The concentrations of 0.77μm particles achieve the maximum at around 25s. However, 7μm particles cannot be sampled until 55s at the exhaust. Since the concentration of 2.5μm particles is not significantly higher than the background, Figure D8 does not show a substantial peak at the exhaust, P5.

The transport performance of latex particles and Arizona Test Dust (ATD)

The mono-dispersed latex particles, 0.77 and 2.5μm, enable the particle sensors to analyze particle concentration without the uncertainty of particle sizing. However, ATD contains particles in a large range of sizes. The accuracy of 7μm particle sampling depends on the capacity of size categorization of the particle sensors. In addition, the latex particle and Arizona Test Dust show different characteristics, such as density and

refractive index. Therefore, the results using the two types of particles (latex and ATD) may lead to increasing uncertainties. To examine the extent to which the measured concentration varied using latex and ATD, this study compared the concentration of 2.5μm particles at location P1 obtained from using mono-dispersed particles and ATD. The comparison plotted in Figure DS1 shows that the two curves agree well with each other. The uncertainty of the results obtained from ATD is not shown here. The deviation of the peak concentrations using the two particle types is approximately 8%. The comparison indicates that the experiments using latex particles and ATD can generate repeatable results. In these experiments, however, care must be taken to ensure that the size distributions in the cough box and at each location do not vary significantly when ATD is used.

Limitations

The paper employs a simply artificial cough jet that has a square wave manner of velocity profile to investigate the transport of coughed particles. The cough jet with such profile might create a different velocity field from real ones in the jet region even though the total air volume of the artificial cough is reasonable in the range of real coughs. Future studies should examine how different velocity profiles affect flow entrainment, velocity field and consequently particle transport in the cough jet and vicinity of the recipient. In addition, the study concerns the transmission of airborne particles smaller than or equal to 7μm. Nevertheless, further exploration is required to include a larger size range and the shrink of large droplets to nuclei by evaporation, especially for low relative humidity environments. The effects of buoyancy force because warm cough jets and

turbulent mixing of particles during transmission should be also addressed in the future studies.

Conclusion

The transport characteristics of coughed particles in the jet region and the vicinity of a receiver occupant were examined analytically and experimentally. The stream-wise penetration distance and the velocity field of a cough jet were determined through a combination of dimensional analysis and flow visualization. In addition, the transport of coughed particles in the vicinity of a receiver occupant 1.1m away from the coughing source was determined by measuring the concentration variation of particles with three sizes, 0.77, 2.5 and 7μm. The findings of this study show that:

A cough jet has a lower axial velocity but higher expansion rate than a steady jet with an identical discharge velocity. Therefore, coughed particles take longer time to transport to a specified location in the stream-wise direction. The transport of coughed particles based on steady jet theory is not valid for coughed particles.

The particle trajectory of coughed particles in the jet region states that the size of coughed particle nuclei (0.35 to 10μm) has a negligible effect on transmission. Large particles, 7μm, only settle few millimeters due to gravity in the jet region. However, different size particles exhibit different performance in the vicinity of the receiver occupant. Overall, large particles have a decreased concentration in this zone because the airflow velocity is relatively low.

The normalized concentrations based on the source value in the breathing zone of the receiver occupant at a distance of 1.1m from the source occupant are 4.93%, 3.68% and 1.74% for 0.77, 2.5 and 7μm particles, respectively.

The peak concentrations show decreased levels at the position directly above the occupant when compared to the receiver occupant's surroundings. This indicates that a cough jet presents a greater impact on dispersing particles than thermal plume, especially for a short distance between the two occupants. Furthermore, the concentration level in the position behind the receiver occupant suggests that a cough jet is able to overcome human thermal plume and travel past the receiver occupant.

(Origin is shown in Figure 2)

Locations	Measurement			Coordinates (m)		
	0.77μm	2.5μm	7μm	X	Y	Z
P1	×	×	×	1.2	1.157	1.765
P2	×	T.L.	×	1.2	1.94	1.945
P3	N.M.	×	N.M.	1.2	1.307	1.765
P4	×	×	×	1.2	1.157	2.25
P5	×	×	×	0.83	2.2	1.54
P6	×	×	T.L.	0.745	1.157	1.945
P7	×	T.L.	T.L.	1.655	1.157	1.945
P8	N.M.	×	N.M.	1.505	1.157	1.945

N.M.: not measured; T.L.: too low concentration

Table DS1: Measurement locations and corresponding coordinates.

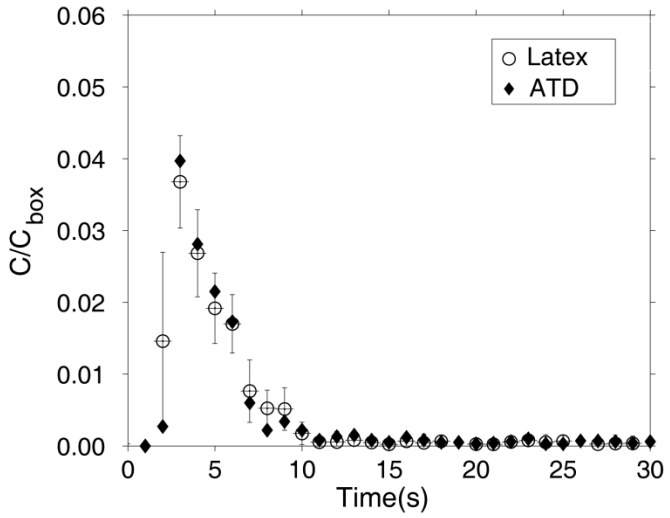

Figure DS1: Normalized particle (2.5μm) concentrations obtained from mono-dispersed particles and Arizona Test Dust (ATD).

References

Abanto, J., D. Barrero, M. Reggio and B. Ozell (2004). "Airflow modelling in a computer room." Building and Environment 39(12): 1393-1402.

ASHRAE (2006). " ANSI/ASHRAE Standard-70: Method of testing the performance of air outlets and air inlets. " American Society of Heating, Refrigerating and Air Conditioning Engineers, Atlanta, GA

ASHRAE (2007). "ASHRAE Handbook - HVAC Applications, Chaper 56." American Society of Heating, Refrigerating and Air Conditioning Engineers, Atlanta, GA

ASHRAE (2009). "ANSI/ASHRAE Standard-113: Method of testing for room air diffusion." American Society of Heating, Refrigerating and Air Conditioning Engineers, Atlanta, GA

ASHRAE (2009). "ASHRAE Handbook-Fundamentals." American Society of Heating, Refrigerating and Air Conditioning Engineers, Atlanta, GA

ASHRAE (2010). "Standard 55 - Thermal Environmental Conditions for Human Occupancy." Atlanta, GA: Refrigerating and Air Conditioning Engineers.

Armbruster, L. and H. Breuer (1982). "Investigations into defining inhalable dust." Annals of Occupational Hygiene 26(1): 21-32.

Aziz, M.A., I.A. Gad, E.S.F. Mohammed and R.H. Mohammed (2012). "Experimental and numerical study of influence of air ceiling diffusers on room air flow characteristics." Energy and Buildings 55: 738-746.

Baldwin, P.E. and A.D. Maynard (1998). "A survey of wind speeds in indoor workplaces." Annals of Occupational Hygiene 42(5): 303-313.

Beghein, C., Y. Jiang and Q.Y. Chen (2005). "Using large eddy simulation to study particle motions in a room." Indoor Air 15(4): 281-290.

Bennett, J.S., C.E. Feigley, J. Khan and M.H. Hosni (2000). "Comparison of mathematical models for exposure assessment with computational fluid dynamic simulation." Applied occupational and environmental hygiene 15(1): 131-144.

Berrouk, A.S., A.C.K. Lai, A.C.T. Cheung and S.L. Wong (2010). "Experimental measurements and large eddy simulation of expiratory droplet dispersion in a mechanically ventilated enclosure with thermal effects." Building and Environment 45(2): 371-379.

Bennett, J.S., C.E. Feigley, J. Khan and M.H. Hosni (2000). "Comparison of mathematical models for exposure assessment with computational fluid dynamic simulation." Applied occupational and environmental hygiene 15(1): 131-144.

Bin, Y. and S.C. Sekhar (2007). "Three-dimensional numerical simulation of a hybrid fresh air and recirculated air diffuser for decoupled ventilation strategy." Building and Environment 42(5): 1975-1982.

Bocksell, T.L. (1998). "An enhanced DRW model for turbulent particle diffusion", Master's thesis, University of Illinois at Urbana-Champaign.

Bolster, D.T. and P.F. Linden (2009). "Particle transport in low-energy ventilation systems. Part 2: Transients and experiments." Indoor Air 19(2): 130-144.

Boor, B.E., J.A. Siegel and A.Novoselac (2013). "Monolayer and Multilayer Particle Deposits on Hard Surfaces: Literature Review and Implications for Particle Resuspension in the Indoor Environment." Aerosol Science and Technology 47(8): 831-847.

Bouilly, J., K. Limam, C. Beghein and F. Allard (2005). "Effect of ventilation strategies on particle decay rates indoors: An experimental and modelling study." Atmospheric Environment 39(27): 4885-4892.

Buratti, C., E. Moretti, E. Belloni and F. Cotana (2013). "Unsteady simulation of energy performance and thermal comfort in non-residential buildings." Building and Environment 59: 482-491.

Cao, G., M. Ruponen and J. Kurnitski (2010). "Experimental investigation of the velocity distribution of the attached plane jet after impingement with the corner in a high room." Energy and Buildings 42(6): 935-944.

Cao, G., M. Ruponen, R. Paavilainen and J. Kurnitski (2011). "Modelling and simulation of the near-wall velocity of a turbulent ceiling attached plane jet after its impingement with the corner." Building and Environment 46(2): 489-500.

Cehlin, M. and B. Moshfegh (2010). "Numerical modeling of a complex diffuser in a room with displacement ventilation." Building and Environment 45(10): 2240-2252.

Chang, K.H., H.M. Kao and T.J. Chang (2012). "Lagrangian modeling of particle concentration distribution in indoor environment with different kernel functions and particle search algorithms." Building and Environment 57: 81-87.

Chang, T.J. and T.S. Hu (2008). "Transport mechanisms of airborne particulate matters in partitioned indoor environment." Building and Environment 43(5): 886-895.

Chang, T.J., H.M. Kao and R.S.W. Yam (2013). "Lagrangian modeling of the particle residence time in indoor environment." Building and Environment 62: 55-62.

Chang, T.J., Y.F. Hsieh and H.M. Kao (2006). "Numerical investigation of airflow pattern and particulate matter transport in naturally ventilated multi-room buildings." Indoor Air 16(2): 136-152.

Chao, C.Y.H., M.P. Wan, L. Morawska, G.R. Johnson, Z.D. Ristovski, M. Hargreaves, K. Mengersen, S. Corbett, Y. Li, X. Xie and D. Katoshevski (2009). "Characterization of expiration air jets and droplet size distributions immediately at the mouth opening." Journal of Aerosol Science 40(2): 122-133.

Chen, C., W. Liu, F. Li, C.H. Lin, J. Liu, J. Pei and Q. Chen (2013). "A hybrid model for investigating transient particle transport in enclosed environments." Building and Environment 62(0): 45-54.

Chen, Q. (1995). "Comparison of different k-epsilon models for indoor air flow computations." Numerical Heat Transfer Part B-Fundamentals 28(3): 353-369.

Chen Q., and A. Moser (1991). "Simulation of a multiple-nozzle diffuser." AIVC 12th Conference, Ottawa, Canada.

Chen, X., A. Li and R. Gao (2012). "Effects of near-wall heat source on particle deposition." Building Simulation, 5(4): 371-382.

Cho, Y. and H. B. Awbi (2007). "A study of the effect of heat source location in a ventilated room using multiple regression analysis." Building and Environment 42(5): 2072-2082.

Cho, Y.H. and M. Liu (2009). "Minimum airflow reset of single duct VAV terminal boxes." Building and Environment 44(9): 1876-1885.

Choi, J.I. and J.R. Edwards (2008). "Large eddy simulation and zonal modeling of human-induced contaminant transport." Indoor Air 18(3): 233-249.

Choi, J.I. and J.R. Edwards (2012). "Large-eddy simulation of human-induced contaminant transport in room compartments." Indoor Air 22(1): 77-87.

Chow, W.K. and L.T. Wong (1996). "Experimental Studies on the Air Flow Characteristics Induced by a High Sidewall Grill in a Climate Chamber." Indoor and Built Environment 5(2): 82-98.

Chow, W.K. and L.T. Wong (1994). "Experimental studies on air diffusion of a linear diffuser and associated thermal comfort indices in an air-conditioned space." Building and Environment 29(4): 523-530.

Chow, W.K., L.T. Wong and W.Y. Fung (1996). "Field measurement of the air flow characteristics of big mechanically ventilated spaces." Building and Environment 31(6): 541-550.

Chow, W.K. and L.T. Wong (1999). "Local air speeds measurement in mechanically ventilated spaces." Building and Environment 34(5): 553-563.

Chung, K.C. and S.P. Hsu (2001). "Effect of ventilation pattern on room air and contaminant distribution." Building and Environment 36(9): 989-998.

Chung, K.C. and C.Y. Lee (1996). "Predicting air flow and thermal comfort in an indoor environment under different air diffusion models." Building and Environment 31(1): 21-16.

Chung, K. C. (1999). "Three-dimensional analysis of airflow and contaminant particle transport in a partitioned enclosure". Building and Environment 34(1): 7-17.

Clausen, P.A., Z. Liu, Y. Xu, V. Kofoed-Sørensen and J. C. Little (2010). "Influence of air flow rate on emission of DEHP from vinyl flooring in the emission cell FLEC: Measurements and CFD simulation." Atmospheric Environment 44(23): 2760-2766.

Corgnati, S., M. Perino, G. Fracastoro and P. V. Nielsen (2009). "Experimental and numerical analysis of air and radiant cooling systems in offices." Building and Environment 44(4): 801-806.

Duguid, J.P. (1946). "The size and the duration of air-carriage of respiratory droplets and droplet-nuclei." Journal of Hygiene 44(6): 471-479.

Emmerich, S. J., and K.B. McGrattan (1998). "Application of a large eddy simulation model to study room airflow." ASHRAE Transactions 104: 1128-1140.

EPA (2003). "Particle pollution and your health." Washington, DC, U.S. Environmental Protection Agency.

Fanger, P. O. (1970) "Thermal comfort". Copenhagen: Danish Technical Press.

Fennelly, K.P., J.W. Martyny, K.E. Fulton, I.M. Orme, D.M. Cave and L.B. Heifets (2004). "Cough-generated aerosols of Mycobacterium tuberculosis: a new method to study infectiousness." American Journal of Respiratory and Critical Care Medicine 169(5): 604-609.

Fisk, W.J. (2000). "Health and productivity gains from better indoor environments and their relationship with building energy efficiency." Annual Review of Energy and the Environment 25: 537-566.

Fontanini, A., M.G. Olsen and B. Ganapathysubramanian (2011). "Thermal comparison between ceiling diffusers and fabric ductwork diffusers for green buildings." Energy and Buildings 43(11): 2973-2987.

Frontczak, M. and P. Wargocki (2011). "Literature survey on how different factors influence human comfort in indoor environments." Building and Environment 46(4): 922-937.

Gao, C.F. and W.L. Lee (2009). "Optimized design of floor-based air-conditioners for residential use." Building and Environment 44(10): 2080-2088.

Gao, N.P. and J.L. Niu (2007). "Modeling particle dispersion and deposition in indoor environments." Atmospheric Environment 41(18): 3862-3876.

Gao, Z, and J.S. Zhang (2010). "Numerical analysis for evaluating the Exposure Reduction Effectiveness of room air cleaners." Building and Environment 45(9): 1984-1992.

Germano, M. (1986). "A proposal for a redefinition of the turbulent stresses in the filtered Navier-Stokes equations." Physics of Fluids 29(7): 2323-2324.

Ghaem-Maghami, E. and H. Johari (2010). "Velocity field of isolated turbulent puffs." Physics of Fluids (1994-present) 22(11): 115105.

Goldasteh, I., G. Ahmadi and A.R. Ferro (2013). "Wind tunnel study and numerical simulation of dust particle resuspension from indoor surfaces in turbulent flows." Journal of Adhesion Science and Technology 27(14): 1563-1579.

Gomes, C., J. Freihaut and W. Bahnfleth (2007). "Resuspension of allergen-containing particles under mechanical and aerodynamic disturbances from human walking." Atmospheric Environment 41(25): 5257-5270.

Gralton, J., E. Tovey, M.L. McLaws and W.D. Rawlinson (2011). "The role of particle size in aerosolized pathogen transmission: A review." Journal of Infection 62(1): 1-13.

Gupta, J.K., C.H. Lin and Q. Chen (2009). "Flow dynamics and characterization of a cough." Indoor Air 19(6): 517-525.

Gupta, J.K., C.H. Lin and Q. Chen (2011). "Transport of expiratory droplets in an aircraft cabin." Indoor Air 21(1): 3-11.

Hafner, S.D., F. Montes and C.A. Rotz (2012). "A mass transfer model for VOC emission from silage." Atmospheric Environment 54(0): 134-140.

Hanzawa, H., A. Melikow and P. Fanger (1987). "Airflow characteristics in the occupied zone of ventilated spaces." ASHRAE Transactions 93: 524-539.

Havel, R.J., H.A. Eder and J.H. Bragdon (1955). "The distribution and chemical composition of ultra-centrifugally separated lipoproteins in human serum." Journal of Clinical Investigation 34(9): 1345-1353.

He, G., X. Yang and J. Srebric (2005). "Removal of contaminants released from room surfaces by displacement and mixing ventilation: modeling and validation." Indoor Air 15(5): 367-380.

Heymann, B. (1899). "Ueber die Ausstreuung infectiöser Tröpfchen beim Husten der Phthisiker." Medical Microbiology and Immunology 30(1): 139-162.

Holmberg, S. and Q. Chen (2003). "Air flow and particle control with different ventilation systems in a classroom." Indoor Air 13(2): 200-204.

Houghten, F., C. Gutberlet and E. Witkowski (1938). "Draft temperatures and velocities in relation to skin temperature and feeling of warmth." ASHRAE Transactions 44: 289-308.

Hu, S. (2003). "Airflow characteristics in the outlet region of a vortex room air diffuser." Building and Environment 38(4): 553-561.

Hu, S.C. (2003). "Airflow characteristics in the outlet region of a vortex room air diffuser." Building and Environment 38(4): 553-561.

Huang, Y. and H. Zhang (1999). "Commercial heating and cooling loads component analysis." Energy Analysis Program: 7.

Ibrahim, A.H., P.F. Dunn and R.M. Brach (2003). "Microparticle detachment from surfaces exposed to turbulent air flow: controlled experiments and modeling." Journal of Aerosol Science 34(6): 765-782.

Int-Hout, D. (2002). "Avoiding Sick Buildings while Assuring Occupant Productivity and Building Optimization." Texas A&M University.

Int-Hout, D. (1983) "Analysis of three perimeter heating systems by air-diffusion methods." ASHRAE Transactions 89(1B), 101-112.

Jia, X. L., McLaughlin, J.B. Derksen, J. and G. Ahmadi (2013). "Simulation of a mannequin's thermal plume in a small room." Computers & Mathematics with Applications 65(2): 287-295.

John, D.A. (2012). "Designing Air-Distribution Systems to Maximize Comfort." ASHRAE Journal 54(9): 20-26.

King, M.F., C. Noakes, P. Sleigh and M. Camargo-Valero (2013). "Bioaerosol deposition in single and two-bed hospital rooms: A numerical and experimental study." Building and Environment 59: 436-447.

Klepeis, N.E., W.C. Nelson, W.R. Ott, J.P. Robinson, A.M. Tsang, P. Switzer, J.V. Behar, S.C. Hern and W.H. Engelmann (2001). "The National Human Activity Pattern Survey (NHAPS): a resource for assessing exposure to environmental pollutants." Journal of exposure analysis and environmental epidemiology 11(3): 231-252.

Koestel, A. and G. Tuve (1955). "Performance and evaluation of room air distribution systems." ASHRAE Transactions 61: 533-550.

Kosonen, R. and F. Tan (2004). "Assessment of productivity loss in air-conditioned buildings using PMV index." Energy and Buildings 36(10): 987-993.

Kovasznay, L.S., H. Fujita and R.L. Lee (1975). "Unsteady turbulent puffs." Adv. Geophys. B 18: 253.

Krajčík, M., Simone, A. and Olesen, B. W. (2012). "Air distribution and ventilation effectiveness in an occupied room heated by warm air." Energy and Buildings 55,

Krarti, M. (2008). "Energy efficient systems and strategies for heating, ventilating, and air conditioning (HVAC) of buildings." Journal of Green Building 3(1), 44-55.

Kouros, H., Medina R., and Johari, H. (1993). "Spreading rate of an unsteady turbulent jet." AIAA journal 31(8):1523-1526.

Kwon, S.B., J. Park, J. Jang, Y. Cho, D. S. Park, C. Kim, G. N. Bae and A. Jang (2012). "Study on the initial velocity distribution of exhaled air from coughing and speaking." Chemosphere 87(11): 1260-1264.

Lai, A.C.K. and S.L. Wong (2010). "Experimental Investigation of Exhaled Aerosol Transport Under Two Ventilation Systems." Aerosol Science and Technology 44(6): 444-452.

Lai, A.C.K. and S.L. Wong (2011). "Expiratory Aerosol Transport in a Scaled Chamber under a Variety of Emission Characteristics: An Experimental Study." Aerosol Science and Technology 45(8): 909-917.

Lee, E., J.A. Khan, C.E. Feigley, M.R. Ahmed and J.R. Hussey (2007). "An investigation of air inlet types in mixing ventilation." Building and Environment 42(3): 1089-1098.

Lee, J.H.W. and G.Q. Chen (1998). "A numerical study of turbulent line puffs via the renormalization group (RNG) k-epsilon model." International Journal for Numerical Methods in Fluids 26(2): 217-234.

Li, A. and G. Ahmadi (1992). "Dispersion and deposition of spherical particles from point sources in a turbulent channel flow." Aerosol Science and Technology 16(4): 209-226.

Li, Y., A. Chwang, W. Seto, P. Ho and P. Yuen (2008). "Understanding droplets produced by nebulisers and respiratory activities." Hong Kong Med J 14(Suppl 1): 29-32.

Li, Y., Leung, G.M., Tang, J.W., Yang, X., Chao, C.Y.H., Lin, J.Z., Lu, J.W., Nielsen, P.V., Niu, J., Qian, H., Sleigh, A.C., Su, H.J.J., Sundell, J., Wong, T.W., and P.L. Yuen (2007). "Role of ventilation in airborne transmission of infectious agents in the built environment-a multidisciplinary systematic review." Indoor Air 17(1): 2-18.

Li, Z., J. Zhang, A. Zhivov and L. Christianson (1993). "Characteristics of diffuser air jets and airflow in the occupied regions of mechanically ventilated rooms-a literature review." ASHRAE Transactions 99: 1119-1119.

Lilly, D.K. (1992). "A proposed modification of the Germano subgrid-scale closure method." Physics of Fluids A: Fluid Dynamics 4(3): 633-635.

Lindsley, W.G., T.A. Pearce, J.B. Hudnall, K.A. Davis, S.M. Davis, M.A. Fisher, R. Khakoo, J.E. Palmer, K.E. Clark, I. Celik, C.C. Coffey, F.M. Blachere and D.H. Beezhold (2012). "Quantity and size distribution of cough-generated aerosol particles produced by influenza patients during and after illness." Journal of Occupational and Environmental Hygiene 9(7): 443-449.

Liu, S.C., Mak, C.M. and J.L. Niu (2011). " Numerical evaluation of louver configuration and ventilation strategies for the windcatcher system." Building and Environment 46(8): 1600-1616.

Liu, S.C. and A. Novoselac (2014). "Lagrangian particle modeling in the indoor environment: A comparison of RANS and LES turbulence methods (RP-1512)." HVAC&R Research 20(4): 480-495.

Liu, S.C. and A. Novoselac (2014). "Transport of airborne particles from an unobstructed cough jet." Aerosol Science and Technology 48(11): 1183-1194.

Liu, W., Mazumdar, S., Zhang, Z., Poussou, S.B., Liu, J., Lin, C.H., and Q. Chen (2012). "State-of-the-art methods for studying air distributions in commercial airliner cabins." Building and Environment 47: 5-12.

Loudon, R. and S. Spohn (1969). "Cough frequency and infectivity in patients with pulmonary tuberculosis." The American review of respiratory disease 99(1): 109.

Lu, W.Z., A.T. Howarth, N. Adam and S.B. Riffat (1996). "Modelling and measurement of airflow and aerosol particle distribution in a ventilated two-zone chamber." Building and Environment 31(5): 417-423.

Luo, S. and B. Roux (2004). "Modeling of the HESCO nozzle diffuser used in IEA Annex-20 experiment test room." Building and Environment 39(4): 367-384.

Mallick, F.H. (1996). "Thermal comfort and building design in the tropical climates." Energy and Buildings 23(3): 161-167.

Marr, D.R., Spitzer, I.M., and M.N. Glauser (2008). "Anisotropy in the breathing zone of a thermal manikin." Experiments in Fluids 44(4): 661-673.

Martinez-Almansa, J., A. Fernandez-Gutierrez, L. Parras and C. del Pino (2014). "Numerical and experimental study of a HVAC wall diffuser." Building and Environment 80: 1-10.

Matthews, T. G., C. V. Thompson, D. L. Wilson, A. R. Hawthorne and D. T. Mage (1989). "Air velocities inside domestic environments: An important parameter in the study of indoor air quality and climate." Environment International 15(1–6): 545-550.

Miguel, A.F., M. Aydin and A.H. Reis (2005). "Indoor deposition and forced re-suspension of respirable particles." Indoor and Built Environment 14(5): 391-396.

Miller, P. and R. Nevins (1972). "An analysis of the performance of room air distribution systems." ASHRAE Transactions 78(Part 2).

Miller, P.L. (1971). "Room air distribution performance of four selected outlets." ASHRAE Transactions 77(2): 194.

Miller, P.L. (1979). "Design of room air diffusion systems using the air diffusion performance index (ADPI)." ASHRAE Journal 10: 85.

Miller, P.L. and R.T. Nash (1971). "A further analysis of room air distribution performance." ASHRAE Transactions 77(2): 205.

Miller, P.L. and R.G. Nevins (1969). "Room air distribution with an air distributing ceiling - Part II." ASHRAE Transactions 75: 118.

Miller, P.L. and R.G. Nevins (1970). "Room air distribution performance of ventilation ceilings and cone-type circular ceiling diffusers." ASHRAE Transactions 76(1): 186.

Morawska, L., G. Johnson, Z. Ristovski, M. Hargreaves, K. Mengersen, C. Chao, M. P. Wan, Y. Li, X. Xie and D. Katoshevski (2008). "Droplets expelled during human expiratory activities and their origin". International Conference on Indoor Air Quality and Climate. Copenhagen, Denmark.

Morsi, S. and A. Alexander (1972). "An investigation of particle trajectories in two-phase flow systems." Journal of Fluid Mechanics 55(02): 193-208.

Mundt, E. (2001). "Non-buoyant pollutant sources and particles in displacement ventilation." Building and Environment 36(7): 829-836.

Nevins, R.G. and P.L. Miller (1972). "Analysis, evaluation and comparison of room air distribution performance-a summary." Research Report, ASHRAE RP-55 and 88.

Ng, K.C., K. Kadirgama and E.Y.K. Ng (2008). "Response surface models for CFD predictions of air diffusion performance index in a displacement ventilated office." Energy and Buildings 40(5): 774-781.

Nishimura, H., S. Sakata and A. Kaga (2013). "A new methodology for studying dynamics of aerosol particles in sneeze and cough using a digital high-vision, high-speed video system and vector analyses." Plos One 8(11): e80244.

Novoselac, A., and J.A. Siegel (2009). "Impact of placement of portable air cleaning devices in multizone residential environments." Building and Environment 44(12): 2348-2356.

Novoselac, A. and Srebric, J. (2003). "Comparison of air exchange efficiency and contaminant removal effectiveness as IAQ indices." ASHRAE Transactions 109(2), 339-349.

Ogden, T. and J. Birkett (1975). "The human head as a dust sampler." Inhaled particles 4: 93-105.

Pérez-Lombard, L., J. Ortiz and C. Pout (2008). "A review on buildings energy consumption information." Energy and Buildings 40(3): 394-398.

Platt, G., J. Li, R. Li, G. Poulton, G. James and J. Wall (2010). "Adaptive HVAC zone modeling for sustainable buildings." Energy and Buildings 42(4): 412-421.

Posner, J., C. Buchanan and D. Dunn-Rankin (2003). "Measurement and prediction of indoor air flow in a model room." Energy and Buildings 35(5): 515-526.

Richmond-Bryant, J., Eisner, A.D., Brixey, L.A., and R.W. Wiener (2006). "Short-term dispersion of indoor aerosols: can it be assumed the room is well mixed?" Building and Environment 41(2): 156-163.

Rim, D. and A. Novoselac (2008). "Transient Simulation of Airflow and Pollutant Dispersion Under Mixing Flow and Buoyancy Driven Flow Regimes in Residential Buildings". ASHARE Transactions 2008, 114(2): 130-142.

Rim, D. and A. Novoselac (2009). "Transport of particulate and gaseous pollutants in the vicinity of a human body." Building and Environment 44(9): 1840-1849.

Rim, D. and A. Novoselac (2010). "Ventilation effectiveness as an indicator of occupant exposure to particles from indoor sources." Building and Environment 45(5): 1214-1224.

Rutman, E., C. Inard, A. Bailly and F. Allard (2005). "A global approach of indoor environment in an air-conditioned office room." Building and Environment 40(1): 29-37.

Rydberg, J., P. Norback and S. Stockholm (1949). "Air distribution and draft." ASHVE Transactions 55: 225-240.

Sadrizadeh, S., A. Tammelin, P. Ekolind and S. Holmberg (2014). "Influence of staff number and internal constellation on surgical site infection in an operating room." Particuology 13: 42-51.

Salmanzadeh, M., G. Zahedi, G. Ahmadi, D.R. Marr and M. Glauser (2012). "Computational modeling of effects of thermal plume adjacent to the body on the indoor airflow and particle transport." Journal of Aerosol Science 53(0): 29-39.

Sangras, R., O. Kwon and G. Faeth (2002). "Self-preserving properties of unsteady round nonbuoyant turbulent starting jets and puffs in still fluids." Journal of Heat Transfer 124(3): 460-469.

Schiavon, S. and A.K. Melikov (2008). "Energy saving and improved comfort by increased air movement." Energy and Buildings 40(10): 1954-1960.

Seepana, S. and A.C.K. Lai (2012). "Experimental and Numerical Investigation of Interpersonal Exposure of Sneezing in a Full-Scale Chamber." Aerosol Science and Technology 46(5): 485-493.

Song, L. and J. Abraham (2003). "Entrainment Characteristics of Transient Turbulent Round, Radial and Wall-Impinging Jets: Theoretical Deductions." Journal of Fluids Engineering 125(4): 605-612.

Spitzer, I. M., Marr, D.R., and M.N. Glauser (2010). "Impact of manikin motion on particle transport in the breathing zone." Journal of Aerosol Science 41(4): 373-383.

Srebric, J. and Q.Y. Chen (2002). "Simplified numerical models for complex air supply diffusers." HVAC&R Research 8(3): 277-294.

Sun, Y. and T. F. Smith (2005). "Air flow characteristics of a room with square cone diffusers." Building and Environment 40(5): 589-600.

Talbot, L., R. Cheng, R. Schefer and D. Willis (1980). "Thermophoresis of particles in a heated boundary layer." Journal of Fluid Mechanics 101(04): 737-758.

Tang, J.W., T.J. Liebner, B.A. Craven and G. S. Settles (2009). "A schlieren optical study of the human cough with and without wearing masks for aerosol infection control." Journal of the Royal Society Interface 6: S727-S736.

Tang, J.W., A. Nicolle, J. Pantelic, G.C. Koh, L. De Wang, M. Amin, C.A. Klettner, D.K. Cheong, C. Sekhar and K.W. Tham (2012). "Airflow dynamics of coughing in healthy human volunteers by shadowgraph imaging: an aid to aerosol infection control." Plos One 7(4): e34818.

Tang, J.W. and G.S. Settles (2008). "Coughing and Aerosols." New England Journal of Medicine 359(15): e19.

Tian, Z.F., J.Y. Tu and G.H. Yeoh (2007). "CFD studies of indoor airflow and contaminant particle transportation." Particulate Science and Technology 25(6): 555-570.

Tian, Z.F., J.Y. Tu, G.H. Yeoh and R.K.K. Yuen (2006). "On the numerical study of contaminant particle concentration in indoor airflow." Building and Environment 41(11): 1504-1514.

Tomasi, R., Krajčík, M., Simone, A. and B.W. Olesen (2013). "Experimental evaluation of air distribution in mechanically ventilated residential rooms." Thermal comfort and ventilation effectiveness. *Energy and Buildings* 60: 28-37.

Tripathi, B. and S.G. Moulic (2007). "Investigation of the buoyancy affected airflow patterns in the enclosure subjected at the different wall temperatures." Energy and Buildings 39(8): 906-912.

U.S. Department of Energy, 2012. "2011 Buildings Energy Data Book." Washington, DC: U.S. Department of Energy.

Vakiloroaya, V., B. Samali, A. Fakhar and K. Pishghadam (2014). "A review of different strategies for HVAC energy saving." Energy Conversion and Management 77: 738-754.

VanSciver, M., S. Miller and J. Hertzberg (2011). "Particle Image Velocimetry of Human Cough." Aerosol Science and Technology 45(3): 415-422.

Vincent, J. and D. Mark (1982). "Applications of blunt sampler theory to the definition and measurement of inhalable dust." Annals of Occupational Hygiene 26(1): 3-19.

Walker, I.S. and M.H. Sherman (2013). "Effect of ventilation strategies on residential ozone levels." Building and Environment 59: 456-465.

Wan, M.P., and C.Y.H. Chao (2007). "Transport characteristics of expiratory droplets and droplet nuclei in indoor environments with different ventilation airflow patterns." Journal of Biomechanical Engineering-Transactions of the ASME 129(3): 341-353.

Wang, M., C.H. Lin and Q. Chen (2012). "Advanced turbulence models for predicting particle transport in enclosed environments." Building and Environment 47(0): 40-49.

Wang, Q. and K.D. Squires (1996). "Large eddy simulation of particle-laden turbulent channel flow." Physics of Fluids 8(5): 1207-1223.

Wargocki, P., D.P. Wyon, J. Sundell, G. Clausen and P. Fanger (2000). "The effects of outdoor air supply rate in an office on perceived air quality, sick building syndrome (SBS) symptoms and productivity." Indoor Air 10(4): 222-236.

Waring, M.S., and J.A. Siegel (2008). "Particle loading rates for HVAC filters, heat exchangers, and ducts." Indoor Air 18(3): 209-224.

Wasiolek, P.T., J.J. Whicker, H. Gong and J.C. Rodgers (1999). "Room airflow studies using sonic anemometry." Indoor Air 9(2): 125-133.

Wells, W.F. (1955). "Airborne Contagion and Air Hygiene. An Ecological Study of Droplet Infections." Royal Society of Health Journal 76(9): 600-600.

Whicker, J.J., G.D. Baker and P.T. Wasiolek (2000). "Quantitative measurements of airflow inside a nuclear laboratory." Health Physics 79(6): 712-721.

Whicker, J.J., P.T. Wasiolek and R.A. Tavani (2002). "Influence of room geometry and ventilation rate on airflow and aerosol dispersion: Implications for worker protection." Health Physics 82(1): 52-63. .

Wilkins, E. (1954). "Air pollution and the London fog of December, 1952." The Journal of the Royal Society for the Promotion of Health 74(1): 1-21.

Worth Longest, P. and S. Vinchurkar (2007). "Validating CFD predictions of respiratory aerosol deposition: Effects of upstream transition and turbulence." Journal of Biomechanics 40(2): 305-316.

Wygnanski, I. and H. Fiedler (1969). "Some measurements in the self-preserving jet." Journal of Fluid Mechanics 38(03): 577-612.

Xie, X., Li, Y., Chwang, A.T.Y., Ho, P.L. and W.H. Seto (2007). "How far droplets can move in indoor environments–revisiting the Wells evaporation–falling curve." Indoor Air 17(3): 211-225.

Xie, X.J., Y.G. Li, H.Q. Sun and L. Liu (2009). "Exhaled droplets due to talking and coughing." Journal of the Royal Society Interface 6: S703-S714.

Xu, H.T. and J.L. Niu (2004). "Numerical simulation and experimental validation of the swirling turbulent air flow and mixing processes." Numerical Heat Transfer, Part A: Applications 46(6): 571-586.

Xu, Y. and J.C. Little (2006). "Predicting emissions of SVOCs from polymeric materials and their interaction with airborne particles." Environmental Science & Technology 40(2): 456-461.

Xu, Y., Z. Liu, J. Park, P.A. Clausen, J.L. Benning and J.C. Little (2012). "Measuring and predicting the emission rate of phthalate plasticizer from vinyl flooring in a specially-designed chamber." Environmental Science & Technology 46(22): 12534-12541.

Yang, S.H., G.W.M. Lee, C.M. Chen, C.C. Wu and K.P. Yu (2007). "The size and concentration of droplets generated by coughing in human subjects." Journal of Aerosol Medicine-Deposition Clearance and Effects in the Lung 20(4): 484-494.

Yin, Y., Xu, W., Gupta, J.K., Guity, A, Marmion, P., Manning, A., Gulick, B., Zhang, X., and Q. Chen (2009). "Experimental Study on Displacement and Mixing Ventilation Systems for a Patient Ward." HVAC &R Research 19(3): 57-61.

Yin, Y., J.K. Gupta, X. Zhang, J. Liu and Q. Chen (2011). "Distributions of respiratory contaminants from a patient with different postures and exhaling modes in a single-bed inpatient room." Building and Environment 46(1): 75-81.

Zhang, H., E. Arens, S. A. Fard, C. Huizenga, G. Paliaga, G. Brager and L. Zagreus (2007). "Air movement preferences observed in office buildings." International journalof biometeorology 51(5): 349-360.

Zhang, L. and Y.G. Li (2012). "Dispersion of coughed droplets in a fully-occupied high-speed rail cabin." Building and Environment 47: 58-66.

Zhang, T., K. Lee and Q. Chen (2009). "A simplified approach to describe complex diffusers in displacement ventilation for CFD simulations." Indoor Air 19(3): 255-267.

Zhang, Z., Chen, X., Mazumdar, S., Zhang, T., and Q. Chen (2009). "Experimental and numerical investigation of airflow and contaminant transport in an airliner cabin mockup." Building and Environment 44 (1):85-94.

Zhang, Z., and Q. Chen (2006). "Experimental measurements and numerical simulations of particle transport and distribution in ventilated rooms." Atmospheric Environment 40(18): 3396-3408.

Zhang, Z., and Q. Chen (2007). "Comparison of the Eulerian and Lagrangian methods for predicting particle transport in enclosed spaces." Atmospheric Environment 41(25): 5236-5248.

Zhang, Z. and Q. Chen (2009). "Prediction of particle deposition onto indoor surfaces by CFD with a modified Lagrangian method." Atmospheric Environment 43(2): 319-328.

Zhao, B., C. Yang, X. Yan and S. Liu (2008). "Particle dispersion and deposition in ventilated rooms: Testing and evaluation of different Eulerian and Lagrangian models." Building and Environment 43(4): 388-397.

Zhao, B., Y. Zhang, X. Li, X. Yang and D. Huang (2004). "Comparison of indoor aerosol particle concentration and deposition in different ventilated rooms by numerical method." Building and Environment 39(1): 1-8.

Zhao, B., Z. Zhang and X. Li (2005). "Numerical study of the transport of droplets or particles generated by respiratory system indoors." Building and Environment 40(8): 1032-1039.

Zhou, L. and F. Haghighat (2007). "Simplified method for modeling swirl diffusers." Proceedings of IAQVEC conference, Sendai, Japan.

Zhu, S., S. Kato and J.H. Yang (2006). "Study on transport characteristics of saliva droplets produced by coughing in a calm indoor environment." Building and Environment 41(12): 1691-1702.

Zhu, S., Srebric, J., Spengler, J.D., and P. Demokritou (2012). "An advanced numerical model for the assessment of airborne transmission of influenza in bus microenvironments." Building and Environment 47: 67-75.

Vita

Shichao Liu was born in a county of Anyang city that was the capital of ancient China around 2000 BC. Here he spent his whole childhood with inspiring parents and brothers who nurtured his curiosity in science. In 2007, he obtained his B. Eng. degree from Tianjin University where he met his wife, Yi. As one of the best universities, Tianjin University provided him a thorough education and fired up his enthusiasm in sustainable and healthy buildings. After two-year research on particle filtration, he received his M. Eng. degree and conducted approximately one year study on sustainable buildings using natural ventilation at The Hong Kong Polytechnic University, Hong Kong. He considers it a great privilege to be a Longhorn and to join Indoor Air Quality Group at The University of Texas at Austin.

Permanent email address: chaoshiliu@hotmail.com
This dissertation was typed by Shichao Liu.